

© 1975

GORDON PAUL TREWEEK

ALL RIGHTS RESERVED

THE FLOCCULATION OF E. COLI  
WITH POLYETHYLENEIMINE

Thesis by  
Gordon P. Treweek

In Partial Fulfillment of the Requirements  
for the Degree of  
Doctor of Philosophy

California Institute of Technology  
Pasadena, California

1975

(Submitted May 29, 1975)

## ACKNOWLEDGMENTS

I would like to express my sincere appreciation to Professor James J. Morgan who unfailingly encouraged my efforts in this research, patiently understood the shortcomings, and invariably posed the right question to guide my understanding of the subject matter. I also wish to acknowledge the continued interest of Professor Jack E. McKee, who started my career in environmental engineering, and of Professor Charles R. O'Melia, who critically evaluated much of the research data and suggested new interpretations.

The transition from conception of research to final thesis form was greatly aided by the efforts of Mr. Elton Daly and Mr. Larry McClellan in constructing research apparatus, Mr. Robert S. Schultz in preparing drawings, and Ms. Helen Fabel in typing the manuscript.

This investigation was supported directly by a U.S. Public Health Service Training Grant, and indirectly by the U.S. Veterans Administration. The financial support by both agencies is gratefully acknowledged.

Finally, I thank my wife Sally for her understanding and devotion throughout the course of this study, and my parents for their enthusiastic support of all my efforts.

## ABSTRACT

A comprehensive study was made of the flocculation of dispersed E. coli bacterial cells by the cationic polymer polyethyleneimine (PEI). The three objectives of this study were to determine the primary mechanism involved in the flocculation of a colloid with an oppositely-charged polymer, to determine quantitative correlations between four commonly-used measurements of the extent of flocculation, and to record the effect of varying selected system parameters on the degree of flocculation. The quantitative relationships derived for the four measurements of the extent of flocculation should be of direct assistance to the sanitary engineer in evaluating the effectiveness of specific coagulation processes.

A review of prior statistical mechanical treatments of adsorbed polymer configuration revealed that at low degrees of surface site coverage, an oppositely-charged polymer molecule is strongly adsorbed to the colloidal surface, with only short loops or end sequences extending into the solution phase. Even for high molecular weight PEI species, these extensions from the surface are theorized to be less than 50 Å in length. Although the radii of gyration of the five PEI species investigated were found to be large enough to form interparticle bridges, the low surface site coverage at optimum flocculation doses

indicates that the predominant mechanism of flocculation is adsorption coagulation.

The effectiveness of the high-molecular weight PEI species in producing rapid flocculation at small doses is attributed to the formation of a charge mosaic on the oppositely-charged E.coli surfaces. The large adsorbed PEI molecules not only neutralize the surface charge at the adsorption sites, but also cause charge reversal with excess cationic segments. The alignment of these positive surface patches with negative patches on approaching cells results in strong electrostatic attraction in addition to a reduction of the double-layer interaction energies. The comparative ineffectiveness of low-molecular weight PEI species in producing E.coli flocculation is caused by the size of the individual molecules, which is insufficient to both neutralize and reverse the negative E.coli surface charge. Consequently, coagulation produced by low-molecular weight species is attributed solely to the reduction of double-layer interaction energies via adsorption.

Electrophoretic mobility experiments supported the above conclusions, since only the high-molecular weight species were able to reverse the mobility of the E.coli cells. In addition, electron microscope examination of the seam of agglutination between E.coli cells flocculation by PEI revealed tightly-bound cells, with intercellular separation distances of less than 100-200 Å in most instances. This

intercellular separation is partially due to cell shrinkage in preparation of the electron micrographs.

The extent of flocculation was measured as a function of PEI molecular weight, PEI dose, and the intensity of reactor chamber mixing. Neither the intensity of mixing, within the common treatment practice limits, nor the time of mixing for up to four hours appeared to play any significant role in either the size or number of E. coli aggregates formed. The extent of flocculation was highly molecular-weight dependent: the high-molecular-weight PEI species produce the larger aggregates, the greater turbidity reductions, and the higher filtration flow rates. The PEI dose required for optimum flocculation decreased as the species molecular weight increased. At large doses of high-molecular-weight species, redispersion of the macroflocs occurred, caused by excess adsorption of cationic molecules. The excess adsorption reversed the surface charge on the E. coli cells, as recorded by electrophoretic mobility measurements.

Successful quantitative comparisons were made between changes in suspension turbidity with flocculation and corresponding changes in aggregate size distribution. E. coli aggregates were treated as coalesced spheres, with Mie scattering coefficients determined for spheres in the anomalous diffraction regime. Good quantitative comparisons were also found to exist between the reduction in

refiltration time and the reduction of the total colloid surface area caused by flocculation. As with turbidity measurements, a coalesced sphere model was used since the equivalent spherical volume is the only information available from the Coulter particle counter. However, the coalesced sphere model was not applicable to electrophoretic mobility measurements. The aggregates produced at each PEI dose moved at approximately the same velocity, almost independently of particle size.

PEI was found to be an effective flocculant of E. coli cells at weight ratios of 1 mg PEI:100 mg E. coli. While PEI itself is toxic to E. coli at these levels, similar cationic polymers could be effectively applied to water and wastewater treatment facilities to enhance sedimentation and filtration characteristics.

## TABLE OF CONTENTS

Part	Title	Page
Chapter 1	INTRODUCTION	1
1.1	Removal of Biocolloids from Wastewater with Cationic Polymers	1
1.2	Definition of Flocculation	4
1.3	Purpose of Thesis	4
1.4	Importance of Aggregate Diameter in Flocculation Process	5
1.4.1	Sedimentation	8
1.4.2	Centrifugation	9
1.4.3	Filtration	10
1.4.4	Vacuum Filtration	11
	REFERENCES CITED CHAPTER 1	16
Chapter 2	THEORIES OF POSSIBLE MECHANISM OF BIOLOGICAL AGGREGATION	18
2.1	Introduction	18
2.2	Physical Double-Layer Theory	20
2.3	Adsorption Coagulation Theory	23
2.4	Polymer Bridging Theory	24
2.5	<u>Zoogloea ramigera</u> Theory	28
2.6	Capsular Theory	29
2.7	Flagella Interaction Theory	29
2.8	Protozoa Theory	29
2.9	Poly-beta-hydroxybutyric Acid Theory	30
2.10	Summary of Theories of Biological Aggregation	31
	REFERENCES CITED CHAPTER 2	33

Chapter 3	THEORETICAL AND EXPERIMENTAL EVIDENCE IN SUPPORT OF MAJOR THEORIES	40
3.1	Polymer Adsorption	40
3.1.1	Introduction	40
3.1.2	Adsorption Models	42
3.1.3	Adsorption Experiments with Polymers	59
3.1.4	Direct Measurement of Adsorbed Layer Thickness	63
3.1.5	Summary of Prior Adsorption Theory and Experiments	64
3.2	Electrophoretic Mobility	70
3.3	Polymer Molecular Weight and Size from Light Scattering	74
3.3.1	Rayleigh Scattering in Gases	75
3.3.2	Rayleigh Scattering in Liquids	76
3.3.3	Rayleigh Scattering from Molecules in Solution	77
3.4	Optimum Polymer Dose from Refiltration Theory	81
3.5	Intercellular Structure from Electron Microscopy	85
3.5.1	Biocolloids Flocculated with Anionic Polymers	85
3.5.2	Colloids Flocculated with Cationic Polymers	87
	REFERENCES CITED CHAPTER 3	89
Chapter 4	MECHANISM OF <u>E. COLI</u> AGGREGATION BY PEI	96
4.1	Experimental Materials	98
4.2	Experimental Methods	102
4.2.1	Light Scattering from PEI Solutions	102
4.2.2	Determination of Residual PEI Concentration	103

	4.2.3	Electrophoretic Mobility Experiments	106
	4.2.4	Refiltration Rate Experiments	108
	4.2.5	Preparation of Flocculated Cells for Electron Microscopy	108
4.3		Experimental Results	110
	4.3.1	PEI Molecular Weight and Size	110
	4.3.2	Results of Adsorption Studies	115
		4.3.2.1 PEI Adsorption to <u>E. coli</u> Surface	115
		4.3.2.2 Surface Site Coverage	118
		4.3.2.3 Monolayers of Surface Coverage	121
	4.3.3	Electrophoretic Mobility of <u>E. coli</u> -PEI Aggregates	124
	4.3.4	PEI Dose at Optimum Refiltration Rate	125
	4.3.5	Examination of <u>E. coli</u> Floccs with a Scanning Electron Microscope	130
		REFERENCES CITED CHAPTER 4	140
Chapter 5		METHODS OF MEASURING AGGREGATE NUMBER AND DIAMETER	143
	5.1	Introduction - Available Measurement Techniques	143
	5.2	Aggregate Count and Size Distribution	148
		5.2.1 Prior Applications of Electronic Particle Counting	148
		5.2.2 Theory of Electronic Particle Counting	153
		5.2.3 Proposed Modification to Theory for Aggregate Passage	160
	5.3	Light Scattering by Aggregated Particles	171
		5.3.1 Rayleigh-Gans Scattering	172
		5.3.1.1 Suspensions of Medium-Sized Particles	172

	5.3.1.2	Aggregates of Medium-Sized Particles	175
	5.3.2	Mie Scattering	177
	5.3.2.1	Suspension of Large Particles	177
	5.3.2.2	Approximations for Mie Scattering Coefficients	183
	5.3.2.3	Aggregates of Large Particles	188
5.4		Refiltration Rate	191
	5.4.1	Determination of Specific Surface Area	191
	5.4.2	Porosity of the Filter Cake	193
5.5		Electrophoretic Mobility of Aggregates	196
		REFERENCES CITED CHAPTER 5	200
Chapter 6		EXTENT OF <u>E. COLI</u> AGGREGATION BY PEI	205
6.1		System Parameters	205
	6.1.1	Particle Size and Concentration	205
	6.1.2	Polymer Concentration and Configuration	209
	6.1.3	Intensity and Time of Agitation	214
	6.1.4	Solution pH and Ionic Strength	218
6.2		Experimental Methods	222
	6.2.1	Application of Coulter Counter/PHA/MCA	223
	6.2.1.1	Calibration Techniques	223
	6.2.1.2	Aggregate Count and Size Distribution	226
	6.2.2	Light Scattering by <u>E. coli</u> Cells	227
	6.2.3	Light Scattering by <u>E. coli</u> Aggregates	229
	6.2.3.1	Correlation of Turbidity with Aggregate Size Distribution	229
	6.2.3.2	Relative Scattering Intensity of Flocculating <u>E. coli</u>	236

	6.2.3.3	Residual Relative Scattering Intensity of Flocculating <u>E. coli</u>	237
	6.2.4	Refiltration Rate of <u>E. coli</u> Aggregates	240
	6.2.4.1	Verification of Constant Porosity Assumption	240
	6.2.4.2	Influence of Velocity Gradient in Stirrer-Reactor on the Refiltration Rate	243
	6.2.5	Preparation of Electron Micrographs of <u>E. coli</u> Filter Cake	244
6.3		Experimental Results	244
	6.3.1	Influence of PEI Molecular Weight, Dose, and Velocity Gradient on Reduction in Particle Count	244
	6.3.2	Influence of PEI Molecular Weight and Dose on Particle Size Distributions	248
	6.3.3	Aggregate Light Scattering Results	259
	6.3.3.1	Correlation of Predicted Turbidity with Measured Turbidity	259
	6.3.3.2	Relative Scattering Intensity of Flocculating <u>E. coli</u> Suspensions	268
	6.3.3.3	Residual Relative Scattering Intensity of Flocculating <u>E. coli</u> Suspensions	270
	6.3.4	Refiltration Rate Results	277
	6.3.4.1	Influence of PEI Molecular Weight, Dose, and Velocity Gradient on Reduction of Refiltration Time	277
	6.3.4.2	Correlation of Refiltering Times with Surface Areas Changes in a Flocculating Suspension	279
	6.3.5	Electron Micrographs of <u>E. coli</u> Filter Cake	282

	6.3.6	Electrophoretic Mobility of <u>E.coli</u> Aggregates	285
		REFERENCES CITED CHAPTER 6	296
Chapter 7		SUMMARY AND CONCLUSIONS	301
	7.1	Mechanisms of <u>E.coli</u> Flocculation by PEI	303
		7.1.1 PEI Adsorption to <u>E.coli</u> Surface	306
		7.1.2 Electrophoretic Mobility of <u>E.coli</u> Floccules	309
		7.1.3 Light Scattering from PEI Solutions	311
		7.1.4 Refiltration Rate of Filtrate Through <u>E.coli</u> Filter Cake	312
		7.1.5 Electron Micrographs of Flocculated <u>E.coli</u> Cells	312
		7.1.6 The Mechanism of <u>E.coli</u> Flocculation by PEI	313
	7.2	Comparison of Methods of Measuring Extent of Aggregation	316
		7.2.1 Electronic Particle Counting and Size Distribution	317
		7.2.2 Light Scattering Intensity of Aggregated Particles	318
		7.2.3 Refiltration Rate Through Filter Bed of Aggregated Particles	320
		7.2.4 Electrophoretic Mobility of Aggregated Particles	320
		7.2.5 Quantitative Correlation of Experimental Data	322
	7.3	Influence of Selected Variables on the Extent of <u>E.coli</u> Aggregation by PEI	324
	7.4	Engineering Applications	329
	7.5	Modeling of Flocculation Process	333
	7.6	Summary	339
		REFERENCES CITED CHAPTER 7	341
Appendix A		Differential Volume Distribution Spectrums	343

## LIST OF TABLES

Number	Title	Page
4.1	Summary of Anticipated Characteristics of <u>E. coli</u> -PEI Floccs Based on Three Major Coagulation Models.	97
4.2	Molecular Weight Data for PEI Species	100
4.3	Molecular Weights and Radii of Gyration of PEI Species from Light Scattering Measurements	114
4.4	Monolayers of Surface Coverage as Function of PEI Molecular Weight and Dosage	123
4.5	Optimum Flocculant Dose and Associated Surface Site Coverage for Five PEI Species	129
5.1	Typical Value of Aggregate Porosity as a Function of Number of Cells Per Aggregate and Cell Diameter	161
5.2	Approximate Values of Scattering Coefficients $\alpha = 2\pi r/\lambda$ , $\rho = 2\alpha(m-1)$	185
5.3	Influence of Size Regime on Coalescence Assumption Using Jobst Approximations for Mie Scatterers	190
6.1	Theoretical Reductions in Particle Concentration from Perikinetic and Orthokinetic Flocculation	219
6.2	Summary of Calibration Data for Coulter Counter	224
6.3	Recent Applications of Turbidity Measurements to Flocculating Systems	231
7.1	Summary of Characteristics of <u>E. coli</u> -PEI Floccs as a Function of PEI Species	314
7.2	Summary of PEI Effectiveness in Producing Flocculation as a Function of PEI Molecular Weight	325

A.1	Diameters of Largest Volume Concentration, and Range of Aggregate Diameters in Equilibrium with Coagulation and Shear Conditions as Functions of PEI $MW_n$ and PEI Dose.	345
-----	---	-----

## LIST OF FIGURES

Number	Title	Page
1.1	Single Collector Efficiency as a Function of Particle Size. Adapted from Yao et al. (6)	12
3.1	Fraction of Adsorbed Segments $F_a$ Versus Segment Surface Interaction Parameter $K_{SS}$ for Molecules of 100, 1000, and 10,000 Segments. Adapted from Higuchi (10).	45
3.2	Fraction of Adsorbed Segments $F_a$ and Number of Segments in a Loop $N_L$ Versus Normalized Adsorption Energy $E_{SS}/kT$ . Adapted from Silberberg (11).	46
3.3	Average Number of Adsorbed Segments $N_a$ Versus Normalized Adsorption Energy $E_{SS}/kT$ for Molecules of 50, 100, 200 and $\infty$ Segments. Adapted from DiMarzio and McCrackin (14).	48
3.4	Fraction of Adsorbed Segments $F_a$ Versus Normalized Adsorption Energy $E_{SS}/kT$ for Molecules of 50, 200, and $\infty$ Segments. Adapted from DiMarzio and McCrackin (14).	49
3.5	Density Distribution of Polymer Segments $\rho(\zeta)$ Versus Distance from the Surface for Five Values of Normalized Adsorption Energy $E_{SS}/kT$ for Molecules of 200 Segments. Adapted from DiMarzio and McCrackin (14).	51
3.6	Average Length of Loops $L_L$ Versus Normalized Adsorption Energy $E_{SS}/kT$ for Flexible and Stiff Molecules of 20, 200, 1000 and 5000 Segments. Adapted from Roe (16).	52
3.7	Average Length of End Sequences $L_e$ Versus Normalized Adsorption Energy $E_{SS}/kT$ for Flexible and Stiff Molecules of 20, 100, 1000, and 10,000 Segments. Adapted from Roe (16).	54

3.8	Maximum Normal Distance from Polymer Segment to Adsorbing Surface Versus Normalized Adsorption Energy $E_{ss}/kT$ for Molecules of 50, 150, 200, and 300 Segments. Adapted from McCrackin (18).	55
3.9	Average Length of Loops $L_L$ Versus Normalized Adsorption Energy $E_{ss}/kT$ for a Range of Polymer Concentrations at Two Solvent-Polymer Interaction Energies $E_{sp}/kT$ . Adapted from Silberberg (20).	57
3.10	Fraction of Adsorbed Segments $F_a$ Versus Normalized Adsorption Energy $E_{ss}/kT$ for a Range of Polymer Concentration at Two Solvent-Polymer Interaction Energies $E_{sp}/kT$ . Adapted from Silberberg (20).	58
3.11A	Zeta Potential Caused by Specific Adsorption of PEI Molecules	71
3.11B	Reversed Zeta Potential Caused by Superequivalent Specific Adsorption of PEI Molecules.	71
4.1	Solution Configuration of PEI Molecule. Branch Points Account for Approximately 25% of Total Amino Nitrogens.	99
4.2	Stirrer-Reactor Assembly Used to Produce <u>E. coli</u> -PEI Flocculation for Electrophoretic Mobility, Refiltration, Turbidity, and Particle Size Distribution Experiments.	107
4.3	Weight-Average Molecular Weight of PEI 350 by Light Scattering Measurements.	111
4.4	Weight-Average Molecular Weight of PEI 600 by Light Scattering Measurements.	112
4.5	Adsorption of PEI to the Surface of <u>E. coli</u> as a Function of PEI Molecular Weight and Dose (0.0 to 10.0 mg/l).	116
4.6	Adsorption of PEI to the Surface of <u>E. coli</u> as a Function of PEI Molecular Weight and Dose (0.0 to 50.0 mg/l).	117

4.7	Fraction of Surface Site Coverage as a Function of PEI Molecular Weight and Dose.	120
4.8	Electrophoretic Mobility as a Function of PEI Molecular Weight and Dose.	126
4.9	Refiltration Rate as a Function of PEI Molecular Weight and Dose.	128
5.1	Deaggregation of a 1. % Hexadecane Emulsion with 0.09% AOT. Adapted from Higuchi et al. (8).	150
5.2	Schematic Diagram of Aperture Unit: A, Aperture; B, Test Tube with Aperture; C, Electrode within B; D, Electrode outside B; E, Dilute Cell Suspension; F and G, Control Stopcocks; H and I, Electrode Leads to Amplifier and Power Supply; J, Mercury Column and Reservoir R; K, L, and M, Electrodes to Activate and Stop Counter at Measured Volumes of Flow. Adapted from Mattern et al. (4).	154
5.3	Diagram of Aperture with Small Cylindrical Particle.	156
5.4A	Schematic Representation of Aperture, Current Density Lines, and Critical Volume.	159
5.4B	Particle Separation Distances in Critical Volume.	159
5.4C	Resulting Voltage Pulses. Adapted from Mattern et al. (4).	159
5.5	Aggregate Porosity as a Function of the Number of Cells per Aggregate.	163
5.6	Record of Voltage Pulses for Suspension of Three Different Monodisperse Particle Sizes.	168
5.7	Relative Intensity of Scattering about a Small Isotropic Particle. Adapted from Bender (33).	179
5.8	Relative Intensity of Scattering about an Isotropic Particle of Radius $0.13\lambda$ . $m=1.25$ . Adapted from Blumer (34).	180

5.9	Relative Intensity of Scattering about an Isotropic Particle of Radius $0.65 \lambda$ . $m=1.25$ . Adapted from Blumer (34).	181
5.10	Scattering Coefficient Curves from Mie's Formulae for $m=1.33$ , $1 + \epsilon$ , $0.93$ , and $0.80$ . Adapted from van de Hulst (36).	184
5.11	Comparison of Jobst Approximation for Scattering Coefficient with Mie Theory Values ( $m=1.05$ , $1.10$ ) and Rayleigh-Gans Approximation ( $m=1.00 + \epsilon$ ). Adapted from Koch (27).	187
6.1	Growth Curve for <u>E. coli</u> CR63.	207
6.2	Simple Extended Configuration of PEI Molecule.	212
6.3	Light Scattering Intensity from Equal Weight Concentrations of Polystyrene Latex Spheres of Increasing Diameter. Adapted from Busch (37).	233
6.4	Plot of $\Delta Pt/w$ Versus $\Delta P$ (Equivalent to Plot of Specific Resistance Versus $\Delta P$ ) for Varying Doses of PEI 6 and PEI 350.	242
6.5	Log $MW_n$ -Log [PEI] Domains of Percent Reduction in Number of Particles after 60 Minutes of Flocculation at $G = 20 \text{ sec}^{-1}$ .	246
6.6	Percent Reduction in Number of Particles as a Function of PEI $MW_n$ , [PEI], and Time of Flocculation at $G = 20 \text{ sec}^{-1}$ .	247
6.7	Percent Reduction in Number of Particles as a Function of PEI $MW_n$ , [PEI], and Magnitude of Velocity Gradient for 60 Minutes.	249
6.8	Differential Size Distribution Spectrum, Molecular Weight=0.0, Polymer Dose = 0.0 mg/l.	251
6.9	Differential Size Distribution Spectrum, Molecular Weight = 600.0, Polymer Dose = 0.50 mg/l.	252

6.10	Differential Size Distribution Spectrum, Molecular Weight = 600.0, Polymer Dose = 5.00 mg/l.	253
6.11	Differential Size Distribution Spectrum, Molecular Weight = 600.0, Polymer Dose = 50.00 mg/l.	254
6.12	Differential Size Distribution Spectrum, Molecular Weight = 1200., Polymer Dose = 0.50 mg/l.	255
6.13	Differential Size Distribution Spectrum, Molecular Weight = 1200., Polymer Dose = 5.00 mg/l.	256
6.14	Differential Size Distribution Spectrum, Molecular Weight = 1200., Polymer Dose = 50.00 mg/l.	257
6.15	Differential Size Distribution Spectrum, Molecular Weight = 1800., Polymer Dose = 5.00 mg/l.	260
6.16	Differential Size Distribution Spectrum, Molecular Weight = 1800., Polymer Dose = 50.00 mg/l.	261
6.17	Differential Size Distribution Spectrum, Molecular Weight = 35000., Polymer Dose = 0.05 mg/l.	262
6.18	Differential Size Distribution Spectrum, Molecular Weight = 35000., Polymer Dose = 0.50 mg/l.	263
6.19	Differential Size Distribution Spectrum, Molecular Weight = 35000., Polymer Dose = 50.00 mg/l.	264
6.20	Differential Size Distribution Spectrum, Molecular Weight = 60000., Polymer Dose = 0.05 mg/l.	265
6.21	Differential Size Distribution Spectrum, Molecular Weight = 60000., Polymer Dose = 0.50 mg/l.	266
6.22	Differential Size Distribution Spectrum, Molecular Weight = 60000., Polymer Dose = 50.00 mg/l.	267
6.23-6.26	Log $MW_n$ - Log[PEI] Domains of Percent Reduction in Relative Scattering Intensity.	269

6.27	Percent Reduction in Relative Scattering Intensity as a Function of [PEI], PEI MW <sub>n</sub> , and Intensity of Agitation for 60 Minutes.	271
6.28-6.31	Log MW <sub>n</sub> -Log[PEI] Domains of Percent Reduction in Residual Relative Scattering Intensity after 20 Minutes of Flocculation at G = 20 sec <sup>-1</sup> .	273
6.32	Percent Reduction in Residual Relative Scattering Intensity as a Function of [PEI], Intensity of Agitation, and Time of Settling. PEI MW <sub>n</sub> =600.	275
6.33	Percent Reduction in Residual Relative Scattering Intensity as a Function of [PEI], Intensity of Agitation, and Time of Settling. PEI MW <sub>n</sub> =35,000.	276
6.34	Log MW <sub>n</sub> -Log [PEI] Domains of Percent Reduction in Refiltration Time after 60 Minutes of Flocculation at G = 20 sec <sup>-1</sup> .	278
6.35	Percent Reduction in Refiltration Time as a Function of PEI 350 Concentration and Magnitude of Velocity Gradient.	280
6.36	Comparison between Plots of the Product Specific Surface Times Surface Versus PEI Dose and Refiltration Time Versus PEI Dose.	283
6.37	Comparison between Plots of the Product Specific Surface Times Surface Versus PEI Dose and Refiltration Time Versus PEI Dose.	284
A.1	Differential Volume Distribution Spectrum, Molecular Weight = 0.0, Polymer Dose=0.0 mg/l	346
A.2	Differential Volume Distribution Spectrum, Molecular Weight = 600.0, Polymer Dose=0.50 mg/l	347
A.3	Differential Volume Distribution Spectrum, Molecular Weight=600.0, Polymer Dose=5.00 mg/l	348
A.4	Differential Volume Distribution Spectrum, Molecular Weight=600.0, Polymer Dose=50.00 mg/l	349

A. 5	Differential Volume Distribution Spectrum, Molecular Weight=1200, Polymer Dose=0.50 mg/ℓ	350
A. 6	Differential Volume Distribution Spectrum, Molecular Weight=1200, Polymer Dose=5.00 mg/ℓ	351
A. 7	Differential Volume Distribution Spectrum, Molecular Weight=1200, Polymer Dose=50.00 mg/ℓ	352
A. 8	Differential Volume Distribution Spectrum, Molecular Weight=1800, Polymer Dose=5.00 mg/ℓ	353
A. 9	Differential Volume Distribution Spectrum, Molecular Weight=1800, Polymer Dose=50.00 mg/ℓ	354
A. 10	Differential Volume Distribution Spectrum, Molecular Weight=35000, Polymer Dose=0.05 mg/ℓ	355
A. 11	Differential Volume Distribution Spectrum, Molecular Weight=35000, Polymer Dose=0.50 mg/ℓ	356
A. 12	Differential Volume Distribution Spectrum, Molecular Weight=35000, Polymer Dose=50.00 mg/ℓ	357
A. 13	Differential Volume Distribution Spectrum, Molecular Weight=60000, Polymer Dose=0.05 mg/ℓ	358
A. 14	Differential Volume Distribution Spectrum, Molecular Weight=60000, Polymer Dose=0.50 mg/ℓ	359
A. 15	Differential Volume Distribution Spectrum, Molecular Weight=60000, Polymer Dose=50.00 mg/ℓ	360

## LIST OF PHOTOGRAPHS

Number	Title	Page
4.1	Electron Micrograph of <u>E. coli</u> Cells Flocculated with PEI 6. Total Magnification $1.8 \times 10^4$ .	132
4.2	Electron Micrograph of <u>E. coli</u> Cells Flocculated with PEI 6. Total Magnification $4.0 \times 10^4$ .	133
4.3	Electron Micrograph of <u>E. coli</u> Cells Flocculated with PEI 6. Total Magnification $1.2 \times 10^5$ .	134
4.4	Electron Micrograph of <u>E. coli</u> Cells Flocculated with PEI 350. Total Magnification $8.0 \times 10^4$ .	135
4.5	Electron Micrograph of <u>E. coli</u> Cells Flocculated with PEI 350. Total Magnification $1.2 \times 10^5$ .	136
4.6	Electron Micrograph of <u>E. coli</u> Cells Flocculated with PEI 350. Total Magnification $2.0 \times 10^5$ .	137
4.7	Electron Micrograph of <u>E. coli</u> Cells Flocculated with PEI 350. Total Magnification $4.0 \times 10^4$ .	138
4.8	Electron Micrograph of <u>E. coli</u> Cells Flocculated with PEI 350. Total Magnification $1.2 \times 10^5$ .	139
6.1	Electron Micrograph of Surface of Filter Cake Produced by Vacuum Filtration of <u>E. coli</u> Cells Flocculated with PEI 6. Total Magnification $6.0 \times 10^3$ .	286
6.2	Electron Micrograph of Surface of Filter Cake Produced by Vacuum Filtration of <u>E. coli</u> Cells Flocculated with PEI 6. Total Magnification $1.0 \times 10^4$ .	287
6.3	Electron Micrograph of Surface of Filter Cake Produced by Vacuum Filtration of <u>E. coli</u> Cells Flocculated with PEI 6. Total Magnification $1.8 \times 10^4$ .	288
6.4	Electron Micrograph of Surface of Filter Cake Produced by Vacuum Filtration of <u>E. coli</u> Cells Flocculated with PEI 6. Total Magnification $2.0 \times 10^4$ .	289

6.5	Electron Micrograph of Surface of Filter Cake Produced by Vacuum Filtration of <u>E. coli</u> Cells Flocculated with PEI 350. Total Magnification $4.0 \times 10^3$ .	290
6.6	Electron Micrograph of Surface of Filter Cake Produced by Vacuum Filtration of <u>E. coli</u> Cells Flocculated with PEI 350. Total Magnification $1.0 \times 10^4$ .	291
6.7	Electron Micrograph of Surface of Filter Cake Produced by Vacuum Filtration of <u>E. coli</u> Cells Flocculated with PEI 350. Total Magnification $1.8 \times 10^4$ .	292
6.8	Electron Micrograph of Surface of Filter Cake Produced by Vacuum Filtration of <u>E. coli</u> Cells Flocculated with PEI 350. Total Magnification $4.0 \times 10^4$ .	293

## Chapter 1

## INTRODUCTION

1.1 Removal of Biocolloids from Wastewater  
with Cationic Polymers

Dissolved and colloidal organic wastes are currently biosynthesized to bacterial and higher biota by the application of various aerobic biological treatment processes. The most cost-effective of these processes, the activated-sludge system, relies on a three-step procedure for the production of an acceptable effluent. The first step is the adsorption of the suspended colloidal material in the wastewater by microorganisms, and the biological absorption of dissolved organic matter. This sorption step is followed by biosynthesis of the organic material, producing "log phase" bacterial growth, and resulting in final products of carbon dioxide, water, refractory organic substances, inert material, and recyclable microorganisms. The third step is the bioflocculation of the microorganisms, now in their endogeneous respiration phase, producing readily settleable floccules and a clear, low-BOD supernatant.

Unfortunately, in the activated-sludge treatment system, a trade-off exists between the requirements for large substrate utilization rates (high growth rate, short detention time) and the requirements for maximum bioflocculation (low growth rate, long

detention time). Thus "high rate" activated-sludge systems achieve good adsorption of particulate matter, but fail to remove dissolved organic matter and to separate microorganisms from the suspension. "Extended aeration" processes, on the other hand, achieve optimum conditions for biosynthesis and bioflocculation, but provide reduced overall efficiency since operation is in the endogeneous or declining growth phase.

While the efficient and cost-effective removal of soluble and colloidal organic matter in sewage requires biological treatment, the subsequent flocculation of dispersed microorganisms and non-assimilated macro-molecular material can be accomplished very effectively with chemical flocculants. An activated-sludge system combining "high rate" substrate adsorption and assimilation with chemically assisted flocculation of biocolloids can achieve greater throughput of sewage than an "extended aeration" process.

Until recently, the chemical flocculants added to wastewater systems to promote aggregation consisted of hydrolyzed metal ions (Fe III or Al III) and occasionally natural polymeric substances such as starches, proteins, and gums. Unfortunately, hydrolyzed metal ions tend to produce a voluminous floc of poor filterability and they add to the total dissolved solids (TDS) of the effluent. Natural polymeric substances are generally anionic or nonionic in solution, and therefore are electrostatically repelled from biocolloids in the normal

pH range. These limitations led to the introduction of synthetic cationic polymers, which adsorb quickly to the biocolloid surface, and produce a floc of excellent filterability.

In general, the removal of biocolloids by cationic polymers can be divided into three stages:

1. Destabilization - modification of the surface properties of the colloids so that interparticle repulsion is reduced and the effectiveness of each collision is enhanced.
2. Transport - movement of the particles into contact via perikinetic (Brownian) or orthokinetic motion.
3. Phase separation - removal of particle aggregates from the bulk suspension.

Many experimental techniques (settling velocity, residual scattering intensity, refiltration rate) used to analyze the polymer effectiveness rely solely on measuring the final phase separation of biocolloid from suspension. While these methods show the end result of successful flocculation, the word flocculate itself means to form a loose fibrous structure, such as a tuft of wool. Consequently, in order to study the actual flocculation of E. coli by polyethyleneimine (PEI) per se, experimental methods (particle size distribution, electrophoretic mobility, and relative scattering intensity) were selected which emphasized the destabilization and transport stages. For completeness,

residual scattering intensity and refiltration rate experiments were conducted to measure the effectiveness of PEI in producing phase separation of the E. coli suspension.

### 1.2 Definition of Flocculation

LaMer and Healy (1,2) have restricted the term flocculation to a special case of coagulation in which the final structure, usually achieved by the bridging action of the polyelectrolyte, is a loose three-dimensional network having pores which permit easy filtration. In this thesis, flocculation will refer to the formation of polycellular aggregates through the action of polymer molecules: the mechanism of formation and the aggregate structure will be studied through a variety of experimental methods for possible inclusion within the LaMer-Healy definition.

### 1.3 Purpose of Thesis

The purpose of this thesis is to make a comprehensive study of the ability of the cationic, polymer polyethyleneimine (PEI), to induce the flocculation of suspended bacterial cells, E. coli CR63. The reactant PEI was selected as representative of the broad range of cationic polymers that can possibly be utilized to flocculate biocolloids and inorganic colloids in water and wastewater systems; similarly, the E. coli are

representative of the heterogeneous mass of biocolloids found in these treatment systems.

This study has been divided into three major areas of interest: first, a determination of the mechanism involved in the aggregation of biocolloids with a cationic polymer (Chapters 2, 3 and 4); second, an analysis of techniques available to measure quantitatively the extent of aggregation (Chapter 5); and third, the application of these techniques to determine the extent of E. coli flocculation by PEI, as a function of selected system parameters (Chapter 6).

The first portion of this research will be directed toward determining the primary means by which polymer molecules destabilize oppositely-charged colloidal particles. The mechanism of flocculation is of interest to polymer scientists and manufacturers in their synthesis of cationic polymers to meet the flocculation requirements of wastewater systems. Similarly, the sanitary engineer can utilize this information to aid in his selection of the proper polymeric flocculant for his particular wastewater treatment problem.

The second portion of this research will attempt to ascertain the exact physical characteristics (size, number, porosity, residual electrostatic charge, etc.) of the flocculating system which are being measured by electronic, optical, filtration, and electrostatic techniques. A quantitative comparison of these techniques can be made only if the

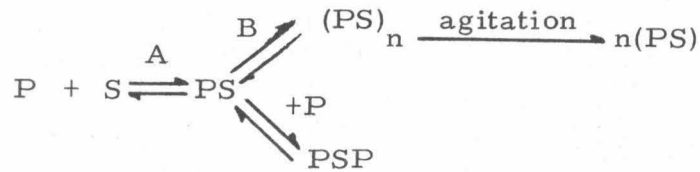
influence of these physical characteristics on the measurement is clearly identified. The relative advantages and disadvantages of each technique in recording the extent of flocculation can then be compared.

The final portion of this research will be directed at determining the influence of four control variables: PEI molecular weight, PEI dose, intensity of agitation, and duration of agitation; upon the extent of flocculation, as recorded by the above measuring techniques. Numerous experiments have shown that the interaction between polymer and colloid is dependent on a wide range of variables including properties of solution, polymer, and colloid, as well as the experimental conditions under which observations are made. Of primary importance are the concentrations of polymer and colloid, the properties of the colloidal surface, the intensity and time of agitation, the molecular weight and structure of the polymer, and the pH and ionic strength of the suspension. For reasons discussed in Chapter 6, the four control variables listed above were selected as being the most meaningful in normal wastewater treatment practice.

#### 1.4 Importance of Aggregate Diameter in Flocculation Process

The end result of successful destabilization and transport processes is the formation of large, compact, equally-sized aggregates from the small, dispersed, primary particles. As represented

by LaMer (1), the flocculation process appears as follows:



where P and S represent polymer molecules and colloidal surface respectively. The unit floc PS can form into a macro floc  $(\text{PS})_n$  whose size is limited by the shear gradient imposed by the degree of agitation. If the polymer-surface bond is too weak to withstand the shearing forces, unit flocs  $n(\text{PS})$  result. Alternatively, an excess of polymer can result in saturation of the colloid surface groups and the formation of polymer stabilized species PSP. Black, Birkner, and Morgan (3,4) and Kasper (5) have determined that the rate "A" at which polymer is adsorbed onto the colloidal surface is much more rapid than the rate "B" at which multiparticle aggregates are formed from unit flocs.

From the above schematic, the degree of flocculation can be determined from a measurement of the relative concentrations of  $(\text{PS})$  and  $(\text{PS})_n$ ; i. e., from a particle size distribution. This technique will measure the growth in the mean aggregate diameter  $d_a$  as a function of the polymer concentration and degree of agitation. To the sanitary engineer, this change in the mean aggregate diameter  $d_a$  is important insofar as it affects the removal of the suspended colloid from the

water or wastewater by one of the phase separation processes. The contribution of flocculation to increases in the mean aggregate diameter can be seen directly in the equations for removal velocities for sedimentation and centrifugation; removal efficiencies for filtration; and filtrate flow rate for vacuum filtration.

#### 1.4.1 Sedimentation

In sedimentation, the impelling force  $F_i$  acting on the aggregate equals the buoyant weight of the aggregate in the fluid.

$$F_i = m_a g = V_a (\rho_a - \rho_o) g = \pi d^3 (\rho_a - \rho_o) g / 6 \quad (1-1)$$

where  $m_a$  = aggregate mass

$g$  = gravitational acceleration

$V_a$  = aggregate volume

$\rho_a$  = aggregate density

$\rho_o$  = fluid density

$d$  = aggregate diameter

Opposing the impelling force is the fluid drag force  $F_d$  caused by friction.

$$F_d = C_d \pi d^2 \rho_o v_a^2 / 8 \quad (1-2)$$

where  $C_d$  = drag coefficient for viscous flow  
 $= 24 u / v_a d \rho_o$  (0.1  $\leq$  R  $\leq$  0.5)  
 $v_a$  = aggregate velocity  
 $u$  = absolute fluid viscosity  
 $R$  = Reynolds number

Under equilibrium conditions,

$$F_i = F_d$$

$$v_a = gd^2(\rho_a - \rho_o) / 18u \quad (\text{Stokes Law}) \quad (1-3)$$

Since  $\rho_a V_a = \rho_p V_p + \rho_o (V_a - V_p)$

where  $\rho_p$  = density of particulate matter in aggregate

$V_p$  = volume of particulate matter in aggregate and the aggregate porosity  $f$  is given by

$$f = (V_a - V_p) / V_a$$

the aggregate sedimentation velocity is therefore directly proportional to the square of the aggregate diameter times the porosity factor (1-f).

$$v_a = gd^2((\rho_p - \rho_o)(1-f)) / 18u \quad (1-4)$$

#### 1.4.2 Centrifugation

In centrifugation, the impelling acceleration  $r\omega^2$  replaces the gravitational acceleration  $g$  in equation (1-4). Therefore,

$$v_a = r\omega^2 d^2((\rho_p - \rho_o)(1-f)) / 18u \quad (1-5)$$

where  $r$  = distance from center of rotation to aggregate

$\omega$  = angular velocity

### 1.4.3 Filtration

For filtration, Yao, Habibian, and O'Melia (6) have derived equation (1-6) relating the effluent particulate concentration  $n$  from a packed bed filter to the single collector efficiency  $\eta$  of each media particle within the filter:

$$\ln(n/n_o) = -3(1-\Phi)\kappa\eta(L/d_g)/2 \quad (1-6)$$

where  $n$  = effluent particulate concentration

$n_o$  = influent particulate concentration

$\Phi$  = filter bed porosity

$L$  = filter bed depth

$d_g$  = filter bed grain diameter

$\kappa$  = collision efficiency factor

The single collector efficiency  $\eta$  is the sum of three theoretical collection efficiencies which reflect the possible transport mechanisms of diffusion, interception, and sedimentation.

$$\eta = \eta_o + \eta_I + \eta_G \quad (1-7)$$

Levich (7) derived the value of the diffusion collection efficiency as

$$\eta_o = 0.9(kT/ud d_g v_o)^{2/3} \quad (1-8)$$

where  $k$  = Boltzmann's constant

$T$  = absolute temperature

$v_o$  = mean fluid velocity in filter bed

Yao (8) derived the equations for interception collection efficiency and sedimentation collection efficiency as

$$\eta_I = 3(d/d_g)^2/2 \quad (1-9)$$

$$\eta_G = (\rho_a - \rho_o)gd^2/18uv_o \quad (1-10)$$

The resulting numerical solution of equation (1-7) for colloidal particles in the size range  $10^{-2} \mu\text{m}$  to  $10^2 \mu\text{m}$  is shown in Figure 1.1.

Although diffusion collection efficiency is important for particle diameters up to  $1 \mu\text{m}$ , larger aggregate removal is primarily dependent on interception and sedimentation collection efficiencies, and therefore proportional to the square of the aggregate diameter. Other theoretical (9) and experimental (6, 10) results suggest that the overall collection efficiencies vary from the first to the second power of the aggregate diameter when interception and settling are the dominant transport mechanisms.

#### 1.4.4 Vacuum Filtration

In the case of vacuum filtration, suspended colloidal particles

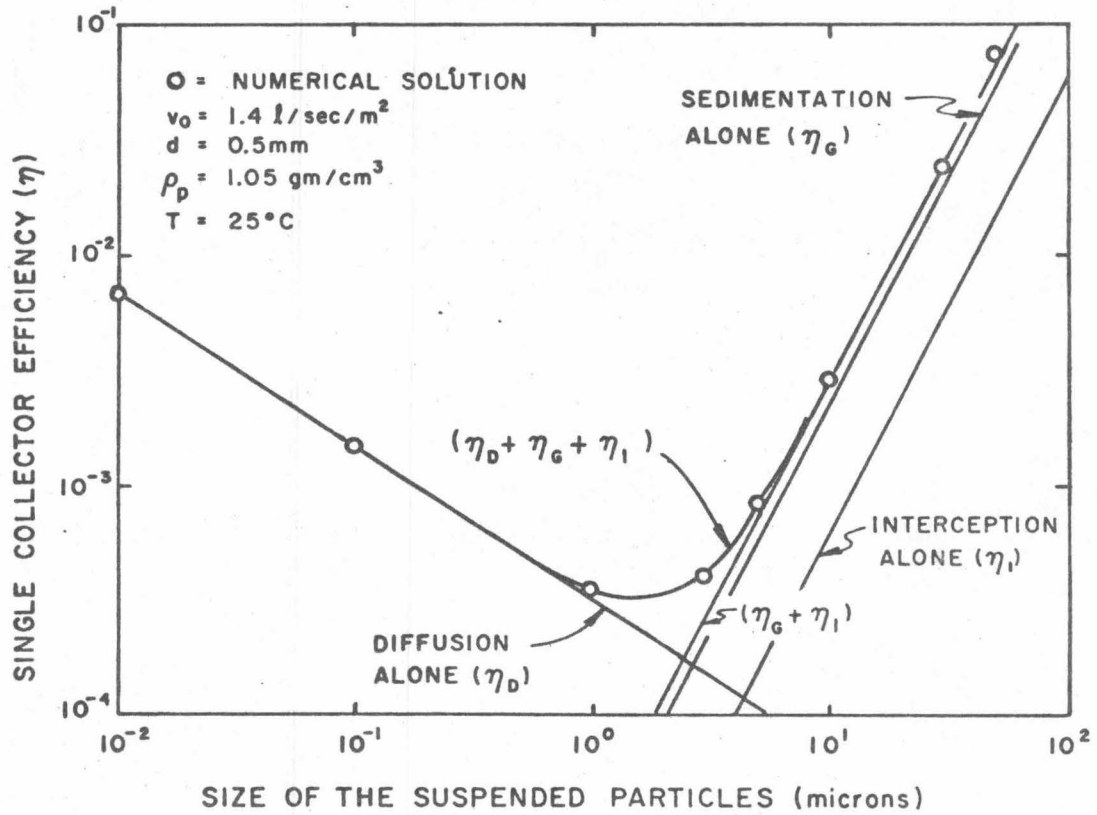


Figure 1.1 Single Collector Efficiency as a Function of Particle Size. Adapted from Yao et al. (6)

are deposited on the filter septum, while the filtrate passes through. The applied pressure differential serves to force the filtrate successively through the filter cake and the filter septum by overcoming the friction of passage. A thorough discussion of the experimental and theoretical background underlying the basic equations of vacuum filtration is presented by Carman (11).

The Kozeny-Carman filtration equation, originally proposed by Kozeny (12) as a simplified model for the flow of liquid through a packed bed and further developed by Carman (11), is given by:

$$Q = \Delta P g A \bar{\phi}^3 / (k_1 u L S_o^2 (1 - \bar{\phi})^2) \quad (1-11)$$

where  $Q$  = volume rate of filtrate flow

$\Delta P$  = pressure drop across the bed

$A$  = cross sectional area of the bed

$\bar{\phi}$  = bed porosity

$k_1$  = constant  $\cong 5$ .

$u$  = absolute viscosity of fluid passing through bed

$L$  = depth or thickness of bed

$S_o$  = specific surface of aggregates in the bed

Equation (1-11) can be derived from either the Poiseuille equation for flow in a circular capillary or from the Darcy-Weisbach equation for flow in a pipe. Its significance lies in the relationship expressed

between the volume rate of flow and the square of the specific surface area: previous equations had related the volume flow rate to either a mean capillary diameter or a mean particle diameter. The reason for choosing the specific surface is that for any fluid in steady, laminar flow past a solid surface, the resistance depends upon the extent of the surface.

By definition,

$$S_o = \pi d^2 / (\pi d^3 / 6) = 6/d \quad (1-12)$$

where  $d$  = mean aggregate diameter in filter cake.

Consequently, the volume rate of flow of filtrate through the filter cake is directly proportional to the square of the mean aggregate diameter in the filter cake, as can be seen by substituting equation (1-12) into equation (1-11).

The importance of the mean aggregate diameter in the preceding equations for phase separation (1-4, 1-5, 1-6, and 1-11) emphasizes the destabilization and transport roles in achieving rapid colloid removal. These equations suggest that, irrespective of the phase separation process, efforts should be directed toward maximizing the interparticle collision efficiency factor and minimizing the adverse effects of shear on aggregate diameter. Successful modification of the chemistry of the colloid-polymer system would lead directly to larger

aggregate diameters and consequently to greater phase separation efficiencies. This modification would complement any design improvements made with respect to the conventional physical parameters, such as  $d_g$ ,  $v_o$ ,  $L$ ,  $r$ ,  $\omega$ , and  $A$ .

## REFERENCES CITED

## CHAPTER 1

1. LaMer, V. K., and Healy, T. W., "Adsorption-Flocculation Reactions of Macromolecules at the Solid Liquid Interface", Review Pure and Applied Chemistry, 13 (1963), 112-133.
2. LaMer, V. K., and Healy, T. W., "The Role of Filtration in Investigating Flocculation and Redispersion of Colloidal Dispersions", Journal Physical Chemistry, 67 (1963), 2417-2420.
3. Black, A. P., Birkner, F. B., and Morgan, J. J., "The Effect of Polymer Adsorption on the Electrokinetic Stability of Dilute Clay Suspension", Journal Colloid and Interface Science, 21 (1966), 626-648.
4. Black, A. P., Birkner, F. B., and Morgan, J. J., "Destabilization of Dilute Clay Suspensions with Labeled Polymers", Journal American Water Works Association, 57 (1965), 1547-1560.
5. Kasper, D. R., "Theoretical and Experimental Investigations of the Flocculation of Charged Particles in Aqueous Solutions by Polyelectrolytes of Opposite Charge", Ph.D. Thesis, California Institute of Technology, 1971.
6. Yao, K. M., Habibian, M. Y., and O'Melia, C. R., "Water and Wastewater Filtration: Concepts and Applications", Environmental Science and Technology, 5 (1971), 1105-1112.
7. Levich, V. G., Physicochemical Hydrodynamics, Prentice Hall, Englewood Cliffs, N. J., 1962.
8. Yao, K. M., "Influence of Suspended Particle Size of the Transport Aspect of Water Filtration", Ph.D. Thesis, University of North Carolina, Chapel Hill, N. C., 1968.
9. Spielman, L. A., and Goren, S. L., "Capture of Small Particles by London Forces from Low-Speed Liquid Flows", Environmental Science and Technology, 4 (1970), 135-140.

10. Ives, K. J., "Rational Design of Filters", Proceedings Institution of Civil Engineers, 16 (1960), 189-193.
11. Carman, P. C., "Fundamental Principles of Industrial Filtration", Transactions - Institution of Chemical Engineers, 16 (1938), 168-185.
12. Kozeny, J., as described by Foust, A. L., Wenzel, L. A., Clump, C. W., Maus, L., and Anderson, L. B., Principles of Unit Operations, John Wiley and Sons, New York, 1960.

## Chapter 2

THEORIES OF POSSIBLE MECHANISM  
OF BIOLOGICAL AGGREGATION2.1 Introduction

Although natural coagulants have been used for thousands of years as a means of clarifying water (1), Bordet (2) published the first article discussing the agglutination of bacteria by flocculants (blood antibodies) in 1899. He proved that in specific agglutination there are two distinct phases; first, the sensitization of the bacterial cell by agglutinins, and second the aggregation of the cells through the action of salts. This analysis served as the forerunner of the chemical bridging model introduced by Heidelberger and Kendall (3) in 1935 to explain observed interactions between antibodies and antigens. This early research eventually led to at least three major (physical double-layer, adsorption coagulation, and polymer bridging) and five minor (Zoogloea ramigera, capsular, flagella interaction, protozoa, and poly-beta-hydroxybutyric acid) theories of explanation for the common phenomenon of bacterial agglutination (4). In addition to bacteria, other biocolloids were similarly observed to aggregate upon the addition of salts, acids, naturally-produced and synthetic polyelectrolytes, and hydrolyzed metal ions. Of this total biological aggregation

classification, flocculation will refer only to the aggregation of bio-colloids by polymer molecules.

While the mechanism of destabilization of many colloidal systems is easily identified (e. g. , the addition of indifferent electrolyte to a lyophobic colloid produces double-layer coagulation, and the addition of an anionic polyelectrolyte to a negatively-charged dispersion produces destabilization via polymer bridging), the destabilization of negatively-charged bacterial cells by a cationic polymer is not so readily understood.

The cationic polymer can effectively reduce the total potential energy of interaction between the electrical double-layers of two approaching cells (double-layer coagulation), and simultaneously, if the polymer has sufficient chain length, it can enmesh the cells in an open three-dimensional floc by the formation of bridging structures between cells (polymer bridging). Chapters 2, 3 and 4 will attempt to answer the question; which mechanism predominates in the flocculation of E. coli by PEI?

The following paragraphs summarize the characteristics of the eight theories of explanation of bacterial agglutination as observed by prior investigators.

## 2.2 Physical Double-Layer Theory

In 1919, Buchanan (5) summarized the data of many investigators who successfully coagulated bacteria with hydrogen ions; univalent, divalent, and trivalent cations; and polyvalent bases. Later researchers equated the ability of cations to coagulate bacteria by themselves with the hydrophobic behavior exhibited by certain species. For example, Mudd (6) and White (7, 8) classified bacteria into three categories: those with predominantly hydrophobic behavior, those with both hydrophobic and hydrophilic groups, and those with predominantly hydrophilic behavior.

Hydrophobic behavior, a phenomenon common to inorganic colloids such as clays and metal oxides, usually originates from imperfections in the crystal lattice, isomorphous substitutions, or surface chemical reactions, which result in an unbalanced surface charge. The destabilization of hydrophobic colloids has been treated as a reduction in the repulsive potential between approaching particles. Initially, the magnitude of the surface potential of a hydrophobic colloid and the thickness of the ionic double layer, or the diffuse layer of counterions surrounding the particles, determine the approach distance between the particles. The addition of salts to a stable hydrophobic suspension leads to compression or elimination of the diffuse double layer, permitting the attractive van der Waals forces to draw the

particles together. The extent of reduction of the electrostatic repulsion is dependent upon the molarity and valence of the counterions in the bulk solution; the quantity of counterions adsorbed to the particulate surface being insignificant in comparison. Once the counterions have reduced the double-layer thickness, the London-van der Waals forces due to dipole moments between molecules overwhelm residual electrostatic repulsion, causing the particles to coagulate (9, 10).

The theory for the destabilization of the diffuse double layer as developed by Gouy and Chapman has been expanded in a rigorous mathematical treatment by Derjaguin and Landau (11) and by Verwey and Overbeek (12). The mathematical analysis for constant potential surfaces has been presented by Kruyt (13) and for weak interactions between constant charged surfaces by Van Olphen (14).

Although there exists a continuous transition between hydrophobic and hydrophilic colloids, all biocolloids (viruses, bacteria, algae) are now classified as hydrophilic, i. e., they exhibit a strong affinity to water. Hydrophilic colloids are created by the hydration of certain functional groups of surface macromolecules; for bacteria, the hydration points are typically hydroxo, sulfato, phosphato, carboxo, amino, or mercapto surface groups. As with hydrophobic colloids, the effect of electrolytes upon the stability of hydrophilic colloids is one of screening the mutual electrostatic interaction of these surface charge

groups, an effect which may or may not produce colloid destabilization depending on the pH, the composition of the ionized groups, and the degree of hydration.

In the case of hydrophobic particles, when the electrokinetic potential difference in the double layer of the particles falls below a certain limiting value (the critical potential), aggregation of the particles takes place. In the case of dispersions of hydrophilic particles, Kruyt (15) has shown that the condition of hydration must be considered as a stabilizing factor in addition to the electrokinetic potential. Kruyt demonstrated that some bacteria formed stable dispersions even when the repelling force, as measured by the electrokinetic potential, was reduced to zero. The addition of alcohol to these isoelectric dispersions caused them to precipitate; the alcohol acting to dehydrate the particles. The stabilizing action associated with the hydrous condition of the particles is attributed to the much lower surface tension against the aqueous medium than that of hypothetical anhydrous particles. Thus the stability of hydrophilic colloids depends not only on the ability of the electrokinetic potential difference to prevent collisions, but also on the small size of the free energy change which occurs upon contact.

Mudd (6) states that bacteria exist which display a wide range of surface types, from those which are strongly hydrophobic to those which are markedly hydrophilic. Smooth variants of intestinal bacteria, such as E. coli CR63, fall into the latter grouping.

### 2.3 Adsorption Coagulation Theory

This theory serves as a transition between the physical double-layer and polymer bridging theories since both electrostatic interaction and chemical adsorption participate in the destabilization process. Essentially the flocculant, either a multinuclear, multivalent hydrolysis species of a metal ion or an oppositely-charged polyelectrolyte, adsorbs to the colloid surface, thereby reducing the energy of interaction between electrical double-layers. Aggregation of the destabilized particles then occurs via van der Waals forces or chemical interaction. Along the seam of agglutination, short loops of a flocculant molecule adsorbed on one particle may adsorb through available charge groups to the surface of an adjacent destabilized particle. However, the normal extension of these loops from the surface is inadequate to cause destabilization by polymer bridging alone.

Stoichiometry between flocculant dose and colloid surface is possible, but does not always occur. Also, the aggregates can exhibit widely varying shear strength, density, and filterability.

In addition to the many flocculation studies of colloids and metallic-ion hydrolysis species, the following articles are representative of biocolloid flocculation with cationic polyelectrolytes: Burger and Stahmann (16), Bacillus subtilis and E. coli with poly-l-lysine, Avi-Dor and Yaniv (17), avirulent strains of Pasteurella tularensis

with protamine sulfate and poly-l-lysine; Rubini et al. (18), red blood cells with poly-l-lysine; Katchalsky et al. (19), E. coli and Bacillus subtilis with poly-l-lysine; Nevo et al. (20) and Katchalsky et al. (21), red blood cells with poly-l-lysine; Tenney and Stumm (22), sewage bacteria with commercial cationic polymer; Johnson et al. (23), tobacco mosaic virus with divinyl benzene maleic anhydride copolymer; Dixon and Zielyk (24), E. coli with polyethyleneimine; Tenney et al. (25), algae with polyamine; Thorup et al. (26), E. coli phage T-2 with Nalcolyte; and Tilton et al. (27), algae with polyethyleneimine.

#### 2.4 Polymer Bridging Theory

In 1904, Bechhold (28) observed that negatively-charged bacteria cells could be agglutinated by antibodies provided that trace quantities of cations were present; neither the antibodies nor the trace cations alone were adequate. Two years later, Porges (29) noticed that an excess of agglutinating serum inhibited the agglutination of many bacterial strains. By 1909, Buxton and Rahe (30, 31) had differentiated clearly between two distinct types of coagulation of colloids, the electrolyte type in which dilution of the colloid has no effect upon the coagulation (double-layer theory), and the bridging type in which the flocculation limits are dependent upon the relative concentration of the colloid and flocculant. Eggerth and Bellows (32)

in 1922, successfully flocculated Bacterium coli with six different proteins in both the presence and absence of salts. Through pH variations in the isoelectric region, they illustrated the electrostatic nature of the attraction between the bacterial cells and the added flocculants. Most significantly, Eggerth and Bellows recorded an "anti-agglutinoid" region created by protein concentrations greater than optimum, again illustrating effects not accounted for by the double-layer theory.

Essentially the bridging theory proposes that a polymer molecule can attach itself to the surface of a colloidal particle at one or more adsorption sites with the remainder of the molecule extending into the solution. These extended segments can then adsorb onto the surface of another colloidal particle (resulting in destabilization), or they can loop back onto the surface of the original particle. Anionic and nonionic polymers attach to negative surfaces via hydrogen bonding, anion interchange with adsorbed anions, or interaction with cations in the diffuse double layer.

The bridging model gained additional credibility in 1951 when Jenckel and Rumbach (33), reasoning inductively from measurements of total polymer surface adsorption, concluded that only a few segments of each polymer molecule adsorb directly on the particle surface; the remaining segments extend into the surrounding solvent. In 1952,

Ruehrwein and Ward (34) concluded from clay sedimentation experiments that flocculation is caused by a system of polymer bridges extending between clay particles. They also discovered that long-chain bacterial polysaccharides were capable of bridging between particle surfaces.

The polymer bridging theory adequately explains the destabilization of many biocolloid-polymer systems in which double-layer effects play a subordinate role, for example: Avi-Dor and Yaniv (17), avirulent strains of Pasteurella tularensis with dyes and electrolytes; Northrop and DeKruif (35), Bacillus typhosus with egg albumin and serum; Heidelberger and Kendall (36), Pneumococcus with horse antiserum; Hodge and Metcalfe (37), bacteria with negatively-charged hydrophilic molecules and trace quantities of cations (Hodge and Metcalfe also found that when the extended chain molecules were enzymatically digested to lower molecular weight components, their flocculating ability was destroyed); Moscona (38, 39), sponge cells with long-chain carbohydrates obtained from other living sponge cells; Curds (40), india ink particles with protein linked polysaccharide from Paramecium caudatum; Tenney and Stumm (22), sewage bacteria with complex polysaccharides and polyamino acids excreted by the cells during declining growth and endogeneous respiration; Dunican and Seeley (41), Lactobacillus with heteropolysaccharide, an autolytic

product; Humphreys (42), sponge cells with 200 Å-diameter particles containing protein and polysaccharide; Wessman and Miller (43), Pasteurella pestis with extracellular nucleic acids; Jones (44), Aerobacter aerogenes with extracellular nucleoprotein; Cripps and Work (45), Staphylococcus aureus with extracellular macromolecules consisting of protein, RNA, and DNA; Busch and Stumm (46), Aerobacter aerogenes and E. coli with extracellular polymeric material and with synthetic anionic and nonionic polyelectrolytes; Friedman et al. (47, 48) Zoogloea ramigera and Pseudomonas with exocellular fibrils; Pavoni et al. (4, 49), algae and sewage bacteria with exocellular biopolymers; and Harris (50), bacteria with extracellular polymers containing a carbohydrate fraction.

In summarizing the results of the many investigations of biocolloid-polymer systems, the polymer bridging theory is characterized by:

1. Polymer adsorption to the biocolloid surface; possible adsorption mechanisms for anionic and nonionic polymers onto negative colloid surfaces are hydrogen bonding, anion interchange, and interactions with cations in the double layer.

2. Polymer molecules of sufficient length to reach between approaching colloidal particles and adsorb on the surface of both particles.

3. A stoichiometric relationship between the polymer concentration and the biocolloid surface area. Excess amounts of one colloid over the other leads to either inadequate bridging or redispersion. Optimum destabilization occurs when only a portion of the available adsorption sites on the surface of the colloidal particles are covered.

#### 2.5 Zoogloea ramigera Theory

In an early study of bioflocculation in the activated sludge process, Butterfield (51) observed a capsular slime produced by zoogloea organisms in every good activated sludge system. The isolated bacterium, grown in pure culture by Butterfield, and later by Heukelekian and Littman (52) and Wattie (53), produced a floc which simulated activated sludge. However, McKinney (54, 55) showed that floc formation was not a special property of any particular group of bacteria when he found 14 different floc forming species out of 72 species isolated from activated sludge. Friedman et al. (47) stated that bacteria producing the gelatinous slime are common in aquatic habitats, and that the classification zoogloea is properly attributed to the growth condition of these bacteria rather than to a definite species.

## 2.6 Capsular Theory

McKinney (54, 55) attributed bacterial flocculation to the interaction between capsular matrices of two approaching cells. The bacterial capsules, composed of high molecular weight polysaccharides excreted from the cell, would attract each other via van der Waals forces at cell separation distances greater than the range of double-layer repulsive forces. Following this initial contact, additional agitation would cause floc formation. Although successful flocculations with non-encapsulated bacteria have negated the specifics of this theory, the idea of appendages to the cell, either organic macromolecules or synthetic polymers, making the initial contact with another cell and its appendages reappears in the polymer bridging theory.

## 2.7 Flagella Interaction Theory

Ellis (56) and Pijper (57) have proposed that bacterial aggregation is due to adhesion or interlocking of flagella. Although flagella interactions may assist aggregation in some species, many non-flagellated species also bioflocculate, and consequently this theory has very limited applications.

## 2.8 Protozoa Theory

Watson (58), Barker (59), Sugden and Lloyd (60), and

Curds (40) have all shown that various species of protozoa induce flocculation by secreting mucoproteins that produce particle aggregation. However, no specific mechanism was developed to explain the observed interaction.

## 2.9 Poly-beta-hydroxybutyric Acid Theory

Recent studies by Crabtree, Boyle, et al. (61, 62) have directly correlated the intracellular accumulation of poly-beta-hydroxybutyric (PHB) granules with bacterial aggregation. Simultaneously with this accumulation, the authors noticed that orderly cell division was incomplete, producing instead irregular laterally-linked cells. Collisions between these linked cells resulted in mechanically entangled clusters. Crabtree et al. felt that the cell surfaces in these clusters were bound by polyester-linked PHB. Eventually, the cell clusters became nuclei for larger flocs incorporating many heterogeneous non-floc-forming bacteria, fungi, and colloids.

Considerable research (63 - 68) prior to the PHB theory definitely showed that PHB granules are initiated as food reserves during periods of rapid growth, and later metabolized during endogeneous respiration. Friedman, Dugan, et al. (69) observed the presence of PHB granules in some cells with the electron microscope, but concluded that their presence was unrelated to the fibrous network of polymeric strands linking various cells.

## 2.10 Summary of Theories of Biological Aggregation

Although some evidence exists to support bacterial aggregation via the Zoogloea ramigera theory, the capsular theory, the flagella interaction theory, the protozoa theory, and the poly-beta-hydroxybutyric acid theory, each suffers from a lack of generality. In addition, these theories do not present a new mechanism of aggregation, but rather only discuss the specific organism or growth condition which produces this effect. Invariably the mechanisms of aggregation for the above theories are included in either the physical double-layer, adsorption coagulation, or polymer bridging theories.

In the polymer bridging theory, the electrostatic interaction which plays the dominant role in the physical double-layer theory is subordinated to the adsorption-bridging phenomenon. The degree of subordination is dependent upon the nature of the polymer (charge density, configuration, concentration) and of the colloid (charge density). Although many colloid-polymer systems flocculate in accordance with the criteria of the bridging theory, Kasper (70) questioned the applicability of this theory to systems exhibiting strong electrostatic attraction between colloid and polymer. In lieu of the polymer molecule attaching itself to the colloid surface at only a few adsorption sites, with the remainder of the molecule extending into solution, Kasper presents evidence of virtually complete polymer

adsorption onto the colloid surface. Each adsorbed molecule then forms part of a total charge mosaic with alternating regions of positive (polymer) and negative (colloid) charge. Flocculation occurs when the charge mosaics of two particles align to provide strong electrostatic attraction. Thus, Kasper's model resembles the physical double-layer theory with the exception that the repulsive potential is reduced not by counterions in the diffuse double layer, but by adsorbed polyelectrolyte molecules.

## REFERENCES CITED

## CHAPTER 2

1. Cohen, J. M., Rourke, G. A., and Woodward, R. L., "Natural and Synthetic Polyelectrolytes as Coagulant Aids", Journal American Water Works Association, 50 (1958), 463-478.
2. Bordet, J., "Le Mechanisms de L'Agglutination", Annales de L'Institute Pasteur, 13 (1899), 225-250.
3. Heidelberger, M., and Kendall, F. E., "Presipitin Reaction between Type III Pneumococcus Polysaccharide and Homologous Antibody. II. Conditions for Quantitative Precipitation of Antibody in Horse Serums. III. A Quantitative Study and a Theory of the Reaction Mechanism", Journal Experimental Medicine, 61 (1935), 559-591.
4. Pavoni, J. L., "Fractional Composition of Microbially-Produced Exocellular Polymers and Their Relationship to Biological Flocculation", Ph.D. Thesis, Department of Civil Engineering, Notre Dame, 1970.
5. Buchanan, R. E., "Agglutination", Journal Bacteriology, 4 (1919), 73-105.
6. Mudd, S., "Agglutination", Cold Spring Harbor Symposia on Quantitative Biology, 1 (1933), 65-76.
7. White, P. B., "On the Relation of the Alcohol-Soluble Constituents of Bacteria to Their Spontaneous Agglutination", Journal Pathology and Bacteriology, 30 (1927), 113-132.
8. White, P. B., "Further Notes on Spontaneous Agglutination", Journal Pathology and Bacteriology, 31 (1928), 423-433.
9. Glasstone, S., Textbook of Physical Chemistry, Van Nostrand, New York, 1946.
10. London, F., "Über einige Eigenschaften und Anwendungen der Molekülarkraft", Zeitschrift für Physikalische Chemie, 811 (1930), 222-251.

11. Derjaguin, B. V., and Landau, L., Acta Physicochimica URSS, 14 (1941), 633.
12. Verwey, E. J., and Overbeek, T. G., Theory of the Stability of Lyophobic Colloids, Elsevier, Amsterdam, 1948.
13. Kruyt, H. R., Colloid Science, Volume I: Irreversible Systems (1952), Volume II: Reversible Systems (1949), Elsevier, Amsterdam.
14. Van Olphen, H., An Introduction to Clay Colloid Chemistry, Interscience, New York, 1963.
15. Kruyt, H. R., translated by van Klooster, H. S., Colloids, New York, 1927.
16. Burger, W., and Stahmann, M., "The Agglutination and Growth Inhibition of Bacteria by Lysine Polypeptides", Archives of Biochemistry and Biophysics, 29 (1952), 27-36.
17. Avi-Dor, Y., and Yaniv, H., "The Stability of Suspensions of Pasteurella Tularensis in the Presence of Electrolytes", Journal Bacteriology, 66 (1953), 1-5.
18. Rubini, J., Stahmann, M., and Rasmussen, A., "Agglutination of Red Cells by Synthetic Lysine Polypeptides", Proceedings Society Experimental Biology and Medicine, 76 (1951), 659-662.
19. Katchalsky, E., Bichowski-Slomnitzki, L., and Volcani, B., "The Action of Some Water Soluble Poly-a-amino Acids on Bacteria", Biochemical Journal, 55 (1953), 671-680.
20. Nevo, A., DeVries, A., and Katchalsky, E., "Interaction of Basic Polyamino Acids with the Red Blood Cells", Biochimica Et Biophysica Acta, 17 (1955), 536-547.
21. Katchalsky, E., Danon, D., and Nevo, A., "Interactions of Basic Polyelectrolytes with the Red Blood Cell. II. Agglutination of Red Blood Cells by Polymeric Bases", Biochimica Et Biophysica Acta, 33 (1959) 120-138.
22. Tenney, M. W., and Stumm, W., "Chemical Flocculation of Microorganisms in Biological Waste Treatment", Journal Water Pollution Control Federation, 37 (1965), 1370-1388.

23. Johnson, J., Fields, J., and Darlington, W., "Removing Viruses from Water by Polyelectrolytes", Nature, 213 (1967), 665-667.
24. Dixon, J. K., and Zielyk, M. W., "Control of the Bacterial Content of Water with Synthetic Polymeric Flocculants", Environmental Science and Technology, 3 (1969), 551-558.
25. Tenney, M. W., Echelberger, W. F., Scheussler, R. G., and Pavoni, J. L., "Algal Flocculation with Synthetic Organic Polyelectrolytes", Applied Microbiology, 18 (1969), 965-971.
26. Thorup, R., Nixon, F., Wentworth, D., and Sproul, O., "Virus Removal by Coagulation with Polyelectrolytes", Journal American Water Works Association, 62 (1970), 97-101.
27. Tilton, R., Murphy, J., and Dixon, J., "The Flocculation of Algae with Synthetic Polymeric Flocculants", Water Research, 6 (1972), 155-164.
28. Bechhold, H., "Die Ausflockung von Suspensionen bzw. Kolloiden und die Bakterienagglutination", Zeitschrift für Physikalische Chemie, 48 (1904), 385-423.
29. Porges, O., and Prantschoff, A., "Über die Agglutinabilität von Bakterien, besonders des B. typhi", Zentralblatt für Bakteriologie Abt. 1, Originale, 41 (1906), 466.
30. Buxton, B. H., and Rahe, A. H., "Effect of Dilution upon the Flocculation of Colloids, I", Journal Medical Research, 20 (1909), 113.
31. Buxton, B. H., and Rahe, A. H., "Effect of Dilution upon the Flocculation of Colloids, II", Journal Medical Research, 20 (1909), 311-325.
32. Eggerth, A. M., and Bellows, M., "The Flocculation of Bacteria by Proteins", Journal General Physiology, 7 (1922), 669-680.
33. Jenckel, E., and Rumbach, B., "The Adsorption of High Molecular Weight Materials from Solution", Zeitschrift Electrochemie, 55(1951), 612-618.
34. Ruehrwein, R. A., and Ward, D. W., "Mechanism of Clay Aggregation by Polyelectrolytes", Soil Science, 73 (1952), 485-492.

35. Northrop, J., and DeKruif, P., "The Stability of Bacterial Suspensions. II. Agglutination in the Presence of Proteins, Normal Serum, and Immune Serum", Journal General Physiology, 6 (1922), 655-667.
36. Heidelberger, M., and Kendall, F., "The Precipitin Reaction Between Type IV Pneumococcus Polysaccharide and Homologous Antibody", Journal Experimental Medicine, 61 (1935), 559.
37. Hodge, H. M., and Metcalfe, S. N., "Flocculation of Bacteria by Hydrophilic Colloids", Journal Bacteriology, 75 (1958), 258-264.
38. Moscona, A. A., "Analysis of Cell Recombinations in Experimental Synthesis of Tissues in Vitro", Journal Cellular Comparative Physiology, 60 (1962), 65-80.
39. Moscona, A. A., "Studies on Cell Aggregation: Demonstration of Materials with Selective Cell-Binding Activity", Proceedings National Academy of Sciences, 49 (1963), 742-747.
40. Curds, C. R., "The Flocculation of Suspended Matter by *Paramecium caudatum*", Journal General Microbiology, 33 (1962), 357-363.
41. Dunican, L. K., and Seeley, H. W., "Extracellular Polysaccharide Synthesis by Members of the Genus Lactobacillus: Conditions for Formation and Accumulation", Journal General Microbiology, 40 (1965), 297-308.
42. Humphreys, T., "Cell Surface Components Participating in Aggregation: Evidence for a New Cell Particulate", Experimental Cell Research, 40 (1965), 539-543.
43. Wessman, G. E., and Miller, D. J., "Biochemical and Physical Changes in Shaken Suspensions of Pasteurella pestis", Applied Microbiology, 14 (1966), 636-642.
44. Jones, D. L., "Ropy Milk. III. Chemical Studies of a Ropy Substance", Food Research, 19 (1954), 254.
45. Cripps, R. E., and Work, E., "The Accumulation of Extracellular Macromolecules by Staphylococcus aureus Grown in the Presence of Sodium Chloride and Glucose", Journal General Microbiology, 49 (1967), 127-137.

46. Busch, P. L., and Stumm, W., "Chemical Interactions in the Aggregation of Bacteria", Environmental Science and Technology, 2 (1968), 49-53.
47. Friedman, B. A., Dugan, P. R., Pfister, R. M., and Remsen, C. C., "Structure of Exocellular Polymers and Their Relationship to Bacterial Flocculation", Journal Bacteriology, 98 (1969), 1328-1334.
48. Friedman, B. A., and Dugan, P. R., "Identification of Zoogloea Species and the Relationship of Zoogloea Matrix and Floc Formation", Journal Bacteriology, 95 (1968), 1903-1909.
49. Pavoni, J. L., Tenney, M. W., and Echelberger, W. F., "Bacterial Exocellular Polymers and Biological Flocculation", Journal Water Pollution Control Federation, 44 (1972), 414-431.
50. Harris, R. H., "The Effect of Extracellular Polymers and Inorganic Colloids on the Colloidal Stability of Bacteria", Ph.D. Thesis, Division of Engineering and Applied Physics, Harvard, 1971.
51. Butterfield, C. T., "Studies of Sewage Purification. II. A Zoogloea-Forming Bacterium Isolated from Activated Sludge", USPHS Reports, 50 (1935), 671-683.
52. Heukelekian, H., and Littman, M. L., "Carbon and Nitrogen Transformations in the Purification of Sewage by the Activated Sludge Process. II. Morphological and Biochemical Studies of Zoogloea Organisms", Sewage Works Journal, 11, (1939), 752-763.
53. Wattie, E., "Cultural Characteristics of Zoogloea-Forming Bacteria Isolated from Activated Sludge and Trickling Filters", USPHS Reports, 57 (1942), 1519-1534.
54. McKinney, R. E., and Horwood, M. P., "Fundamental Approach to the Activated Sludge Process. I. Floc-Producing Bacteria", Sewage and Industrial Wastes, 24 (1952), 117-123.
55. McKinney, R. E. and Weichlein, R. G., "Isolation of Floc-Producing Bacteria from Activated Sludge", Applied Microbiology, 1 (1953), 259-261.

56. Ellis, D., "Untersuchungen über Sarcina, Streptococcus and Spirillum", Centrum Bacteriologie, 33 (1903), 1-17, 81-96, 161-166.
57. Pijper, A., "Dark Ground Studies of Flagellar and Somatic Agglutination of B. typhosus", Journal Pathology and Bacteriology, 47 (1938), 1-17.
58. Watson, J. M., "Mechanisms of Bacterial Flocculation Caused by Protozoa", Nature, 155 (1945), 271-272.
59. Barker, A. N., "The Ecology and Function of Protozoa in Sewage Purification", Annals of Applied Biology, 33 (1946), 314.
60. Sugden, B., and Lloyd, L. L., "The Clearing of Turbid Waters by Means of the Ciliate Carchesium; A Demonstration", Journal Institute for Sewage Purification, 1 (1950), 16.
61. Crabtree, K., McCoy, E., Boyle, W. C., and Rohlich, G. A., "Isolation Identification, and Metabolic Role of the Sudanophilic Granules of Zoogloea ramigera", Applied Microbiology, 13 (1965), 218-226.
62. Crabtree, K., Boyle, W., McCoy, E., and Rohlich, G. A., "A Mechanism of Floc Formation by Zoogloea ramigera", Journal Water Pollution Control Federation, 38 (1966), 1968-1980.
63. Lemoigne, M., "Etudies Sur l'autolyse Microbienne-Origine de l'acide B-oxybutyrique Forme Par Autolyse", Annals Institute Pasteur, 41 (1927), 148-165.
64. Macrae, R. M., and Wilkinson, J. F., "Poly-B-hydroxybutyrate Metabolism in Washed Suspension of Bacillus cereus and Bacillus megaterium", Journal General Microbiology, 19 (1958), 210-222.
65. Lemoigne, M., Grelet, N., Croxon, M., and LeTreis, M., "Formalion of Lipide B-hydroxybutyrique aux Depends du Glucose par la Bacillus megaterium. Donnes Quantitatives", Bulletin Sociiite de Chimie Biologique, 27 (1945), 90-95.
66. Doudoroff, M., and Stanier, R. Y., "Role of Poly-B-hydroxybutyric Acid in the Assimilation of Organic Carbon by Bacteria", Nature, 183 (1959), 1540-1542.

67. Rouf, M. A., and Stokes, J. L., "Isolation and Identification of the Sudanophilic Granules of Sphaerotilis natans", Journal Bacteriology, 83 (1962), 343-347.
68. Dias, F. F., and Bhat, J. V., "Microbial Ecology of Activated Sludge. I. Dominant Bacteria", Applied Microbiology, 12 (1964), 412-417.
69. Friedman, B. A., Dugan, P. R., Pfister, R. M., and Remsen, C. C., "Fine Structure and Composition of the Zoogloal Matrix Surrounding Zoogloea ramigera", Journal Bacteriology, 96 (1968), 2144-2153.
70. Kasper, D. R., "Theoretical and Experimental Investigations of the Flocculation of Charged Particles in Aqueous Solutions by Polyelectrolytes of Opposite Charge", Ph.D. Thesis, California Institute of Technology, 1971.

## Chapter 3

THEORETICAL AND EXPERIMENTAL EVIDENCE  
IN SUPPORT OF MAJOR THEORIES

The observed characteristics of the three major theories of aggregation (physical double-layer, adsorption coagulation, and polymer bridging) have been summarized by Stumm and O'Melia (1), and by Stumm and Morgan (2). This chapter presents theoretical and experimental evidence of prior investigators which supports and/or delimits certain characteristics of each theory. The discussion, in this chapter, of adsorption, electrophoretic mobility, light scattering, refiltration, and electron microscope studies of various colloid-polymer systems provides insight into the application of these methods (in Chapter 4) to determine the mechanism of E. coli flocculation with PEI.

3.1 Polymer Adsorption3.1.1 Introduction

In 1918, Langmuir (3) published a quantitative theory for the simple adsorption of gas molecules onto plane surfaces. By adsorbing CO, CO<sub>2</sub>, and N<sub>2</sub> in monomolecular layers on glass, mica, and platinum, Langmuir verified his theoretical expression for adsorption:

$$d\theta/dt = k_a(1-\theta)C - k_d\theta \quad (3-1)$$

where  $\theta$  = fraction of total surface site coverage

$C$  = solution concentration of adsorbate

$k_a$  = adsorption rate constant

$k_d$  = desorption rate constant

Under equilibrium conditions,  $d\theta/dt = 0$ , and equation (3-1) becomes

$$\theta = (k_a/k_d)C / (1 + (k_a/k_d)C) = bC / (1 + bC) \quad (3-2)$$

where  $b$  represents the ratio of adsorption to desorption rate constants. Equations (3-1) and (3-2) were subsequently found to represent a wide range of adsorption phenomena, especially for molecules adsorbed flat on a surface, or for vertically-oriented adsorbed molecules with particularly strong intermolecular attraction (65).

The first systematic study on the adsorption of high molecular weight molecules from solution onto solid adsorbents, conducted by Jenckel and Rumbach (66), produced a picture of Langmuirian adsorption with vertically-oriented molecules. Measuring the adsorption of polystyrene (PSt), polymethyl methacrylate (PMMA), and polyvinyl chloride (PVC) on aluminum granules, quartz sand, and glass wool, Jenckel and Rumbach calculated "coating factors" (monomolecular layers) ranging from 1 (PSt on glass) to 70 (PMMA on aluminum).

They reasoned that since the attractive forces between polymer and adsorbent were inadequate to extend beyond a few monolayers, the polymer molecules must be adsorbed in the form of loops or bristles.

### 3.1.2 Adsorption Models

Following the experimental investigations of Jenckel and Rumbach; Simha, Frisch, and Eirich (SFE) (4-9) developed a theoretical model of the adsorption of a flexible random coil molecule onto an adsorbent surface. Via appropriate solution of the diffusion equation, assuming a Gaussian distribution of end-to-end distances for adsorbed segments, Simha et al. derived an adsorption isotherm which predicted short sequences on the adsorbent surface and long loops of segments. In its simplest form, the SFE isotherm is

$$(e^{2k_1\theta})/(\theta/(1-\theta)) = (k_2C)^{1/\nu} \quad (3-3)$$

where  $k_1$  = surface-polymer interaction constant

$k_2$  = solvent-polymer interaction constant

$\nu$  = average number of adhering segments in each molecule

Frisch (7) realized that this derivation corresponded to weak adsorption forces between segment and surface, and to perfect reflection of an adsorbed segment from the adsorbent surface. He derived an equation for the fraction  $F_a$  of the total number of segments  $s$  which

are anchored to the absorbent surface:

$$F_a = 2\kappa [(1-\theta) / (\pi D_s)^{1/2}] (1 + \gamma + \dots) \quad (3-4)$$

where  $\kappa$  = probability of successful contact

$D_s$  = segment diffusion coefficient, including the effects of restrictions of valence angles and bond rotation

$s$  = number of polymer statistical segments

$\gamma = E_{ss}/kT$

$kT$  = Boltzmann's constant  $k$  times absolute temperature  $T$

$E_{ss}$  = segment-surface interaction energy

The expression in brackets pertains only to the geometric restrictions placed upon the polymer chain while the expression in parentheses contains the energy of interaction between segment and surface. A modified equation for strong forces ( $E_{ss} \gg kT$ ), such as those found in biological substrate systems, predicts that all segment chains will collapse onto the substrate surface.

Higuchi (10) modified the SFE model to account for attractive forces varying between very weak forces ( $E_{ss} \ll kT$  yielding large loops) and very strong forces ( $E_{ss} \gg kT$  yielding long surface trains). He determined the segment-surface interaction energy parameter

$K_{ss}$  to be

$$K_{ss} = \kappa (1-\theta) e^{E_{ss}/kT} \quad (3-5)$$

which determines the segment adsorption curves given in Figure 3.1. In general, when anchoring occurs with the formation of a hydrogen bond or other strong dipolar interaction,  $E_{ss}$  may easily exceed several  $kT$  per mole. If  $\kappa$  is of the order of unity and  $\theta$  is not too large, then  $K_{ss} = 7$  for  $E_{ss} = 2kT$ ,  $K_{ss} = 20$  for  $E_{ss} = 3kT$  and  $K_{ss} = 150$  for  $E_{ss} = 5kT$ . In the last two cases, the polymer chains are essentially collapsed to the surface.

Silberberg (11,12) recognized that by considering the absorbing surface as a reflecting wall, Simha et al. biased their random walk model into configurations of small surface trains and long loops. Consequently, Silberberg derived adsorption equations, without the reflection bias, for flexible macromolecules whose segments adsorb in either a three-dimensional hexagonal or cubic lattice. In addition, Silberberg placed restrictions on the number of adsorbable polymer segments and on the siting of adsorbing surface molecules. Figure 3.2 illustrates the fraction of the total number of segments adsorbed  $F_a$ , and the number of segments in an extended loop  $N_L$ , as functions of the normalized adsorption energy.

Silberberg determined that for large macromolecules, the size and structure of adsorbed segments and loops are results of the nature and morphology of the surface and of the polymer molecule, and not necessarily results of the molecular weight. In cases where all

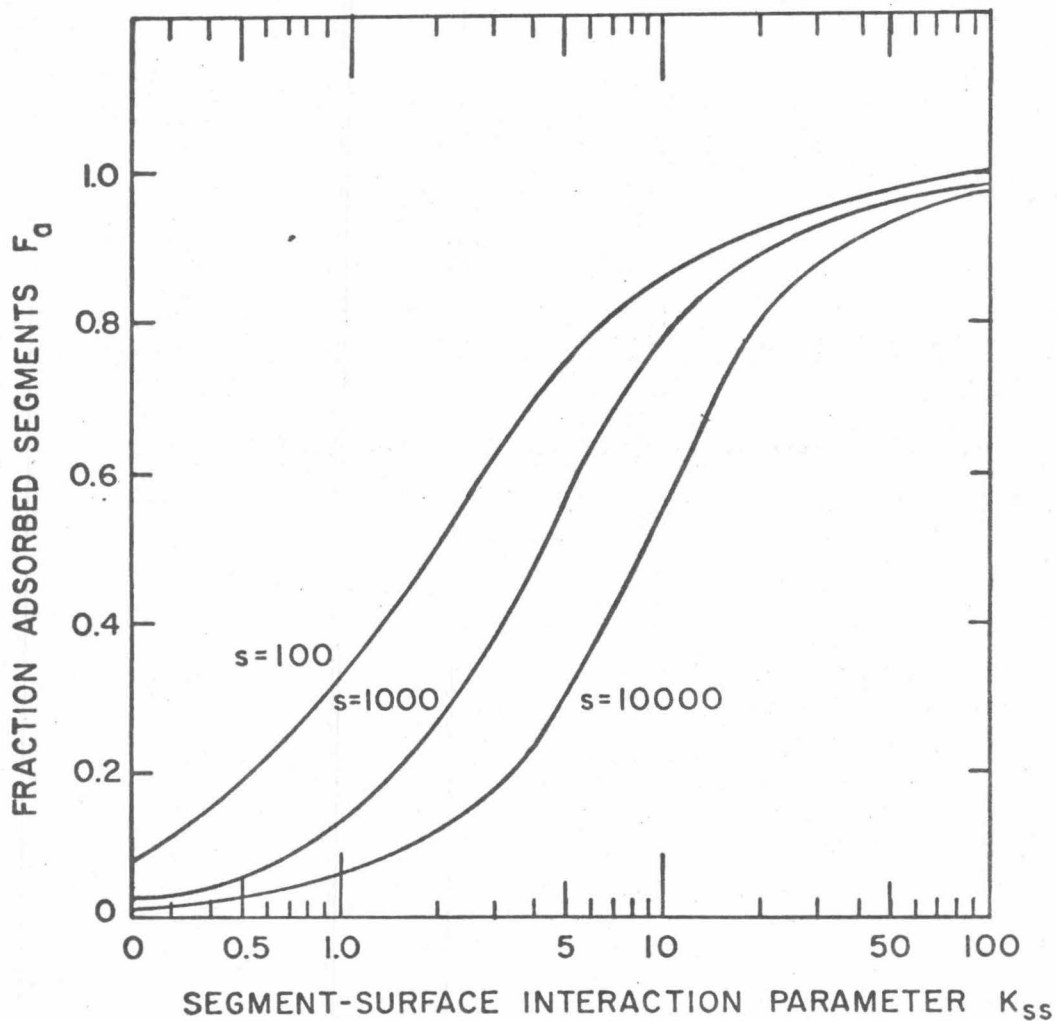


Figure 3.1 Fraction of Adsorbed Segments  $F_a$  versus Segment Surface Interaction Parameter  $K_{ss}$  for Molecules of 100, 1000, and 10000 Segments. Adapted from Higuchi (10).

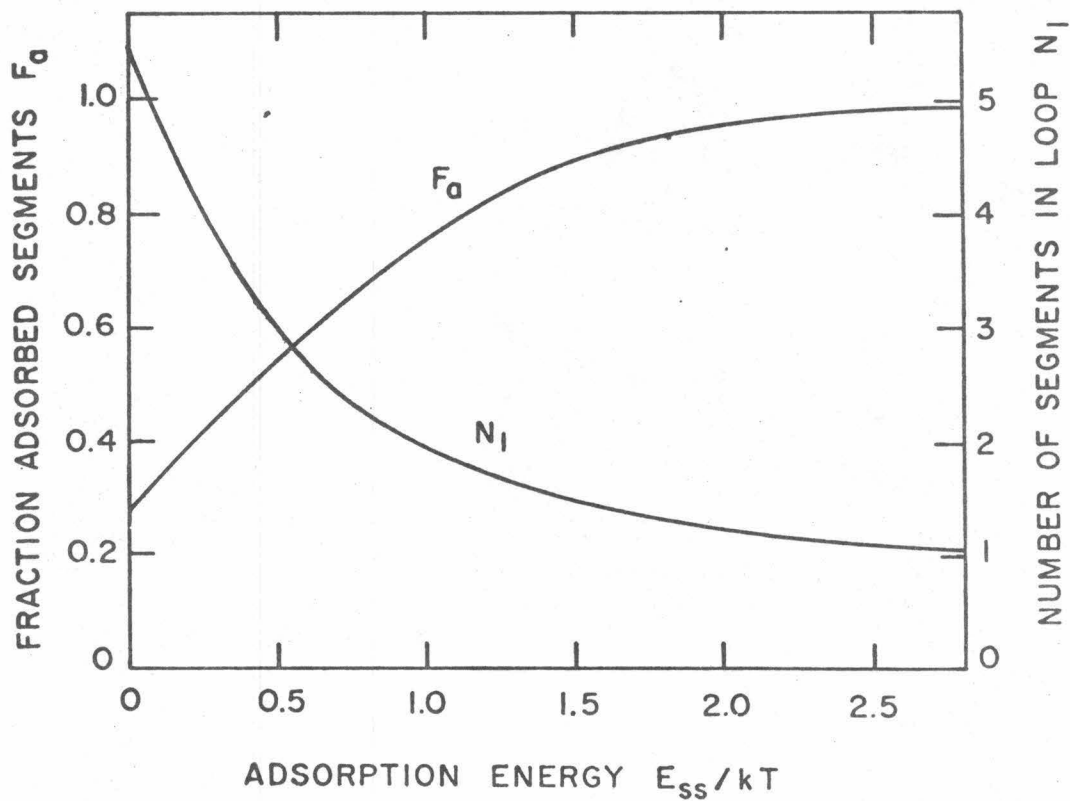


Figure 3.2 Fraction of Adsorbed Segments  $F_a$  and Number of Segments in a Loop  $N_L$  Versus Normalized Adsorption Energy  $E_{ss}/kT$ . Adapted from Silberberg (11).

surface sites and polymer segments are adsorbing and the molecule is reasonably flexible, the adsorption loops are short and the polymer molecule lies close to the surface. At about 1 kT energy change per mole, more than 70% of the polymer segments are in contact with the surface. However, steric hinderance resulting from inflexibility of bond angles or lack of adsorption centers rapidly increases the size of the loops and increases the energy requirements for total adsorption.

To equations derived from the projection of Silberberg's three dimensional cubic lattice onto one dimension, DiMarzio (13), and DiMarzio and McCrackin (14) applied Monte Carlo computer techniques for adsorption energies of 0-4 kT and polymer molecules larger than 50 segments. Figure 3.3 depicts the number of adsorbed segments of each molecule  $N_a$  as a function of normalized adsorption energy and of total number of segments  $s$ .

Figure 3.4, derived from the computer analysis of DiMarzio and McCrackin (14), illustrates the fraction of adsorbed segments  $F_a$  as a function of normalized adsorption energy and number of segments in each molecule. The close correlation of this one-dimensional model with previous three-dimensional work by Higuchi is seen in a comparison of Figures 3.1 and 3.4, both of which show a high degree of adsorption at low interaction energies.

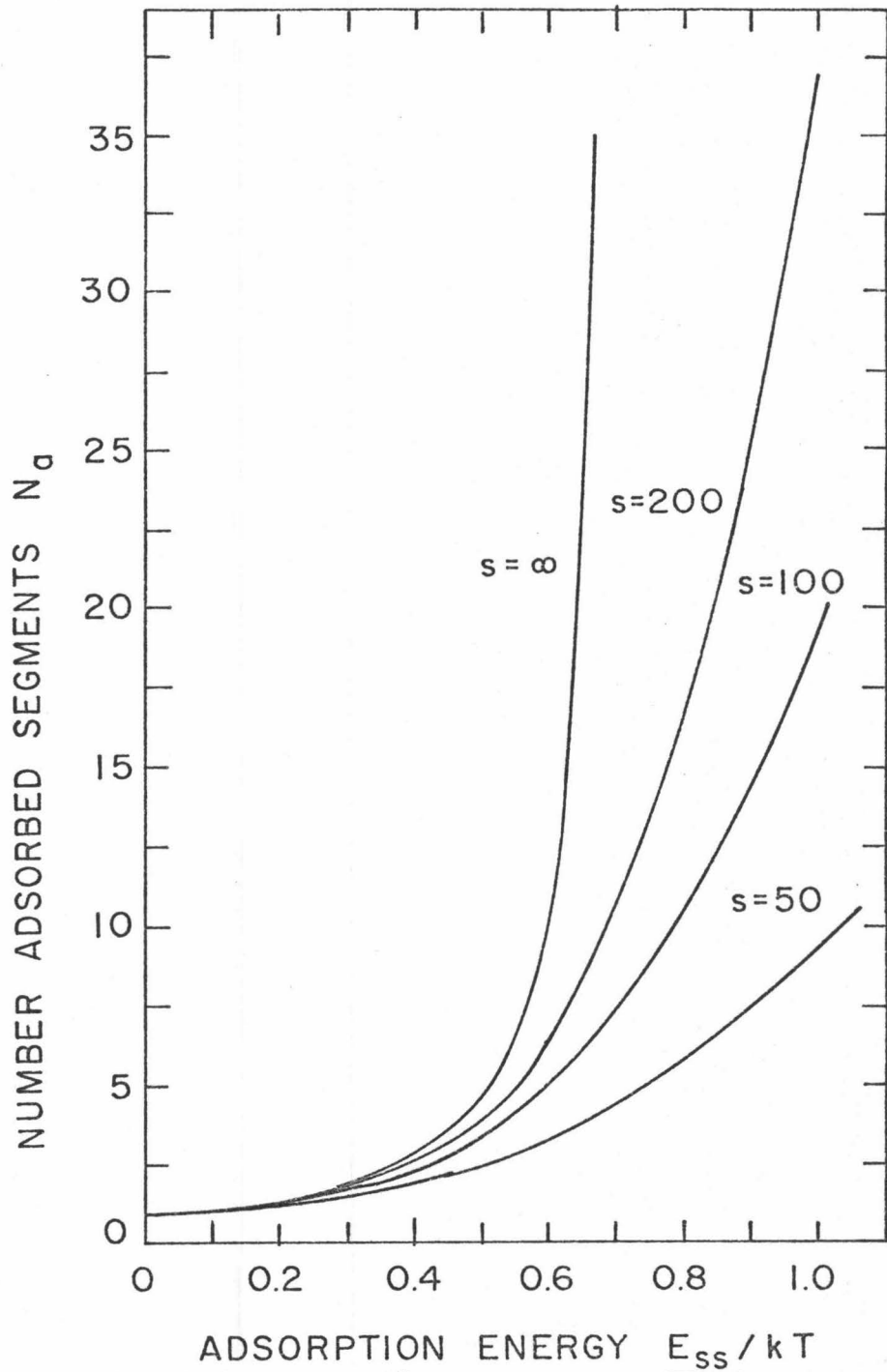


Figure 3.3 Average Number of Adsorbed Segments  $N_a$  Versus Normalized Adsorption Energy  $E_{ss}/kT$  for Molecules of 50, 100, 200 and  $\infty$  Segments. Adapted from DiMarzio and McCrackin (14).

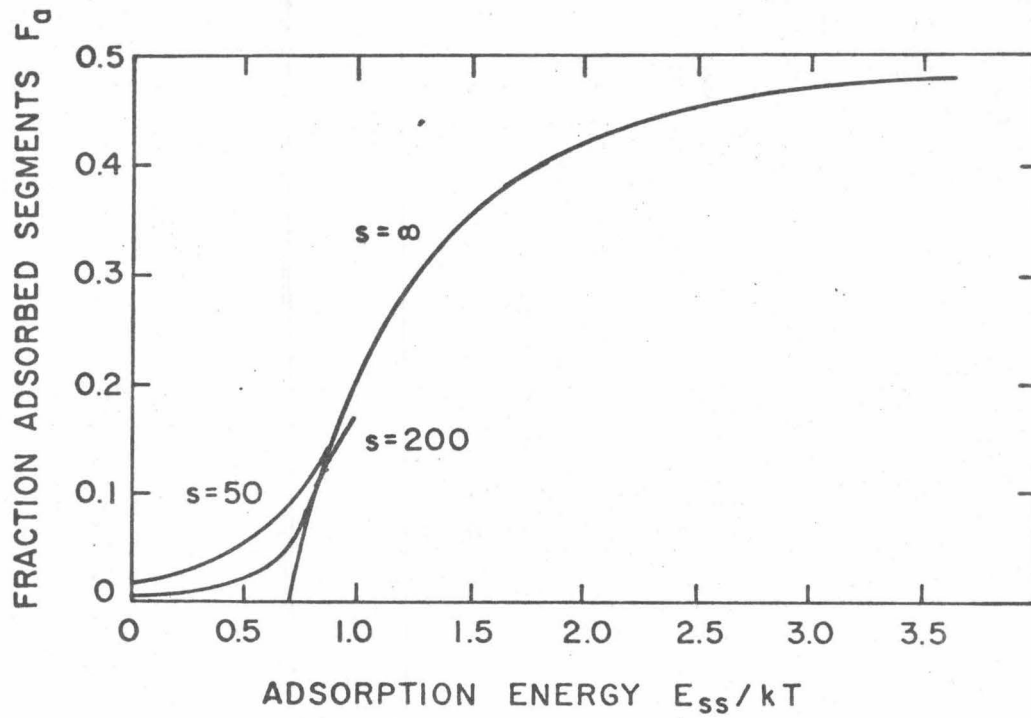


Figure 3.4 Fraction of Adsorbed Segments  $F_a$  Versus Normalized Adsorption Energy  $E_{ss}/kT$  for Molecules of 50, 200, and  $\infty$  Segments. Adapted from DiMarzio and McCrackin (14).

Figure 3.5 is a display of the polymer density  $\rho(\delta)$  as a function of distance  $\delta$  from the surface for five values of attraction energy. This computer simulation depicts virtually complete adsorption of polymer segments to the surface for segment adsorption energies greater than 1 kT, and only limited expectation for long loops of polymer extending into solution. For  $E_{ss} \gg kT$ , Hovee (15) derived an exponential decay in  $\rho(\delta)$  with  $\delta$ , in good agreement with the results of DiMarzio and McCrackin.

Roe (16) extended the computer simulation of the three-dimensional random walk adsorption model to include end effects, which previously had been considered insignificant. His solution revealed a critical energy,  $E_c$ , at which the local free energy change accompanying the adsorption of a segment just balanced the entrophy effect arising from polymer adsorption and solvent desorption. When adsorption is strongly favored ( $E_{ss} \gg E_c$ ), the polymer chain end effects are negligible, desorbed loops are only a few segments long, and the polymer chains lie essentially flat on the surface. However when  $E_{ss} \cong E_c$ , approximately 70% of the total number of segments are in free chain ends, and the adsorbed sequences are very short. Figure 3.6 illustrates the dependence of average length of polymer loops  $L_L$  on the degree of flexibility and the normalized adsorption energy for 20, 100, 1000, and 5000 segment polymer molecules.

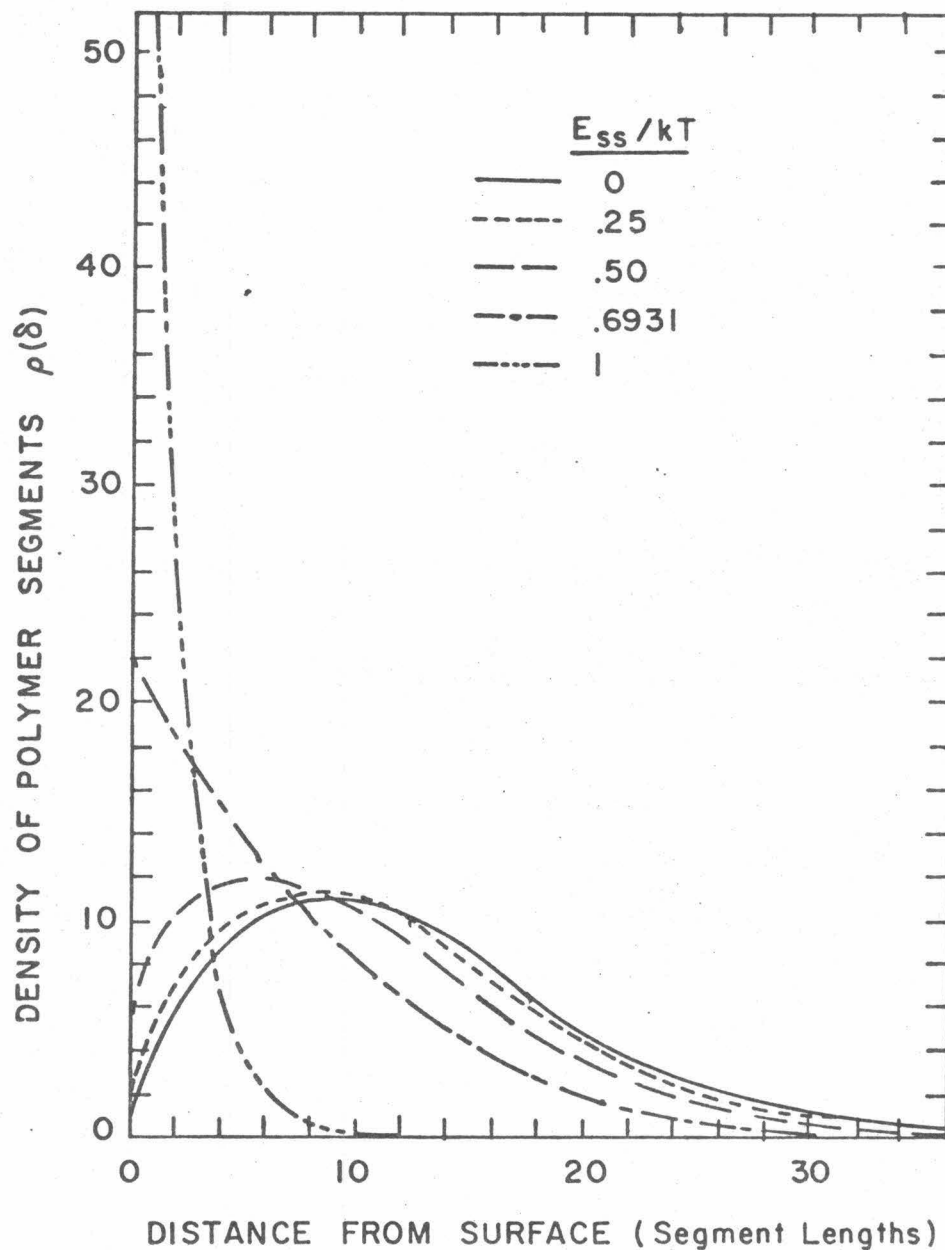


Figure 3.5 Density Distribution of Polymer Segments  $\rho(\zeta)$  Versus Distance from the Surface for Five Values of Normalized Adsorption Energy  $E_{ss}/kT$  for Molecules of 200 Segments. Adapted from DiMarzio and McCrackin (14).

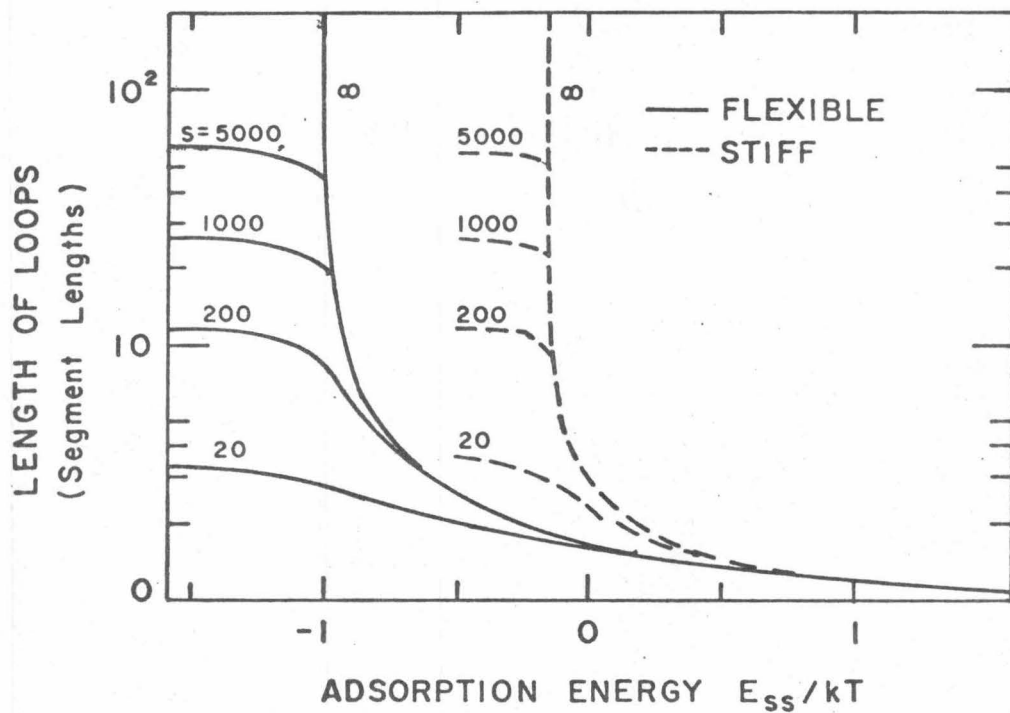


Figure 3.6 Average Length of Loops  $L_L$  Versus Normalized Adsorption Energy  $E_{SS}/kT$  for Flexible and Stiff Molecules of 20, 200, 1000 and 5000 Segments. Adapted from Roe (16).

In Figure 3.7, the average length of the desorbed sequences at the polymer chain ends  $L_e$  is plotted as a function of the normalized interaction energy for both flexible and stiff molecules. Significantly, the chain end sequences are an order of magnitude longer than the interior loops of an adsorbed polymer for all degrees of polymerization, at roughly the same energy levels.

Numerous additional statistical-mechanical treatments of the configuration of polymer molecules adsorbed on solid surfaces have been published by Rubin (17), McCrackin (18), Silberberg (19, 20), and Motomura (21). McCrackin extended the Monte Carlo computer simulations by taking into account the excluded volume effect:

Figure 3.8 illustrates the maximum normal distance to an adsorbing surface for different size molecules as a function of normalized adsorption energy when the excluded volume effect is considered. McCrackin determined that the fraction of adsorbed segments is reduced by a factor of about 2 for molecules up to 300 segments. He also calculated a critical adsorption energy of about 0.25 kT, below which a small fraction of the segments of the molecule lie on the surface and the remaining segments form long loops; and above which, the opposite holds.

Silberberg (19) revised his previous equations to allow for nonintersection (volume exclusion) effects, and concluded that for

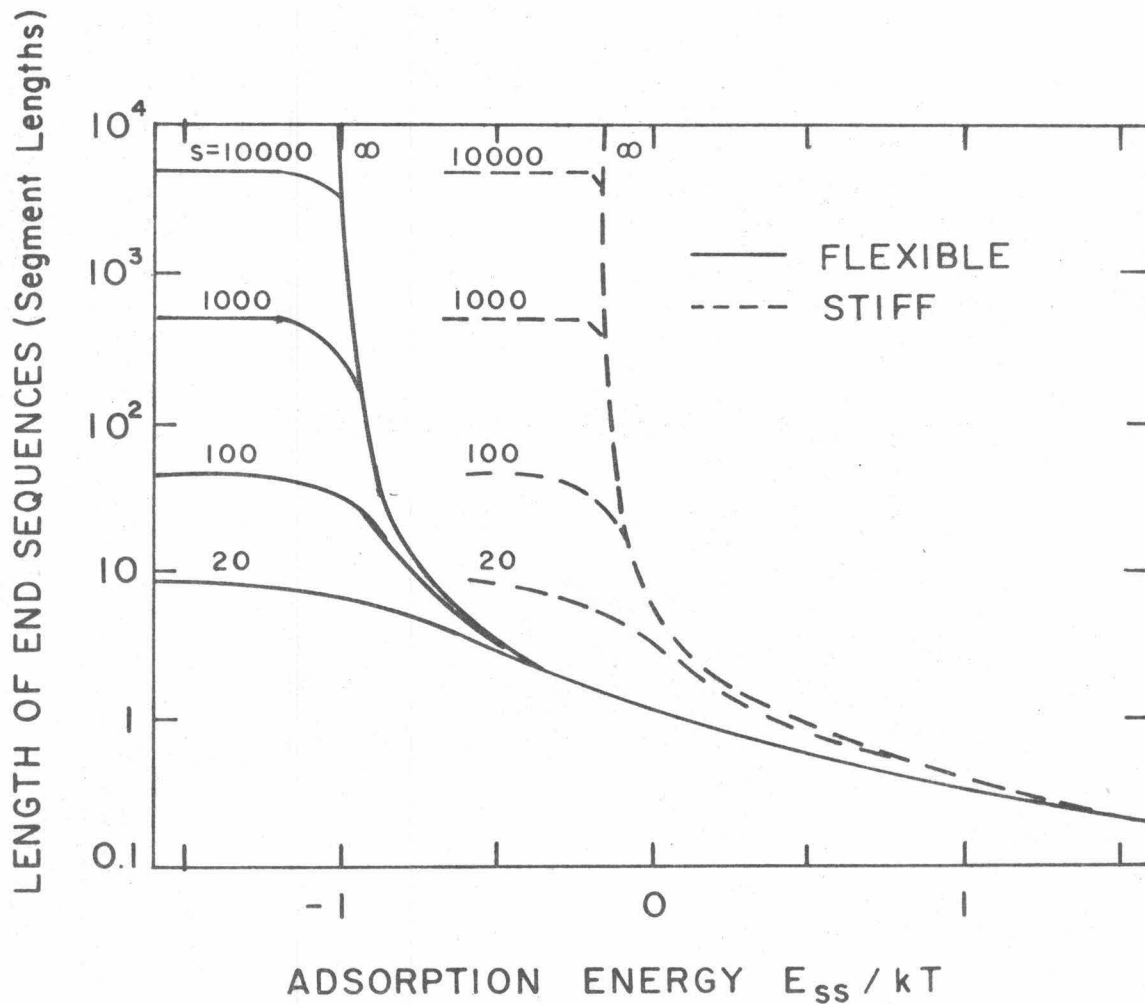


Figure 3.7 Average Length of End Sequences  $L$  Versus Normalized Adsorption Energy  $E_{ss}/kT$  for Flexible and Stiff Molecules of 20, 100, and 10,000 Segments. Adapted from Roe (16).

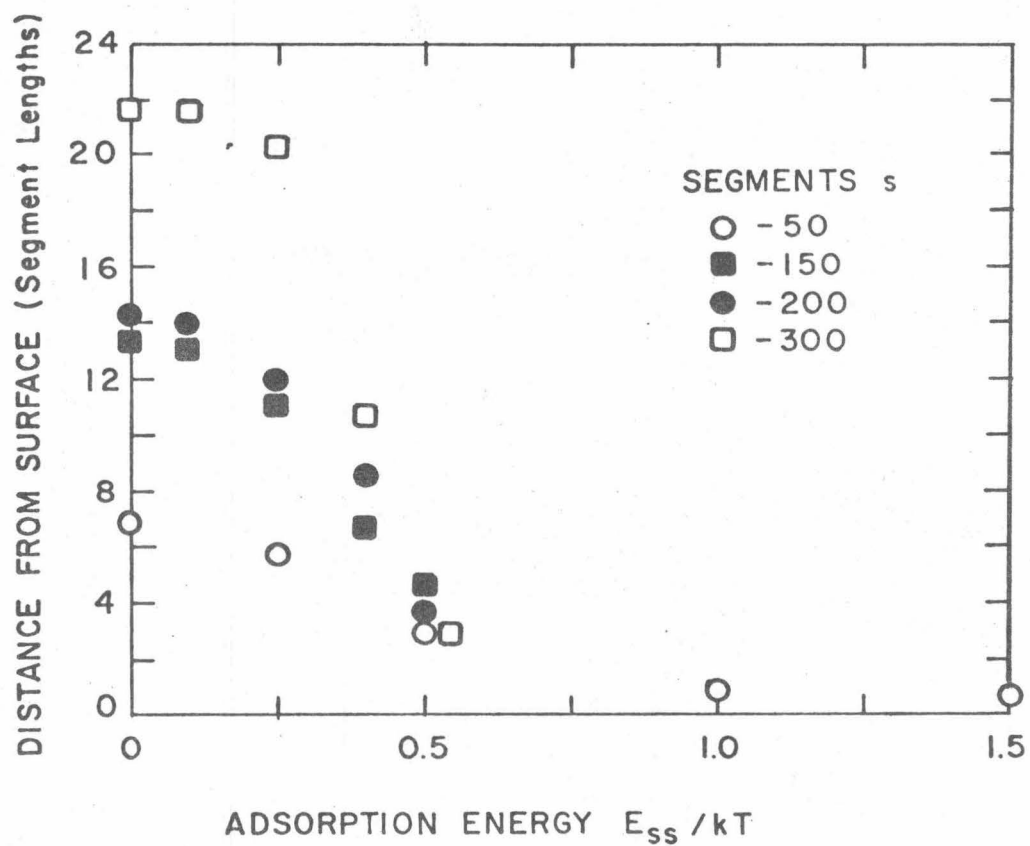


Figure 3.8 Maximum Normal Distance from Polymer Segment to Adsorbing Surface Versus Normalized Adsorption Energy  $E_{SS}/kT$  for Molecules of 50, 150, 200, and 300 Segments. Adapted from McCrackin (18).

segment-surface attraction energies  $E_{ss}/kT > 0.0$ , the average surface train length of adsorbed polymer was at least an order of magnitude greater than the average loop length. In addition, the fraction of segments in contact with the surface at adsorption energies greater than zero was estimated to lie between 0.6 and 1.0 depending on polymer flexibility. Further revisions to Silberberg's model included adsorbed and bulk phase polymer concentrations, polymer flexibility parameters, and polymer-solvent energy interaction parameters.

Essentially, previous models considered adsorption from very dilute solutions, i. e., isolated coils onto flat surfaces. Silberberg's revisions provided a more realistic picture of the adsorption process, yielding closer correlation of theoretical predictions to experimental results. For example, Figure 3.9 depicts the combined effect of solvent-polymer interaction energy ( $E_{sp}$ ) and polymer concentration ( $C$ ) upon the average loop length  $L_L$  as a function of the normalized segment-surface interaction energy ( $E_{ss}/kT$ ). Under normal polymer concentrations ( $C = 0.1$  to  $10.0$  mg/l) only the shape of the  $L_L$  versus  $E_{ss}/kT$  curve remains similar to the  $C = 0$  condition: there are major quantitative differences in that the adsorbed layers are much thicker, in agreement with many experimental results.

Figure 3.10 illustrates that far fewer segments are in the surface than would have been expected on the basis of the previous

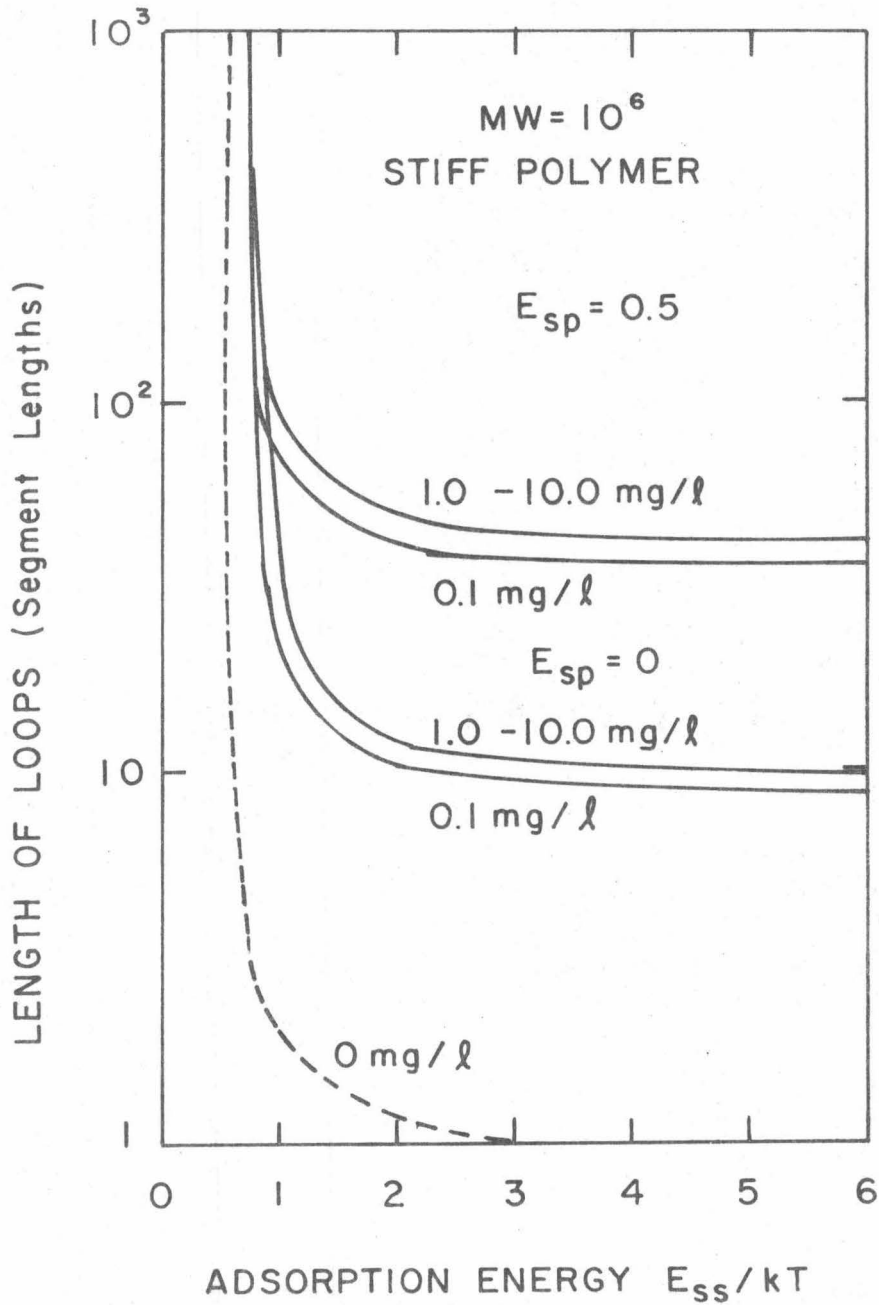


Figure 3.9 Average Length of Loops  $L_L$  Versus Normalized Adsorption Energy  $E_{ss}/kT$  for a Range of Polymer Concentrations at Two Solvent-Polymer Interaction Energies  $E_{sp}/kT$ . Adapted from Silberberg (20).

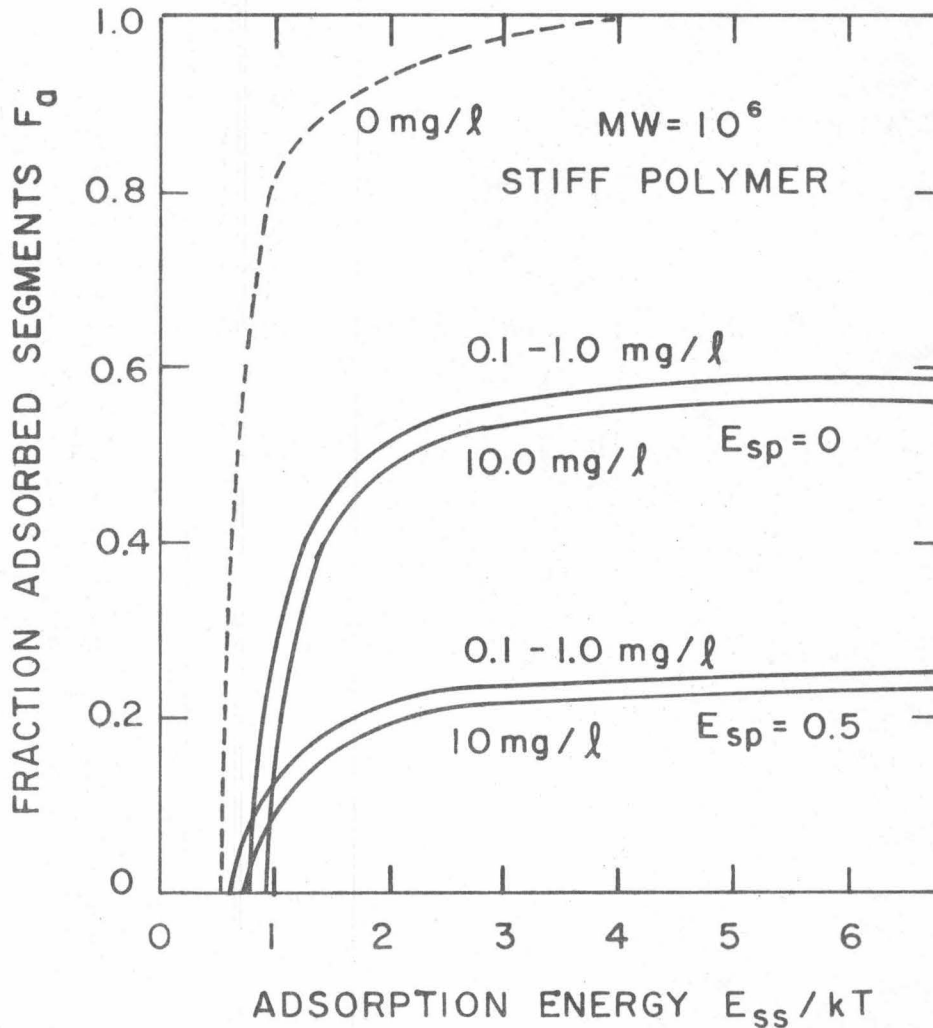


Figure 3.10 Fraction of Adsorbed Segments  $F_a$  Versus Normalized Adsorption Energy  $E_{ss}/kT$  for a Range of Polymer Concentration at Two Solvent-Polymer Interaction Energies  $E_{sp}/kT$ . Adapted from Silberberg (20).

isolated macromolecule models. Once again, the experimental data giving the range of  $F_a$  between 0.2 and 0.5 are now in good agreement with the theoretical model. For  $E_{ss}/kT$  greater than 3.0, Silberberg predicted that  $\theta$ , the fraction of the surface sites covered by polymer segments, approaches unity, and is independent of the bulk concentration over a wide range of conditions.

### 3.1.3 Adsorption Experiments with Polymers

Continuing the work of Jenckel and Rumbach; Koral, Ullman, and Eirich (22) studied the adsorption of polyvinyl acetate (PVA) onto iron powder, tin powder, and activated alumina, from a variety of solvents. Although the Langmuir isotherm was originally derived for individual rigid molecules, most of the results for PVA adsorption were shown to fit the Langmuir isotherm (Equation 3-2); i. e., a steep rise and then a plateau in which the amount of polymer adsorbed per gram of adsorbent does not change appreciably with increasing solution concentration. Koral et al. (22) determined that with a monomeric unit of PVA covering  $26 \text{ \AA}^2$  of adsorbent surface, the maximum adsorption values of the polymer corresponded to 10-20 molecular layers of material. This fact plus the similarity between single molecule adsorption and polymer adsorption (both plot as Langmuir isotherms) led Koral et al. (22) to conclude that the polymer

molecules adsorb at single points with long loops. In order to adsorb thusly, the polymer molecules must be laterally compressed into a cylindrical or ellipsoidal form, and must allow a certain degree of intermolecular entanglement.

Binford and Gessler (23) determined that polyisobutylene adsorbed completely onto the surface of carbon black particles: however, their conclusion was based solely on a comparison of the number of adsorption sites with the number of available polymer methyl groups. Peterson and Kwei (24), in their studies of the kinetics of polyvinyl acetate adsorption onto a chrome plate surface, determined that their adsorption met the conditions of a Langmuir isotherm, with "plateau" equilibrium attained in under 120 seconds. They calculated that with maximum adsorption of PVA, most but not all segments are lying flat on the surface, but only with dilute polymer solutions. Peterson and Kwei suggested a model, similar to that of Gottlieb (36), which postulated essentially two-dimensional adsorption followed by an "overfilm" of polymer molecules projecting into the third dimension with at least some segments in contact with the surface.

Perkel and Ullman (25), conducting adsorption experiments of polydimethyl siloxanes (PDS) on iron and glass particles, concluded that: (a) The quantity of PDS adsorbed is far in excess of that which could be packed into a monolayer, (b) the shape of the adsorption

isotherm (Langmuir) is characteristic of single point adsorption, and (c) the amount of polymer adsorbed when monolayer coverage is complete increases as a low power of molecular weight; i. e. ,

$$A_s = c(MW_n)^\beta \quad 0.1 < \beta < 0.5 \quad (3-6)$$

where  $A_s$  = saturation adsorption, milligram polymer per gram adsorbent

$c$  = constant

$MW_n$  = number-average molecular weight

In their model, the polymer adsorbs through only a small fraction of the available polar groups; the unadsorbed segments extend into the surrounding solution in configurations determined by bonds to the surface and by polymer-solvent interactions.

By measuring the shift in the normal carbonyl frequency caused by hydrogen bonding of polylauryl methacrylate (PLMA) to silica particles, Fontana and Thomas (26) quantitatively measured  $F_a$ , the fraction of polymer segments attached to the silica surface. Their result that 36% of the segments are attached to the surface is in accord with the statistical theory of Simha-Frisch-Eirich (4-6), as extended by Frisch (7) for strong interactions (5-8 kT for hydrogen bonding). The adsorption data for PLMA and for polyalkyl methacrylate vinyl pyrrolidone (PAM-VP) appear to fit the Langmuir isotherm, even

though the adsorption of long trains of segments is indicated by the value of  $F_a$ . From sedimentation studies, Fontana and Thomas conclude that PLMA is adsorbed relatively flat and extended parallel to the surface with 40% of the ester segments attached (films of 30 Å thickness), while PAM-VP is extended away from the surface with only 10% or less of the ester segments attached (films of 200 Å thickness).

Further investigations by Fontana (27) with polyalkyl methacrylate-polyglycol (PAM-PG) on silica revealed a 2.5 fold increase in the amount of polymer adsorbed from solution, but a fourfold decrease in  $F_a$ , the fraction of the ester carbonyl groups in an adsorbed polymer molecule which are directly attached to silica surface hydroxyls via hydrogen bonds. This effect is due to the preferential adsorption of polyethylene oxide groups to the exclusion of the ester carbonyl groups: an effect already noticed in the preferential adsorption of the strongly polar pyrrolidone groups of PAM-VP.

Steinberg (28) performed a variety of adsorption experiments with polylauryl methacrylate (PLMA) and polyalkyl methacrylate vinyl pyridine (PAM-VP) onto iron powder. Using carbon-14 labeled polymers to measure solution depletion, Steinberg presented a two-step adsorption model: the first polymer molecules at a surface uncoil and adsorb in a two-dimensional configuration. Initially, the fraction of segments adsorbed at the interface,  $F_a$ , approaches one. As the

surface site coverage  $\theta$  increases, the configuration progressively changes to a three-dimensional random coil configuration. An overlayer may begin to form with interpenetration of adsorbed molecules. After a longer time period (order of 100 hours), Steinberg noted desorption and displacement of polymer molecules - evidence that surface rearrangement can take place.

Other adsorption studies by Black, Birkner, and Morgan (29, 30), Birkner and Edzwald (31), and Kasper (67), in conjunction with flocculation experiments, present data indicative of Langmuirian adsorption behavior.

#### 3.1.4 Direct Measurement of Adsorbed Layer Thickness

The experimental investigations cited thus far provide only indirect evidence of the actual configuration of the adsorbed molecule. However a small amount of direct evidence is available from precision-viscosity measurements. Ohrn (32) determined the thickness of an adsorbed layer of polystyrene (MW = 500,000) on the walls of the glass capillary of an Ostwald viscometer by measuring the relative increase in flow times of a polystyrene solution in toluene for two capillaries of different radius. Ohrn found this thickness to be about 1500 Å, or roughly 2.5 times the hydrodynamic diameter of 600 Å. In a similar experiment, Tuijnman and Hermans (33) measured the thickness of

a layer of polyvinyl acetate (MW = 800,000) adsorbed from a toluene solution on a glass capillary to be approximately 5000 Å, or roughly 5.0 times the hydrodynamic diameter of 1000 Å. Huque, Fishman, and Goring (34) obtained thicknesses of 700-900 Å for cellulose trinitrate in acetone, and 300-600 Å for cellulose trinitrate in ethyl acetate. Finally, Fendler, Rohleder, and Stuart (35), determining layer thicknesses from changes in specific viscosity caused by polymer adsorption, measured  $750 \pm 250$  Å for polystyrene (MW = 400,000) in toluene,  $1480 \pm 290$  Å for polystyrene (MW = 620,000) in decalin, and  $2500 \pm 300$  Å for polystyrene (MW = 400,000) in butanol.

Fontana and Thomas (26) measured the adsorbed film thicknesses of PLMA and PAM-VP on uniform carbon particles by a sedimentation velocity technique. Particle fractionation gave particle size distribution sufficiently narrow to allow determination of film thicknesses of  $25 \pm 10$  Å for PLMA and  $210 \pm 40$  Å for PAM-VP. In both the viscosity and sedimentation velocity experiments, uncoiling of the molecules may occur due to flow, resulting in extended molecules and in too large an adsorption thickness.

### 3.1.5 Summary of Prior Adsorption Theory and Experiments

In general, three approaches have been used to determine the geometrical configuration of adsorbed macromolecules: statistical

mechanical treatments based on random walk theory, interpretation of experimental adsorption data, and direct measurement of adsorbed layer thickness. As improvements were made to the original SFE adsorption isotherm, the statistical mechanical model began to better explain the behavior noticed in experimental polymer adsorption systems. Although the primary factor controlling the adsorption of polymer onto a solid surface and the subsequent polymer configuration is the total free energy change (chemical and electrical), accurate representation of the process must include: (a) adsorbent surface conditions (smooth or porous) and charge distribution, (b) adsorbate concentration, flexibility, molecular weight, and charge distribution, and (c) solvent interaction with surface and polymer.

Initial statistical mechanical models considered only the adsorption of isolated polymer molecules from extremely dilute solutions onto large, flat surfaces. At even small values of the segment-surface free energy change ( $E_{ss}/kT = 1.0$ ), this resulted in the collapse of the three-dimensional molecule in solution to a two-dimensional molecule on the surface. For an isolated macromolecule, the surface interaction will cause the polymer molecule to form short trains of segments all in the surface connected together by short loops. For this type of adsorption, the polymer configuration is independent of molecular weight, and dependent only on the energy

change per segment-surface contact and on steric hindrance factors of the surface or polymer molecule.

Kasper (67) felt that the large adsorption energies ( $1.0 < E_{ss}/kT < 10.0$ ) for polymer segments attracted to oppositely-charged surfaces negated the possibility of polymer bridging via long loops or end tails. Consequently, he postulated that adsorbed polymer molecules created a surface mosaic of alternate positive and negative charge regions, resulting in the coagulation of normally repelling particles. However, as Figures 3.9 and 3.10 have shown, the revised model of Silberberg predicts long loops and moderate fractions of adsorbed segments when adsorbate concentration, adsorbate flexibility, and solvent interaction effects are considered. From Silberberg's analysis, a two-phase model of polymer adsorption emerges which depends primarily on the degree of surface site coverage. Initially, at low-surface-site coverages and with adsorption energies of  $2 kT$  or greater, the polymers adsorb in relatively flat configurations with: (a) essentially no loops extending ten or more segment lengths from the surface, (b) more than 95% of the segments attached directly to the surface, and (c) no free tails longer than a few segments in length (67). As the fraction of surface site coverage approaches one, increasing numbers of polymer molecules will adsorb to small uncovered surface areas by only a few monomer segments. Because of the strong segment-surface attraction,

the adsorbed monomer segments will be firmly anchored, but the remainder of the molecule will remain unattached. This effect was observed by Gottlieb (36) in his surface potential measurements:

The region in which the potential is independent of surface coverage is believed to correspond to the adsorption of polymer molecules with only a small fraction of the segments in contact with the surface, the remainder extended into solution in a coiled configuration. An alternate explanation of the plateau in the surface potential-surface coverage plot is that the plateau region corresponds to the adsorption of randomly coiled polymer molecules on top of the first layer of oriented polymer.

If only the polymer molecular weight is varied during adsorption experiments, then a picture of the adsorbed polymer configuration can be obtained from the molecular weight dependence of such adsorption. Perkel and Ullman (25) have presented five variations of the dependence of maximum adsorption,  $A_s$ , on molecular weight which can be compared with experimental results. Generally,

$$A_s = c(MW_n)^\beta \quad (3-6)$$

where  $c$  and  $\beta$  are constants. The configuration of adsorbed molecules can be related to the values of  $\beta$  as follows:

1.  $\beta = 0$  : Either all polymer segments lie in the plane of the adsorbent, or loops exist in which the number of segments is a constant fraction of the total number of segments adsorbed.
2.  $\beta = 1$  : A single monomer attaches each polymer molecule to the surface

3.  $\beta = 1/3$  : The polymer, coiled in spherical configuration, has adsorbed with a radius proportional to the radius of gyration of the molecule in solution.
4.  $0 < \beta < 1$  : The polymer molecules, tangled and intertwined on the adsorbent, nevertheless adsorb with the number of attached segments in proportion to the molecular weight.
5.  $A_s = c_1 + c_2 (MW_n)^\beta$  : This equation represents two stage polymer adsorption; i. e., virtually complete surface coverage followed by isolated segment adsorption. The constant term  $c_1$  represents initial adsorption of all segments, while  $c_2 (MW_n)^\beta$  meets one of the criteria discussed in 1 through 4 above.

The following statements summarize prior experimental results:

1. The adsorption data can in general be fitted to a Langmuir isotherm, the best linear fits being obtained for the highest molecular weights. The amount of polymer adsorbed per unit surface area increases rapidly with polymer concentration in the equilibrium solution and then reaches a plateau value which does not change appreciably with further increases in bulk concentration. Randomly-coiled molecules tend to adsorb with each monomer segment competing individually with solvent molecules for surface sites; shaped molecules tend to adsorb as units (66, 22-23, 25-31).

2. The initial polymer uptake by the adsorbent is extremely rapid, approximately 85% of the polymer being adsorbed within 30

seconds of addition. Equilibrium, however, takes a very long time to establish, particularly with high molecular weight samples or with porous adsorbents (66, 22-26, 28-31, 37).

3. As the molecular weight increases, the amount of polymer adsorption increases up to limiting values where it becomes less and less dependent on the size of the macromolecule (11, 26).

4. Segment adsorption energies of the order of  $kT$  are usually adequate to flatten coiled molecules onto the adsorbent surface, creating trains of adsorbed segments and small loops. These loops are generally only 30-50 Å in length (7, 10, 12, 16, 18, 21).

5. Larger pendant loops are found in these situations:

- a. during the period which immediately follows the initial successful attachment of the macromolecule to the surface (3-6, 12, 22, 28-31, 38),
- b. when steric hinderance, caused by polymer inflexibility or adsorbent surface porosity, restricts the macromolecule configuration (37-40),
- c. when only a few interspersed surface sites are available for adsorption of monomer segments, resulting in firmly-anchored monomers with larger pendant loops (20, 23, 25, 28, 36).

### 3.2 Electrophoretic Mobility

When a bacterial suspension is subjected to an electric field, the cells in consequence of their charge will migrate to one or another of the electrodes. The mobility of the cells is directly proportional to the applied potential gradient  $E$  and to the zeta potential  $\zeta$ . The zeta potential is defined as the potential existing at the shear plane between the bulk electrolyte and the liquid layer which moves with the particle. The location of this slipping plane, and its associated zeta potential, is shown in Figure 3.11A for finite specific adsorption in which the net adsorbed counterion charge is less than the initial surface charge; and in Figure 3.11B for superequivalent specific adsorption in which the net adsorbed counterion charge is greater than the initial surface charge.

Because of its experimental accessibility, the zeta potential has been used for years in determining double-layer parameters. A major problem in this approach has been the lack of information on the thickness of the diffuse layer which accompanies the colloid particle in its motion. Some investigators have equated the zeta potential with the Inner Helmholtz Plane (IHP) potential because of the presence of additional counterions in the liquid layer which moves with the particle.

If the segment adsorption energy  $E_{ss}$  is strong enough, sufficient polymer molecules can be adsorbed to create a reversal of the IHP potential, in spite of the normal Coulombic repulsion between

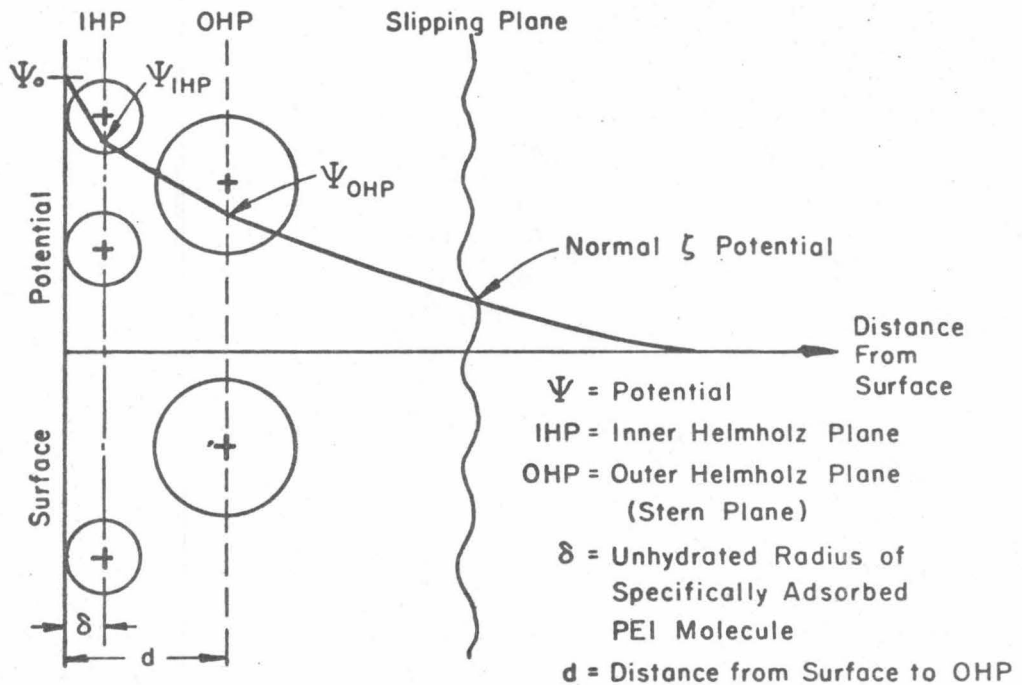


Figure 3.11A Zeta Potential Caused by Specific Adsorption of PEI Molecules.

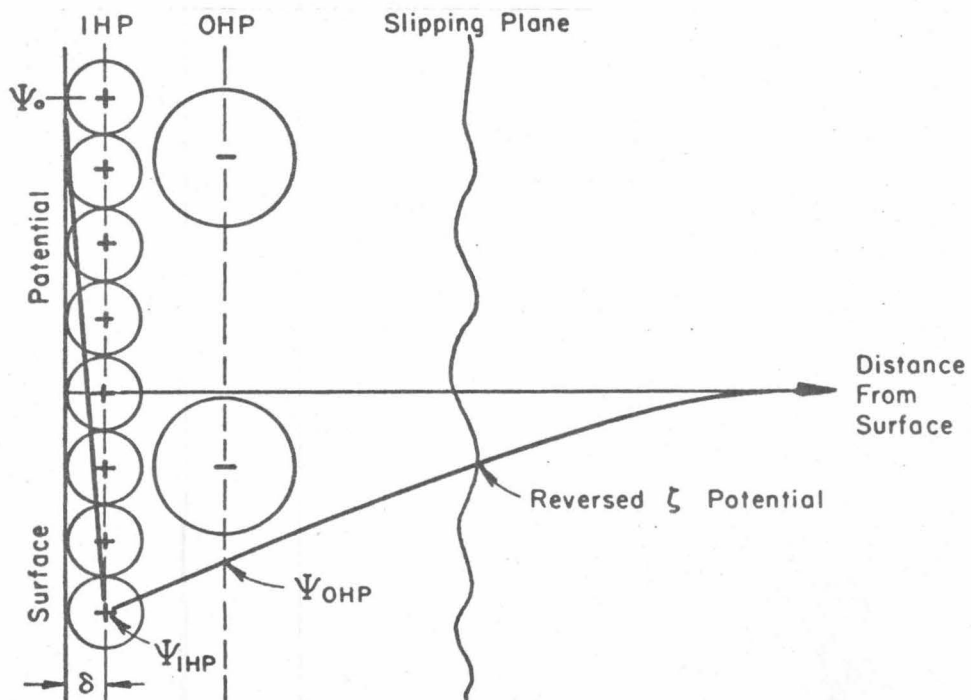


Figure 3.11B Reversed Zeta Potential Caused by Superequivalent Specific Adsorption of PEI Molecules.

similarly charged species. Figure 3.11B illustrates the reversal of the IHP potential and of the zeta potential, such as might occur with the adsorption of a complete monolayer of polymer.

Electrophoretic measurements of E. coli by Moyer (41) under carefully-controlled conditions revealed that the surface factors which determine the electrokinetic potential of bacteria in mature cultures are constant during long periods of cultivation. Electrophoretic changes which occur during physiological youth (0-6 hours after seeding of culture) were not evident in later growth stages. In addition, Moyer noted that there was no change in the mobility of E. coli with pH in the range 4.0 to 7.0, when suspended in buffers of constant ionic strength.

One of the first studies of the effect of surface-active agents upon the electrophoretic mobility of bacteria was conducted by Dyar and Ordall (42). Using cetyl pyridinium chloride (CPC), a cationic surface-active agent, in concentrations of  $1 \times 10^{-6}$  to  $1 \times 10^{-3}$  M, they observed a general pattern of decreasing negative mobility, reversal of mobility, and finally stabilization of mobility at positive values. Doses of CPC that barely decreased the negative mobility were found lethal to E. coli within 10 minutes of addition.

The mechanism of biological aggregation can be related to changes in the electrophoretic mobility as polymer is placed in the

colloidal suspension. Specific information is gained from the mobility at the optimum aggregation concentration, and from the mobility when excess polymer is added.

In the physical double-layer model, optimum aggregation is produced when the electrokinetic potential difference falls below the critical potential. This reduction in electrokinetic potential coincides approximately with a decrease in electrophoretic mobility to zero, i. e., as the zeta potential approaches zero, the interaction between diffuse double layers becomes small enough to enable effective collisions to occur. Addition of excess polymer in the double-layer model has little or no effect on the particle mobility.

In the adsorption coagulation model, aggregation is produced by the reduction of the electrostatic interaction energy between particles by chemical adsorption of polymer molecules to the particle surface. In this case, the zeta potential will also be reduced because of the adsorption of oppositely-charged polymer. Coagulation can occur, however, within a range of values on either side of zero mobility. Kasper (67), for example, showed theoretically and experimentally that coagulation could be produced by a charge mosaic of strongly adsorbed cationic polymer on an anionic colloid at optimum surface site coverages of 20-30%. At this level of surface site coverage, the mobility should remain negative, as was verified in electrophoretic

measurements. The addition of polymer in excess of optimum doses results in continued adsorption and possible charge reversal.

In the chemical bridging model, electrostatic interaction plays a subordinate role to surface chemical interactions and bridging at optimum doses. Consequently the zeta potential is usually not zero. As excess polymer of opposite charge is added, the molecules reduce and may reverse the IHP potential thereby producing restabilization. As excess polymer of similar charge is added, restabilization can occur because of complete surface site coverage on each particle, and the resulting lack of bridging sites.

### 3.3 Polymer Molecular Weight and Size from Light Scattering Experiments

Polymer bridging, one of the proposed mechanisms in achieving flocculation, obviously requires molecules of sufficient length to anchor onto receptive sites of two approaching particles. The weight-average molecular weight, expressed as,

$$MW_w = \frac{\sum n_i MW_i^2}{\sum n_i MW_i} \quad (3-7)$$

where  $n_i$  = number of molecules of each molecular weight

$MW_i$  = molecular weight of individual molecules

is particularly sensitive to the number of large molecules. Thus the weight-average molecular weight, determined by light scattering

methods, would provide evidence as to whether polymer bridging between approaching particles was physically possible.

### 3.3.1 Rayleigh Scattering in Gases

Lord Rayleigh (43) in 1871 laid the foundation of light scattering by his application of electromagnetic theory to the problem of the scattering of light by molecules in a gas. According to Rayleigh, the electric field of the light incident upon an optically isotropic particle, whose radius is small compared to the wavelength of the light, induces an oscillating electric moment in the particle. The particle thus acts as a source of light whose intensity of scattering per unit volume is  $I$  when observed at a distance  $D$  and at an angle  $\Psi$  with respect to the incident beam. This light is perfectly plane polarized when viewed at right angles to the incident beam.

The complete equation for the intensity of light scattered by  $n$  independent small isotropic particles per unit volume has been derived in treatises on electromagnetic theory (44, 45) and is given by

$$I = 8\pi^4 B^2 n(1 + \cos^2 \Psi) I_0 / \lambda^4 D^2 \quad (3-8)$$

where  $I$  = intensity of scattered light per unit volume of the scattering system

$I_0$  = intensity of the incident beam

$D$  = distance of observer from the scattering system

$\Psi$  = angle between observer and incident beam

$\lambda$  = wavelength of light incident on the particles

$B$  = polarizability or induced dipole moment per unit electrical field strength of small isotropic particle

For small isotropic scatterers the angular intensity distribution is symmetrical; i. e., the intensity of scattered light in the forward direction is equal to that in the backward direction, and the fractional decrease in the intensity of the incident beam, now scattered in all directions, can be calculated. The logarithm of this fractional decrease in transmitted intensity,  $\ln I/I_0$  is termed the turbidity  $\tau$  (also called the attenuation or extinction coefficient due to scattering), where  $I = I_0 \exp(-\tau \ell)$  and  $\ell$  is the path length in the scattering system. Calculations (44, 45) show that for  $I$  perpendicular to the incident beam ( $\Psi = 90^\circ$ )

$$\tau = 16\pi D^2 I / 3I_0 \quad (3-9)$$

or on combining with equation (3-8)

$$\tau = 128\pi^5 B^2 n / 3\lambda^4 \quad (3-10)$$

### 3.3.2 Rayleigh Scattering in Liquids

A basic assumption of Rayleigh scattering in gases is the randomness of the relative positions of the gas molecules. In liquids this is not the case, and the scattered light intensity is reduced about

fifty-fold due to destructive interference between scattered light waves from different liquid molecules. Smoluchowski (46) and Einstein (47) traced the source of the existing scattered light to local thermal fluctuations in density that make the liquid optically inhomogeneous. Since the inhomogeneities in density are randomly distributed within the liquid, Rayleigh's equation can be modified to calculate the magnitude of solvent light scattering. In terms of experimentally measurable quantities, the turbidity is expressed as

$$\tau = 32\pi^3 (\mu\rho(d\mu/d\rho)kT K_o / 3\lambda^4) \quad (3-11)$$

where  $\mu$  = fluid refractive index

$\rho$  = fluid density

$k$  = Boltzmann's constant

$T$  = absolute temperature

$K_o$  = compressibility of liquid

### 3.3.3 Rayleigh Scattering from Molecules in Solution

In the case of an ideal gas, Maxwell (48) related the polarizability  $B$  of the isotropic particles to the dielectric constant of the gas  $\epsilon$ , and to the dielectric constant of the medium in which the gas particles reside,  $\epsilon_o$ , which in this case is a vacuum and  $\epsilon_o = 1$ . For a mixture of  $n$  isotropic particles, Maxwell's relation is

$$(\epsilon - \epsilon_0) / \epsilon_0 = 4\pi n B \quad (3-12)$$

Substituting equation (3-12) into equation (3-10) and using  $NC/MW$  for  $n$  (where  $N$  is Avogadro's number,  $C$  the weight concentration, and  $MW$  the molecular weight), results in

$$\tau = 8\pi^3 (MW)C ([\epsilon - \epsilon_0] / C)^2 / 3\lambda^4 N \quad (3-13)$$

In the case of small solute particles in solution, an analogy is made with the case of gas molecules in vacuum. The solute particles are assumed isotropic, small compared to the wavelength of light ( $r < \lambda/20$ ), and randomly distributed in the solvent. In addition, we assume that the scattering from the solute molecules alone can be obtained if the scattering from the solvent is subtracted from that of the solution. The specific dielectric increment,  $(\epsilon - \epsilon_0) / C$ , of equation (3-13) may be expressed in terms of the specific index of refraction increment  $(\mu - \mu_0) / C$ , where  $\mu$  and  $\mu_0$  are the indices of refraction of solute and solvent respectively, by

$$(\epsilon - \epsilon_0) / C = (\mu^2 - \mu_0^2) / C \approx d\mu^2 / dC \approx 2\mu_0 (\mu - \mu_0) / C \quad (3-14)$$

With this relationship, and knowing that additional light scattering arises from irregular changes in density and in refractive index due to fluctuations in composition, Debye (49) calculated the solution turbidity as

$$\tau = 32\pi^3 \mu_o^2 ((\mu - \mu_o)/C)^2 C(MW)/3N\lambda^4 \quad (3-15)$$

Putzeys and Brosteaux (50) were the first to verify the light scattering method as a useful means of determining the molecular weight of large molecules in solution by measuring the relative intensity of scattering from dilute protein solutions.

Substituting equation (3-14) into equation (3-12), and using  $NC/MW$  for  $n$  yields

$$B^2 = (\mu - \mu_o)^2 \mu_o^2 (MW)^2 / 4\pi^2 N^2 C^2 \quad (3-16)$$

and upon substituting this expression into equation (3-8), there results

$$I/I_o = 2\pi^2 \mu_o^2 (\mu - \mu_o)^2 (1 + \cos^2 \Psi) C(MW) / \lambda^4 D^2 NC^2 \quad (3-17)$$

The Rayleigh Ratio, defined as,

$$R_\Psi = ID^2 / I_o (1 + \cos^2 \Psi) \quad (3-18)$$

can be determined from equation (3-17) as

$$R_\Psi = 2\pi^2 \mu_o^2 (d\mu/dC)^2 C(MW) / \lambda^4 N = K_1 C(MW) \quad (3-19)$$

where  $K_1 = 2\pi^2 \mu_o^2 (d\mu/dC)^2 / N\lambda^4$

Consequently, the species molecular weight can be determined from the weight concentration and from two experimentally measured parameters,  $R_\Psi$  and  $K_1$ . These equations assume solution ideality in that the

scattering of  $n$  particles was equated with  $n$  times the scattering from a single particle, a situation valid only if the particles are entirely independent of one another. In actual solutions, the scattering must be modified to account for interference between molecules, such as the excluded volume effect, resulting in the introduction of virial coefficients to account for concentration fluctuations. Consequently for an ideal solution,

$$K_1 C / R_\Psi = 1 / MW \quad (3-20)$$

whereas for a nonideal solution

$$K_1 C / R_\Psi = 1 / MW + 2A_1 C + 3A_2 C^2 + \dots \quad (3-21)$$

whereas  $A_1$  and  $A_2$  are virial coefficients.

In addition to the virial coefficients introduced by concentration fluctuations, compensation must be made to include the interference between light scattered from points within a molecule of dimensions larger than  $\lambda/20$ , i. e., the Rayleigh-Gans factor  $P(\Psi)$ . Tanford (51) shows that  $P(\Psi)$  can be related to the particle radius of gyration by

$$P(\Psi) = 1 - (16\pi^2 R_g^2 / 3\lambda^2) \sin^2 \Psi / 2 \quad (3-22)$$

Introducing equation (3-22) into equation (3-21) results in

$$K_1 C / R_\psi = [1/P(\psi)] (1/MW + 2A_1 C) \quad (3-23)$$

or, using the approximate value of  $1/P(\psi)$  from equation (3-22)

$$K_1 C / R_\psi = [1 + (16\pi^2 R_g^2 / 3\lambda^2) \sin^2 \psi / 2] (1/MW + 2A_1 C) \quad (3-24)$$

Thus the polymer size, expressed as the radius of gyration  $R_g$ , can also be determined from the experimentally measured parameters  $R_\psi$  and  $K_1$ .

#### 3.4 Optimum Polymer Dose from Refiltration Theory

While studying the use of flocculating agents to improve the subsidence and filtration rates of phosphate slimes, LaMer, Smellie, and Lee (52-56) observed that the flow rate  $Q$  during refiltration was inversely proportional to the square of the effective particle surface area in a unit volume of filter cake,  $S_o$ .

$$Q = K_f S_o^{-2} \quad (3-25)$$

In addition, the amount of flocculating agent required to produce a maximum in filtration rate was also found to be directly related to the square of the specific surface area.

Smellie and LaMer (57) stated that the aggregating process was dependent upon the degree of particle surface site coverage  $\theta$  and upon the amount of uncovered surface sites per particle  $(1-\theta)$ . The rate of

floc formation,  $df/dt$ , was then proportional to the product of nuclei covered by flocculant  $n_o \theta$  times the concentration of nuclei with available open surface  $n_o (1-\theta)$ .

$$df/dt = k_1 n_o^2 \theta(1-\theta) \quad (3-26)$$

The resulting equation (3-26) is similar to Smoluchowski's equation for the coagulation of primary particles. The disintegration of flocs,  $-df/dt$ , was hypothesized to be proportional to the size (volume) of the floc, and inversely proportional to the surface of the floc times the binding factor  $\theta(1-\theta)$ .

$$-df/dt = k_2 d^3 / (d^2 \theta(1-\theta)) \quad (3-27)$$

At equilibrium,

$$d = k_1 n_o^2 \theta^2 (1-\theta)^2 / k_2 \quad (3-28)$$

Upon squaring (3-28) and substituting into equation (3-25) there results:

$$C_o^{1/2} / (Q - Q_o)^{1/8} = a + pC_o \quad (3-29)$$

where  $C_o$  = flocculant dosage

$Q$  = refiltration rate of flocculated suspension

$Q_o$  = refiltration rate of untreated suspension

The optimum flocculation dose,  $C_{opt}$ , is equal to the ratio of intercept to slope, i. e.,  $C_{opt} = a/p$ . If the optimum flocculant dose as determined by the refiltration technique corresponds to the optimum dose as measured by other independent methods, such as changes in the particle size distribution or changes in suspension turbidity, then this result supports the theory underlying equation (3-29).

The Smellie-LaMer refiltration technique for determination of optimum polymer dose has been successfully applied to many polymer-colloid systems. The method must be utilized with caution however as both theoretical and experimental difficulties have been encountered.

1. Smellie and LaMer assumed that for theoretical purposes, the flocs can be considered as essentially spherical in shape and composed of closely-packed primary particles. These tightly-bound aggregates have a smaller specific surface area than the dispersed primary particles, and consequently produce more rapid refiltration rates. The filter cake porosity was assumed to constant irrespective of flocculation condition, an assumption which must be verified independently for each polymer-colloid system.

2. The theoretical derivation of equation (3-29) contains an unjustifiable mathematical step (equation (18) of reference (57)) which leads to the equation:

$$Q - Q_o = Q_o k_1^2 w^4 \theta^4 (1-\theta)^4 / r^2 k_2^2 \quad (3-30)$$

where  $r$  = radius of primary particle

$w$  = solid content of suspension

$k_1, k_2$  = rate constants

Equation (3-30) states that the value of  $\theta = 0.5$ , i. e.,  $\theta^4(1-\theta)^4 = 1/256$ , leads to a maximum in  $Q - Q_o$ . If equation (3-30), and subsequently equation (3-29) are correct, then surface site coverages of the order 0.5 should be measured at the optimum flocculant dose in polymer studies.

The value of  $\theta = 0.5$  led Healy and LaMer (58-60) to postulate that polymer flocculation involved "bridging" between adjacent colloidal particles by extended polymer segments. The degree of flocculation at a particular polymer concentration was postulated to depend on the length and number of extended segments, and the available surface sites onto which the extended segments can bridge. Simultaneous adsorption and refiltration experiments revealed that the fraction of adsorbed segments to extended segments was less than 1/4 (59), and that optimum flocculation occurred when approximately one-half of available surface sites are covered by adsorbed polymer (60). Values of  $\theta$  greater than 0.5 resulted in oversaturation of surface sites with polymer, leaving too few sites available for bridging, and the particles remained dispersed.

3. Determination of the optimum polymer dose from equation (3-29) can be difficult due to the lack of sensitivity of the 8<sup>th</sup> root of the filtration rate. If a particular polymer species produces only limited flocculation over a broad concentration range, equation (3-29) will be especially difficult to apply.

### 3.5 Intercellular Structure from Electron Microscopy

Direct evidence as to the mechanism of agglutination and the structure of the aggregates is at least theoretically available through electron microscope studies of the aggregates. In spite of inherent difficulties in sample preparation, especially surface tension forces which pull the colloid-polymer system together on evaporation of the dispersing medium, the electron microscope offers the possibility of unequivocally establishing or disproving polymeric bridging.

#### 3.5.1 Biocolloids Flocculated with Anionic Polymers

In three early studies on the clumping of bacteria cells, the investigators (61-63) utilized the electron microscope to visualize the final structure of the cell aggregates. Warren and Gray (61) observed a viscous, extracellular, polymeric material binding cells of Pseudomonas aeruginosa. The cementing properties of this intercellular substance, isolated and identified as a polysaccharide, were removed upon incubation of the cells in hyaluronidase. Clark (62) photographed cells

of Nocardia corallina clumped together with the sticky slime layer which normally adheres tightly to the cells. Clark stated that shrinkage (dehydration) of the cells during grid preparation accentuated the appearance of the slime layer, since it was observed only between cells which were close together and which had probably, at some time prior to preparation of the specimens, been in direct contact. Stanley and Rose (63) also noted an electron-dense material distributed over the surface of Corynebacterium xerosis cells, which bound the cells together. These clumps were formed only in the presence of salts, indicating that the stickiness may have been caused by formation of salt bridges between protein groups on the surfaces of adjacent bacteria. The ability of the bacteria in the clumps to remain at least partially in contact after preparation for electron microscopy testified more to the mechanical strength of the adhesive material than to a bridging mechanism of formation.

A thorough study of the structure and composition of the zoogloal matrix surrounding Zoogloea ramigera by Friedman et al. (68,69) revealed exocellular fibrillar polymers, which produced flocculation either through entanglement of cells among fibrils, or adsorption of cells to fibrils. The fibril polymer produced by the Zoogloea ramigera was determined to be a polyglucose, susceptible to cellulase. Using three different grid preparation techniques; freeze-etching,

shadow casting, and thin sectioning, Friedman et al. (68,69) observed the exocellular polymer forming a matrix-like structure linking the bacteria cells, thereby supporting the polymer bridging theory.

### 3.5.2 Colloids Flocculated with Cationic Polymers

In 1959, Katchalsky et al. (70) used the electron microscope to study the seam of agglutination between red blood cells agglutinated by the polybase, poly-L-lysine. They noted significant deformation in shape of the red blood cells agglutinated by polylysine, and "bridges" in the narrow area of contact. The length of these bridges, or the thickness of the seam of agglutination, was found to correspond to the length of the fully-extended polylysine molecule, based on the known degree of polymerization. Washing the polybase-induced aggregates with physiological saline removed surface polylysine, but enough remained between the cells to maintain the state of aggregation. Since the agglutinated red blood cells were dehydrated prior to thin-sectioning, it is possible that the cells were in direct contact after flocculation, but the dehydration process caused the cells to separate to the extent allowed by the length of the lysine molecule.

In a study of the flocculant behavior of cationic polymers on inorganic colloids, Ries and Meyers (64) obtained electron micrographs showing ribbon-like polymeric fibers stretching between aggregates of both silica and polystyrene latex. Some fiber diameters

appear to be 20 to 30 Å in diameter, which approximates the expected diameter for single polymer chains of the cationic polymer (2-vinylimidazole) used. Other fiber diameters appear to be from 200 to 300 Å, attributed to surface tension forces pulling together the polymer molecules upon evaporation of the dispersing medium. The electron micrographs, prepared by shadow-casting with a gold-palladium alloy, show bridging fibers extending radially between aggregates of cells, but present no information as to the structure between cells of an aggregate. Both the silica and polystyrene latex particles appear very tightly bound together, with no recognizable seam of agglutination.

## REFERENCES CITED

## CHAPTER 3

1. Stumm, W., and O'Melia, C. R., "Stoichiometry of Coagulation", Journal American Water Works Association, 60 (1968), 514-539.
2. Stumm, W., and Morgan, J. J., Aquatic Chemistry, Wiley-Interscience, New York, 1970.
3. Langmuir, I., "The Adsorption of Gases on Plane Surfaces of Glass, Mica, and Platinum", American Chemical Society, 40 (1918), 1361-1389.
4. Frisch, H. L., Simha, R., and Eirich, F. R., "Statistical Mechanics of Polymer Adsorption", Journal Chemical Physics, 21 (1953), 365-366.
5. Simha, R., Frisch, H. L., and Eirich, F. R., "The Adsorption of Flexible Macromolecules", Journal Physical Chemistry, 57 (1953), 584-589.
6. Frisch, H. L., and Simha, R., "The Adsorption of Flexible Macromolecules II", Journal Physical Chemistry, 58 (1954), 507-512.
7. Frisch, H. L., "Polymer Chain Configuration Near a Boundary Exerting Forces", Journal Physical Chemistry, 59 (1955), 633-636.
8. Frisch, H. L., and Simha, R., "Monolayers of Linear Macromolecules", Journal Chemical Physics, 24 (1956), 652-655.
9. Frisch, H. L., and Simha, R., "Statistical Mechanics of Flexible High Polymers at Surfaces", Journal Chemical Physics, 27 (1957), 702-706.
10. Higuchi, W. I., "Effects of Short Range Surface-Segment Forces on the Configuration of an Adsorbed Flexible Chain Polymer", Journal Physical Chemistry, 65 (1961), 487-491.

11. Silberberg, A., "The Adsorption of Flexible Macromolecules. Part I. The Isolated Macromolecule at a Plane Interface", Journal Physical Chemistry, 66 (1962), 1872-1883.
12. Silberberg, A., "The Adsorption of Flexible Macromolecules. Part II. The Shape of the Adsorbed Molecule; The Adsorption Isotherm, Surface Tension, and Pressure", Journal Physical Chemistry, 66 (1962), 1884-1907.
13. DiMarzio, E. A., "Proper Accounting of Conformations of a Polymer Near a Surface", Journal Chemical Physics, 42 (1965), 2101-2106.
14. DiMarzio, A. E. and McCrackin, F. L., "One-Dimensional Model of Polymer Adsorption", Journal Chemical Physics, 43 (1965), 539-547.
15. Hovee, C. A., "Density Distribution of Polymer Segments in the Vicinity of an Adsorbing Interface", Journal Chemical Physics, 43 (1965), 3007-3008.
16. Roe, R. J., "Conformation of an Isolated Polymer Molecule at an Interface. II. Dependence on Molecular Weight", Journal Chemical Physics, 43 (1965), 1591-1598.
17. Rubin, R. J., "A Random Walk Model of Chain Polymer Adsorption at a Surface. II. Effect of Correlation Between Neighboring Steps", Journal Research of National Bureau of Standards, 69B (1965), 301-312.
18. McCrackin, F. L., "Configuration of Isolated Polymer Molecules Adsorbed on Solid Surfaces Studied by Monte Carlo Computer Simulations", Journal Chemical Physics, 47 (1967), 1980-1986.
19. Silberberg, A., "Adsorption of Flexible Macromolecules. III. Generalized Treatment of the Isolated Macromolecule; The Effect of Self- Exclusion", Journal Chemical Physics, 46 (1967), 1105-1114.
20. Silberberg, A., "Adsorption of Flexible Macromolecules. IV. Effect of Solvent-Solute Interactions, Solute Concentration, and Molecular Weight", Journal Chemical Physics, 48 (1968), 2835-2851.

21. Motomura, K., and Mutuura, R., "Conformation of Adsorbed Polymeric Chain, II", Journal Chemical Physics, 50 (1969), 1281-1287.
22. Koral, J., Ullman, R., and Eirich, F., "The Adsorption of Polyvinyl Acetate", Journal Physical Chemistry, 62 (1958), 541-550.
23. Binford, J. S., and Gessler, A M , "Multisegment Adsorption of Long Chain Polymers on Carbon Black", Journal Physical Chemistry, 63 (1959), 1376-1378.
24. Peterson, C., and Kwei, T. K., "The Kinetics of Polymer Adsorption onto Solid Surfaces", Journal Physical Chemistry, 65 (1961), 1330-1333.
25. Perkel, R., and Ullman, R., "The Adsorption of Polydimethylsiloxanes from Solution", Journal Polymer Science, 54 (1961), 127-148.
26. Fontana, B. J., and Thomas, J. R., "The Configuration of Adsorbed Alkyl Methacrylate Polymers by Infrared and Sedimentation Studies", Journal Physical Chemistry, 65 (1961), 480-487.
27. Fontana, B. J., "The Configuration of an Adsorbed Polymeric Dispersant by Infrared Studies", Journal Physical Chemistry, 67 (1963), 2360-2362.
28. Steinberg, G., "On the Configuration of Polymers at the Solid Liquid Interface", Journal Physical Chemistry, 71 (1967), 292-301.
29. Black, A. P., Birkner, F. B., and Morgan, J. J., "Destabilization of Dilute Clay Suspensions with Labeled Polymers", Journal American Water Works Association, 57 (1965), 1547-1560.
30. Black, A. P., Birkner, F. B., and Morgan, J. J., "The Effect of Polymer Adsorption on the Electrokinetic Stability of Dilute Clay Suspensions", Journal Colloid and Interface Science, 21 (1966), 626-648.

31. Birkner, F. B., and Edzwald, J. K., "Nonionic Polymer Flocculation of Dilute Clay Suspensions", Journal American Water Works Association, 61 (1969), 645-651.
32. Ohrn, O. E., "Preliminary Report on the Influence of Adsorption on Capillary Dimensions of Viscometers", Journal Polymer Science, 17 (1955), 137-140.
33. Tuijnman, C. A., and Hermans, J. J., "Precision Viscometry of Polyvinyl Acetate in Toluene", Journal Polymer Science, 25 (1957), 385-401.
34. Huque, M. M., Fishman, M., and Goring, D. A., "The Sorption Effect of Cellulose Trinitrate in Capillary Viscometry", Journal Physical Chemistry, 63 (1959), 766-768.
35. Fendler, H. G., Rohleder, H., and Stuart, H. A., "Adsorption Effects Determined by the Measurement of Specific Viscosity", Makromolekulare Chemie, 18/19 (1956), 383-396.
36. Gottlieb, M. H., "Measurement of the Surface Potentials of Metals Due to Adsorption of Organic Compounds from Solution", Journal Physical Chemistry, 64 (1960), 427-432.
37. Thies, C., "The Adsorption of Polystyrene-Poly(methyl methacrylate) Mixtures at a Solid-Liquid Interface", Journal Physical Chemistry, 70 (1966), 3783-3790.
38. Peyser, P., Tutas, D. J., and Stromberg, R. R., "Conformation of Polyesters Adsorbed on Solid Surfaces", Journal Polymer Science Part A-1, 5 (1967), 651-663.
39. Kipling, J. J., Adsorption from Solutions of Non-Electrolytes, Academic Press Inc., New York, 1965.
40. Thies, C., Peyser, P., and Ullman, R., Proceedings 4th International Congress Surface Activity, Brussels, 1967.
41. Moyer, L. S., "Changes in the Electrokinetic Potential of Bacteria at Various Phases of the Culture Cycle", Bacteriology, 32 (1936), 433-464.
42. Dyar, M. T., and Ordal, E. J., "The Effects of Surface-active Agents on the Electrophoretic Mobilities of Bacteria", Bacteriology, 51 (1946), 149-167.

43. Rayleigh, O. M., Philosophical Magazine, 41 (1871), 447.
44. Born, M., Optik, J. Springer, Berlin, 1933.
45. Stratton, J. A., Electromagnetic Theory, McGraw-Hill Book Co., Inc., New York, 1944.
46. Smoluchowski, M. V., "Molekular kinetische Theorie der Opaleszenz von Gasen im Kritischen Zustande, sowie einiger verwandter Erscheinungen", Annalen Der Physik, 25 (1908), 205-226.
47. Einstein, A., "Theorie der Opaleszenz von homogenen Flussigkeiten und Flussigkeitgemischen in der Nahe des kritischen Zustandes", Annalen Der Physik, 33 (1910), 1275-1298.
48. Jeans, J., Electricity and Magnetism, 5th Edition, Cambridge University Press, London, 1925.
49. Debye, P., "Light Scattering in Solutions", Journal Applied Physics, 15 (1944), 338-342.
50. Putzeys, P., and Brosteaux, J., "The Scattering of Light in Protein Solutions", Transactions of the Faraday Society, 31 (1935), 1314-1325.
51. Tanford, C., Physical Chemistry of Macromolecules, John Wiley and Sons, New York, 1961, 302-305.
52. LaMer, V. K., and Smellie, R. H., "Flocculation, Subsidence, and Filtration of Phosphate Slimes. I. General", Journal Colloid Science, 11 (1956), 704-709.
53. LaMer, V. K., and Smellie, R. H., "Flocculation, Subsidence, and Filtration of Phosphate Slimes. II. Starches as Agents for Improving Flocculation, Subsidence, and Filtration of Phosphate Slimes", Journal Colloid Science, 11 (1956), 710-719.
54. Smellie, R. H., and LaMer, V. K., "Flocculation, Subsidence, and Filtration of Phosphate Slimes. III. Subsidence Behavior", Journal Colloid Science, 11 (1956), 720-731.

55. LaMer, V. K., Smellie, R. H., and Lee, P. K., "Flocculation, Subsidence, and Filtration of Phosphate Slimes. IV. Flocculation by Gums and Polyelectrolytes, and Their Influence on Filtration Rate", Journal Colloid Science, 12 (1957), 230-239.
56. LaMer, V. K., Smellie, R. H., and Lee, P. K., "Flocculation, Subsidence, and Filtration of Phosphate Slimes. V. The Optimum Filtration Rate as a Function of Solid Content and Specific Area", Journal Colloid Science, 12 (1957), 566-574.
57. Smellie, R. H., and LaMer, V. K., "Flocculation, Subsidence, and Filtration of Phosphate Slimes. VI. A Quantitative Theory of Filtration of Flocculated Suspensions", Journal Colloid Science, 13 (1958), 589-599.
58. Healy, T. W., and LaMer, V. K., "The Adsorption-Flocculation Reactions of a Polymer with an Aqueous Colloidal Dispersion", Journal Physical Chemistry, 66 (1962), 1835-1838.
59. LaMer, V. K., and Healy, T. W., "Adsorption-Flocculation Reactions of Macromolecules at the Solid-Liquid Interface", Review of Pure and Applied Chemistry, 13 (1963), 112-133.
60. LaMer, V. K., and Healy, T. W., "The Role of Filtration in Investigating Flocculation and Redispersion of Colloidal Dispersions", Journal Physical Chemistry, 67 (1965), 2417-2420.
61. Warren, G. H., and Gray, J., "Studies on the Properties of a Polysaccharide Constituent Produced by Pseudomonas aeruginosa", Journal Bacteriology, 70 (1955), 152-157.
62. Clark, J. B., "Slime as a Possible Factor in Cell Clumping in Nocardia corallina", Journal Bacteriology, 75 (1958), 400-402.
63. Stanley, S. O., and Rose, A. H., "On the Clumping of Corynebacterium xerosis as Affected by Temperature", Journal General Microbiology, 48 (1967), 9-23.
64. Ries, H. E., and Meyers, B. L., "Microelectrophoresis and Electron Microscope Studies of Polymeric Flocculants", Journal Applied Polymer Science, 15 (1971), 2023-2034.

65. Giles, C. H., MacEwan, T. H., Nakhwa, S. N., and Smith, D., "Studies in Adsorption. Part XI. A System of Classification of Solution Adsorption Isotherms, and its Use in Diagnosis of Adsorption Mechanisms and in Measurement of Specific Surface Areas of Solids", Chemical Society (London), 1960 (1960), 3973-3993.
66. Jenckel, E., and Rumbach, B., "The Adsorption of High Molecular Weight Materials from Solution", Zeitschifte Electrochemie, 55 (1951), 612-618.
67. Kasper, D. R., "Theoretical and Experimental Investigations of the Flocculation of Charged Particles in Aqueous Solutions by Polyelectrolytes of Opposite Charge", Ph.D. Thesis, California Institute of Technology, 1971.
68. Friedman, B. A., Dugan, P. R., Pfister, R. M., and Remsen, C. C., "Structure of Exocellular Polymers and Their Relationship to Bacterial Flocculation", Journal Bacteriology, 98 (1969), 1328-1334.
69. Friedman, B. A., Dugan, P. R., Pfister, R. M., and Remsen, C. C., "Fine Structure and Composition of the Zoogloal Matrix Surrounding Zoogloea ramigera", Journal Bacteriology, 96 (1968), 2144-2153.
70. Katchalsky, E., Danon, D., and Nevo, A., "Interactions of Basic Polyelectrolytes with the Red Blood Cell. II. Agglutination of Red Blood Cells by Polymeric Bases", Biochimica Et Biophysica Acta, 33 (1959), 128-138.

## Chapter 4

MECHANISM OF E. COLI AGGREGATION BY PEI

In the preceding chapter much of the evidence for flocculation of a colloid with an oppositely-charged polyelectrolyte points to the adsorption coagulation mechanism, though phenomena attributed to either the physical double-layer theory or the polymer bridging theory are also observed in some systems. Experiments in this chapter were designed to compare the characteristics of the negative colloid (E. coli)-cationic polymer (PEI) system with those anticipated for the three major coagulation models (1,2). These experiments, and the results anticipated for each aggregation model, are summarized in Table 4.1.

PEI polymers of varying molecular weights were selected for this research as a means to investigate further the charge mosaic model of colloid flocculation. Strongly-adsorbed high-molecular-weight species should produce areas of high positive charge density surrounded by large expanses of weak negative charge, resulting in strong mutual attraction between particles. With low-molecular-weight species, the adsorbed charge should be spread more uniformly over the particle surface, resulting in a lesser electrostatic attraction and poorer flocculation.

If the PEI molecules, known to possess an open three-dimensional branched structure in solution, are literally pancaked onto

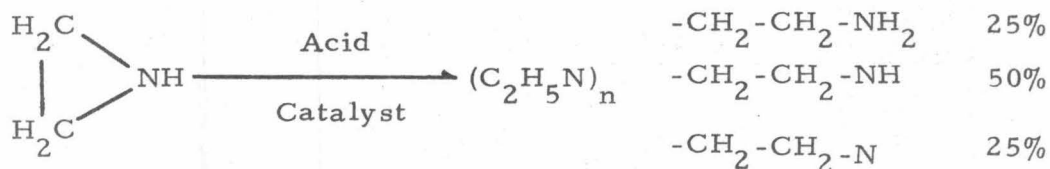
<u>Phenomena Adsorption</u>	<u>Physical Double Layer</u>	<u>Adsorption Coagulation</u>	<u>Polymer Bridging</u>
configuration of adsorbed polymer molecules at saturation	no effect	$A_s = c(MW)^\beta$ $0 < \beta < 1$	$A_s = c(MW)^\beta$ $\beta \approx 1$
surface site coverage	no effect	$\theta < 0.5$ at optimum $0 < \theta < 1.0$ in general	$\theta = 0.5$ at optimum $0 < \theta < 1.0$ in general
monolayers of surface coverage	no effect	monolayers limited by strength of adsorption forces	many monolayers possible
addition of excess polymer	no effect	possible restabilization from charge reversal	restabilization from complete site coverage or charge reversal
<u>Electrophoretic Mobility</u>			
mobility at optimum aggregation	near zero	not necessarily zero	usually not zero
mobility at excess cationic polymer	no effect	possible reversal from excess adsorption	possible reversal from excess adsorption
<u>Polymer Size and Configuration</u>	no effect	size sufficient to create charge mosaic	length sufficient to bridge particles
<u>Refiltration Rate</u>	poor filterability	widely-varying filterability	excellent filterability
<u>Intercellular Structure</u>	closely packed	closely packed	open, three-dimensional

Table 4.1 Summary of Anticipated Characteristics of E. coli-PEI Floccs Based on Three Major Coagulation Models.

the E. coli surface by the electrostatic attraction (degree of surface site coverage  $\theta \ll 0.5$ ), then successful flocculation provides good evidence of the charge mosaic model. Alternatively, the PEI molecules may adsorb through only a few monomer segments closest to the surface (degree of surface site coverage  $\theta \geq 0.5$ ), resulting in a tumbleweed configuration sticking out from the surface. The polymer molecule, prevented by steric hindrance from totally adsorbing could then serve as a polymer bridge between colliding particles. The degree of surface site coverage will determine which mechanism is predominant at optimum flocculation.

#### 4.1 Experimental Materials

A series of polyethyleneimine (PEI) polymers were selected because of the range of molecular weights available from 600 to 60,000 corresponding to 14 to 1400 monomer ( $C_2NH_5$ ) units. Polyethyleneimine is highly-branched polyamine produced by the acid-catalyzed polymerization of the monomer, ethyleneimine. The polymer is composed of units which have two carbons per nitrogen, and these units are randomly distributed in the approximate ratios of one primary amino nitrogen/two secondary amino nitrogens/one tertiary amino nitrogen.



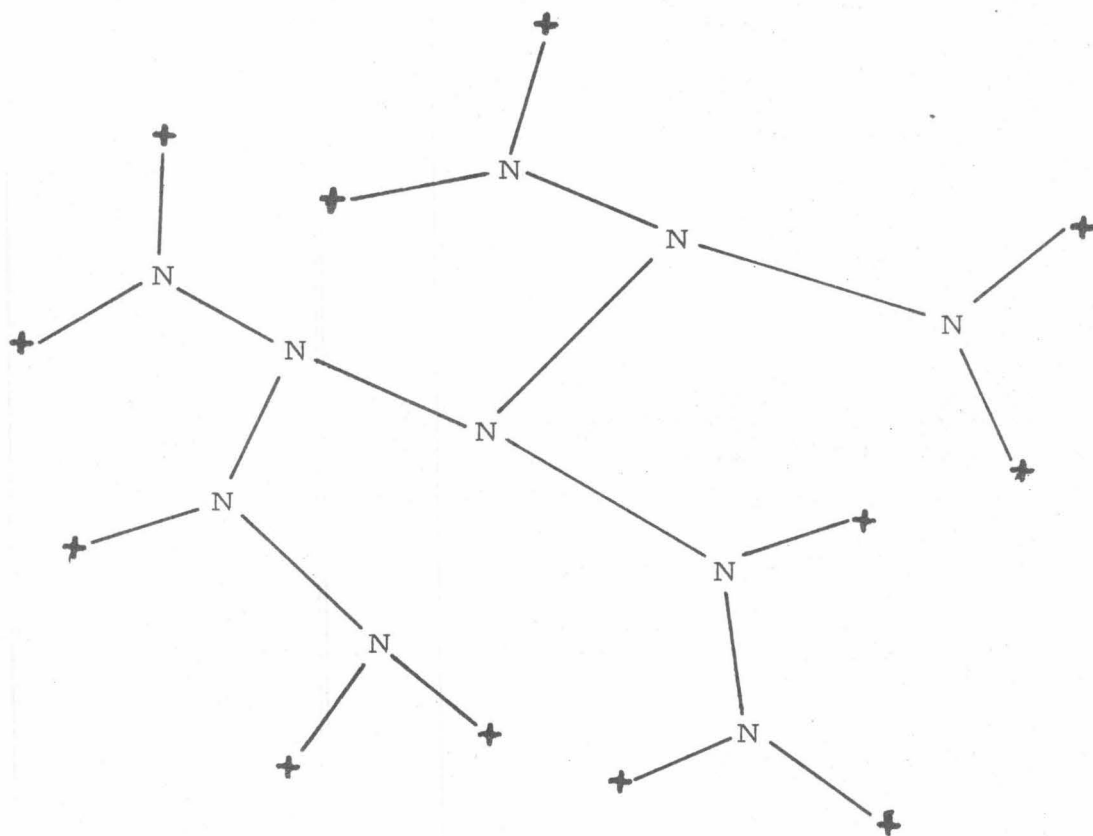


Figure 4.1 Solution Configuration of PEI Molecule. Branch Points Account for Approximately 25% of Total Amino Nitrogens.

<u>Property</u>	<u>PEI 6</u>	<u>PEI 12</u>	<u>PEI 18</u>	<u>PEI 350</u>	<u>PEI 600</u>
Manufacturer	DOW	DOW	DOW	Borden	DOW
Nominal MW (number-average)MW <sub>n</sub>	600	1200	1800	35,000 <sup>(1)</sup>	40,000-60,000 <sup>(1)</sup>
Molecular Weight <sup>(2)</sup> (number-average)MW <sub>n</sub>	500	1300	1900	---	---
Monomer Units (C <sub>2</sub> H <sub>5</sub> N)	14	28	42	810	930-1400
Molecular Weight <sup>(3)</sup> (weight-average)MW <sub>w</sub>	3.4x10 <sup>4</sup>	6.7x10 <sup>4</sup>	1.0x10 <sup>5</sup>	1.0x10 <sup>6</sup>	3.4x10 <sup>6</sup>
Radius of Gyration <sup>(3)</sup> (R <sub>g</sub> in Å)	70	110	150	750	1760

(1) Number-average molecular weight determined by manufacturer via gel chromatography.

(2) Number-average molecular weights determined from freezing point depression in 0.06 M NaCl. Higher molecular weight species cannot be measured in this way.

(3) Weight-average molecular weights and radius of gyration determined from light scattering measurements. (Section 4.3.1).

Table 4.2 summarizes the molecular weight data for the five molecular weight species of PEI used in all experiments.

Table 4.2 Molecular Weight Data for PEI Species

This distribution of amino nitrogens yields a spheroid-shaped molecule with many branched segments: the tertiary amino nitrogens being the branching sites and the primary amino nitrogens being the terminal groups of each segment.

When PEI is placed in solution, the amino nitrogens react to form positively-charged nitrogens in the same manner as simple amines, thereby forming alkaline solutions. Since PEI is composed of many nitrogens per molecule, there will be a multiplicity of positive charges on each molecule. The titration of PEI with strong acids demonstrates that the degree of protonation normally does not exceed 80% of the total basic nitrogens. Although the titration of aqueous PEI with an acid (such as HCl) does not yield a break suitable for determination of the end point, titration of PEI in acetic acid solvent with perchloric acid does yield such an inflection. Failure to neutralize all the amino groups is attributed to reduced basicity of specific amino groups as adjacent amino groups become protonated. PEI in solution functions as a cationic polyelectrolyte, strongly attracted to anionically-charged colloids (3).

The E. coli, strain CR63, were grown in batch culture to a cell concentration of  $9.0 (\pm 1.0) \times 10^8$  cells/ml in the following media.

<u>Ingredient</u>	<u>gm/l</u>
Casamino Acid	1.20
Glucose	4.00
NH <sub>4</sub> Cl	1.00
NaCl	1.75
KH <sub>2</sub> PO <sub>4</sub>	0.10
Collidine-HCl Buffer pH 7.0	50 ml/l
MgSO <sub>4</sub> 1M	2 ml/l
FeCl <sub>3</sub> 10 <sup>-3</sup> M	1ml/l

A constant temperature of 25<sup>o</sup>C was maintained in a jacketed chemostat, along with a constant pH of 7.0 (± 0.1). The stationary-phase cells were removed from the chemostat, centrifuged for 30 minutes at 1530 g, and separated from the growth supernatant. The cells were then resuspended in filtered 0.06 M NaCl and the pH adjusted to 7.0 via addition of 0.1 M NaOH. The separation of cells from growth media was essential since the media reacted with the indicator for polyethyleneimine.

## 4.2 Experimental Methods

### 4.2.1 Light Scattering from PEI Solutions

The weight-average molecular weights of three PEI species were determined in 0.6 M NaCl via light scattering measurements at nine angles ranging from 45<sup>o</sup> to 135<sup>o</sup>. A Brice-Phoenix light scattering photometer Model 2000 with a cylindrical cell (Brice-Phoenix catalog

number C101) was used to obtain experimental data. The cylindrical cell was filled with 50 ml of polymer solution and measurements were made at a wavelength of 546 nm monochromatic light (410 nm in solution). The polymer solutions were filtered through a 0.45  $\mu\text{m}$  Millipore filter directly into the light scattering cell to remove dust particles. Data were taken at three different polymer concentrations: 0.05, 0.1, and 0.5 percent by weight.

The refractive indices of the different polymer weight concentrations were measured with a Bausch & Lomb Dipping Refractometer. This instrument accurately measures the polymer solution refractive index to within 0.00004 at 22.0 $^{\circ}\text{C}$  in white light. The instrument was calibrated with NaCl solutions as specified in the Bausch & Lomb Operators Manual. The polymer refractive indices were checked with a Zeiss Abbe Refractometer, operated at 25 $^{\circ}\text{C}$  in yellow sodium light. However, these measurements are accurate only to the fourth decimal place, thereby making them inadequate for use in computing the differential refractive index.

#### 4.2.2 Determination of Residual PEI Concentration

The amount of PEI adsorbed was measured by mixing a known amount of polymer with an E. coli suspension, centrifuging this suspension to remove the polymer-coated bacteria, and then determining

the residual polymer concentration in the supernatant.

Five milliliters of a predetermined concentration of PEI were added to a 45 ml sample of the resuspended cells. This suspension was vigorously shaken for two minutes, then gently swirled for 18 minutes. The suspension was then centrifuged for 30 minutes at 4150 g, which removed more than 99.9% of the E. coli cells from the suspension. The centrifugate was then analyzed for residual polymer by a spectrophotometric method developed by DOW Chemical Company (3). The method involves the complexation of the residual polyethylenimine with 1,2 naphthoquinone-4-sulfonic acid: this colored complex exhibits maximum absorbance at 450 nm and obeys the Beer-Lambert Law in the polymer concentration range of 0 to 12 ppm based on a 50 ml sample. This range can be increased or decreased by varying the sample size.

The DOW procedure requires the following reagents:

1. A freshly prepared 0.05% 1,2 Naphthoquinone-4-sulfonic solution in distilled water.
2. A 2% trisodium phosphate solution in distilled water.
3. A standard 100 ppm polyethylenimine solution in distilled water.

A reference curve is prepared by pipetting 0, 2, 4, 6, 8, 10 and 12 ml of a 100 ppm standard PEI solution into respective polyethylene bottles.

These solutions are diluted to about 50 ml each with distilled water, after which 3 ml of trisodium phosphate and 10 ml of the naphthoquinone reagent are added. The solution is brought to a total volume of 100 ml with distilled water, and then let stand for exactly 60 minutes. The solution absorbance was measured at 450 nm in the 1 cm cell of a Gilford Model 300 Spectrophotometer.

This reference procedure was followed to measure the absorbance of the initial polymer dose, the centrifugate from the polymer-E. coli solution, and the centrifugate from a blank E. coli suspension. Depending on the initial PEI dosage, centrifugate samples from 1 to 50 ml were required. The amount of polymer adsorbed on the surface of the E. coli was calculated as the sum of the polymer dose and the blank E. coli reading minus the residual polymer concentration in the PEI-E. coli centrifugate.

Polyethylene bottles and centrifuge tubes were used with all PEI and PEI-E. coli suspensions to minimize loss of polymer caused by adsorption on the surface of equipment. Rembaum et al. (4) found that the polyethylene surface produced the least amount of adsorption in their experiments with ionene polymers. The polyethylene bottles and centrifuge tubes were presoaked at the polymer dosage of each experiment, then briefly rinsed with distilled water. This presoaking procedure was found effective by Kasper (5) in saturating adsorption sites of the

experimental equipment. In addition, the cell concentration of  $9.0 (\pm 1.0) \times 10^8$  cells/ml provides a surface area for 45 ml of E. coli of  $2,430 \text{ cm}^2$  which is 20 times larger than the  $125 \text{ cm}^2$  interior surface area of the polyethylene bottles used in these experiments. Finally, since the adsorbed polymer was determined as the difference between a blank and a residual concentration, adsorption losses to polyethylene bottles and centrifuge tubes will be compensated for in the calculations.

#### 4.2.3 Electrophoretic Mobility Experiments

The electrophoretic mobilities of E. coli-PEI suspension were measured in a Briggs-type cell (6) following the recommendations for improvement of Black and Smith (7, 8). In addition, palladium electrodes were used since they permitted high current densities without evolving gas. These electrodes were charged daily with atomic hydrogen by cathodic electrolysis, as per Neihof (9). Samples of cell aggregates for electrophoretic mobility determination were removed from the stirrer-reactor assembly (Figure 4.2) and placed directly into the Briggs cell. Settling of flocculated cells at optimum polymer concentrations was minimized by circulating the suspension back and forth through the cell by pressing a rubber bulb attached to the cell. The mobilities of 10 cells (or aggregates of cells) were recorded for both directions of current flow at each polymer concentration.

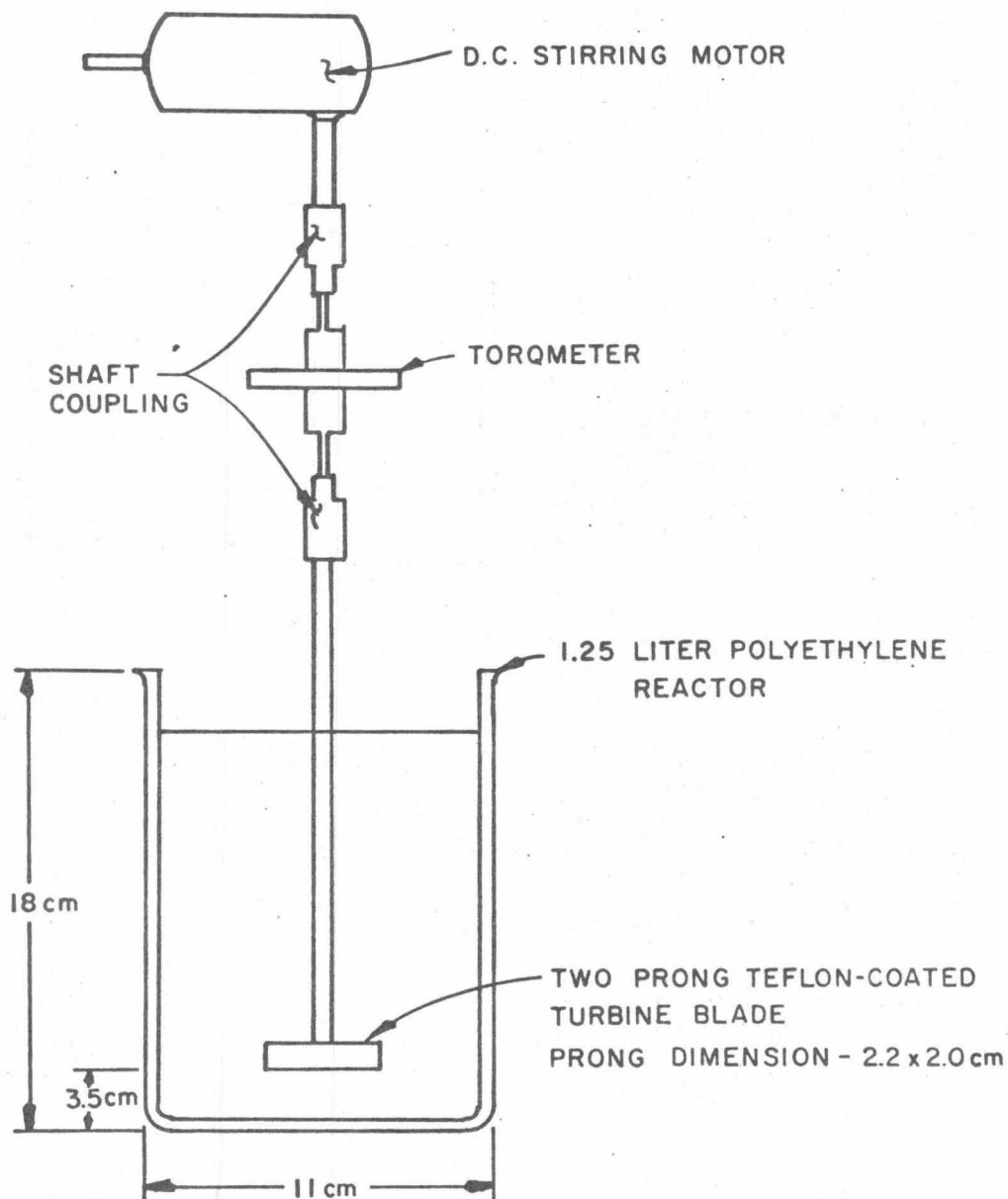


Figure 4.2 Stirrer-Reactor Assembly Used to Produce *E. coli*-PEI Flocculation for Electrophoretic Mobility, Refiltration, Turbidity, and Particle Size Distribution Experiments.

#### 4.2.4 Refiltration Rate Experiments

Refiltration rate experiments were conducted utilizing the procedure of LaMer et al. (10). After 60 minutes of flocculation in the stirrer-reactor assembly (Figure 4.2) at a specified mixing intensity, 50 milliliters of the PEI-E. coli suspensions were removed and forced through a 0.45  $\mu\text{m}$  Millipore filter at a pressure differential  $\Delta P$  of 74 cm Hg. The filtrate was collected and refiltered through the filter cake and 0.45  $\mu\text{m}$  filter. The volume flow rate of the flocculated suspension was recorded as the refiltration rate  $Q$ , and that of an untreated suspension as  $Q_0$ . The cell concentration was  $2.5 (\pm 0.5) \times 10^7$  cells/ml, the pH 7.0, the ionic strength 0.06 M NaCl, and the temperature  $25^\circ\text{C}$ .

#### 4.2.5 Preparation of Flocculated Cells for Electron Microscopy

E. coli cells, grown and washed as per Section 4.1 experiments, were diluted in filtered 0.6 M NaCl to a final cell concentration of  $10^8$  cells/ml. During a two minute rapid mix, 10 milliliters of PEI were added to 90 milliliters of the E. coli suspension to produce final concentrations of either 5.0 mg/l PEI 6 or 0.5 mg/l PEI 350. These doses are approximately the optimum flocculation doses for the representative molecular weight species. The PEI-E. coli suspensions were then gently swirled for 20 minutes. After this flocculation period, a

few milliliters were pipetted from the polyethylene reactor vessel, and placed on a 0.5  $\mu\text{m}$  Nucleopore filter.

Following a 10 minute sedimentation period, the flocs were fixed for 30 minutes in 25% gluteraldehyde in 0.6 M NaCl. The fixation step is required to stop metabolic processes and to stabilize the flocs during subsequent steps. Water was removed from the flocs by taking the sample through a series of alcohol solutions: 15 minutes at 30% alcohol, 15 minutes at 50% alcohol, 30 minutes at 70% alcohol, and 30 minutes at 90% alcohol. The alcohol was removed by critical point drying in freon. The flocs, still on the Nucleopore filter, are placed in freon TC in a chilled bomb. The bomb is sealed, and the freon TC is replaced by freon 13 by diluting it out. The bomb is then heated so that the freon changes from a liquid to a gas. The gas is then released slowly so that condensation does not occur. The dried Nucleopore filter with E. coli flocs was then sliced into small strips, which were glued to scanning microscope studs with silver paint. Finally, these studs were shadowed with gold-platinum alloy to increase the electron density of the surface structures, followed by carbon evaporation to enhance the strength of the floc structure. Flocs which had sedimented to the surface of the Nucleopore filter were examined in an Autoscan Scanning Electron Microscope.

### 4.3 Experimental Results

#### 4.3.1 PEI Molecular Weight and Size

In a method devised by Zimm (11), experimental light scattering data are extrapolated to zero polymer concentration and zero scattering angle on the same graph. The extrapolation to zero concentration is necessary to eliminate molecular interactions at the higher concentrations required for light scattering measurements; the extrapolation to zero angle is required since at a  $0^\circ$  setting, the photocell cannot differentiate between the scattered and transmitted light intensities.

The quantity  $K_1 C / R_\psi$  has been graphed versus  $(\sin^2 \psi / 2 + kC)$ , where  $k$  is an arbitrary constant, providing a convenient graphical scale. For each measurement of  $R_\psi$  (at a particular value of  $\psi$  and  $C$ ) we measure a distance  $\sin^2 \psi / 2 + kC$  on the abscissa and plot the corresponding value of  $K_1 C / R_\psi$  as the ordinate. On the Zimm plot, the molecular weight is determined as the reciprocal of the intercept of the zero concentration line, the zero angle line, and the ordinate axis. The intersection of these three lines at a single point indicates good experimental data.

The resulting Zimm plots for the two high molecular weight PEI species are shown in Figure 4.3 and 4.4. On each figure, the line denoted by  $0^\circ$  represents the sample scattering at various concentrations

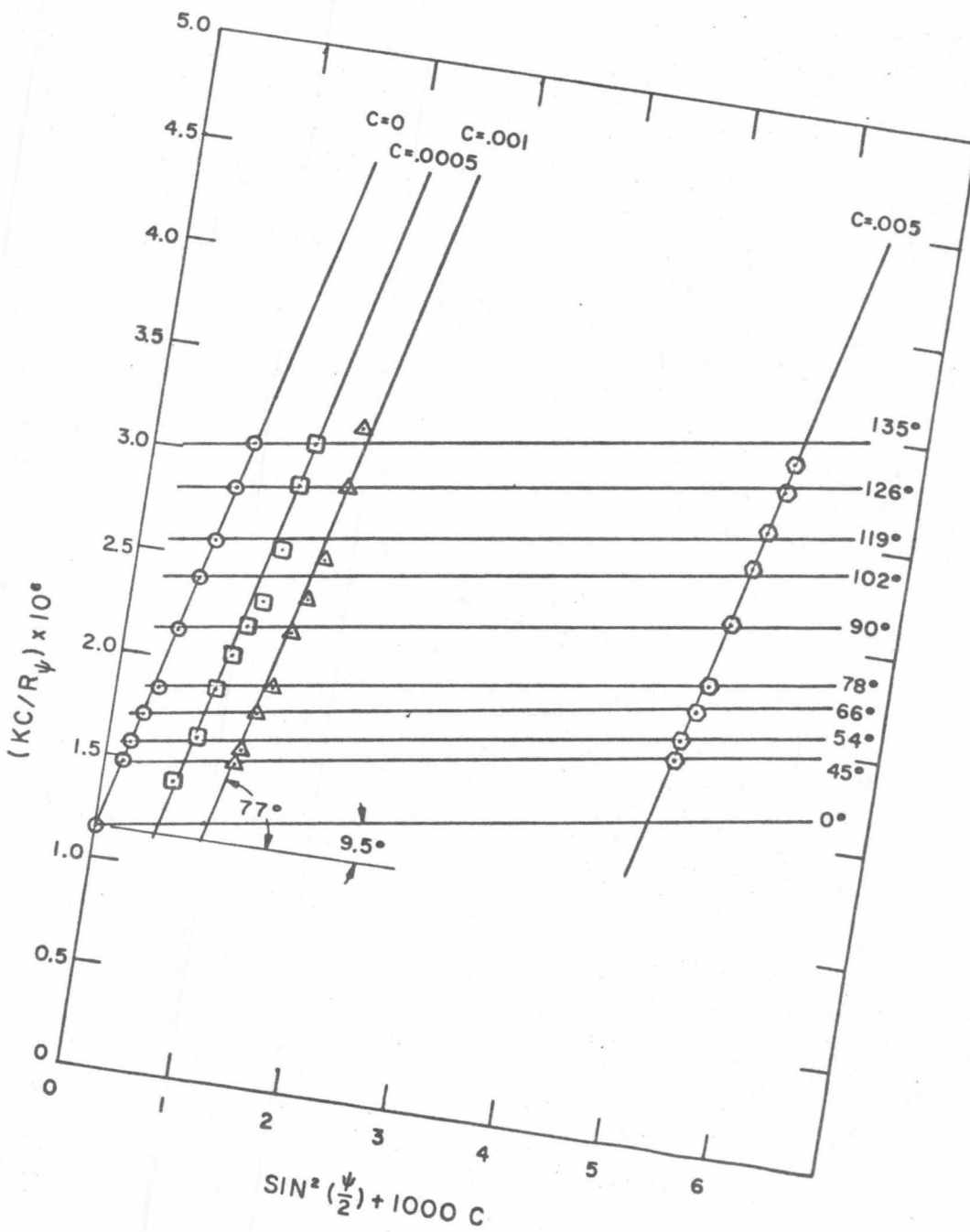


Figure 4.3 Weight-Average Molecular Weight of PEI 350 by Light Scattering Measurements.

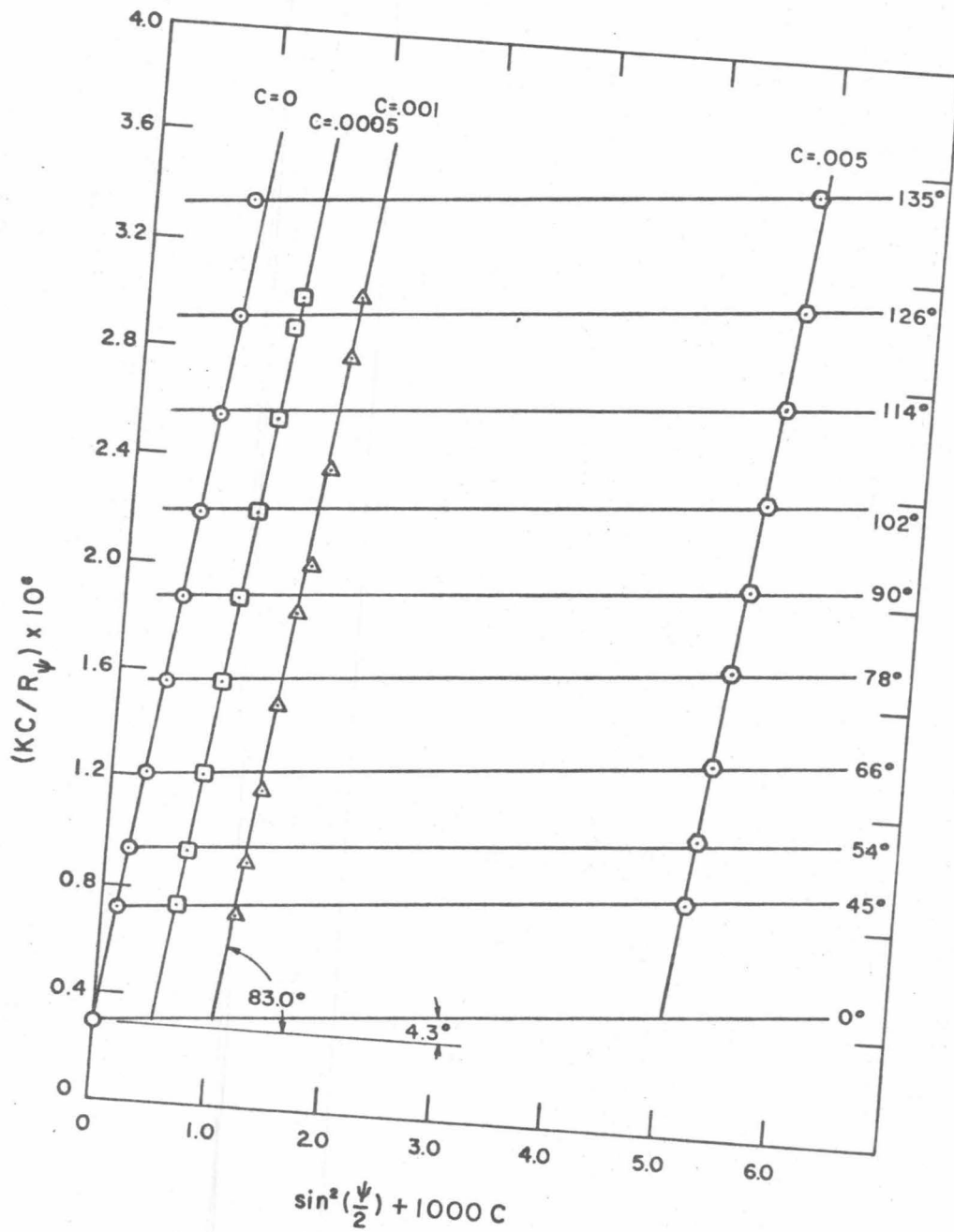


Figure 4.4 Weight-Average Molecular Weight of PEI 600 by Light Scattering Measurements.

and zero angle. From equation (3-24) one finds  $1/MW$  as the intercept and  $2A_1/k$  as the limiting slope. Similarly, extrapolating to  $C = 0$ , one finds the line (denoted by  $C = 0$ ) whose intercept is  $1/MW$  and whose limiting slope is immediately a measure of  $R_g$ . From equation (3-24)

$$R_g^2 = (3\lambda^2 MW / 16\pi^2) \cdot (\text{limiting slope}) \quad (4-1)$$

Table 4.3 summarizes the molecular weight data derived from light scattering measurements.

The radii of gyration of the polyethyleneimine samples were found to be related to the weight-average molecular weight via the equation:

$$R_g = 0.05 MW_w^{0.7} \quad (4-2)$$

Tanford (12) states that when  $R_g$  is proportional to  $MW_w^{1.0}$ , the molecule is a rigid rod, and when  $R_g$  is proportional to  $MW_w^{0.5}$ , the molecule is randomly coiled. Consequently, the experimental value of the exponent, 0.7, for PEI in solution indicates an ellipsoid-shaped molecule, in agreement with earlier discussions of the molecular configuration.

The radii of gyration of all the molecular weight species are large enough to stretch between receptive sites on two approaching particles. Although this is not evidence that bridging exists, it does

<u>Species</u>	<u>Manufacturer</u>	$\frac{MW}{w}$	$\frac{R}{g} (\text{\AA})$	$\frac{MW}{w} / \frac{MW}{n}$	$R = \frac{(R_g^2 / .6)^{\frac{1}{2}} (\text{\AA})}{g}$
PEI 6 <sup>(1)</sup>	DOW	$3.4 \times 10^4$	70	56	90
PEI 12 <sup>(1)</sup>	DOW	$6.7 \times 10^4$	110	56	150
PEI 18	DOW	$1.0 \times 10^5$	150	56	190
PEI 350	Borden Chemical	$1.0 \times 10^6$	750	29	970
PEI 600	DOW	$3.4 \times 10^6$	1760	57	2270

(1) Because the Brice-Phoenix cannot make accurate readings at angles greater than  $135^\circ$ , the full possible range of this method ( $10^3 < MW_w < 10^7$ ) and ( $200A < R_g < 2000A$ ) could not be achieved.

PEI 6 and PEI 12 values are extrapolated from PEI 18 and PEI 600 data.

Table 4.3 Molecular Weights and Radii of Gyration of PEI Species from Light Scattering Measurements.

indicate that bridging is possible. The information on molecule size and shape suffers from two major liabilities when applied to flocculating systems:

1. The solution configuration determined via light scattering may be significantly altered in the adsorption process.
2. The weight-average molecular weight is particularly sensitive to the larger molecules in solution, and therefore biases the results against the many smaller molecules in the sample which may not be capable of bridging.

#### 4.3.2 Results of Adsorption Studies

##### 4.3.2.1 PEI Adsorption to E. Coli Surface

The results of the polymer adsorption experiments for PEI onto E. coli are shown in Figure 4.5 for doses from 0.0 to 10.0 mg/l and in Figure 4.6 for doses from 0.0 to 50.0 mg/l. As anticipated the adsorption data follow a Langmuir isotherm, with the saturation adsorption increasing as the polymer molecular weight increases. An "S" shaped adsorption curve is observed for the adsorption of relatively monodisperse (as determined from molecular weight measurements) PEI 350 onto E. coli. This curve is caused by a distinct two step adsorption as the PEI concentration increases: initially, all the adsorbing PEI molecules are compressed onto the bacteria surface, caused

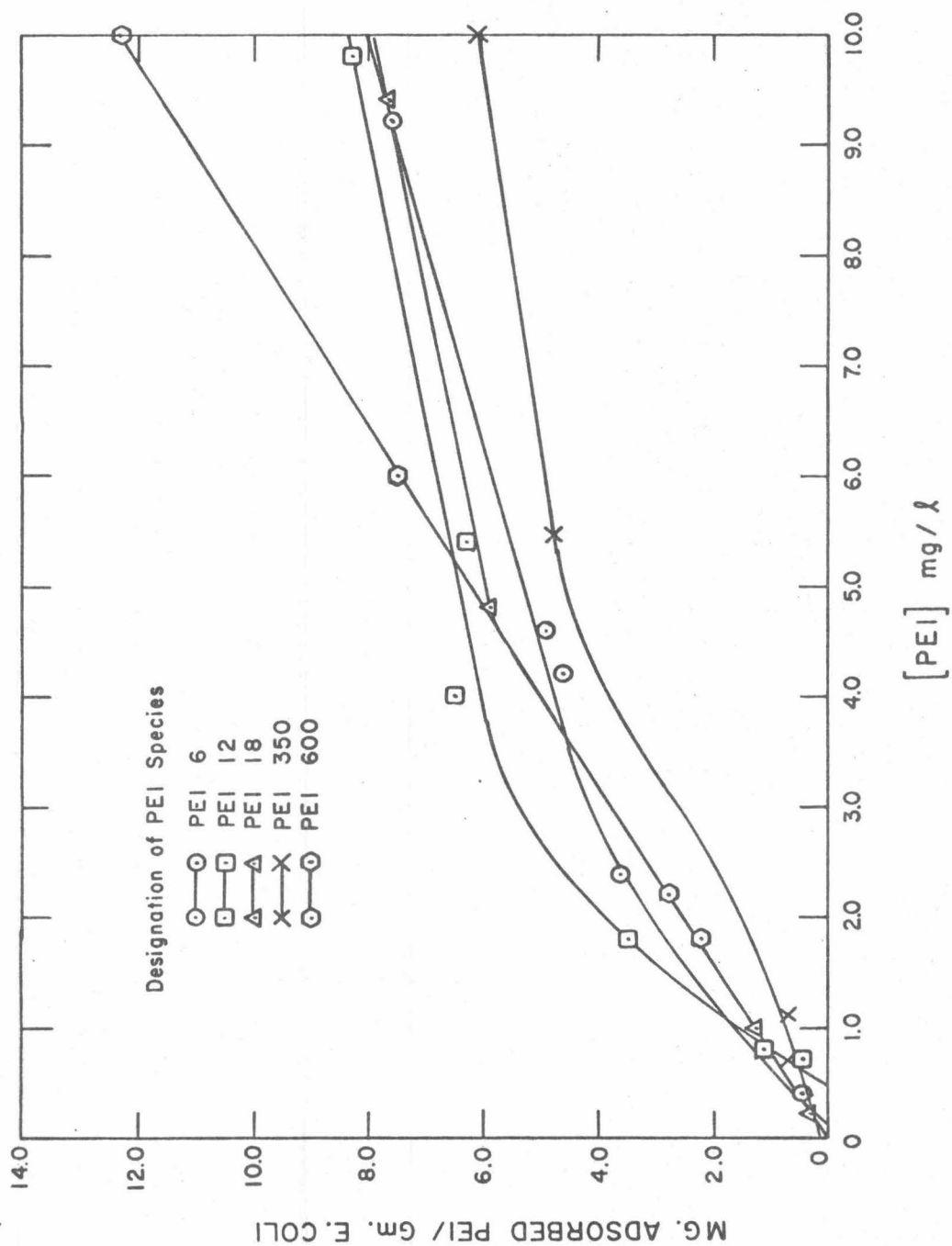


Figure 4.5 Adsorption of PEI to the Surface of *E. coli* as a Function of PEI Molecular Weight and Dose (0.0 to 10.0 mg/l).

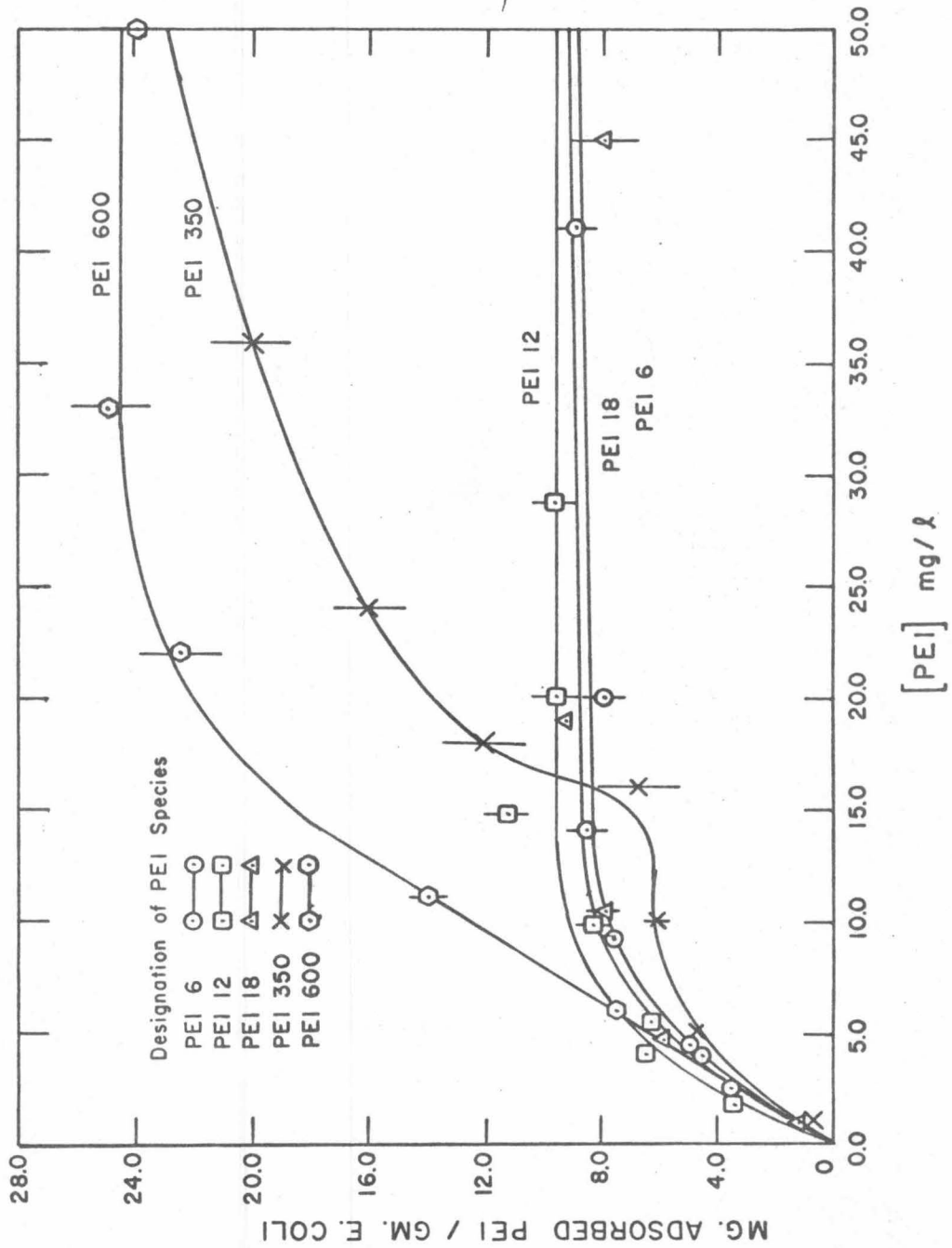


Figure 4.6 Adsorption of PEI to the Surface of *E. coli* as a Function of PEI Molecular Weight and Dose (0.0 to 50.0 mg/l).

by the many strong surface-polymer reaction sites. This horizontal adsorption continues to the first plateau, which corresponds to approximately 10 monolayers in depth. Further PEI concentration increases result in additional PEI molecules adsorbing vertically, with only a few of the polymer segments from each molecule firmly attaching to the bacteria surface (13).

Using the Perkel and Ullman model (14), the saturation adsorptions for the five different molecular weight species (PEI6, PEI12, PEI 18, PEI 350, PEI 600) can be related to the number average molecular weights as follows:

$$A_s = 1.8 MW_n^{0.24} \quad (4-3)$$

The value  $\beta = 0.24$  indicates that the PEI molecules in the overlayer have adsorbed in configurations intermediate between coiled spheres ( $\beta = 0.33$ ) and flat two-dimensional layers ( $\beta = 0.0$ ).

#### 4.3.2.2 Surface Site Coverage

The fraction of surface site coverage,  $\theta$ , can be determined from the linearized form of the Langmuir adsorption isotherm:

$$(X/W)^{-1} = a/C + 1/h \quad (4-4)$$

where  $X$  = weight of adsorbed PEI

$W$  = weight of E. coli

$C$  = equilibrium polymer concentration

$h$  = saturation weight ratio (weight PEI/weight E. coli  
at saturation)

and  $\theta = X/hW$

(4-5)

A graph of  $(X/W)^{-1}$  versus  $C^{-1}$  yields the saturation weight ratio of PEI to E. coli as the reciprocal of the intercept of the least squares line calculated from the adsorption data. Substitution of the value  $1/h$  into equation (4-5) enables the calculation of the fraction of surface site coverage  $\theta$  for a specified PEI dose. Figure 4.7 summarizes the effect of the PEI molecular weight on the fraction of surface site coverage.

At the optimum flocculation doses (3 to 10 mg/l) for low molecular weight species (PEI 6, PEI 12, PEI 18), the fraction of surface site coverage lies between 40 and 80%. From the preceding theoretical discussion, some approaching PEI molecules probably adsorb through only a few of their segments in this range of surface coverage. The remaining segments extend into the solution phase since adjacent adsorption sites are already occupied.

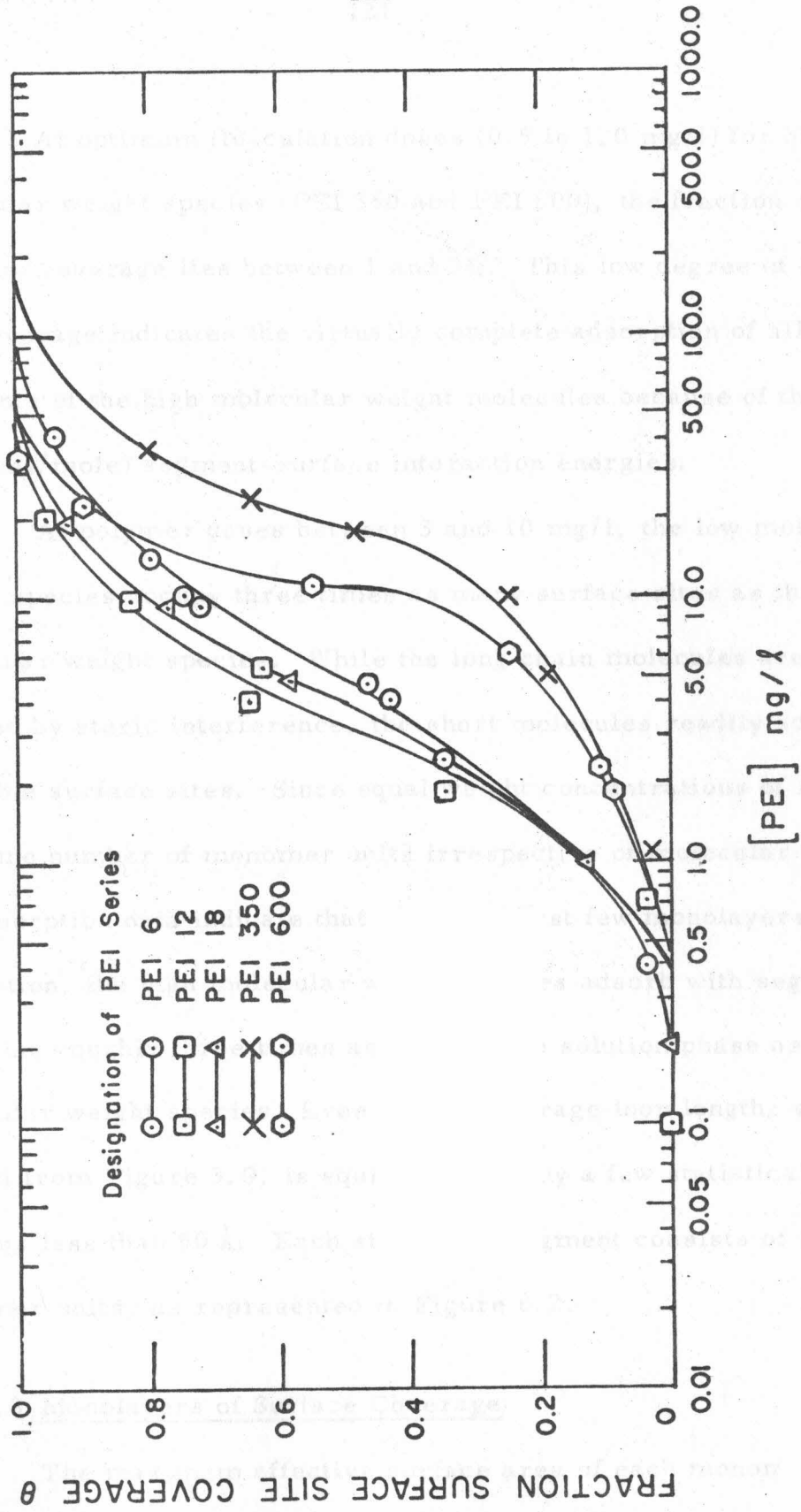


Figure 4.7 Fraction of Surface Site Coverage as a Function of PEI Molecular Weight and Dose.

At optimum flocculation doses (0.5 to 1.0 mg/l) for high molecular weight species (PEI 350 and PEI 600), the fraction of surface site coverage lies between 1 and 3%. This low degree of surface site coverage indicates the virtually complete adsorption of all adsorbing segments of the high molecular weight molecules because of the strong (6-8 kcal/mole) segment-surface interaction energies.

At polymer doses between 3 and 10 mg/l, the low molecular weight species occupy three times as many surface sites as the high molecular weight species. While the long chain molecules are restricted by steric interference, the short molecules readily adsorb to available surface sites. Since equal weight concentrations of PEI have the same number of monomer units irrespective of molecular weight, the adsorption data indicate that after the first few monolayers of adsorption, the high molecular weight species adsorb with segments extending roughly three times as far into the solution phase as low molecular weight species. Even so, the average loop length, extrapolated from Figure 3.9, is equivalent to only a few statistical segments and thus less than 50 Å. Each statistical segment consists of four monomer units, as represented in Figure 6.2.

#### 4.3.2.3 Monolayers of Surface Coverage

The maximum effective surface area of each monomer unit of

PEI molecule can be determined from its chemical structure and known values of packing radii and covalent bond radii. Packing radii, also known as van der Waals radii, give the effective size for non-bonded contacts between atoms packed together in a crystal or liquid.

<u>Packing Radii of Atoms</u>		<u>Covalent Bond Radii of Atoms</u>	
H	1.15 Å	H	0.30 Å
N	1.50 Å	N	0.70 Å
		C	0.77 Å

In a flat extended configuration, each monomer unit ( $C_2H_5N$ ) would cover approximately  $20 \text{ \AA}^2$ . Since the PEI molecule is highly branched, and since the high molecular weight species appear to adsorb with only a fraction of the monomer units in full contact with the surface, the  $20 \text{ \AA}^2$  is the maximum possible surface coverage. Nevertheless, it does provide an estimate of the number of monolayers of surface coverage at each polymer dose.

Using the measured adsorption at each polymer dosage, the effective area of each adsorbed monomer segment, and the available E. coli surface area from Coulter Counter data, one can readily calculate the monolayers of surface coverage at each polymer dosage and molecular weight. Table 4.4 provides the results of these calculations.

The saturation doses of low molecular weight species produce adsorbed polymer "coating factors" of 10 monolayers; while high

Dose mg/l \ MW <sub>n</sub>	600	1200	1800	35000	60000
0.05	---	---	---	0.07	0.07
0.5	0.78	0.58	0.73	0.45	0.82
1.0	---	1.9	1.5	0.87	1.5
5.0	7.8	8.2	7.1	5.4	7.5
10.0	8.4	12.0	10.0	---	---
50.0	11.0	12.0	14.0	22.0	25.0
500	12.0	16.0	16.0	---	---

Table 4.4 Monolayers of Surface Coverage as a Function of PEI Molecular Weight and Dose.

molecular weight species produce "coating factors" of 25 monolayers. These "coating factors" are in accord with those of previous investigators for the adsorption of cationic polymers on anionic surfaces. The fact that more than one monolayer is adsorbed provides evidence that many PEI molecules adsorb through only a few monomer units, with the remainder extending into the solution.

Optimum polymer doses for low molecular weight species are characterized by 4.0 to 10.0 monolayers of surface coverage, whereas optimum doses for high molecular weight species correspond to less than 1.5 monolayers of coverage.

#### 4.3.3 Electrophoretic Mobility of E.coli-PEI Aggregates

The mobility  $M_e$  may be calculated from the equation

$$M_e = xA/tJR_s \text{ } \mu\text{m/sec/volt/cm} \quad (4-6)$$

where  $x$  = distance across a square of the Howard cell in  $\mu\text{m}$

$A$  = cross sectional area of Briggs cell in  $\text{cm}^2$

$t$  = time in seconds to cross distance  $x$

$J$  = current in amperes

$R_s$  = specific resistance of the suspension in ohm-cm

From the mobility, the zeta potential can be calculated via the equation

$$\zeta = 4\pi\mu M_e / K\epsilon_0 \quad \text{volts} \quad (4-7)$$

$K\epsilon_0$  = dielectric constant in coul/volt cm

Figure 4.8 illustrates the change in electrophoretic mobility, and zeta potential, as increasing amounts of PEI are added to the E. coli suspension. Also shown are the regions of optimum flocculant dose as measured by a 90% or greater decrease in the number of particles. For low molecular weight PEI species: PEI 6, PEI 12, and PEI 18, optimum flocculation occurs when the electrophoretic mobility of the cells is reduced from an initial value of -0.85 to the region -0.50 to -0.25  $\mu\text{m}/\text{sec}/\text{v}/\text{cm}$ . Even at high concentrations, PEI 6 and PEI 12 are unable to reverse the negative mobility of the E. coli cells. The two high molecular weight PEI species: PEI 350 and PEI 600 are optimally effective at lower polymer concentrations and over a broader range of mobility values; i. e., -0.75 to +1.05  $\mu\text{m}/\text{sec}/\text{v}/\text{cm}$ . In addition, PEI 350 and PEI 600 produce reversal of mobility and stabilization of mobility at positive values for high polymer concentrations.

#### 4.3.4 PEI Dose at Optimum Refiltration Rate

Figure 4.9 shows the variation of the refiltration rate  $Q-Q_0$  for a flocculated suspension of PEI-E. coli with respect to the initial PEI dose. The ability of the high molecular weight species PEI 350 and PEI 600 to improve the refiltration rate is in sharp contrast with

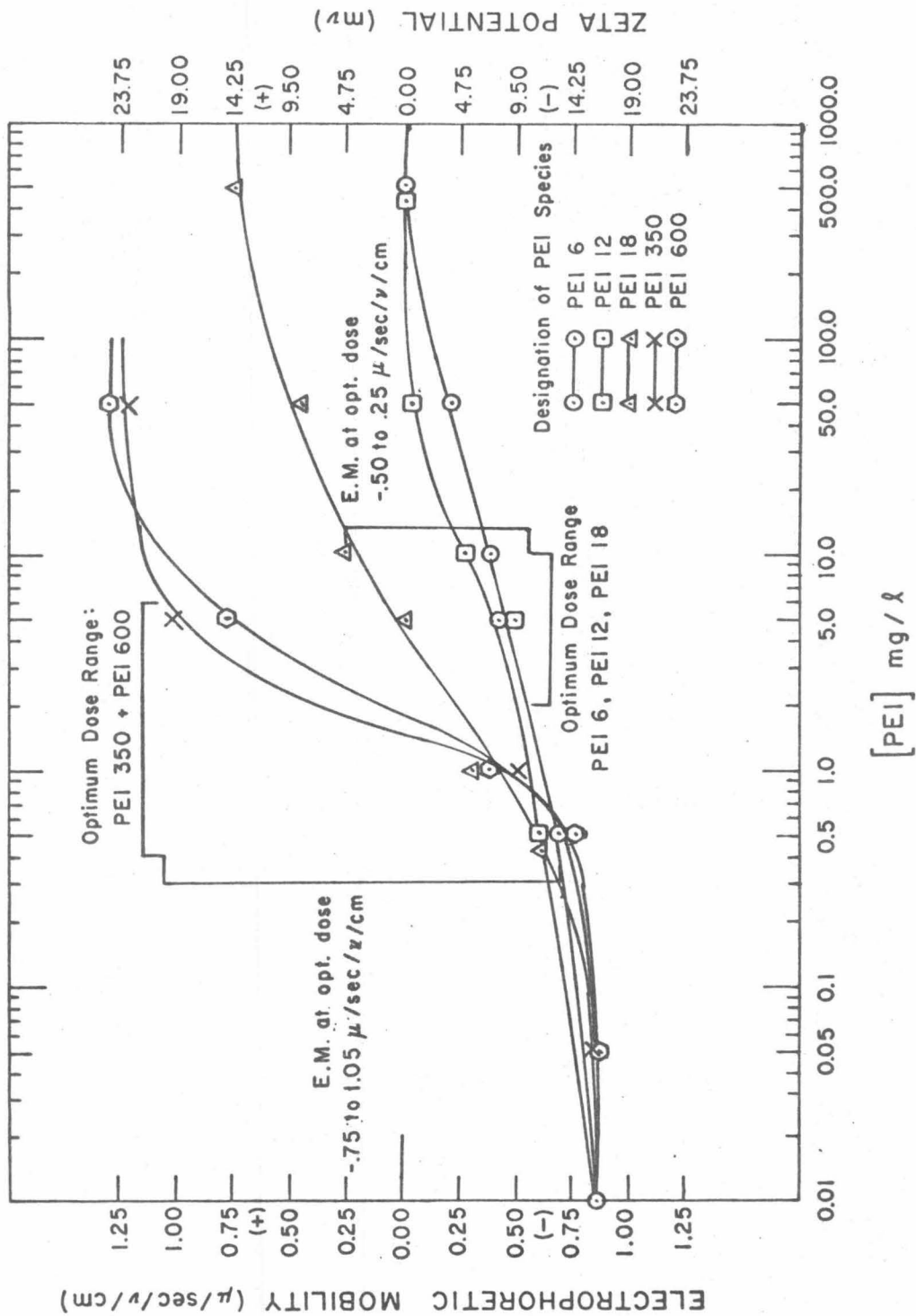


Figure 4.8 Electrophoretic Mobility as a Function of PEI Molecular Weight and Dose.

that of the low molecular weight species; PEI 6, PEI 12, and PEI 18.

Optimum PEI doses were calculated from the values of slope  $p$  and intercept  $a$  obtained from graphs of equation (3-29) for each PEI molecular weight. The optimum flocculation dose determined from refiltration rate experiments for each molecular weight is in the concentration range which produces the greatest percent reduction in the number of primary particles  $n_o$ . Table 4.5 lists the optimum refiltration flocculation doses along with the associated fraction of surface site coverage, taken directly from Figure 4.7.

Table 4.5 shows that  $\theta$  approaches 0.5 only for PEI 6 and PEI 12, both of which produce poor refiltration rates when compared to the higher molecular weight species. Optimum flocculation for the PEI-E. coli system occurred with high molecular weight species at values of  $\theta$  ranging between 0.01 and 0.10; values which are in better accord with a charge mosaic model of flocculation (5) than with the polymer bridging model (15).

From the theoretical derivation of LaMer and Healy (16-21), optimum flocculation doses determined from refiltration experiments using the "eighth-power rule" (equation 3-29) should occur at values of surface site coverage  $\theta$  near 0.5. Although the refiltration technique is useful in determining optimum flocculation doses for the PEI-E. coli system, the doses so measured do not substantiate the bridging theory

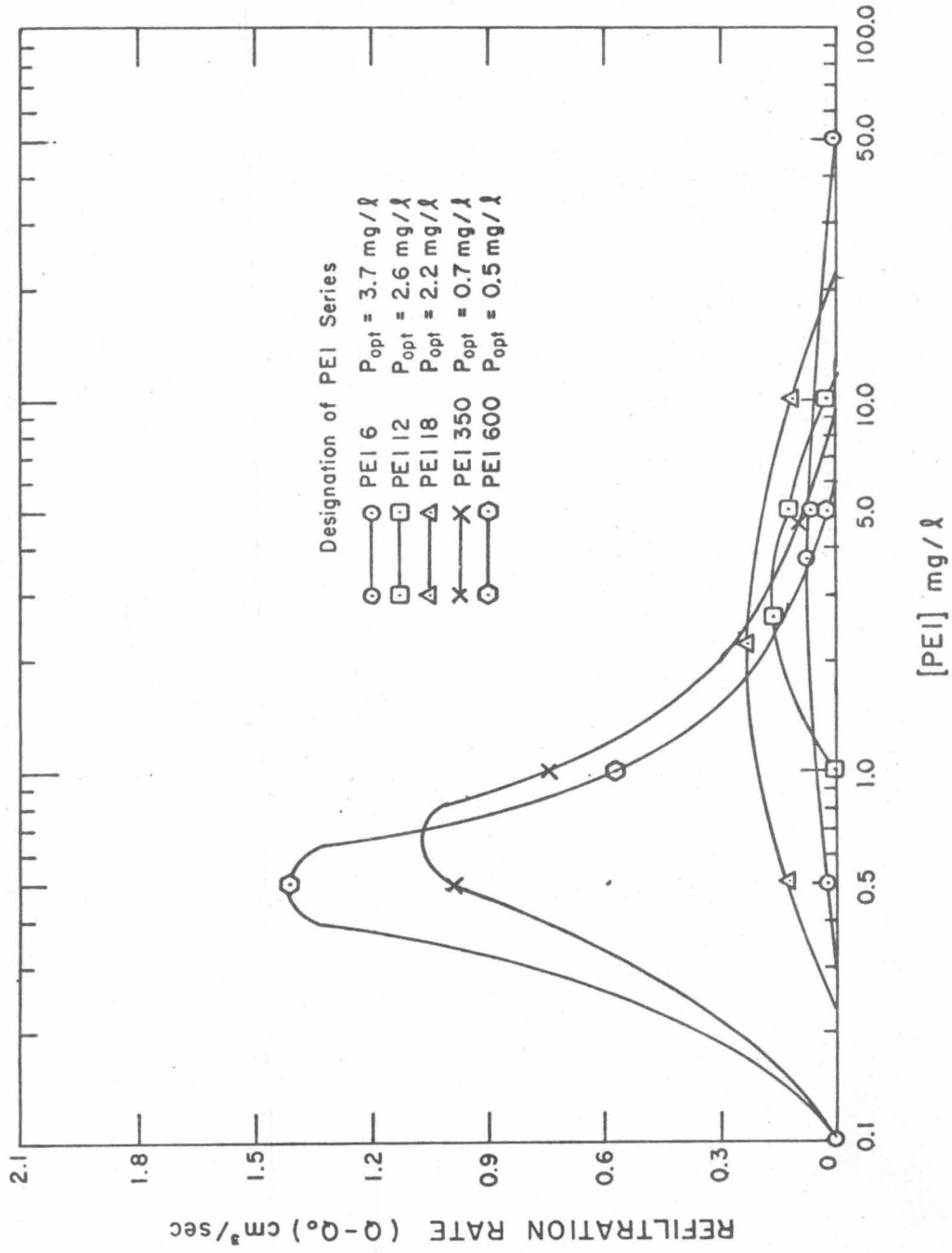


Figure 4.9 Refiltration Rate as a Function of PEI Molecular Weight and Dose.

<u>Polymer Species</u>	<u>Optimum Dose (mg/l)</u>	<u>Surface Site Coverage <math>\theta</math></u>
PEI 6	3.7	0.42
PEI 12	2.6	0.42
PEI 18	2.2	0.29
PEI 350	0.7	0.03
PEI 600	0.5	0.01

Table 4.5 Optimum Flocculant Dose and Associated Surface Site Coverage for Five PEI Species.

of formation as proposed by LaMer and Healy.

Smellie and LaMer (15) attributed the decrease in refiltration rate following the optimum dose (Figure 4.9) to decreasing floc size resulting from excess average coverage of the particles with flocculant molecules and the onset of restabilization. This view was found to be correct for the high molecular weight PEI molecules, which reversed the charge on the E.coli surface at PEI doses slightly larger than optimum. For low molecular weight species, the decrease in refiltration rate was due mostly to obstruction of flow through the interstices of the filter cake and filter septum caused by the adsorption of polymer molecules, rather than to any restabilization phenomenon.

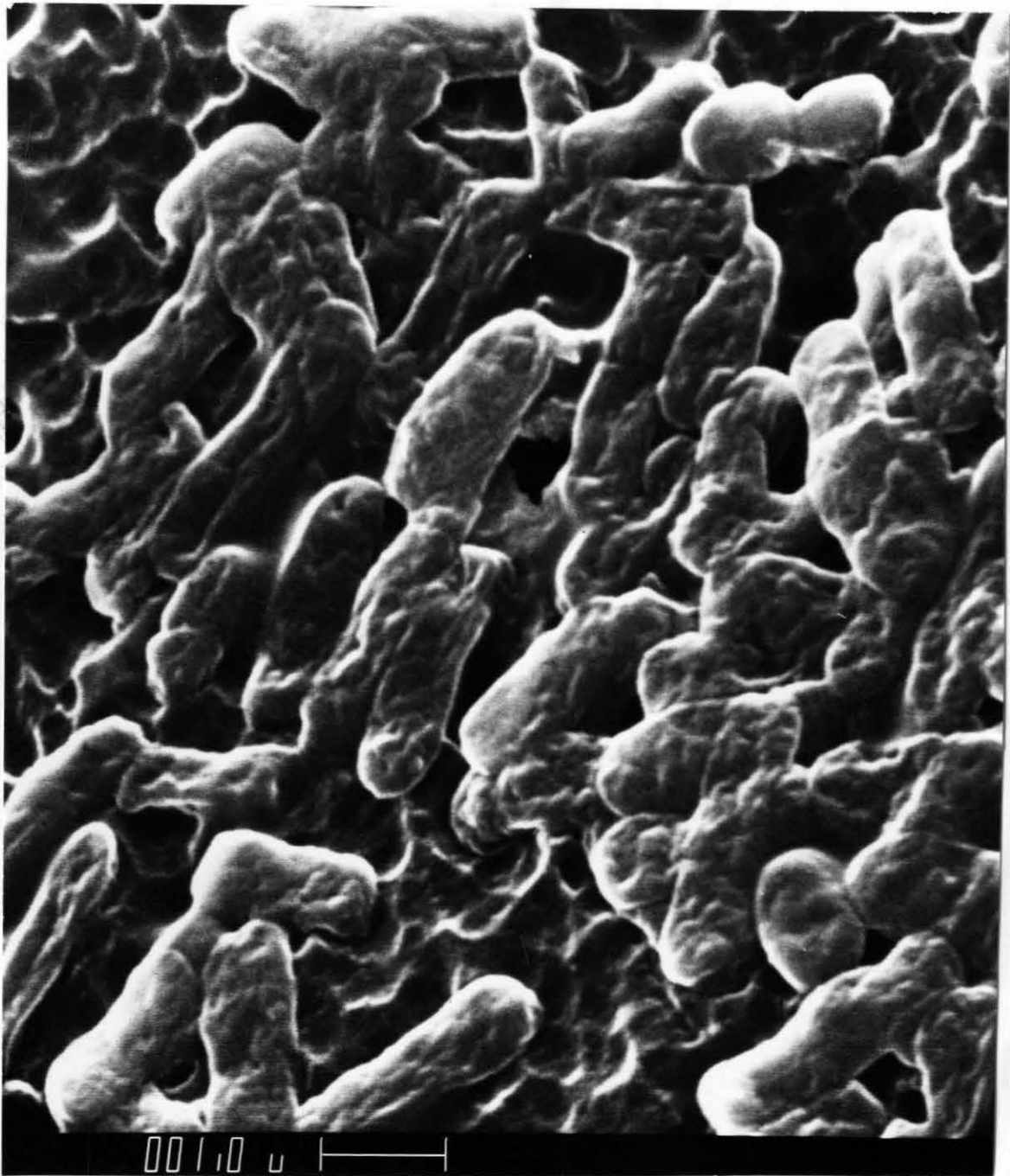
#### 4.3.5 Examination of PEI Flocs with a Scanning Electron Microscope

Photographs 4.1-4.3 illustrate the structure of E.coli cells flocculated with 5.0 mg/l of the low molecular weight species PEI 6. The cell packets appear tightly bound together: Photograph 4.3, for example, indicates a cell separation distance on the order of 100 Å. The diameter of a PEI 6 molecule determined from extrapolated light scattering data (Table 4.3) is less than 200 Å, and therefore this molecule could serve as a bridge holding together two colliding E.coli cells.

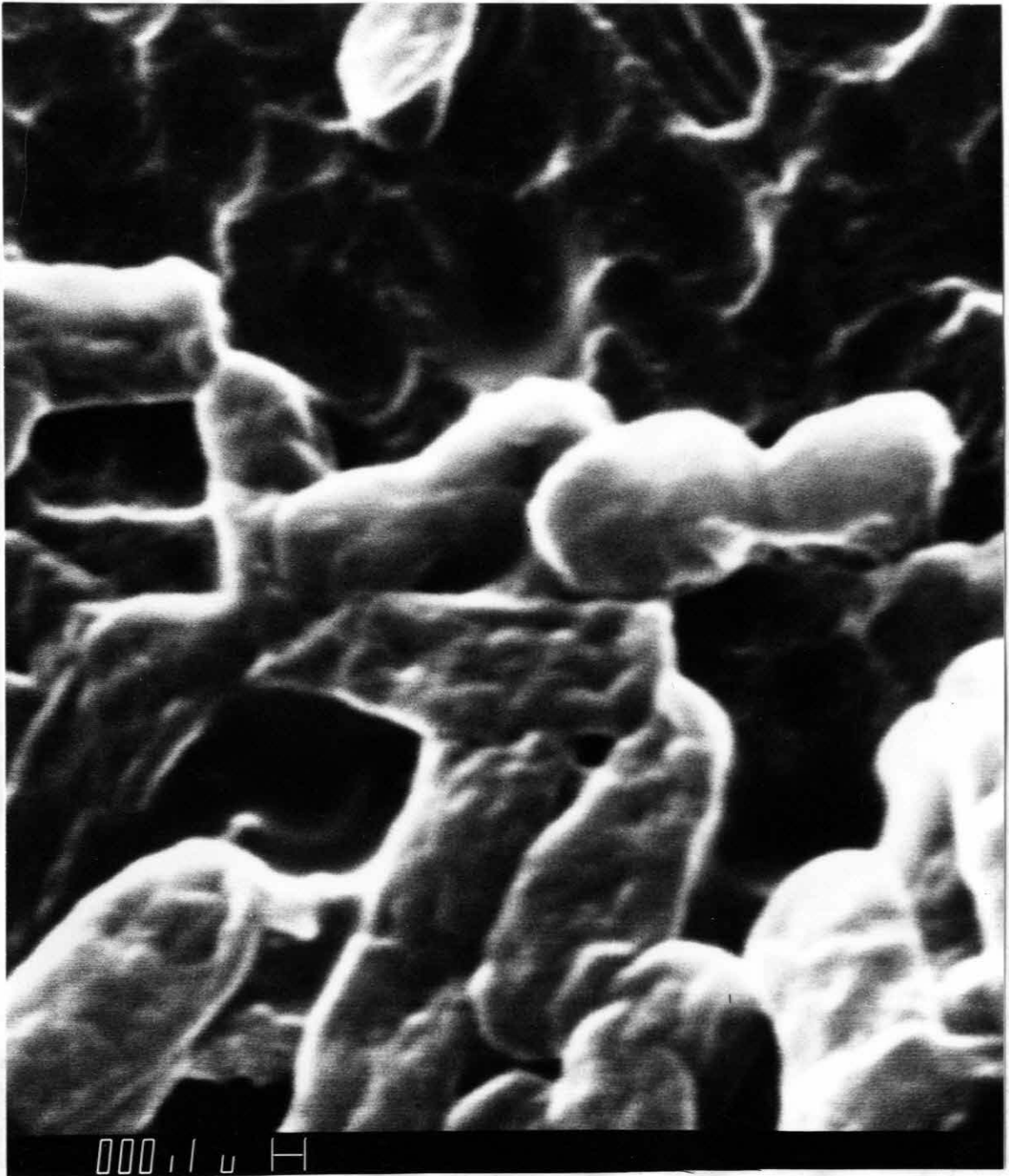
Photographs 4.4-4.8 illustrate the structure of E. coli cells flocculated with 0.5 mg/l of the high molecular weight species PEI 350. The cell packets are firmly bound together, as with PEI 6. In addition, evidence exists of a longer bridging structure between colliding cells, as in the left center of Photograph 4.4. From Photographs 4.5 and 4.6, this bridging structure appears to be on the order of 500 Å in length, compared to a molecular diameter of 1900 Å as determined from light scattering measurements (Table 4.3).

This bridging structure was the exception to the more frequently observed tightly-bound cells (Photographs 4.7 and 4.8) with cell separation distances of 100-200 Å. In spite of the care taken to avoid cell shrinkage in preparation of the electron micrographs, the observed bridging structures may reflect the strength of the E. coli PEI bond more than a bridging mechanism of formation.

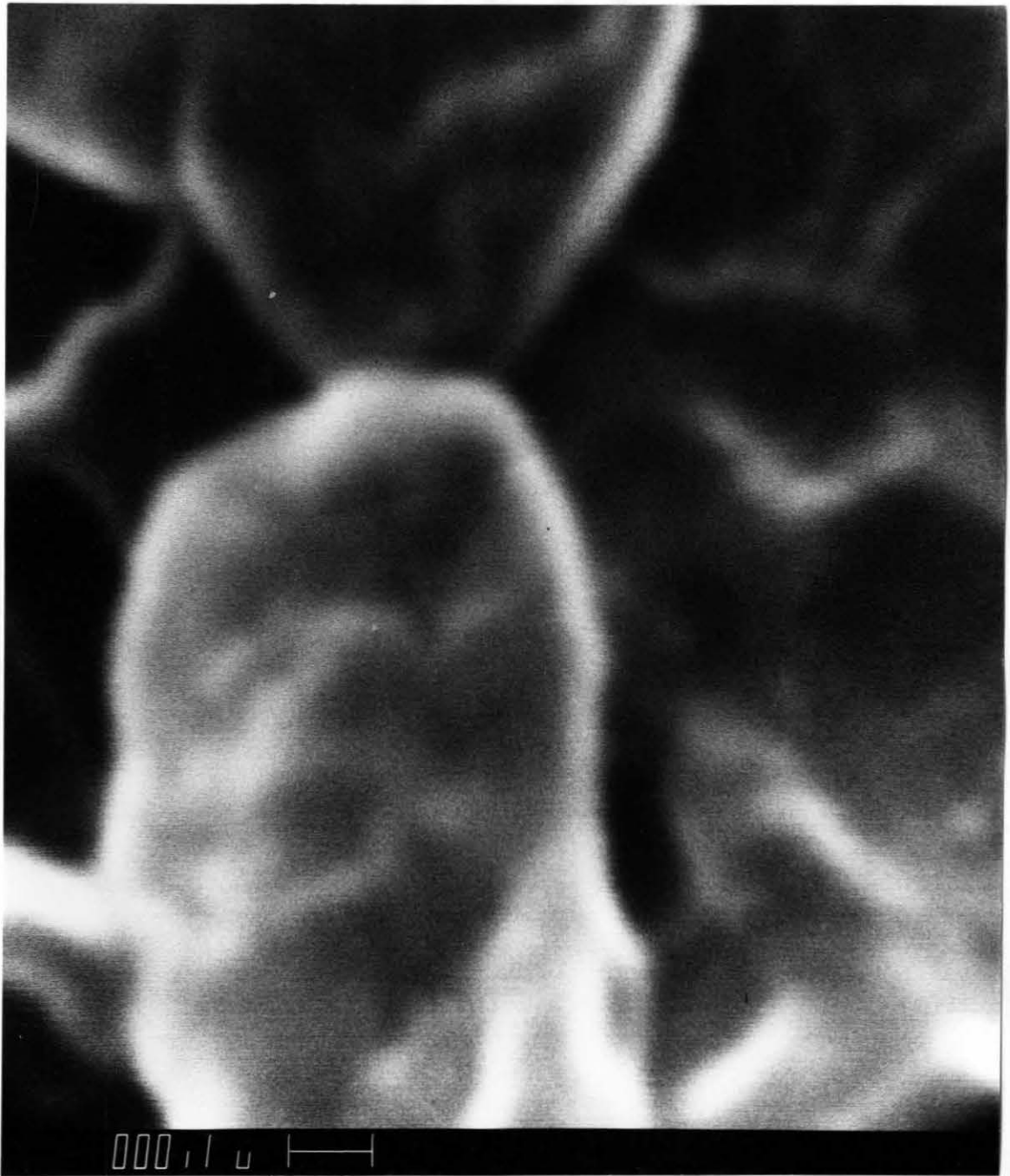
Because of the relatively low molecular weight of all the PEI species, especially when compared to anionic/nonionic polymers with molecular weights in excess of  $10^6$ , and because of the high degree of chain branching (25% of monomer units being branch points), one does not expect to see the long fibrillar structures extending between particles, such as were observed by Friedman et al. (22,23). Instead, the highly-branched PEI molecules appear to serve as a strongly-adsorbed polymeric glue which binds the colliding cells together.



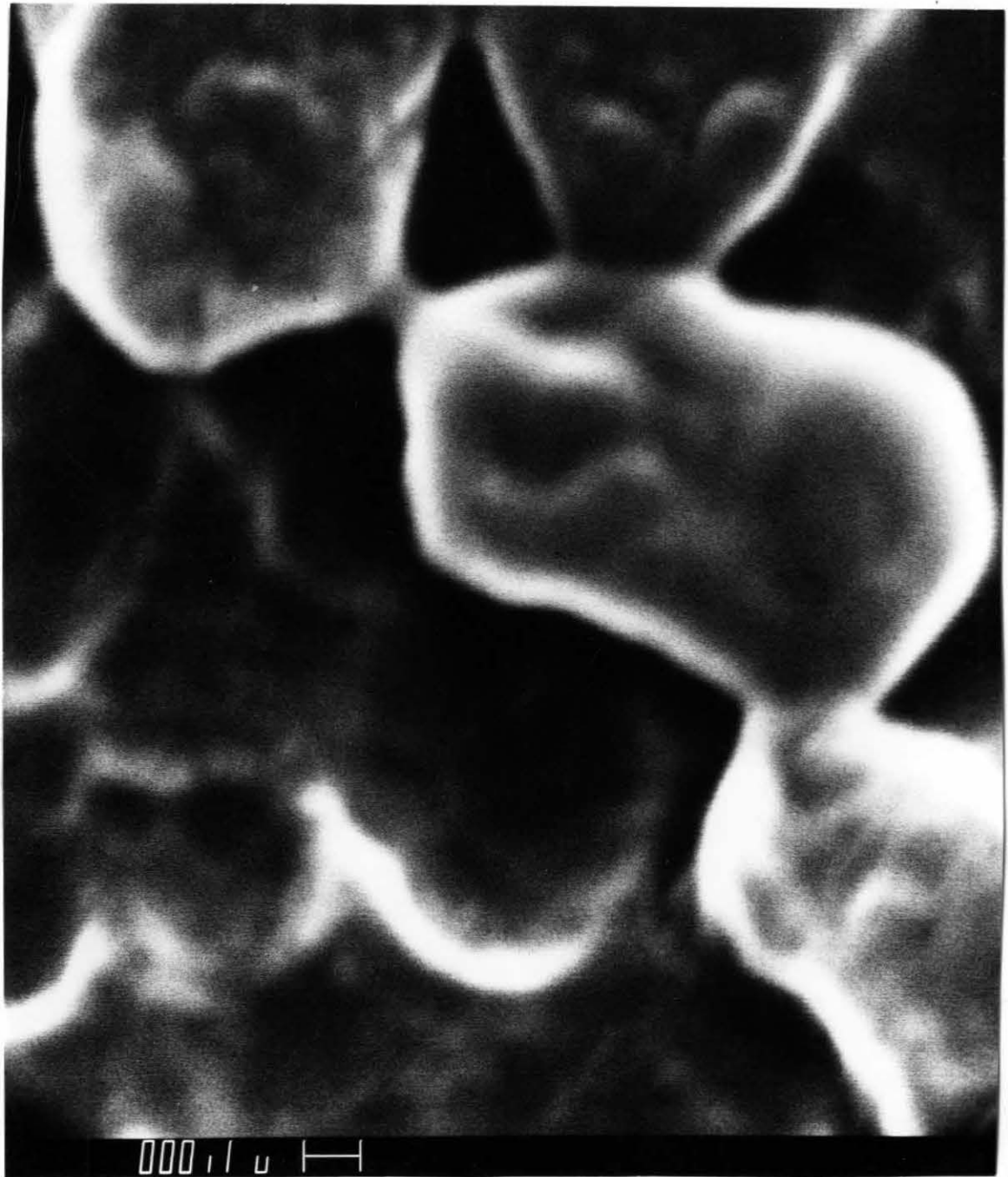
4.1 Electron Micrograph of *E. coli* Cells Flocculated with PEI 6.  
Total Magnification  $1.8 \times 10^4$ .



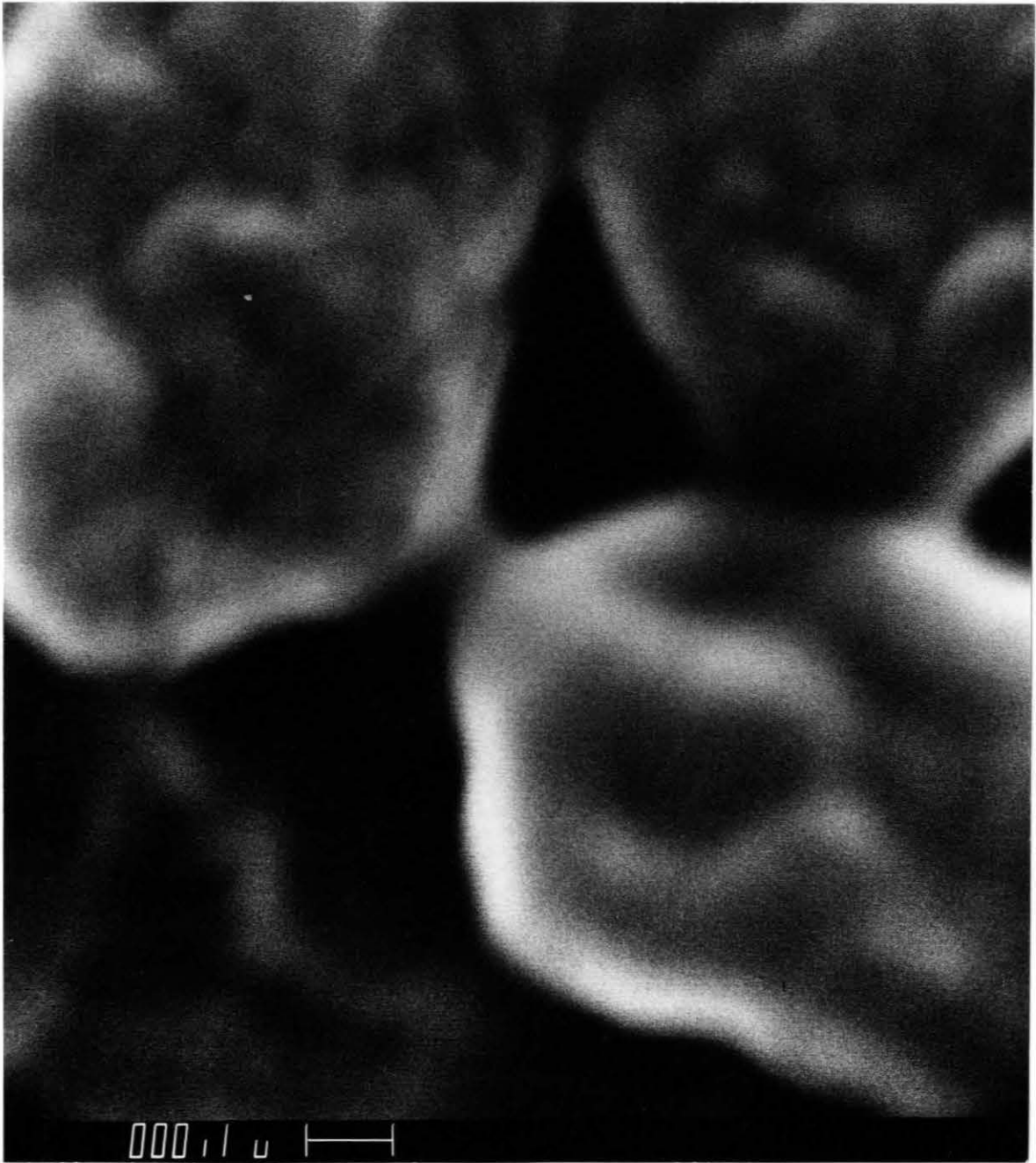
4.2 Electron Micrograph of E. coli Cells Flocculated with PEI 6.  
Total Magnification  $4.0 \times 10^4$ .



4.3 Electron Micrograph of E. coli Cells Flocculated with PEI 6.  
Total Magnification  $1.2 \times 10^5$ .



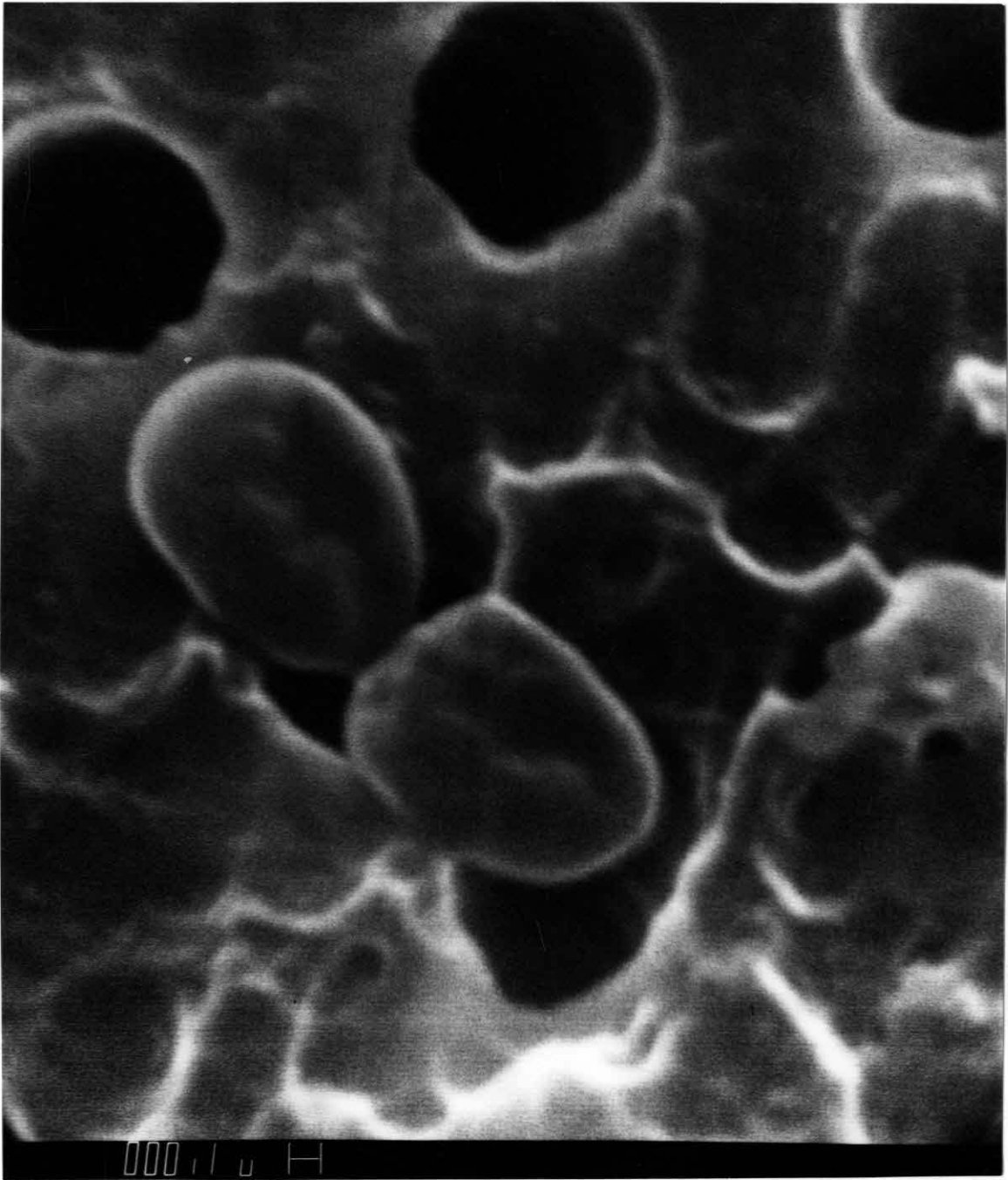
4.4 Electron Micrograph of E. coli Cells Flocculated with PEI 350.  
Total Magnification  $8.0 \times 10^4$ .



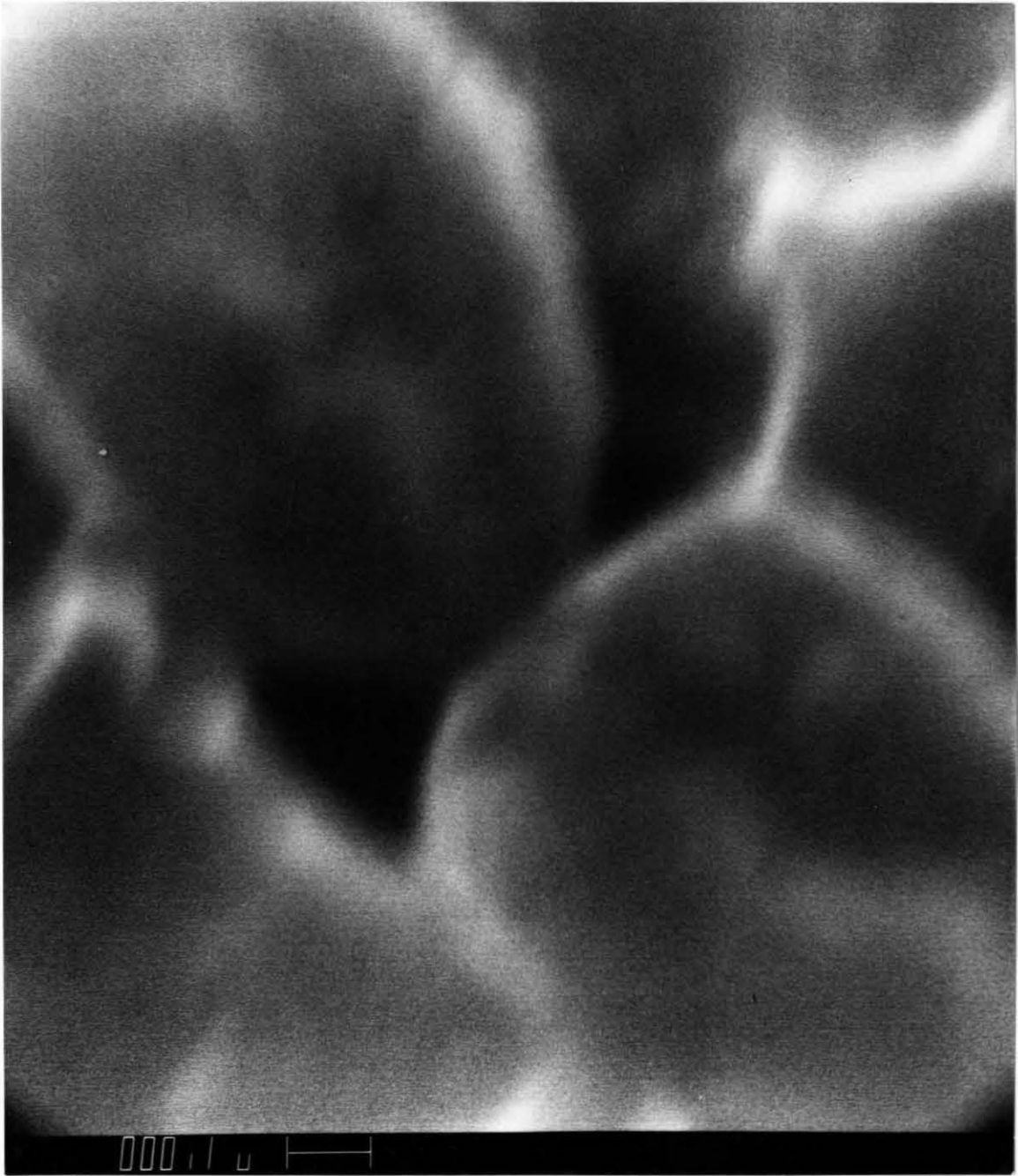
4.5 Electron Micrograph of E. coli Cells Flocculated with PEI 350.  
Total Magnification  $1.2 \times 10^5$ .



4.6 Electron Micrograph of E. coli Cells Flocculated with PEI 350.  
Total Magnification  $2.0 \times 10^5$ .



4.7 Electron Micrograph of *E. coli* Cells Flocculated with PEI 350.  
Total Magnification  $4.0 \times 10^4$ .



4.8 Electron Micrograph of E. coli Cells Flocculated with PEI 350.  
Total Magnification  $1.2 \times 10^5$ .

## REFERENCES CITED

## CHAPTER 4

1. Stumm, W., and O'Melia, C. R., "Stoichiometry of Coagulation", Journal American Water Works Association, 60 (1968), 514-539.
2. Stumm, W., and Morgan, J. J., Aquatic Chemistry, Wiley-Interscience, New York, 1970.
3. PEI Polymers, DOW Chemical Company, Midland, Michigan, 1974.
4. Rembaum, A., Casson, D., and Morgan, J. J., "Flocculation of Colloidal Suspensions with Ionene Polymers", Jet Propulsion Laboratory, Pasadena, California, 1972.
5. Kasper, D. R., "Theoretical and Experimental Investigations of the Flocculation of Charged Particles in Aqueous Solutions by Polyelectrolytes of Opposite Charge", Ph.D. Thesis, California Institute of Technology, 1971.
6. Briggs, D. R., "A Pyrex All-Glass Microelectrophoresis Cell", Industrial and Engineering Chemistry, Analytical Edition, 12 (1940), 703-705.
7. Black, A. P., and Smith, A. L., "Determination of the Mobility of Colloidal Particles by Microelectrophoresis", Journal American Water Works Association, 54 (1962), 926-934.
8. Black, A. P., and Smith, A. L., "Improvements in Instrumentation and Techniques for Microelectrophoresis", Journal American Water Works Association, 57 (1965), 485 - 491.
9. Neihof, R., "Microelectrophoresis Apparatus Employing Palladium Electrodes", Journal Colloid and Interface Science, 30 (1969), 128-133.
10. LaMer, V. K., Smellie, R. H., and Lee, P. K., "Flocculation, Subsidence, and Filtration of Phosphate Slimes. V. The Optimum Filtration Rate as a Function of Solid Content and Specific Area", Journal Colloid Science, 12 (1957), 566-574.

11. Zimm, B. H., "Apparatus and Methods for Measurement and Interpolation of the Angular Variation of Light Scattering, Preliminary Results on Polystyrene Solutions", Journal Chemical Physics, 16 (1948), 1099-1116.
12. Tanford, C., Physical Chemistry of Macromolecules, John Wiley and Sons, New York, 1961, 302-305.
13. Giles, C. H., MacEwan, T. H., Nakhwa, S. N., and Smith, D., "Studies in Adsorption. Part XI. A System of Classification of Solution Adsorption Isotherms, and its Use in Diagnosis of Adsorption Mechanisms and in Measurement of Specific Surface Areas of Solids", Chemical Society (London), 1960 (1960), 3973-3993.
14. Perkel, R., and Ullman, R., "The Adsorption of Polydimethylsiloxanes from Solution", Journal Polymer Science, 54 (1961), 127-148.
15. Smellie, R. H., and LaMer, V. K., "Flocculation, Subsidence, and Filtration of Phosphate Slimes. VI. A Quantitative Theory of Filtration of Flocculated Suspensions", Journal Colloid Science, 13 (1958), 589-599.
16. Healy, T. W., and LaMer, V. K., "The Adsorption-Flocculation Reactions of a Polymer with an Aqueous Colloidal Dispersion", Journal Physical Chemistry, 66 (1962), 1835-1838.
17. LaMer, V. K., and Healy, T. W., "Adsorption-Flocculation Reactions of Macromolecules at the Solid-Liquid Interface", Review of Pure and Applied Chemistry, 13 (1963), 112-133.
18. LaMer, V. K., and Healy, T. W., "The Role of Filtration in Investigating Flocculation and Redispersion of Colloidal Dispersions", Journal Physical Chemistry, 67 (1963), 2417-2420.
19. Healy, T. W., and LaMer, V. K., "The Energetics of Flocculation and Redispersion by Polymers", Journal Colloid Science, 19 (1964), 323-332.
20. Kane, J. C., LaMer, V. K., and Linford, H. B., "The Effect of Solid Content on the Adsorption and Flocculation Behavior of Silica Suspensions", Journal Physical Chemistry, 68 (1964), 3539-3544.

21. LaMer, V. K., "Filtration of Colloidal Dispersions Flocculated by Anionic and Cationic Polyelectrolytes", Discussions Faraday Society, 42 (1966), 248-254.
22. Friedman, B. A., Dugan, P. R., Pfister, R. M., and Remsen, C. C., "Fine Structure and Composition of the Zoogloal Matrix Surrounding Zoogloea ramigera", Journal Bacteriology, 96 (1968), 2144-2153.
23. Friedman, B. A., Dugan, P. R., Pfister, R. M., and Remsen, C. C., "Structure of Exocellular Polymers and Their Relationship to Bacterial Flocculation", Journal Bacteriology, 98 (1969), 1328-1334.

## Chapter 5

## METHODS OF MEASURING

## AGGREGATE NUMBER AND DIAMETER

5.1 Introduction - Available Measurement Techniques

The second goal of this research is to analyze the techniques available to measure quantitatively the effectiveness of PEI in aggregating the E. coli suspension. Over twenty different techniques have been utilized by prior investigators to measure flocculant effectiveness, but aside from the efforts of TeKippe and Ham (1), little has been done to correlate the results of different techniques. In addition, many experiments measure only the phase separation aspect of the flocculation process, which can lead to inaccuracies when laboratory bench tests are scaled up to full-scale plants. To some degree, measurement of phase separation alone biases the investigator toward improvement of the physical parameters of the system, at the expense of possible chemical alterations which would enhance the destabilization stage.

Although experimental techniques have been developed to measure the interparticle collision efficiency factor, these techniques are too sophisticated, time-consuming, and expensive for daily water and wastewater treatment practices. Alternatively, many tests have

been devised which measure, either qualitatively or quantitatively, the change in aggregate diameter due to flocculation. From an engineering viewpoint, the technique selected should be applicable to a wide variety of particulate-flocculant systems, quick and simple to perform, and the results compatible with sophisticated laboratory measurements.

TeKippe and Ham (1) have prepared a detailed survey of available experimental tests, which are listed below according to the type of measurement involved. Descriptions of each method can be found in the work of TeKippe and Ham or in referenced publications.

1. Direct Measurement

- a. Electronic Particle Counting - Electronic counting and sizing of aggregates.
- b. Floc Volume Concentration - Microscopic counting and sizing of aggregates.
- c. Surface Area Concentration - Correlation of surface area (by microscopic examination) with weight concentration.

2. Optical Measurement

- a. Conventional Jar Test - Visual or spectrophotometric measurement of supernatant turbidity following flocculation and settling.

- b. Modified Jar Test - Turbidity measurement after passing flocculated suspension through small granular bed.
  - c. Speed of Floc Formation - Time required for appearance of floc after coagulant addition.
  - d. Visual Floc Size Comparisons - Qualitative visual comparison of floc size.
  - f. Inverted Gauze Filter - Turbidity of filtrate after passing suspension through gauze filter.
3. Sedimentation/Filtration Measurement
- a. Membrane Refiltration - Filtration of coagulated suspension followed by refiltration of filtrate through filter cake.
  - b. Floc Density - Particle volume and settling velocity measurement.
  - c. Settled Floc Volume - Volume of settled floc in continuous-flow settling tank.
  - d. Silting Index - Flow rate of coagulated suspension through Millipore filter.
  - e. Filtrability Number - Ratio of flow rates for coagulated suspension and distilled water.

- f. Filtration Parameters - Measurement of filter headloss and breakthrough.
  - g. Cotton Plug Filters - Gravimetric analysis of particulate matter accumulated on cotton plug filter.
4. Electrostatic Charge Measurement
- a. Zeta Potential - Measurement of particle electrophoretic mobility in an applied electric field.
  - b. Cation Exchange Capacity - Cation exchange capacity of particulate matter.
  - c. Conductivity - Conductivity of suspension before and after flocculant addition.
  - d. Streaming Current Detection - Measurement of particle zeta potential without direct observation of particle.
  - e. Colloid Titration - Color change of indicator when suspension is titrated to electric neutrality.

The best direct quantitative measure of the change in aggregate diameter can be achieved via the electronic particle counting and sizing technique. However, because of the difficult experimental procedure and the high cost of the data acquisition and data reduction equipment, electronic particle sizing is presently confined to laboratory experiments. Flocculation data recorded by this technique were utilized as the basis

against which the data taken by more practical techniques were compared.

A single test was selected from each of the three remaining categories for comparison with the particle size data taken with the Coulter Electronic Particle Counter.

1. In a modification of the conventional jar test, the flocculation process was followed by measuring the ratio of light scattered at  $90^{\circ}$  to that transmitted at  $0^{\circ}$  from an E. coli suspension flocculated with PEI. This scattering ratio was measured for both continuously stirred suspensions and for settled suspensions.

2. The membrane refiltration technique of LaMer et al. (2) was utilized by passing the E. coli-PEI suspension through a  $0.45 \mu\text{m}$  Millipore filter under constant pressure. The collected filtrate was then refiltered through the cake and filter septum, with the time of refiltration recorded. The membrane refiltration technique, with a firm theoretical basis in the Kozeny-Carman equation, was felt to be representative of the many sedimentation/filtration tests.

3. The zeta potential test was selected to provide an indication of the degree of neutralization of the negative surface charge on the E. coli caused by adsorption of cationic PEI. Although the measurement of the aggregate electrophoretic mobility, and the subsequent determination of zeta potential, is ideally suited to systems following

the electrokinetic theory, the test has little validity when the bridging theory is operative, such as with anionic or nonionic flocculants.

## 5.2 Aggregate Count and Size Distribution

Aggregation in suspensions is the formation of agglomerates without coalescence, i. e., without the actual rupture of the interfacial film and the subsequent formation of larger droplets. Generally, the aggregation behavior must be deduced in a qualitative or semi-quantitative fashion from filtration, sedimentation, or light scattering measurements. Because the degree of aggregation is subject to such a wide variety of variables: pH, ionic strength, flocculant dose, particulate concentration, shear intensity, etc., a quantitative measure of the aggregation process is needed to understand the influence of each factor involved. Electronic particle counting and sizing provides this quantitative measure.

### 5.2.1 Prior Applications of Electronic Particle Counting

In 1956, W.H. Coulter announced the development of a precise counter for discrete microscopic particles (3). This counter found immediate application in many medical and industrial situations. Mattern, Brackett, and Olson (4) used a 100  $\mu\text{m}$  aperture to measure the number and size of red blood cells: they found the instrument counts to be more accurate than those obtained via the hemacytometer,

and deduced a linear relationship between pulse height and particle volume. Kubitschek (5,6) extended the instrumental technique to bacteria with the use of a 10  $\mu\text{m}$  aperture, and also found a strictly linear performance of the counter in response to particle volume, as long as the particle diameter was greater than 10%, and less than 40%, of the aperture diameter. Further experimental improvements: coincidence counts, background reduction, and size distributions for discrete particles, are discussed in the work of Wachtel and LaMer (7).

Higuchi, Okada, and Lemberger (8) were among the first to study the aggregation of particles (in this case an oil-in-water emulsion) with a Coulter Counter. They prepared a relatively monodispersed emulsion, with droplets of about 1  $\mu\text{m}$  diameter, by an electrical dispersion technique and then measured the aggregation/deaggregation of this emulsion with varying concentrations of dioctyl sodium sulfosuccinate (AOT). Over a period of 9 to 12 days, a 50% reduction in the number of 1  $\mu\text{m}$  particles was recorded in aggregation experiments with 2% emulsions containing more than 0.2% AOT, and a 600% increase in the number of 1  $\mu\text{m}$  particles was recorded in deaggregation experiments with 1% emulsions containing less than 0.1% AOT. In spite of these large changes in the degree of aggregation, the particle size distributions appear to change very little except within the immediate vicinity ( $\pm 0.5 \mu\text{m}$ ) of the 1  $\mu\text{m}$  monodisperse particles (Figure 5.1).

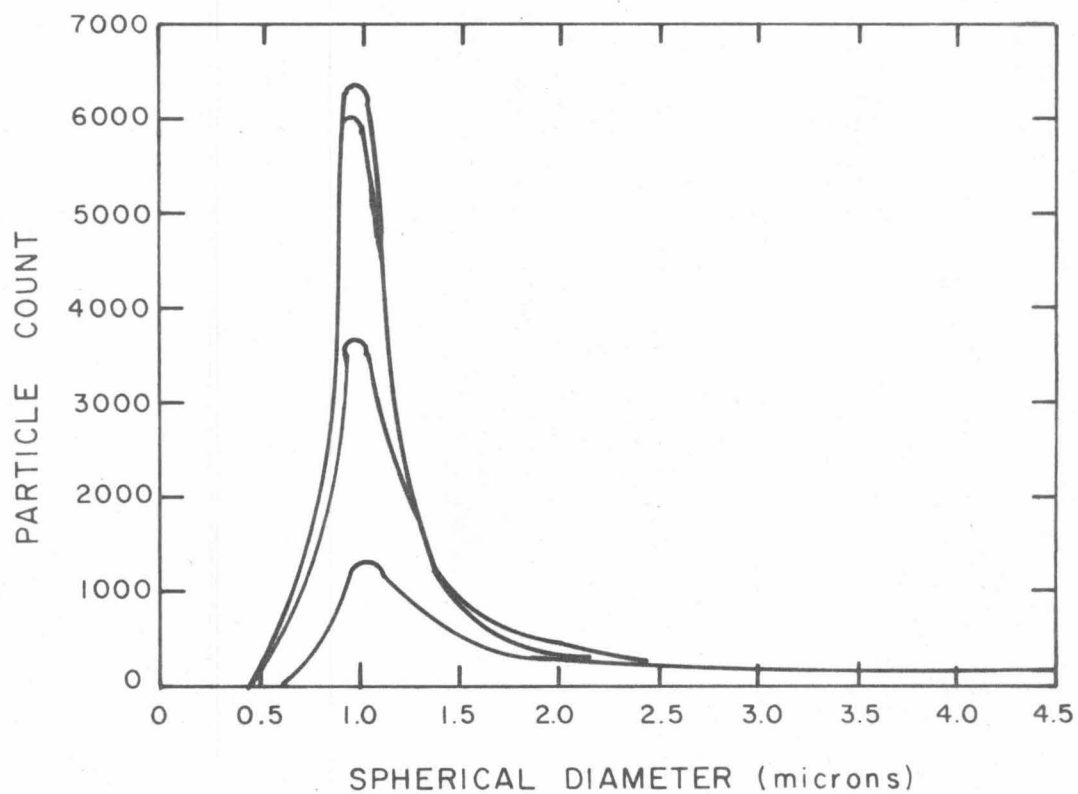


Figure 5.1 Deaggregation of a 1.% Hexadecane Emulsion with 0.09% AOT. Adapted from Higuchi et al. (8).

Further improvements in measuring the particle size distribution of aggregating systems included the introduction of the multi-aperture analysis procedure (9,10), and the application of a pulse height analyzer with multichannel storage (1, 11). Birkner and Morgan (9,10) used interchangeable apertures of 30, 70, 140, 280, and 400  $\mu\text{m}$  diameter to determine the particle size distributions during flocculation of 1.3  $\mu\text{m}$  polystyrene latex particles with polyethyleneimine. The use of the five aperture sizes permitted the study of aggregating particles from 1.3 to 17.0  $\mu\text{m}$  diameter, while minimizing aggregate breakup due to high fluid velocities encountered in the smaller apertures. Ham, Christman, and TeKippe (1,11) fitted the electronic particle counter with a standard 128 channel pulse height analyzer which sized each aggregate pulse and stored the signal in the proper channel. The particle size histogram can then be printed out in one rapid recall, enabling sequential readings to be taken during the coagulation process.

The accuracy of the Coulter Counter in enumerating and sizing single particles within the size range 10-40% of aperture diameter has been verified with both the optical and electron microscope. In the case of particle aggregates, only qualitative checks have been made on particle sizes recorded by the counter. The first indication that the Coulter Counter/multichannel analyzer may not accurately record the aggregate size was noted by Camp (12) in his analysis of a series of

experiments by Hannah, Cohen, and Robeck (13). Hannah et al. (13) evaluated the floc strength of a kaolin-alum floc in a modified Couette mixing apparatus which contained a 70  $\mu\text{m}$  aperture capable of recording six size ranges from 1.3  $\mu\text{m}$  to greater than 9.0  $\mu\text{m}$ . Using their data, Camp estimated the volume fractions for mixing times of 1, 5, and 10 minutes to be 4.7, 3.0, and 2.2 ppm respectively. The initial volume of clay and  $\text{Al}_2\text{O}_3$  was estimated at 4.3 ppm, and the velocity gradient was set at 50  $\text{sec}^{-1}$  to promote rapid floc formation without settling. Camp attributed the recorded loss of volume during flocculation to the dissolution of kaolin within the system.

Camp (14) attempted a similar volumetric analysis of the data of Ham and Christman (11), in which the formation of silica floc with alum was studied with a 240  $\mu\text{m}$  aperture. Camp determined that the volume concentration increased from 1.6 ppm to 3.6 ppm as the flocculation proceeded from 10 to 36 minutes. This result is expected since the 240  $\mu\text{m}$  orifice resolves only the upper end of the total particle size distribution: i. e., due to background noise, small agglomerates and individual silica particles were not detected in the initial size distribution measurement. With flocculation, more large aggregates are detected, but the loss of small particles within the total size distribution goes unnoticed. Using the data of Ham and Christman, Camp calculated the water content of the silica-alum floc to range from 74 to 99.9%.

Recently, Neis, Eppler, and Hahn (15) recorded a decrease in the specific resistance of polystyrene latex agglomerates during flocculation. This decrease was attributed to the higher electrolyte content of the aggregates, and resulted in Coulter Counter responses to the aggregate size which were smaller than the actual aggregate size. Neis et al. (15) presented similar results for the particle size distribution of a suspension of Bacillus Cereus in 0.25 M NaCl.

In spite of this difficulty, the Coulter Counter-multichannel analyzer technique offers the potential for precise quantitative measurement of the flocculation of colloidal particles. In flocculation experiments with PEI-E. coli, three apertures (11  $\mu\text{m}$ , 30  $\mu\text{m}$ , and 70  $\mu\text{m}$ ) were utilized to follow the change in the total particle size distribution. With this three aperture system, all but the very smallest cells ( $d \leq 1.0 \mu\text{m}$ ) and the very largest aggregates ( $d \geq 25 \mu\text{m}$ ) were enumerated and sized. This size range of equivalent spherical diameters corresponds to cell aggregates composed of 1 to 7100 cells of 1.3  $\mu\text{m}$  mean diameter.

### 5.2.2 Theory of Electronic Particle Counting

In the operation of the Coulter counter (Figure 5.2), a vacuum supply (P) is used to draw a sample of the cell suspension through a small orifice (A) in the wall of a nonconducting tube (B). Electrodes

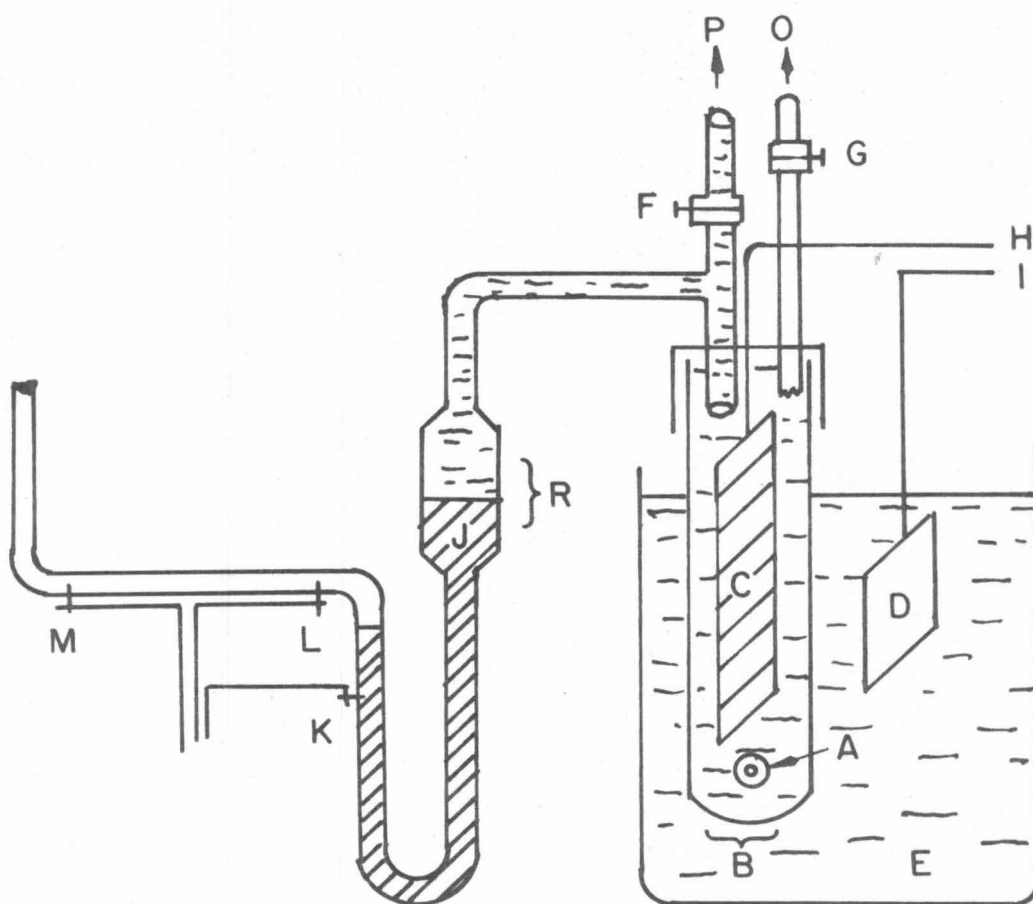


Figure 5.2 Schematic Diagram of Aperture Unit: A, Aperture; B, Test Tube with Aperture; C, Electrode within B; D, Electrode outside B; E, Dilute Cell Suspension; F and G, Control Stopcocks; H and I, Electrode Leads to Amplifier and Power Supply; J, Mercury Column and Reservoir R; K, L, and M, Electrodes to Activate and Stop Counter at Measured Volumes of flow. Adapted from Mattern et al. (4).

(C,D), located in the electrolyte chambers on either side of the orifice, carry a constant current between them. As each particle passes through the aperture, it displaces a volume of electrolyte equal to its own volume within the aperture, thus momentarily changing the resistance between the electrodes. This produces a voltage pulse of short duration having a magnitude proportional to the particle volume: the resulting series of pulses is electronically amplified, scaled, and counted. As shown in Figure 5.2, an external vacuum P initiates flow through the aperture and unbalances the mercury manometer. Closing the stopcock F isolates the system from the external vacuum, and the rebalancing mercury draws measured samples (50  $\mu\text{l}$  for 11  $\mu\text{m}$  apertures, and 500  $\mu\text{l}$  for 30  $\mu\text{m}$  and 70  $\mu\text{m}$  apertures) through the aperture.

Figure 5.3 visualizes the passage of a small cylindrical particle, of length  $ad$  and diameter  $bd$ , through an aperture of diameter  $D$  and thickness  $ad$ . The resistance  $R_o$  of the aperture segment without the particle is given by

$$R_o = 4j_o ad/\pi D^2 \quad (5-1)$$

where  $j_o$  = resistivity of electrolyte

The resistance  $R$  of the aperture segment with the particle, equivalent to the resistance of two resistors in parallel, is given by

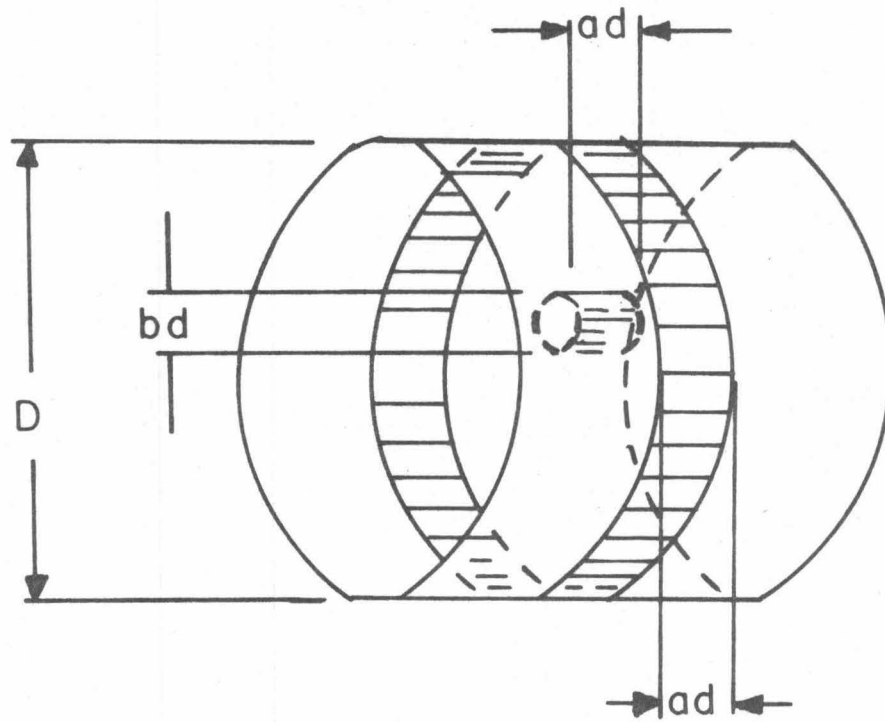


Figure 5.3 Diagram of Aperture with Small Cylindrical Particle.

$$R = \left[ \frac{1}{\frac{j_o a d}{(\pi/4)(D^2 - b^2 d^2)}} + \frac{1}{\frac{j a d}{\pi b^2 d^2 / 4}} \right]^{-1} \quad (5-2)$$

where  $j$  = resistivity of particle

Then the resistance change caused by the particle passage is

$$\Delta R = R - R_o = \left[ \frac{1}{\frac{j_o a d}{(\pi/4)(D^2 - b^2 d^2)}} + \frac{1}{\frac{j a d}{(\pi/4)b^2 d^2}} \right]^{-1} - \frac{4j_o a d}{\pi D^2}$$

$$\Delta R = \frac{j_o a}{\pi D^2 / 4} \frac{d^3 (1 - j_o / j)}{(1/b^2) - (d^2/D^2)(1 - j_o / j)} \quad (5-3)$$

For a spherical particle equivalent in volume to the above cylindrical particle,

$$V = \pi d^3 / 6 = \pi b^2 d^2 a d / 4$$

$$1/b^2 = 1.5a \quad (5-4)$$

and

$$\Delta R = (4j_o / \pi D^4) \frac{d^3}{(1.5/(1 - j_o / j)) - (d^2 / a D^2)} \quad (5-5)$$

Thus the response to a singlet particle is directly proportional to the particle volume, except as modified by the second term in the

denominator. Both Kubitschek (5,6) and Wachtel and LaMer (7) found that  $d/D$  should not exceed 0.4 to minimize aperture jamming and to preserve linearity of response. Furthermore, in most instances  $j \gg j_0$  and equation (5-5) can be written as

$$\Delta R = 4j_0 d^3 / 1.5\pi D^4 \quad (5-6)$$

In the case of aggregates, however, this latter simplification cannot be justified due to the porosity of the aggregate itself. When a large aggregate of tightly bound singlets passes through a small (11  $\mu\text{m}$ ) or medium (30  $\mu\text{m}$ ) aperture, the aggregate tends to feather itself along the streamlines of the rapidly flowing sample volume. This elongation of the aggregate as it passes through the aperture results in a pulse having both height and width. Although the pulse height can be calibrated with monodisperse polystyrene latex particles, the pulse width goes uncalibrated. A similar result was noticed by Mattern, Brackett, and Olsen (4) in their analysis of coincidence passage by singlet particles. Figure 5.4A depicts the critical volume in which the particle size is measured. Figure 5.4B and 5.4C show that the separation distance of two particles during coincident transit of the critical volume determines the relative pulse height and width. For small tightly bound aggregates, the pulse height should be directly proportional to the number of singlets in the aggregate. However, as

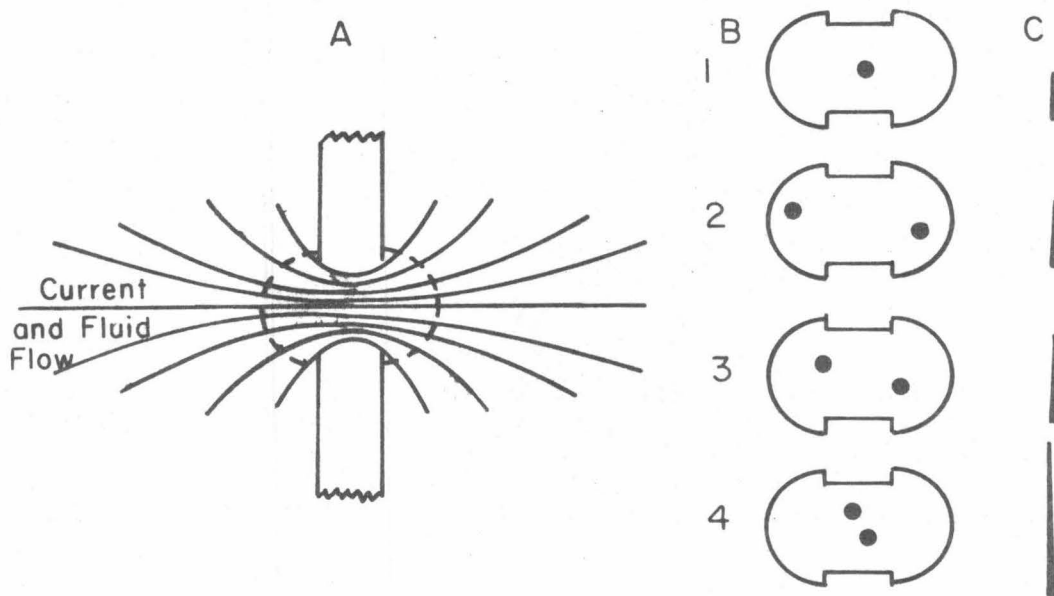


Figure 5.4A Schematic Representation of Aperture, Current Density Lines, and Critical Volume.

Figure 5.4B Particle Separation Distances in Critical Volume.

Figure 5.4C Resulting Voltage Pulses. Adapted from Mattern et al. (4).

the porosity increases and the aggregates elongate within the critical volume, the pulse width increases at the expense of pulse height.

A second problem occurs when a large aggregate passes through a medium (30  $\mu\text{m}$ ) or large (70  $\mu\text{m}$ ) aperture. If the porosity of the aggregate is large, then the aggregate sizing system (aperture, current, and amplification) is required to size and sum the many smaller pulses created by the primary particles which comprise the total aggregate. However, only the small 11  $\mu\text{m}$  aperture is able to precisely detect and size the bacteria cells: the larger 30  $\mu\text{m}$  and 70  $\mu\text{m}$  apertures only partially detect the singlet cells, and thus the system response is only a partial response to the total particulate volume within the aggregate. Neis, Eppler, and Hahn (15) recorded these effects as increases in the calibration factor during the course of coagulation: the calibration factor being the ratio of actual particulate volume to Coulter Counter measured volume.

### 5.2.3 Proposed Modification to Theory for Aggregate Passage

In order to compensate for the effect of aggregate porosity upon the measured volume following flocculation, determinations of aggregate porosity, as a function of the number of primary particles within an aggregate, were made either from calculations or from literature survey. These porosity values are summarized in Table 5.1.

<u>#Cells/ Aggreg.</u>	<u>Configuration</u>	<u>Porosity</u>	<u>Reference</u>
2	Linear	0.20	
3	Linear-triangular	0.25-0.26	
4	Linear-tetrahedral	0.27-0.29	
8	Cubic-rhombohedral	0.26-0.48	Graton & Fraser (16)
	Coarse sand	0.39-0.41	Muskat (17)
	Medium sand	0.41-0.48	"
	Fine sand	0.44-0.49	"
	Fine sandy loam	0.50-0.54	"
	d ≤ 20 μm	0.50	Terzoghi (18)
	d ≤ 2 μm	0.95	"
Silica powder	d ≤ 21 μm	0.38	Shapiro & Kolthoff (19)
"	d ≤ 16 μm	0.43	"
"	d ≤ 6 μm	0.75	"
"	d ≤ 2.3 μm	0.89	"
	d ≤ 5 μm	0.71	Dixon, LaMer, & Linford (20)
Clay & alum	d ≤ 15 μm	0.74-0.99	Camp (14)

Table 5.1 Typical Value of Aggregate Porosity as a Function of Number of Cells per Aggregate and Cell Diameter.

For aggregates of E. coli-PEI, with aggregate diameters ranging between 2.6 and 25  $\mu\text{m}$ , typical values of aggregate porosity would lie between 0.50 to 0.95. Other authors have attributed high porosity values to electrostatic repulsion between primary particles, a condition ameliorated by the adsorption of PEI which neutralizes the negative surface charge, and by the continuous agitation of the suspension during flocculation. Nevertheless, the PEI-E. coli system does produce an open porous structure, as determined by electron microscopy.

Figure 5.5 depicts a smooth curve of porosity versus number of cells per aggregate, drawn from the data of Table 5.1 such that two conditions are satisfied:

1. For aggregates with less than 8 cells, the curve passes through the calculated porosity values.
2. For larger aggregates, the curve is asymptotic to the porosity value between 0.50 and 0.95 which enables a conservation of volume condition to be met between unflocculated and flocculated state.

The shape of the curve relating the calculated porosity  $f$  to the number of cells per aggregate  $B$  suggests an exponential relationship of the form

$$B = ab^f \quad (5-7)$$

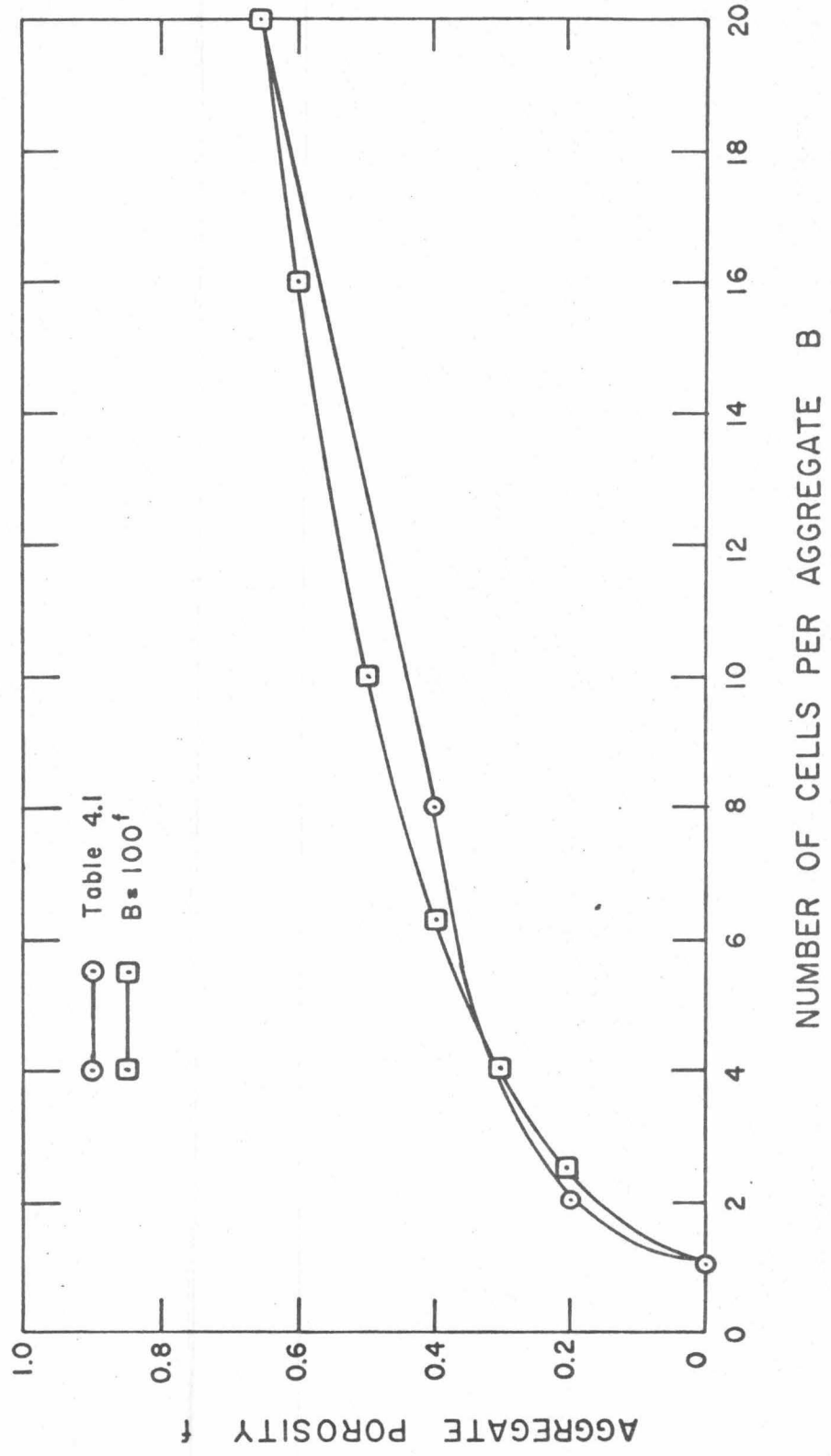


Figure 5.5 Aggregate Porosity as a Function of the Number of Cells per Aggregate.

Since  $B = 1$  at  $f = 0$ ,  $a = 1$ . Further calculation provides a best fit when  $b = 100$ , yielding

$$B = 100^f$$

$$f = \frac{1}{2} \log B \quad (5-8)$$

An asymptotic porosity value of 0.65 provided conservation of volume of the total suspended matter in the unflocculated and flocculated state.

The formation factor  $F$  is defined as the ratio of the resistivity of the porous material,  $j_f$ , saturated with an electrolyte to the bulk resistivity of the same electrolyte,  $j_o$ :

$$F = j_f/j_o$$

Archie (21) has determined an empirical relationship between porosity and formation factor which applies to most porous materials:

$$F = j_f/j_o = f^{-m} \quad (5-9)$$

where  $m = 2.0$  for clean sands, and slightly less than 2.0 for all other materials; i. e.,  $m \approx 1.9$ .

Letting  $m = 1.9$  for the E. coli aggregates, and substituting equation (5-8) into equation (5-9), yields

$$j_f = j_o \left(\frac{1}{2} \log B\right)^{-1.9} \quad (5-10)$$

As derived earlier, the Coulter Counter response to aggregate passage through the orifice is given by

$$\Delta R = (4j_o / \pi D^4) \frac{d^3}{(1.5 / (1 - j_o / j)) - (d^2 / aD^2)} \quad (5-5)$$

where  $j_o$  = electrolyte resistivity

$D$  = aperture diameter

$d$  = equivalent spherical diameter of aggregate material

$a \approx 3$  for rod-shaped E. coli

As the aggregate size increases, larger apertures must be used in order to maintain  $d/D$  less than 0.4, and  $d^2/aD^2$  insignificant.

Substituting equation (5-10) into equation (5-5) yields:

$$\Delta R = 4j_o d^3 (1 - (\frac{1}{2} \log B)^{1.9}) / 1.5\pi D^4 \quad (5-11)$$

In equation (5-11), the response  $\Delta R$  of the Coulter Counter to the aggregate passage is a function of two unknowns:  $d$ , the equivalent spherical diameter of the aggregate, and  $B$ , the number of cells per aggregate. However,

$$B = (\pi d^3 / 6) / (\pi d_m^3 / 6) \quad (5-12)$$

where  $d_m$  = mean cell diameter.

Therefore,

$$\Delta R = 4j_o d^3 (1 - (1.5 \log(d/d_m))^{1.9}) / 1.5 \pi D^4 \quad (5-13)$$

Experimentally, for  $d \leq d_m$

$$\Delta R = 4j_o d^3 / 1.5 \pi D^4 \quad (5-14)$$

and the Coulter counter response is directly proportional to the particle diameter  $d$ . For  $d \gg d_m$ ,

$$(1 - (1.5 \log(d/d_m))^{1.9}) \rightarrow 0 \quad (5-15)$$

and therefore

$$R \rightarrow 0$$

Consequently, as the porosity of the aggregate increases, the response of the Coulter counter decreases. Since the actual volume of aggregate material does not change, the response of the counter must be modified to account for the effect of the aggregate porosity on the instrument response. The following paragraphs discuss the proposed modification to the analysis of the initial Coulter counter data to compensate for the effects of aggregate porosity.

The best method of calibrating the counter/multichannel analyzer is by passing monodisperse particles through the selected aperture. At given current and amplification settings, each different

diameter particle will produce a response which is recorded in a corresponding channel of the multichannel analyzer (MCA). Figure 5.6 is a representation of the display created by the voltage pulses of a sample suspension containing particles of three different diameters. Since the voltages pulses  $v_i$  are proportional to the volume  $V_i$  of the respective particles,

$$v_i \propto V_i = \pi d_i^3 / 6$$

$$v_i = k \pi d_i^3 / 6 = K d_i^3 \quad (5-16)$$

These voltages, upon entering the pulse height analyzer (PHA), are converted to the log mode, thereby enabling a broader spectrum of particles to be displayed by the MCA-oscilloscope.

$$\log_x (v_i) = \log_x K + 3 \log_x (d_i) \quad (5-17)$$

The log of the voltage pulse is stored directly by the MCA into one of its channels, the location being dependent upon the size of the pulse. However, since a coarse gain amplification precedes the logarithmic conversion, and a fine gain amplification follows the logarithmic converter output, the combined system may not yield a linear relationship between respective channels.

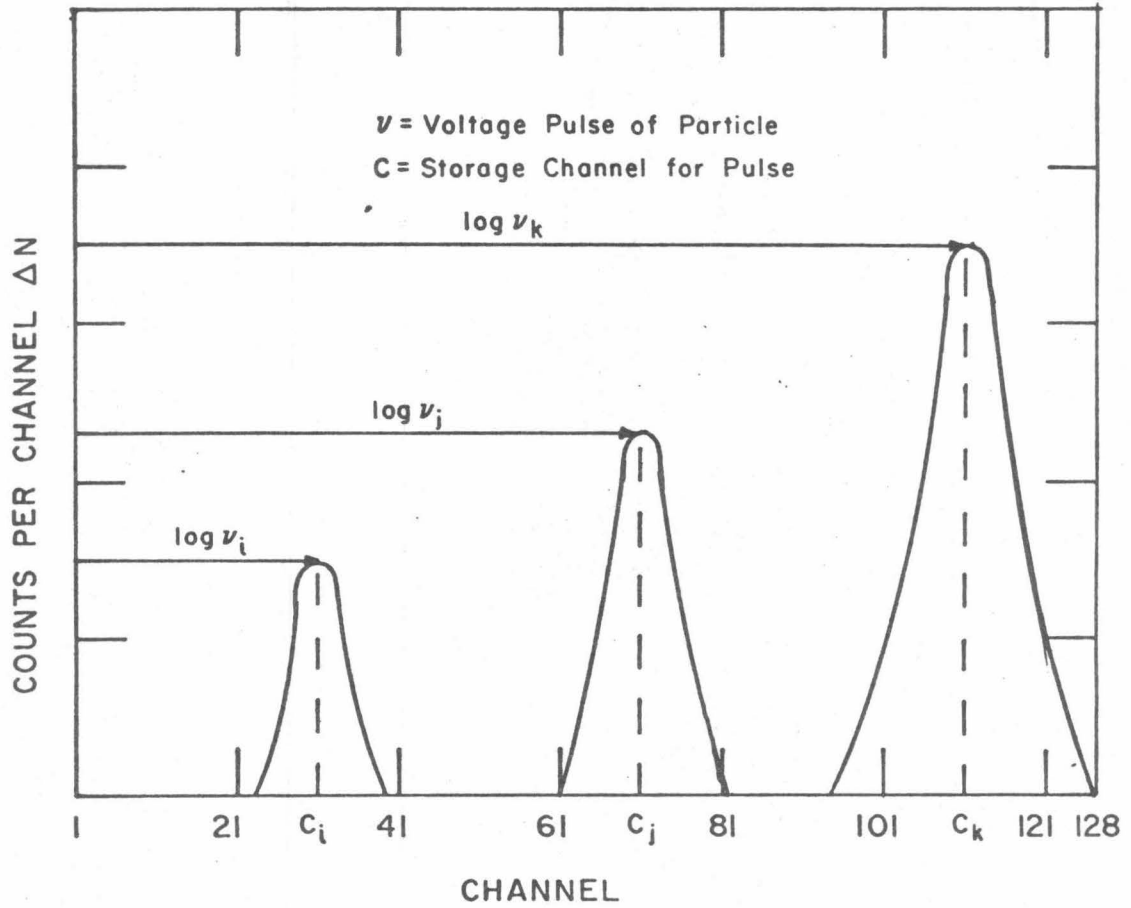


Figure 5.6 Record of Voltage Pulses for Suspension of Three Different Monodisperse Particle Sizes.

Initially, the relationship between voltages pulses ( $v_i, v_j$ ) and channels ( $C_i, C_j$ ) is written as follows:

$$\begin{aligned} C_i &= A \log_x v_i + E \\ C_j &= A \log_x v_j + E \end{aligned} \quad (5-18)$$

where A and E are constants which compensate for the coarse and fine gain amplifications.

$$\begin{aligned} C_j - C_i &= \Delta C = A \log_x (v_j/v_i) \\ \Delta C &= \log_y (v_j/v_i) \\ y &= (v_j/v_i)^{1/\Delta C} = (v_j/v_i)^{1/(C_j - C_i)} \end{aligned} \quad (5-19)$$

where y is the logbase used by the MCA in the storage of the voltage pulses. In addition, upon substituting equation (5-16) into equation (5-17), there results:

$$\begin{aligned} C_j - C_i &= \log_y (Kd_j^3 / Kd_i^3) \\ C_j - C_i &= 3 \log_y (d_j/d_i) \\ d_j &= d_i y^{(C_j - C_i)/3} \end{aligned} \quad (5-20)$$

The setting for the coarse gain on the PHA/MCA was determined with a voltage pulse generator such that a constant logbase y

resulted over the full range of channels, i. e., from channel 1 to 128. Varying the frequency of the voltage pulse, within the recovery time of the electronic circuitry, did not shift the channel of record. By using monodisperse polystyrene latex particles, it is possible to determine the logbase of the Coulter counter/PHA/MCA system for different aperture diameters, current settings, and amplification factors.

If, in equation (5-20),  $d_i$ ,  $C_i$ ,  $C_j$ , and  $y$  are known then  $d_j$  can be computed provided that the particle is not an aggregate. In the case of singlets,

$$\Delta R_j = \Delta R_i y^{(C_j - C_i)} \quad (5-21)$$

when (5-20) is cubed and substituted into (5-6).

For the flocculating PEI-E. coli suspension, equations (5-21) and (5-20) were utilized to determine the particle diameter from the instrument response provided that the diameter was less than or equal to the mean cell diameter, determined from an unflocculated suspension.

When the instrument response indicated an aggregate larger than the mean cell diameter, it was necessary to include the porosity factor of equation (5-13), such that:

$$\Delta R_j = 4j_o d_j^3 (1 - (1.5 \log (d_j/d_m))^{1.9}) / 1.5\pi D^4$$

$$\Delta R_j = \Delta R_{d_m} y^{(C_j - C_{d_m})} = 4j_o (d_m)^3 y^{(C_j - C_{d_m})} / 1.5\pi D^4 \quad (5-13)$$

Therefore:

$$d_j^3 (1 - (1.5 \log (d_j/d_m))^{1.9}) = (d_m^3) y^{(C_j - C_{d_m})} \quad (5-22)$$

In equation (5-22),  $d_m$ ,  $y$ ,  $C_j$ , and  $C_{d_m}$  are known, and therefore  $d_j$  can be calculated via an iterative technique, using an initial estimate that:

$$d_j \geq d_m y^{(C_j - C_{d_m})/3} \quad (5-23)$$

The porosity factor  $(1 - (1.5 \log (d_j/d_m))^{1.9})$  decreases until it reaches 0.5, which corresponds to the asymptotic value of the porosity for large aggregates,  $f = 0.65$ . The overall effect at a porosity of 0.65 is to increase the particle diameter 25% above that recorded by the Coulter Counter.

### 5.3 Light Scattering by Aggregated Particles

There are presently three interpretations of light scattering data derived from coagulating systems. One treats both single particles and aggregates of particles as Rayleigh scatterers, in which an aggregate of  $k$  spheres, each of volume  $v$ , is equivalent to a Rayleigh

sphere of volume  $k^3$ . For such a sphere, the light scattered is  $k^2$  times that from a single sphere. The second, a Rayleigh-Gans type treatment derived by Benoit et al. (22) evaluates the scattering properties of aggregates whose constituent particles have refractive indices close to that of the dispersion medium. And finally, the third interpretation based on Mie theory is used for larger particles of unspecified index of refraction. Since the bacteria are obviously larger than Rayleigh spheres, only the latter two interpretations will be investigated more thoroughly.

### 5.3.1 Rayleigh-Gans Scattering

#### 5.3.1.1 Suspensions of Medium-Sized Particles

If particles possess a linear dimension greater than one-twentieth of the wavelength of the incident light, they are not considered optically small, and the character of the light scattered is more complicated than that given by the dipole radiator theory of Rayleigh. For these particles, the scattered light will be the superposition of the wavelets from various parts of the same particle, resulting in interference between scattering centers. In the general case, the phase and intensity of the wavelets will bear complicated relationships to each other; an exact solution is available only for the case of the homogeneous sphere. However, an approximate solution was

developed by Rayleigh (23) and Gans (24) for the case in which the primary light field is not distorted appreciably in the scattering process. This condition is satisfied for particles smaller than the wavelength of light in media chosen so that the relative refractive index (particle/medium) is less than about 1.20. Under these conditions, the researcher is able to consider the solute molecules as divided into a series of independent dipole submolecules which radiate according to the Rayleigh principle. As long as the difference in optical constants between the particles and the surrounding medium is low, the approximate length and shape of discrete particles can be determined. Rayleigh and Gans obtained a function  $P(\Psi)$  which, if multiplied on the right side of equation (3-8), will correct for interference between wavelets.

$P(\Psi)$ , the ratio of the scattered intensity at an angle  $\Psi$  to that which would be observed if the particles had the same molecular weight but infinitesimal dimensions compared to  $\lambda$ , is given by

$$P(\Psi) = (1/N^2) \sum_{i=1}^N \sum_{j=1}^N \sin hR_{ij} / hR_{ij} \quad (5-29)$$

where  $N$  = number of scattering centers within the molecule

$R_{ij}$  = distance between any pair of centers  $i$  and  $j$

$h = (4\pi/\lambda) \sin \Psi/2$

Debye (25) calculated the diminution factors relative to the intensity of scattering using the average sum of contributions from the submolecules. These factors for spherical, rod-like, and randomly coiled molecules are given below:

$$P(\Psi) = (3(\sin z - z \cos z)/z^3)^2 \quad (\text{spheres}) \quad (5-25)$$

$$P(\Psi) = 2(e^{-y} - (1-y))/y^2 \quad (\text{coils}) \quad (5-26)$$

$$P(\Psi) = \frac{1}{2} \left( \int_0^{2z} (\sin w/w) dw \right)^2 - ((\sin z)/z)^2 \quad (\text{rods}) \quad (5-27)$$

where  $P(\Psi)$  = normalized intensity of scattering at angle  $\Psi$

$$z = (2\pi l/\lambda) \sin \Psi/2$$

$$y = 8/3 (\pi l/\lambda)^2 (\sin \Psi/2)^2$$

$w$  = dummy variable of integration

$l$  = diameter in case of spheres, mean square distance  
between ends for coils, and length in case of rods

These equations relate the amount and direction of scattered light with the size and shape characteristics of the molecules, with allowance for interference between the scattered wavelets from a particle. Using this method, Oster (26) successfully estimated the shape and length of the tobacco mosaic virus.

Overall, the Rayleigh-Gans treatment of the scattering by large particles as an assembly of independent dipole oscillators must meet the condition  $2\alpha(m-1) \ll 1$  where  $\alpha = 2\pi r/\lambda$ , and  $m = \mu/\mu_0$ .

Thus for particles such as bacteria, which have a low relative refractive index ( $m = 1.06$ ) but are large ( $r = 0.65 \mu\text{m}$ ) compared with the wavelength of incident light, this simplified picture may not apply since  $2 \alpha (m-1)$  is about one or a little less. However, Koch (27) has pointed out that the Rayleigh-Gans method may give quite precise results, if only the total amount of light scattered is to be computed. The reason for this is simply that the main influence of the phase shift is to change the direction in which the scattered light wavelets most strongly interfere without influencing the total amount of interference. Thus, the intensity calculated for a particular direction may be strongly in error -- the turbidity may not.

#### 5.3.1.2 Aggregates of Medium-Sized Particles

In the analysis by Benoit et al. (22), primary particles within an aggregate scatter light which interferes immediately with that scattered by its aggregate neighbors. The intensity of the light scattered at an angle  $\Psi$  by an aggregate of  $k$  monodisperse spheres randomly oriented to the incident light beam can be expressed as

$$I_k(\Psi) = kI_1(\Psi) [1 + (2/k)A_k(\Psi)] \quad (5-28)$$

where  $I_1(\Psi)$  is the intensity of light scattered at an angle  $\Psi$  by a single primary sphere (Rayleigh-Gans or Mie Theory) and  $A_k(\Psi)$  is a form

factor which is a function of the geometry of the aggregate and of the scattering angle  $\Psi$ . Benoit et al. (22) analogize the aggregate form factor  $A_k(\Psi)$ , due to interference of particles within an aggregate, to the Rayleigh-Gans form factor  $P(\Psi)$ , due to interference between scattering centers within the same particle.

The form factors and hence the scattering properties of aggregates depend upon the geometrical arrangement of particles within the aggregates. Because there are an infinite number of possible arrangements of particles in a coagulating sol, a precise evaluation of  $A_k(\Psi)$  is not possible. Generally,  $A_k(\Psi)$  can be expressed by

$$A_k(\Psi) = \sum_{i=1}^{k-1} \sum_{j=i+1}^k \frac{\sin[(4h_{ij}/\lambda)\sin\Psi/2]}{[4h_{ij}/\lambda)\sin\Psi/2]} \quad (5-29)$$

where  $h_{ij}$  is the distance between centers of the  $i^{\text{th}}$  and  $j^{\text{th}}$  particle in the aggregate, and  $\lambda$  is the wavelength of incident light. Lips et al. (28,29) assumed a system mixture of three types of aggregates: (1) linear, (2) planar, and (3) close-packed three dimensional, in deriving form factors for singlet particle multiplicities up to thirteen. In coagulation experiments on polystyrene latex, Lips et al. (28) concluded that aggregates greater than thirteen particles accounted for less than 0.5% of scattered light. Their results demonstrated the validity of the interference method in predicting light scattering

intensity from the three types of aggregates.

There appear to be several major complications to the above analysis when applied to suspensions of particles of the size and shape of E. coli. First, the turbidity measurements for the primary particles must be corrected for the rod-shape of the cells by applying equation (5-27). Second, an assumption must be made as to the system mix of aggregates; i. e., the percentage of linear, planar, and three-dimensional aggregates. For particles such as E. coli, with a relatively broad size distribution even in the uncoagulated state, determination of the system mix from the particle size distribution would be most difficult. And finally, form factors  $A_k(\Psi)$  must be calculated from the assumed system mix, and then substituted into equation (5-28) for determination of the turbidity.

### 5.3.2 Mie Scattering

#### 5.3.2.1 Suspensions of Large Particles

For systems more complex than the small particles whose scattering is described by the Rayleigh and Rayleigh-Gans approximations, most problems in light scattering involve the scattering from widely separated spherical particles. The theory for this scattering requires a formal solution of Maxwell's equations. The solution of this boundary value problem of a plane wave incident upon a particle

of arbitrary size, shape, orientation, and index of refraction has not been achieved mathematically, except for spheres via Mie theory (30, 31). Mie obtained a series expression in terms of spherical harmonics for the intensity of scattered light emergent from a sphere of arbitrary size and index of refraction. The coefficients of the series are functions of the ratio,  $m$ , of the index of refraction of the particle and that of the medium, and of the parameter  $\alpha = 2\pi r/\lambda$ , where  $r$  is the sphere radius and  $\lambda$  is the wavelength of the light in the medium.

The pattern given by the Mie series for spherical particles is determined not only by interferences between the wavelets scattered by the volume elements of the same particle, but also by distortions in phase associated with the incident and emergent light. For particles with radii comparable or large compared to the wavelength of incident light, i. e.,  $\alpha \geq 1$ , and with index of refraction ratio  $m$  differing somewhat from unity, say  $m \geq 1.30$ , the calculations of the Mie series are found in the works of Mie (30), Debye (31), and Rayleigh (32). With increasing particle size, the light scattering diagram, consisting of numerous maxima and minima, becomes increasingly complicated. The angular scattering diagrams for a small isotropic particle, determined via Rayleigh theory, and for two spheres of increasing radii, determined via Mie theory are shown in Figures 5.7 - 5.9 respectively. The dotted curves represent the intensity of horizontally

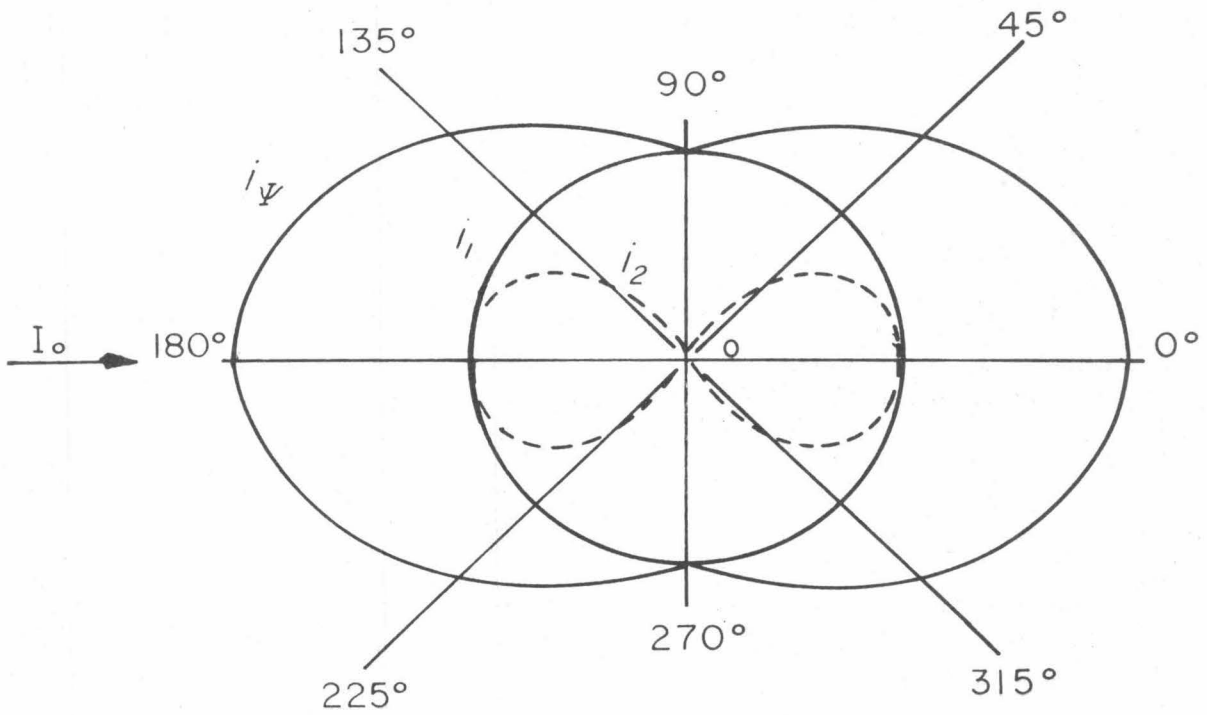


Figure 5.7 Relative Intensity of Scattering about a Small Isotropic Particle. Adapted from Bender (33).

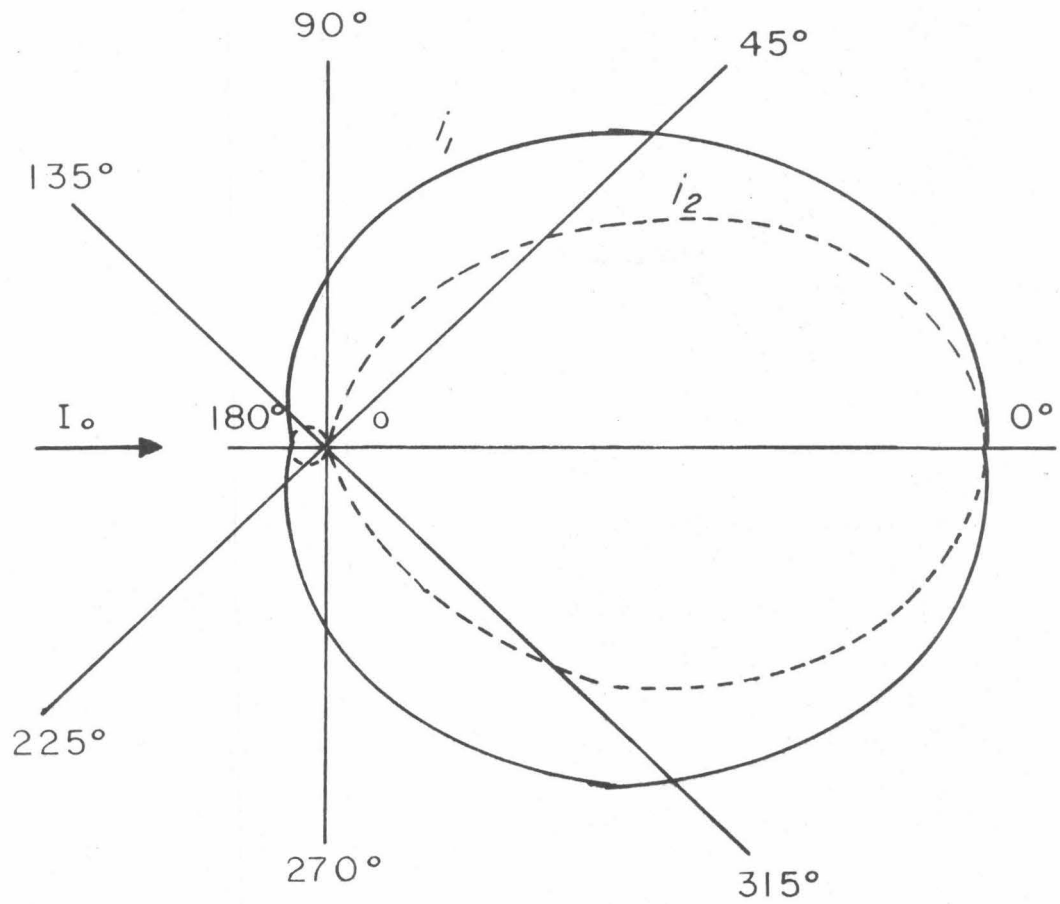


Figure 5.8 Relative Intensity of Scattering about an Isotropic Particle of Radius  $0.13 \lambda$ .  $m = 1.25$ . Adapted from Blumer (34).

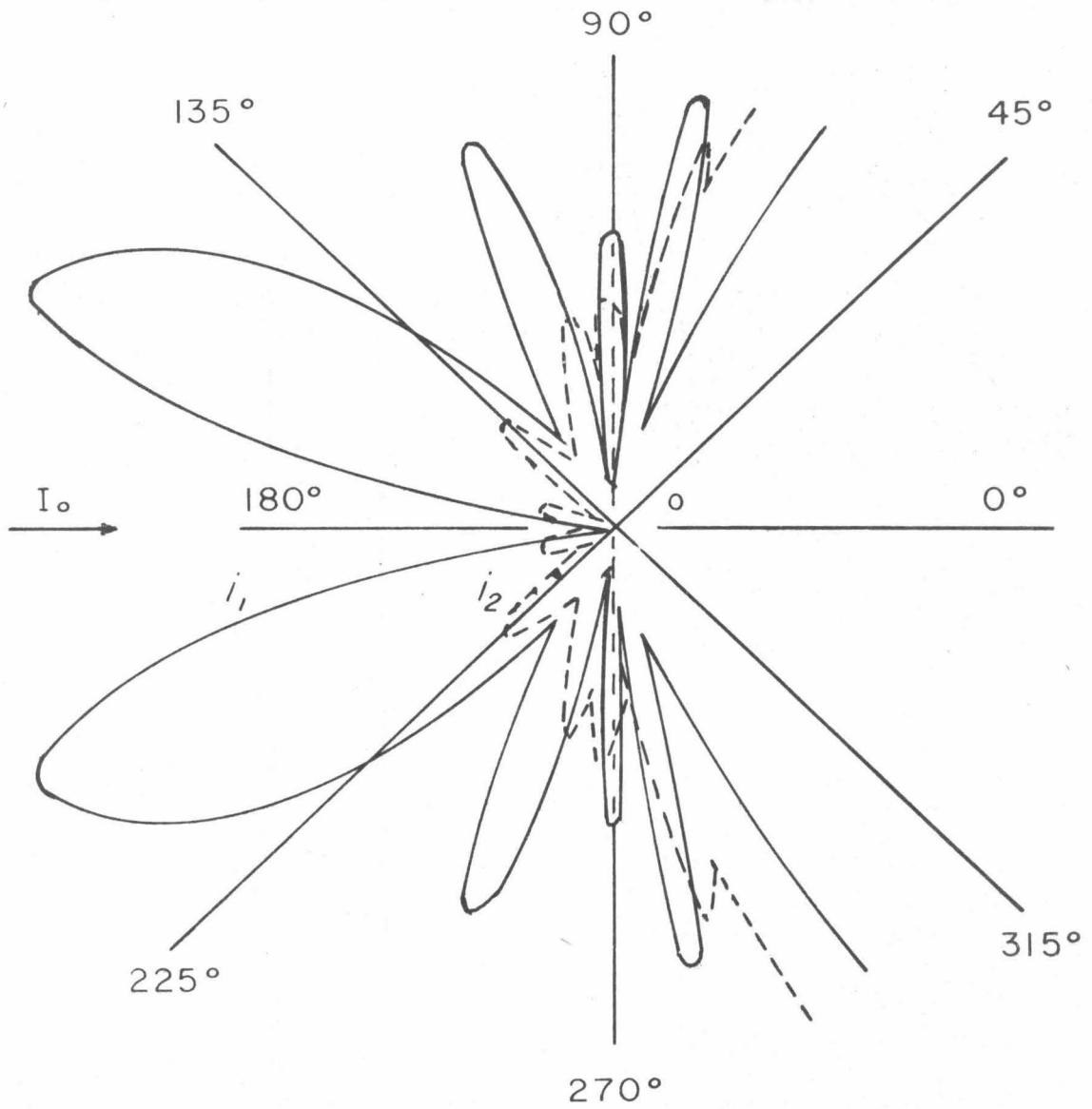


Figure 5.9 Relative Intensity of Scattering about an Isotropic Particle of Radius  $0.65 \lambda$ .  $m = 1.25$ . Adapted from Blumer (34).

polarized light; the solid lines represent intensity of vertically polarized light. The complicated scattering diagrams of Figures 5.8 and 5.9, caused by the higher spherical harmonics in the Mie series, reduce to ordinary defraction and reflection diagrams of geometrical optics for particles which are very large compared to the wavelength of light.

If the intensity of scattered light is integrated over the surface of a large sphere, then the fractional decrease in intensity of the incident light can be calculated. While for small isotropic particles this integration is easily performed (Equation 3-9), this is not the case for Mie scatterers. The total scattered radiation, expressed as the product  $nR$  (where  $n$  = the number of spheres per ml and  $R$  = the total light energy scattered by one sphere), equals the attenuation of the incident beam for the optical path length  $x$ :

$$-dI/Idx = nR \quad (5-30)$$

Integrating over the path length yields

$$\ln (I_0/I) = nRx \quad (5-31)$$

where  $I_0$  is the intensity of the incident beam and  $I$  is the intensity of the beam emerging from the scattering solution. The product  $nR$  represents the coefficient of apparent absorption resulting from light scattering, or the turbidity  $\tau$ . For a fixed path length  $l$

$$\tau = \ln(I_0/I)/l = nR \quad (5-32)$$

If the total scattering cross-section  $R$  of a sphere is divided by the geometrical cross-sectional area,  $\pi r^2$ , then the dimensionless scattering coefficient  $K$  is obtained. Mie's solution for the light scattered by spheres results in expression

$$K = 2/\alpha^2 \sum_{j=1}^{\infty} (A_j^2 + P_j^2)/(2j+1) \quad (5-33)$$

where  $A_j$  and  $P_j$  are the scattering components of the  $j^{\text{th}}$  multipole of the electric and magnetic field respectively. Although  $A_j$  and  $P_j$  are complicated and complex functions of  $\alpha$  and  $m$ , they have been precisely computed and tabulated (35).

Figure 5.10 depicts the complicated relationship between the Mie scattering coefficient  $K$ , where  $K = \tau/n\pi r^2$ , and the size-refractive index parameter  $\rho$ , where  $\rho = 2\alpha(m-1)$ .

#### 5.3.2.2 Approximations for Mie Scattering Coefficients

In 1925, Jobst (37) derived values for  $R$ , the effective area of a light scattering particle, from the Mie equations for four special "particle size - refractive index" regimes. From Jobst's derivations, the values of  $K$ , the dimensionless scattering coefficient, and the restrictions on their application caused by approximations to the Mie coefficients, are listed in Table 5.2. Thus the Jobst approximations

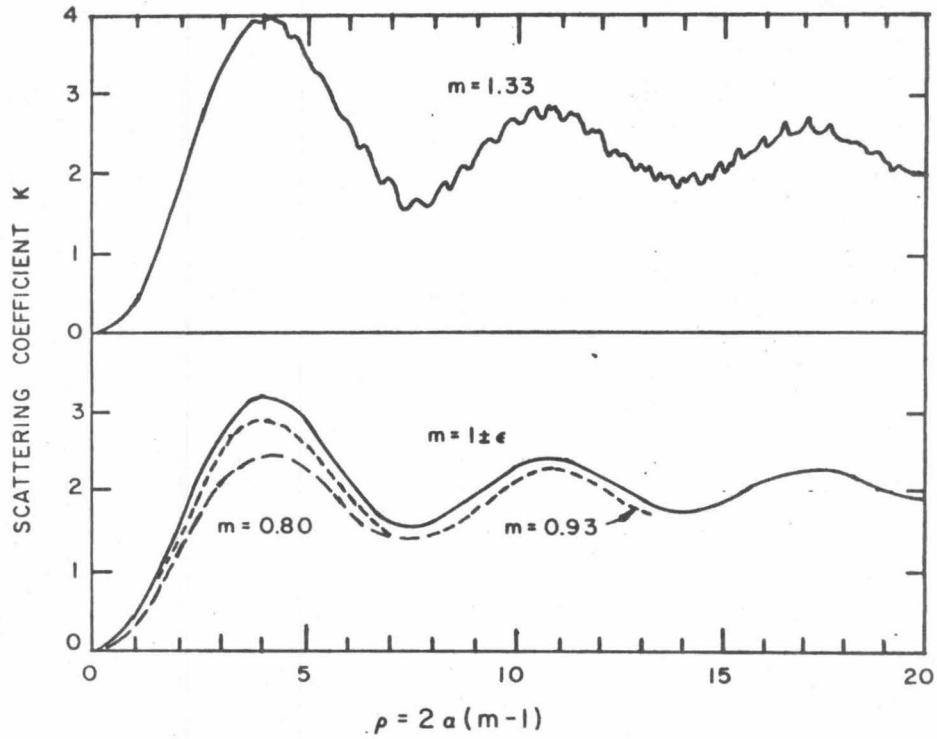


Figure 5.10 Scattering Coefficient Curves from Mie's Formulae for  $m = 1.33$ ,  $1 \pm \epsilon$ ,  $0.93$ , and  $0.80$ . Adapted from Van de Hulst (36).

K	Restrictions	Region
$32\alpha^4 (m-1)^2 / 27$	$\alpha(m-1) \ll \alpha \ll 1$	Rayleigh
$2\alpha^2 (m-1)^2$	$\alpha(m-1) \ll 1 \ll \alpha$	Anomalous
$2 - (4 \sin \rho) / \rho + 4(1 - \cos \rho) / (\rho)^2$	$\alpha(m-1)$ arbitrary	Anomalous Diffraction
2	$1 \ll \alpha(m-1) \ll \alpha$	Diffraction

Table 5.2 Approximate Values of Scattering Coefficients  
 $\alpha = 2\pi r / \lambda$ ,  $\rho = 2\alpha(m-1)$ .

provide simple analytical solutions in the case of particles of the dimension and composition of bacteria, since  $\alpha$  is quite large ( $\alpha \cong 10$ ) and yet  $\alpha(m-1)$  is small ( $\alpha(m-1) = 0.6$ ). Figure 5.11 compares the Jobst solution,  $K = 2\alpha^2(m-1)^2$ , with the exact solution for spheres of relative refractive indices of 1.05 and 1.10, taken from published Mie tables, and with the approximate Rayleigh-Gans solution for relative refractive index  $1.00 + \epsilon$ .

For a given weight (or volume) of material which is monodispersed into particles of very small size so that Rayleigh's Law is obeyed ( $r < \lambda/20$ ), the turbidity will increase as the third power of the radius, since the number of particles per unit volume of the system decreases inversely as the third power of the radius, while the scattering of each particle increases as the sixth power of the radius, and the turbidity is the product of these quantities, i. e.,

$$\tau = K n \pi r^2 \quad \text{where } K = 32\alpha^4(m-1)^2/27 \quad (5-34)$$

When the particles are comparable in size to the wavelength of incident light ( $\alpha(m-1) \ll 1 \ll \alpha$ ), the scattering per particle is proportional to the fourth power of the radius, and the turbidity for a given weight of material will increase linearly with the radius, i. e.,

$$\tau = K n \pi r^2 \quad \text{where } K = 2\alpha^2(m-1)^2 \quad (5-35)$$

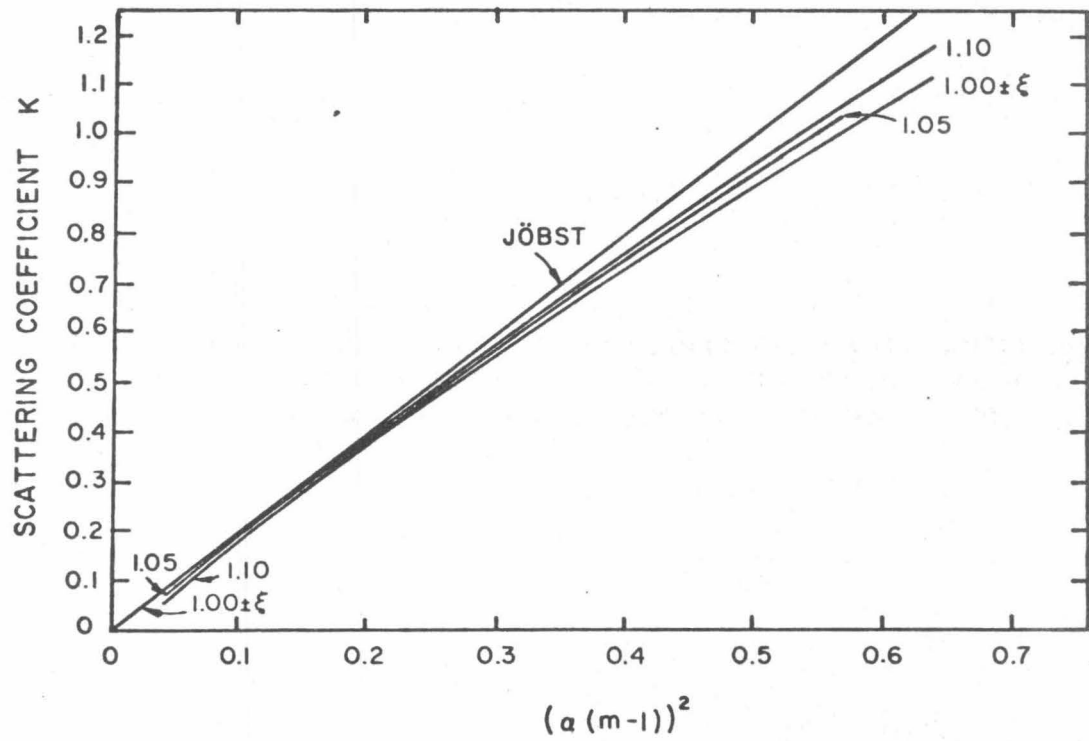


Figure 5.11 Comparison of Jobst Approximation for Scattering Coefficient with Mie Theory Values ( $m = 1.05, 1.10$ ) and Rayleigh-Gans Approximation ( $m = 1.00 \pm \epsilon$ ). Adapted from Koch (27).

For large particles with small refractive indices, and arbitrary values of  $\alpha(m-1)$ , the scattering per particle is approximately proportional to the third power of the radius in the range  $10 < \alpha < 40$ , and proportional to the second power of the radius in the range  $\alpha > 40$ . Thus, in the anomalous diffraction region, the turbidity of a coalescing system is initially insensitive to changes in the particle diameter ( $10 < \alpha < 40$ ), and decreases for larger particle diameters ( $\alpha > 40$ ), i. e.,

$$\tau = K n \pi r^2 \quad \text{where } K = 2 - (4 \sin \rho) / \rho + 4(1 - \cos \rho) / (\rho)^2 \quad (5-36)$$

For still larger particles ( $1 \ll \alpha(m-1) \ll \alpha$ ), the scattering is proportional to the square of the radius, so that the turbidity of the system will always decrease with increasing radius of the particle, i. e.,

$$\tau = K n \pi r^2 \quad \text{where } K = 2 \quad (5-37)$$

### 5.3.2.3 Aggregates of Large Particles

If the aggregates of rod-shaped bacteria cells are assumed to coalesce into spheres, then the turbidity of the flocculating suspension can be represented as

$$\tau = \sum_i n_i \pi r_i^2 K_i \quad (5-38)$$

where  $n_i$  = number of aggregates of radius  $r_i$

$r_i$  = aggregate radius

$K_i$  = Mie scattering coefficient for aggregate of equivalent spherical radius  $r_i$

While this coalescing sphere approach is strictly valid only for emulsions and liquid aerosols, it has been used with aggregated systems of rigid primary particles because of its simplicity and good correlation

with experimental results (38, 39).

The turbidity of an aggregate coalesced from primary particles is highly dependent upon the particle size regime involved. For example, Table 5.3 summarizes the turbidities for coalesced aggregates consisting of up to seven primary particles, using the Jobst approximations for the Mie scattering coefficient in the anomalous region and the diffraction region. Thus for particles in the anomalous region, coalescence leads to increased turbidity, whereas in the diffraction region, coalescence leads to decreased turbidity.

Lichtenbelt et al. (40) made a detailed comparison of extinction cross sections for real doublets and for hypothetical doublets coalesced into spheres. Using Rayleigh-Gans Theory for  $\alpha$  up to 3, Lichtenbelt et al. (40) determined that the coalescence assumption leads to larger values of the scattering cross section by about 10% than for real doublets created in coagulation. This is because a doublet is less compact than a single sphere of the same volume: therefore, the interference between light waves, scattered by different parts of the doublet is stronger because of the longer average difference in path length. Consequently, scattering is less for a real doublet than for a hypothetical coalesced sphere. Lower scattering means greater transmission, and lower turbidity.

Although the coalescence assumption may lead to small errors in the scattering cross section, it does enable the rapid correlation of

<u>Anomalous region</u> <u><math>(\alpha(m-1) \ll 1 \ll \alpha)</math></u>	<u>Diffraction region</u> <u><math>(1 \ll \alpha(m-1) \ll \alpha)</math></u>
$\tau_2 = 1.26 \tau(2)$	$\tau_2 = 0.79 \tau(2)$
$\tau_3 = 1.44 \tau(3)$	$\tau_3 = 0.69 \tau(3)$
$\tau_4 = 1.59 \tau(4)$	$\tau_4 = 0.63 \tau(4)$
$\tau_5 = 1.71 \tau(5)$	$\tau_5 = 0.59 \tau(5)$
$\tau_6 = 1.82 \tau(6)$	$\tau_6 = 0.55 \tau(6)$
$\tau_7 = 1.91 \tau(7)$	$\tau_7 = 0.52 \tau(7)$

$\tau_n$  = turbidity of single sphere coalesced from n independent spheres

$\tau(n)$  = turbidity of n independent spheres

Table 5.3 Influence of Size Regime on Coalescence Assumption Using Jobst Approximations for Mie Scatterers.

turbidity data ( $\tau_i$ ) with Coulter counter data ( $n_i$  and  $d_i$ ) provided the relative refractive index and size regime are known. Because the Coulter counter only measures the aggregate volume, and therefore only determines an equivalent spherical diameter, Coulter counter size distributions relate only to a coalesced sphere approach.

The difficulties in determining aggregate form factors, particle form factors, phase shifts, and distribution functions combine to make the Rayleigh-Gans approach too complicated for practical application. On the other hand, the coalesced sphere approach, using approximations to the Mie theory, enables rapid correlation of turbidity with particle size distribution. Consequently, a coalesced sphere approach was adopted for experimentation in the E. coli-PEI system.

#### 5.4 Refiltration Rate

##### 5.4.1 Determination of Specific Surface Area

In refiltration experiments, LaMer et al. (41) forced a measured amount of flocculated phosphate slime through filter paper at a pressure differential  $\Delta P$  of 74 cm Hg provided by a vacuum filtration apparatus. The initial filtrate was then refiltered through the filter cake and the time rate of flow  $Q$  recorded as the refiltration rate. The difference in volume flow rate between a flocculated suspension and an unflocculated suspension,  $Q - Q_0$ , was attributed to the change in the specific surface area  $S_0$  of the particles. At a given pressure

$\Delta P$ , the porosity of the filter cake  $\phi$  and the thickness of the cake  $L$  were considered to be essentially constant. This was roughly verified by measuring the cake thickness with a traveling microscope.

As stated in Chapter 1, the flow rate  $Q$  of a liquid through a packed bed of constant thickness is given by the Kozeny-Carman filtration equation:

$$Q = \Delta P g A \phi^3 / (k_1 u L S_o^2 (1 - \phi)^2) \quad (1-11)$$

Obviously, if the filter bed porosity remains constant, the time of refiltration will be directly proportional to  $S_o^2$ . For a given series of flocculated samples with the same percent solids,

$$Q = K_1 / S_o^2 \quad (5-39)$$

where  $K_1 = \Delta P g A \phi^3 / k_1 u L (1 - \phi)^2$

$$S_o = 6/d$$

$d$  = mean aggregate diameter in filter cake

This proportionality was recorded by O'Melia and Stumm (42) in refiltration experiments with untreated suspensions of four Min-U-Sil grades of varying specific surfaces; and the assumption was made that effective particle surface areas of treated (hydrolyzed iron) suspensions could be computed directly from refiltration times. If this assumption is correct, then refiltration rate experiments provide a quick and

simple means of determining the increase in the mean aggregate diameter, and the effectiveness of the polymer in producing the desired flocculation.

#### 5.4.2 Porosity of the Filter Cake

Initially, LaMer and Smellie (43, 44) had assumed that the porosity of the filter cake was essentially constant, and therefore independent of flocculation condition. This assumption was based on experiments with untreated phosphate slimes, and was later extended to several polymer-colloid systems. However, in later experiments by Dixon, LaMer, and Linford (20), the concentration of added polymer (PEI) caused significant increases in the porosity of the filter cake. Using a silica-PEI system, Dixon et al. (20) determined the porosity by subtracting the known weight of dry silica from the weight of the wet cake. The porosity increased from 0.5 for untreated silica to 0.7 for silica-PEI suspensions at optimum PEI concentrations. This change in cake porosity would result in an approximate eight-fold increase in the volume flow rate as specified by the Carman-Kozeny filtration equation.

Consequently, in order to determine the changes in the specific surface area via refiltration experiments, it is necessary to first determine if changes occur in the porosity of the polymer-colloid cake. Although the porosity can be measured by compressing the suspension

in a piston type apparatus with a porous bottom (45), or by the method of the preceding paragraph, the very small amounts of E. coli available necessitated other procedures.

A superficial flow velocity  $v$  can be determined by rearranging the Kozeny-Carman equation as follows:

$$v = Q/A = (1/A)(dV_f/dt) = \Delta P g \phi^3 / (k_1 u L S_o^2 (1-\phi)^2) \quad (5-40)$$

where  $V_f$  = volume of filtrate

$t$  = time of filtration

Furthermore,

$$LA(1-\phi)\rho_p = wV_f \quad (5-41)$$

where  $w$  = weight of particles per unit volume of suspension

$\rho_p$  = density of solids

Substituting (5-41) into (5-40), rearranging, and integrating results in

$$V_f/A = ((\Delta P g \phi^3 \rho_p / (k' u w (1-\phi) S_o^2)) t)^{\frac{1}{2}} \quad (5-42)$$

The specific resistance of the material for a unit pressure differential ( $\Delta P = 1$ ) is defined as

$$q = k'(1-\phi) S_o^2 / \rho_p \phi^3 \quad (5-43)$$

which is equivalent to the reciprocal of the permeability. Substituting this expression for the specific resistance into equation (5-42) results in

$$V_f/A = (\Delta P g t / u w q)^{\frac{1}{2}} \quad (5-44)$$

and the volume flow rate can be plotted as a function of (time)<sup>1/2</sup>. The slope will be a measure of q, and the intercept on the V<sub>f</sub>/A axis will be the equivalent cake depth of the filter septum.

Returning to equation (5-43), if the porosity  $\phi$  of the filter cake is dependent on the pressure differential  $\Delta P$ , and independent of the flocculation condition, then a plot of  $\log q$  versus  $\log \Delta P$  can be used to estimate the changes in the specific surface area  $S_o$ .

$$\log q = \log k' (1-\phi) / \rho_p \phi^3 + 2 \log S_o \quad (5-45)$$

For two different flocculation conditions,

$$\begin{aligned} \log q_1 - \log q_2 &= \log (k' (1-\phi) / \rho_p \phi^3) + 2 \log S_1 - \\ &\quad \log (k' (1-\phi) / \rho_p \phi^3) - 2 \log S_2 \end{aligned} \quad (5-46)$$

$$\log q_1 - \log q_2 = 2(\log S_1 - \log S_2) \quad (5-47)$$

$$q_1/q_2 = (S_1/S_2)^2 \quad (5-48)$$

provided that the porosity  $\phi$  at any  $\Delta P$  is the same for each condition of flocculation. This relationship between resistivity and specific surface

area yields, for all  $\Delta P$  values,

$$\log q_1 - \log q_2 = \text{constant}$$

i. e. , curves on the  $\log q$  versus  $\log \Delta P$  graph should be parallel.

Equation (5-44) may be rewritten as follows

$$\Delta Pt/w = quV_f^2/gA^2$$

or

(5-49)

$$\Delta Pt/w \propto q$$

Since  $u, V_f, g,$  and  $A$  are constant, a plot of  $\Delta Pt/w$  with respect to  $\Delta P$  is equivalent to a plot of  $q$  with respect to  $\Delta P$ . Parallel lines on such a graph provide experimental verification that the porosity of the PEI-E. coli filter cake is independent of flocculation condition.

### 5.5 Electrophoretic Mobility of Aggregates

The impelling force on the E. coli cells in the Briggs micro-electrophoresis cell is due to the electric field acting on the unbalanced surface charge as reduced by double-layer effects.

$$F_i = E\sigma nA_o \quad (5-50)$$

where  $F_i$  = impelling force

$E$  = electric field strength =  $V/l$

$V$  = potential difference

$l$  = distance between electrodes

$A_o = \pi d_o^2$  = area of primary particle

$n$  = number of primary particles in aggregate

$\sigma$  = unbalanced charge density at slipping plane

Opposing the impelling force is the fluid drag force due to friction

$$F_d = C_d \pi d_o^2 \rho_o v_a^2 / 8 \quad (5-51)$$

where  $C_d$  = drag coefficient for viscous flow

$$= 24 u / v_a d_o p_o$$

$\rho_o$  = fluid density

$u$  = absolute viscosity

$v_a$  = aggregate velocity

At equilibrium,

$$F_i = F_d$$

$$v_a = n d_o^2 \sigma E / 3 u d \quad (5-52)$$

And from conservation of volume,

$$n \pi d_o^3 / 6 = \pi d^3 (1-f) / 6$$

where  $f$  = porosity of aggregate

Consequently,

$$\begin{aligned}
 v_a &= [(1-f)E/3ud_o] \sigma d_a^2 \\
 &= K \sigma d^2
 \end{aligned}
 \tag{5-53}$$

where K is the product of the constant terms in brackets.

By adsorbing cationic polymer to the E. coli surface,  $\sigma$  is reduced from negative values to zero, and occasionally to positive values. However, simultaneously with the reduction of  $\sigma$ ,  $d$  increases since electrostatic repulsion between primary particles is reduced and collisions become more effective. Since the two effects oppose each other, the combined influence of their product on  $v_a$  is quite complicated.

As shown by equation (5-53), electrophoretic mobility measurements do not solely record the changes in  $d$ , which is the important parameter in all treatment operations discussed (see equations (1-4), (1-5), (1-6), and (1-11)), but multiply the change in  $d^2$  by the change in  $\sigma$ . Unless this change in  $\sigma$  is known precisely, electrophoretic mobility measurements cannot provide direct information on the ability of a flocculant to produce the desired aggregation. The common engineering practice of requiring the zeta potential to be within some limits,  $0 \pm x$  mv, for optimum flocculation is a handy rule of thumb, but one which may bear little or no relationship to the size parameter  $d$  which determines optimum flocculation.

Nevertheless, since the reduction in zeta potential corresponds to reduced repulsive forces between charged particles in solution and to reduced double-layer thicknesses, the technique of electrophoretic mobility measurement has received some acceptance as an indicator of coagulant efficiency. The technique appears to work well for treatment operations using cationic coagulants such as Fe(III) and Al(III) salts. In water treatment operations, Riddick (46) claims that reduction of the zeta potential to  $0 \pm 5$  mv, via addition of Fe(III), Al(III), or cationic polymers, will result in effective coagulation of the colloidal fraction of diameter 1-1000 nm, and reduction of the zeta potential to  $0 \pm 15$  mv will effectively coagulate the colloidal fraction of diameter 1-1000  $\mu\text{m}$ .

Since zeta potential measurement involves only aspects of electrokinetic theory, it may lead to erroneous conclusions when applied to flocculants which operate via bridging or enmeshing techniques. In addition, the method is without value when the polymer is anionic and coagulates negatively-charged particles.

## REFERENCES CITED

## CHAPTER 5

1. TeKippe, R. J., and Ham, R. K., "Coagulation Testing: A Comparison of Techniques - Part I", Journal American Water Works Association, 62 (1970), 594-602; "Coagulation Testing: A Comparison of Techniques - Part II", Journal American Water Works Association, 62 (1970), 620-628.
2. LaMer, V. K., Smellie, R. H., and Lee, P. L., "Flocculation, Subsidence, and Filtration of Phosphate Slimes", Journal Colloid Science, 12 (1957), 230-239.
3. Coulter, W. H., "High Speed Automatic Blood Cell Counter and Cell Size Analyzer", Proceedings National Electronics Conference, 12 (1956), 1034.
4. Mattern, C. F., Brackett, F. S., and Olson, B. J., "Determination of Number and Size of Particles by Electrical Grating: Blood Cells", Journal Applied Physiology, 10 (1957), 56-70.
5. Kubitschek, H. E., "Electronic Counting and Sizing of Bacteria", Nature, 182 (1958), 234-235.
6. Kubitschek, H. E., "Electronic Measurement of Particle Size", Research (London), 13 (1960), 128-135.
7. Wachtel, R. E., and LaMer, V. K., "The Preparation and Size Distribution of Some Monodisperse Emulsions", Journal Colloid Science, 17 (1962), 531-564.
8. Higuchi, W. I., Okada, R., and Lemberger, A. P., "Aggregation in Oil-in-Water Emulsions", Journal Pharmaceutical Sciences, 51 (1962), 683-687.
9. Morgan, J. J., and Birkner, F. B., "Flocculation Behavior of Dilute Clay-Polymer Systems", Progress Report WP 00942-02, USPHS, Sept. 1966.

10. Birkner, F. B., and Morgan, J. J., "Polymer Flocculation Kinetics of Dilute Colloidal Suspensions", Journal American Water Works Association, 60 (1968), 175-191.
11. Ham, R. K., and Christman, R. K., "Agglomerate Size Changes in Coagulation", Proceedings American Society of Civil Engineers, 95 (1969), 481-502.
12. Camp, T. R., "Floc Volume Concentration", Journal American Water Works Association, 60 (1968), 656-673.
13. Hannah, S. A., Cohen, J. M., and Robeck, G. G., "Measurement of Floc Strength by Particle Counting", Journal American Water Works Association, 59 (1967), 843-858.
14. Camp, T. R., "Discussion: Agglomerate Size Changes in Coagulation", Journal Sanitary Engineering Division, ASCE, 95 (1969), 1210-1214.
15. Neis, U., Eppler, B., and Hahn, H., "Quantitative Analysis of Coagulation Processes in Aqueous Systems: An Application of the Coulter Counter Technique", unpublished paper, 1974.
16. Graton, L. C., and Fraser, H. J., "Systematic Packing of Spheres, with Particular Relation to Porosity and Permeability", Journal Geology, 43 (1935), 785-909.
17. Muskat, M., The Flow of Homogeneous Fluids Through Porous Media, McGraw-Hill Book Co., New York, 1937.
18. Terzoghi, K., "Physical Differences Between Sand and Clay", Engineering News Record, 95 (1925), 912-915.
19. Shapiro, I., and Kolthoff, I., "The Bulkiness and Porosity of Silica Powder", Journal Physical and Colloid Chemistry, 52 (1948), 1020-1033.
20. Dixon, J. K., LaMer, V. K., and Linford, H. B., "Factors Affecting Filtration Rates of Flocculated Silica", Journal Water Pollution Control Federation, 39 (1967), 647-658.
21. Archie, G. E., "The Electrical Resistivity Log as an Aid in Determining Some Reservoir Characteristics", Transactions AIME, 146 (1942), 54-67.

22. Benoit, H., Ullman, R., DeVries, A., and Wippler, C., "Diffusion De La Lumiere Par Des Agregats En Suspension Dans Un Liquide", Journal De Chimie Physique, 59 (1962), 889-895.
23. Rayleigh, O. M., Philosophical Magazine, 12 (1881), 81.
24. Gans, R., "Strahlungsdiagramme ultramikroskopischer Teilchen", Annalen Der Physik, 76 (1925), 29-38.
25. Debye, P., "Molecular Weight Determination by Light Scattering", Journal Physical and Colloid Chemistry, 51 (1947), 18-32.
26. Oster, G., "The Scattering of Light and Its Applications to Chemistry", Chemical Reviews, 43 (1948), 319-335.
27. Koch, A. L., "Some Calculations on the Turbidity of Mitochondria and Bacteria", Biochimica Et Biophysica Acta, 51 (1961), 429-441.
28. Lips, A., Smart, C., and Willis, E., "Light Scattering Studies on a Coagulating Polystyrene Latex", Faraday Society Transactions, 67 (1971), 2979-2988.
29. Lips, A., and Willis, E., "Low Angle Light Scattering Technique for the Study of Coagulation", Journal Chemical Society Faraday I, 69 (1973), 1226-1234.
30. Mie, G., "Beitrage zur Optik truber Medien", Annalen Der Physik, 25 (1908), 377-445.
31. Debye, P., "Der Lichtdruck auf Kugeln von beliebigem Material", Annalen Der Physik, 30 (1909), 57-136.
32. Rayleigh, O. M., "The Incidence of Light upon a Transparent Sphere of Dimensions Comparable with the Wavelength", Proceedings Royal Society of London, 84 (1911), 25-46.
33. Bender, M., "The Use of Light Scattering for Determining Particle Size and Molecular Weight and Shape", Journal Chemical Education, 29 (1952), 15-33.
34. Blumer, H., "Strahlungsdiagramme kleiner dielektrischen Kugeln", Zeitschrift Physik, 32 (1925), 119-134.

35. Tables of Scattering Functions for Spherical Particles, National Bureau of Standards, Applied Mathematics, Series 4, US Government Printing Office, Washington, D. C.
36. van de Hulst, H. C., Light Scattering by Small Particles, John Wiley and Sons, New York, 1961, Secs. 17, 18.
37. Jobst, G., "Diffuse Strahlung dielektrisches Kugeln im Grenzfalle, dasz Kugelmateriale und umgebendes Medium fast gleich Brechungsindices haben", Annalen Der Physik, 78 (1925), 157-166.
38. Lips, A., and Levine, S., "Light Scattering by Two Spherical Rayleigh Particles over All Orientations", Journal Colloid and Interface Science, 33 (1970), 455-463.
39. Ottewill, R. H., and Shaw, J. N., "Stability of Monodisperse Polystyrene Latex Dispersions of Various Sizes", Discussions Faraday Society, 42 (1966), 154-163.
40. Lichtenbelt, J. W., Ras, H. J., and Wiersema, P. H., "Turbidity of Coagulating Lyophobic Sols", Journal Colloid and Interface Science, 46 (1974), 522-527.
41. LaMer, V. K., and Smellie, R. H., "Flocculation, Subsidence, and Filtration of Phosphate Slimes, II. Starches as Agents for Improving Flocculation, Subsidence, and Filtration of Phosphate Slimes", Journal Colloid Science, 11 (1956), 710-719.
42. O'Melia, C. R., and Stumm, W., "Aggregation of Silica Dispersions by Iron (III)", Journal Colloid and Interface Science, 23 (1967), 437-447.
43. LaMer, V. K., Smellie, R. H., and Lee, P. K., "Flocculation, Subsidence, and Filtration of Phosphate Slimes. V. The Optimum Filtration Rate as a Function of Solid Content and Specific Area", Journal Colloid Science, 12 (1957), 566-574.
44. Smellie, R. H., and LaMer, V. K., "Flocculation, Subsidence, and Filtration of Phosphate Slimes. VI. A Quantitative Theory of Filtration of Flocculated Suspensions", Journal Colloid Science, 13 (1958), 589-599.

45. Grace, H. P., "Structure and Performance of Filter Media", American Institute of Chemical Engineers Journal, 2 (1956), 307-336.
46. Riddick, T. M., "Zeta Potential and Its Application to Difficult Waters", Journal American Water Works Association, 53 (1961), 1007-1030.

## Chapter 6

EXTENT OF E. COLI AGGREGATION BY PEI6.1 System Parameters6.1.1 Particle Size and Concentration

A species of the coliform group, E. coli CR63, was selected for the experimental work as representative of the heterogeneous mass of biocolloids present in municipal wastewaters. Grown on a glucose-enriched Geneva M9 media (1), the monodisperse coliforms had a cylindrical shape; 0.8  $\mu\text{m}$  in diameter, 2-3  $\mu\text{m}$  in length, with mean equivalent spherical diameter of 1.3  $\mu\text{m}$  at the end of log phase growth. This particular species has a smooth surface, free of fillae or fimbriae.

Growth Media for E. coli CR 63

Casamino Acid	1.200 gm/l
Glucose	1.000 gm/l
$\text{NH}_4\text{Cl}$	1.000 gm/l
$\text{KH}_2\text{PO}_4$	0.100 gm/l
Collidine-HCl Buffer (2)	50 ml/l
$\text{MgSO}_4$	2 ml/l of 1 M
$\text{FeCl}_3$	1 ml/l of $10^{-3}$ M

In addition to the collidine-HCl buffer, minor additions of 0.1 M NaOH were made during the growth cycle to maintain the suspension pH constant at  $7.0 \pm 0.1$ . The jacketed chemostat was maintained at  $25^\circ\text{C}$ . With continuous stirring of the growth media, the seeded culture

grew to a final cell concentration of  $3.0 (\pm 0.5) \times 10^7$  cells/ml as shown in Figure 6.1. Cells were removed from the chemostat at the end of the log phase growth, since several investigators (3,4) have shown that cells in this physiological state are most susceptible to chemical flocculation. Coincidentally, growth of the microorganisms to this point in a wastewater system maximizes the biological assimilation capabilities of the organisms.

In the previous flocculation studies, many investigators (3,4, 5,6) have observed "stoichiometry" or a linear relationship between flocculant dose and total surface area of the colloid. At the same time, this stoichiometry has been shown to be virtually independent of particle size (6,7,8). Because of this, the particle size was chosen to meet other experimental limitations:

1. Since the Counter counter system was unable to distinguish electronic noise from signals for particles with diameters smaller than  $1.1 \mu\text{m}$ , mean cell sizes greater than  $1.1 \mu\text{m}$  in diameter were required.

2. The E. coli cells of diameter  $1.3 \mu\text{m}$  could be counted electronically in the Coulter counter, counted visually in a hemacytometer, and their velocity measured in the Briggs cell using an ordinary light microscope.

3. Because of their size and low relative refractive index,

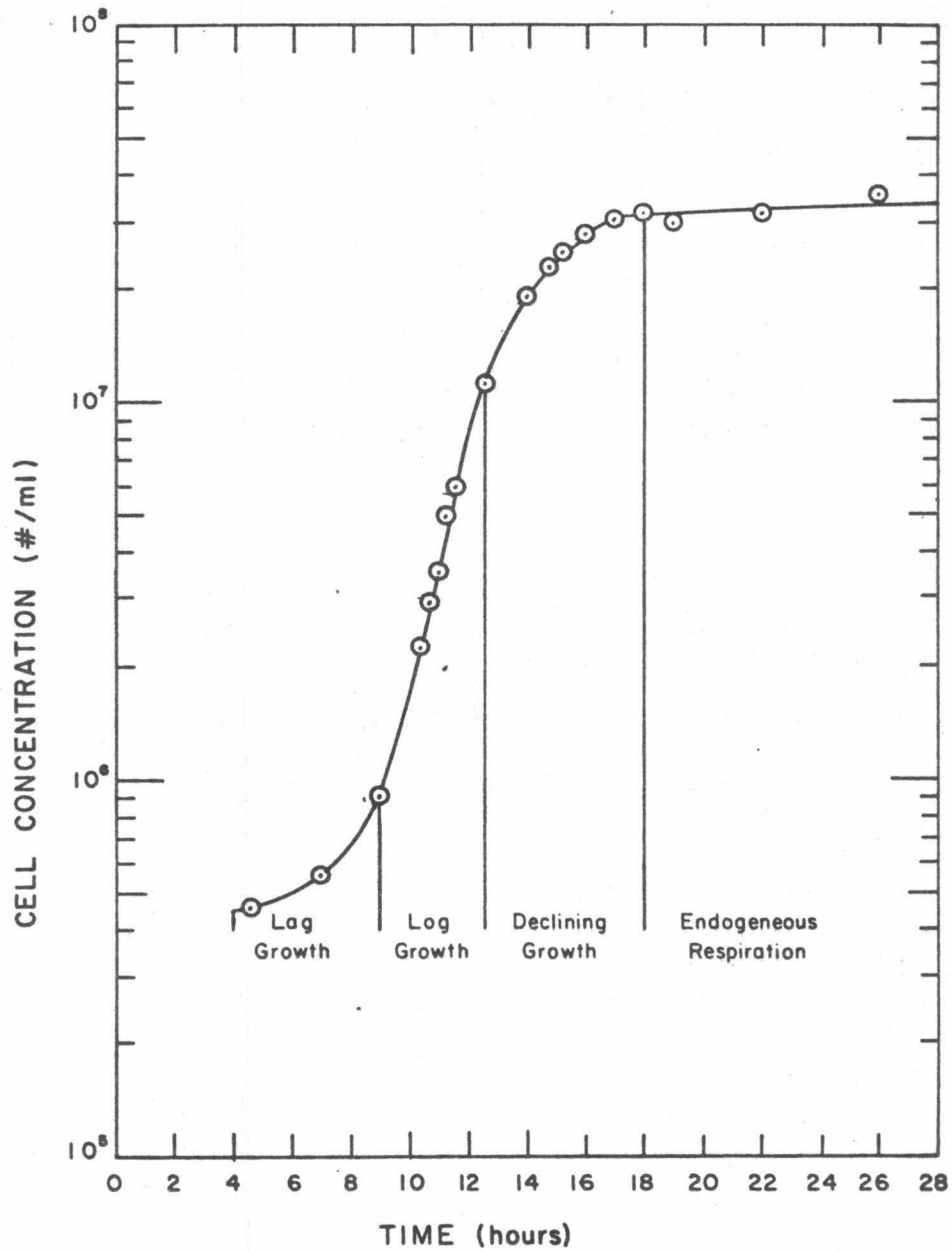


Figure 6.1 Growth Curve for *E. coli* CR63.

E. coli cells could be treated optically as either Rayleigh-Gans or Mie scatterers, utilizing the Mie scattering coefficient approximations (Table 5.2) in the latter case.

The particle concentration participates directly in the Smoluchowski equations describing both the polymer-particle and particle-particle collision rates. The particle-particle collision rate must be large enough to insure that aggregation will occur rapidly, and that polymer rearrangement on the surface of the colloid will not lead to reduced polymer extensibility if interparticle bridging contributes to overall flocculant effectiveness. Linke and Booth (6) hypothesize that when aggregates are broken apart at low particle concentrations, the time of "free travel" is so large that "loose ends" of the adsorbed polymer molecules (former bridges) have a chance of adsorbing totally on one particle, thereby reducing total particle bridging in the system.

The particle concentration was also important from an operational viewpoint:

1. Starting with an initial cell concentration of  $2.5 (\pm 0.5) \times 10^7$  cells/ml, two serial dilutions of 10:1 resulted in  $2.5 \times 10^5$  cells/ml or  $1.25 \times 10^4$  cells/50  $\mu$ l. At this concentration, the 11  $\mu$ m aperture will give a true count of cell concentration without necessitating coincidence corrections (9).

2. The relative scattering intensity  $I_{90}/I_0$  of the undiluted E. coli suspension was found to be linearly related to the cell concentration over the range  $5 \times 10^5$  to  $5 \times 10^7$  cells/ml. At greater cell concentrations, multiple scattering resulted in nonlinearity of relative scattering intensity (10). Consequently, both unflocculated and flocculated suspensions could be removed directly from the reactor vessel, and their relative scattering intensity measured without making dilutions or multiple-scattering corrections.

#### 6.1.2 Polymer Concentration and Configuration

As stated earlier, the known stoichiometry between optimum polymer dose and colloid surface area dictated the range of polymer concentrations to be studied. In addition to optimum doses, underdosed and overdosed conditions were investigated for each molecular weight species.

The polymer configuration in solution is primarily caused by the molecular weight, the number of branch points, the pH, and the ionic strength. The influence of molecular weight and number of branch points on the polymer configuration has been discussed in Section 4.1.

The solution pH and ionic strength control the ionization of functional groups on the polymer molecule. Normally, an uncharged

flexible linear polymer takes a random coil configuration in solution; the degree of coiling being limited by bond lengths, bond angles, and any other steric restrictions. This random coil configuration is further modified by electrostatic repulsion between dissociation groups when ionization of the molecule occurs. The effective range of the repulsion forces between different ionized groups on the polyelectrolyte depends on the ionic strength of the solution, analogous to the situation of colloidal particles (11, 12). A diffuse double layer of oppositely charged "counter" ions is established at the ionization site; this layer acts as a shield to reduce the effective range of the repulsive forces between like-charged segments of the polyion.

At low ionic strengths, the shielding effect is small, and the repulsion between like-charged segments causes an extended configuration of the polymer. At high ionic strengths, the opposite holds and the polymer assumes a more compact, coiled configuration.

Linke and Booth (6) and Kasper (13) have done studies indicating that as the ionic strength increases, the optimum flocculation dose (OFD) decreases to some minimal value, after which further increases in ionic strength are ineffective; for a silica-polyacrylate (MW of  $10^6$ ) system, Linke and Booth found the minimum in flocculant dose at ionic strengths greater than 0.2 M NaCl; for a Min-u-sil-dimethyl vinylpyridinium system, Kasper found that at low ionic

strengths ( $10^{-2}$  -  $10^{-5}$  M  $\text{NaHCO}_3$ ) the OFD decreased with increasing molecular weight; at high ionic strengths (greater than  $10^{-2}$  M  $\text{NaHCO}_3$ ) all molecular weights appeared equally effective at the same flocculation dose.

Unfortunately, the ionic strength affects flocculation via two mechanisms; the reduction of the double-layer thickness of the colloid particle, and the extensibility of the polymer molecule. Flocculation studies of themselves do not differentiate the relative magnitude of each mechanism. In addition, the situation with PEI is different from that of a linear molecule since the large number of branch points somewhat constricts the polymer to a spheroid configuration.

Figure 6.2 illustrates the simplest configuration of the PEI molecule, using 25% primary, 50% secondary, and 25% tertiary amino groups. At pH 7.0 approximately 20% of the total nitrogen groups have been protonated (ultimately 80% of the nitrogen atoms are protonatable). Even in the extended configuration of Figure 6.2, this results in a separation distance of only 10 to 15 Å between protonated nitrogen atoms. Calculating the thickness of the electric double layer extending from each protonated nitrogen atom at an ionic strength of 0.06 M NaCl results in a value of the Debye-Huckel parameter  $\kappa_{\text{DH}} = 7.35 \times 10^6 \text{ cm}^{-1}$ . Then the center of the diffuse counterion double layer falls at a distance of  $1/\kappa_{\text{DH}}$  or 13.6 Å from the protonated charge group.

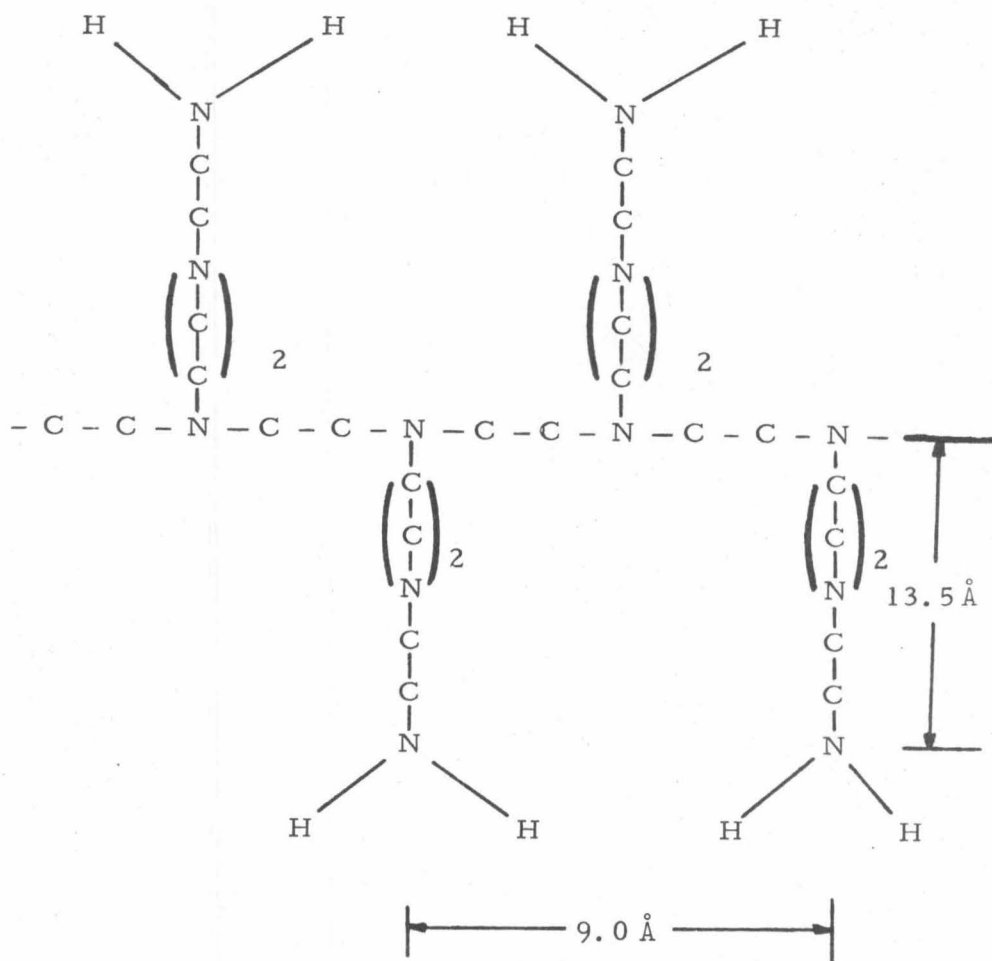


Figure 6.2 Simple Extended Configuration of PEI Molecule.

Consequently, at this ionic strength there exists strong electrostatic interaction between the double layers of protonated nitrogen atoms of the PEI molecule. This strong repulsion between segments of the molecule accounts for the large radii of gyration calculated from light scattering measurements (Table 4.3).

The Debye-Huckel parameter  $\kappa_{DH}$  was calculated via a simplified form of Poisson's equation, in which it was assumed that

$$z\epsilon\Psi/kT \ll 1$$

where  $z$  = valence of mobile ion

$\epsilon$  = charge of proton

$\Psi$  = potential at mobile ion due to neighboring protonated groups

However, in the case of PEI molecules with 20% protonation of amino groups, this simplification is not justified since

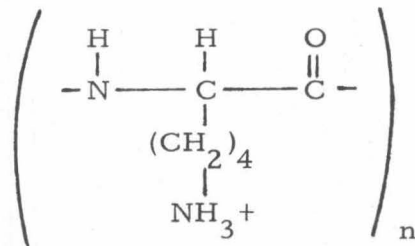
$$z\epsilon\Psi/kT > 1$$

Calculations of  $\kappa_{DH}$  from Poisson's equation directly would lead to a larger value of  $\kappa_{DH}$  than stated above, and thus to a reduced double-layer thickness.

Tanford (12) states that the Debye-Huckel double-layer theory may not be applicable to individual charge groups on highly-charged synthetic polyelectrolytes, although no proof has been given in either

case. This theory has been successfully applied to organic molecules and flexible linear polyelectrolytes (12).

The best verification of the polymer configuration in solution comes from viscosity or light scattering measurements as functions of ionic strength. While a detailed study was not undertaken in this case, a comparison of radii of gyration determined for PEI molecules at  $I = 0.06$  M NaCl from light scattering measurements indicates that the molecules are fully extended. Similarly, Nevo et al. (14) determined that the polylysine molecule was fully ionized under experimental conditions pH 7.2,  $I = 0.15$ ; i. e., every lysine residue carried a positive charge and the polypeptide chain was fully extended.



### 6.1.3 Intensity and Time of Agitation

The influence of mixing intensity on polymer effectiveness was first detected by LaMer et al. (15,16). They noted that it was necessary to add the flocculant slowly in order to provide uniform distribution of the flocculant over the colloid surface area, and that the rate of rotation influenced the floc size, and the subsequent

refiltration rate. In addition, the refiltration rate was minimized for their phosphate slime-anionic polymer system when the number of rotations was between 10 and 1000. Rotations (at 15 rpm) above this amount resulted in reduction of bridge length, shearing of the floc, and further polymer adsorption onto the unit flocs. Tenney and Stumm (3) observed that the number of rotations should be kept between 500 and 5000 (at 15 rpm) for optimum removal of microorganisms with cationic polyelectrolytes.

Black et al. (17), in experiments with kaolinite and cationic polymer, verified the importance of careful flocculant dosing, since approximately 85% of the polymer was adsorbed within 30 seconds of addition. For identical number of rotations, suspensions agitated at 20 rpm consistently exhibited lower residual turbidity than suspensions agitated at 100 rpm. After prolonged agitation (more than 6000 revolutions) the frequency of successful interparticle collisions became so small that the residual turbidity approached a limiting value independent of both mixing intensity and clay concentrations.

Birkner and Morgan (18) quantified the energy input into the suspension by measuring the torque of the stirring shaft at various speeds. The power input into the reactor can be computed from

$$P = \omega T \quad (6-1)$$

where P = power input

$\omega$  = angular velocity

T = measured torque

The root-mean-square velocity gradient is then determined from

$$G = (P/V\rho_0 u)^{\frac{1}{2}} \quad (6-2)$$

where G = root-mean-square velocity gradient

V = reactor volume

$\rho_0$  = density of suspension

u = absolute viscosity

The stirrer reactor assembly of Figure 4.2 was chosen so that the applied torque and angular velocity could be easily measured. The E. coli suspension (900 ml at  $2.5 \times 10^7$  cells/ml) was rapidly stirred at  $G = 190 \text{ sec}^{-1}$  for two minutes during the continuous addition of 100 ml of PEI solution. The high value of G insured even distribution of the PEI throughout the E. coli suspension, and provided for a high initial particle collision frequency. From Smoluchowski's equation,

$$b_{ij} = 2G(r_i + r_j)^3 n_i n_j / 3 \quad (6-3)$$

where  $b_{ij}$  = interparticle collision frequency

r = particle radius

n = particle concentration

and for my system,  $b_{ij} = 1.7 \times 10^5$  collisions/sec  $\text{cm}^3$  initially.

Following the two minute rapid mix, flocculation was continued either by diffusion ( $G=0$ ) or by imposed laminar shear gradients ( $G=20, 40, \text{ or } 60 \text{ sec}^{-1}$ ) for 60 minutes. A thorough review (19) of current treatment practices in the U. S. indicates that operational velocity gradients range from approximately  $20 \text{ sec}^{-1}$  to  $74 \text{ sec}^{-1}$  and that the values of the product  $Gt$  at plant capacity range from approximately 23,000 to 210,000. The shear gradients in my experiments were chosen so as to determine an optimum value of  $G$  within the range  $20 - 60 \text{ sec}^{-1}$ . The products  $Gt$  for my experiments were 72,000 ( $G=20 \text{ sec}^{-1}$ ), 144,000 ( $G=40 \text{ sec}^{-1}$ ), and 216,000 ( $G=60 \text{ sec}^{-1}$ ).

Particle size distributions were recorded every 60 minutes for four hours following rapid mix, primarily to determine if the aggregates would reach an equilibrium size determined by the imposed shear gradient and PEI molecular weight. In addition, relative scattering intensity measurements were made after 60 minutes for comparison with the particle size distributions.

The rate of decrease in the concentration of particles caused by agglomeration under the influence of a velocity gradient,  $G$ , can be described by first order kinetics:

$$-dn/dt = k_g n \quad (6-4)$$

or

$$n = n_o e^{(-k_g t)}$$

where  $k_g = 4\kappa V_m G/\pi$

$\kappa$  = particle collision efficiency factor

$V_m$  = volume of suspended particulate matter per unit volume of medium

$n_o$  = initial number of particle per unit volume

The rate of decrease in the concentration of particles caused by aggregation by Brownian motion ( $G=0$ ) is described by a second-order rate law:

$$-dn/dt = k_b n^2 \quad (6-5)$$

or

$$1/n - 1/n_o = k_b n^2$$

where  $k_b = 4\kappa kT/3\nu$

$\nu$  = kinematic viscosity

Table 6.1 summarizes the theoretical predictions of particle number concentration following the initial two minute rapid mix and the succeeding 60 minute flocculation period. Each interparticle collision was assumed to result in aggregate formation, i. e.,  $\kappa = 1$ . Obviously, particle removal by diffusion ( $G=0$ ) should be ineffective in size range under investigation ( $d \geq 1.3 \mu\text{m}$ ).

#### 6.1.4 Solution pH and Ionic Properties

Solution properties, particularly the pH and cation

Mixing Period	$n_o$ (cells/ml)	G ( $\text{sec}^{-1}$ )	$R^{(1)}$ (Reynolds #)	k (coefficient)	n (cells/ml)
2 min. rapid	$2.5 \times 10^7$	190	$6.3 \times 10^4$	$8.2 \times 10^{-3}$	$9.2 \times 10^6$
6 min. flocculation	$9.2 \times 10^6$	0	0	$6.2 \times 10^{-12}$	$7.6 \times 10^6$
"	$9.2 \times 10^6$	20	$7.2 \times 10^3$	$8.7 \times 10^{-4}$	$4.2 \times 10^5$
"	$9.2 \times 10^6$	40	$2.0 \times 10^4$	$1.7 \times 10^{-3}$	$2.0 \times 10^4$
"	$9.2 \times 10^6$	60	$2.8 \times 10^4$	$2.6 \times 10^{-3}$	$9.2 \times 10^2$

(1) Shinnar and Church (20) indicate that Reynolds Numbers in excess of  $1 \times 10^5$  are necessary if local isotropic turbulence is to exist in a stirred-tank-type reactor.

Table 6.1 Theoretical Reductions in Particle Concentration from Perikineti and Orthokinetic Flocculation.

concentration, have considerable effect on the surface potential and charge of the colloid, the nature of the double layer surrounding each particle, the charge density and chain length or extensibility of the polymer (Section 5.1.1) and the extent of complex formation at the colloid-polymer interface.

As the pH increases from the isoelectric point (pH 2.5) of the E. coli cells, functional groups on the bacterial surface ionize, thereby increasing the negative charge density. Primarily these functional groups consist of amino acids (2-4% of cell wall), polysaccharides (20%), and lipids (10-20%), which ionize through amino or carboxyl groups (21,22). Although bacteria are classified as hydrophilic colloids, in that their stability as a dispersion does not solely depend on the electrostatic repulsion between cells, successful flocculation has been achieved through reduction of the surface potential by addition of cations (23). Consequently, reductions in surface potential, either as a result of changes in pH or ionic strength, would lessen inter-particle repulsion and lower the polymer concentration for optimum aggregation. For a similar E. coli-PEI system, Dixon and Zielyk (24) determined that at pH 4 optimum aggregation is achieved with approximately 1/10 the polymer dose required at pH 6 to 9. This was attributed to the smaller negative charge density of the E. coli surface

at pH 4, thereby requiring less polymer to reduce even further the interparticle energy.

A secondary effect of high surface potentials is the likelihood that adsorbed cationic polymers would tend to flatten onto the colloid surface, instead of bridging between particles. Eventually, as the surface potential is lowered through adsorption, the polymer molecules would exhibit greater extensibility from the surface, the distance of closest approach would be lessened, and bridging could begin if the particles had not already coagulated.

Multivalent cations are especially important in anionic polymer-colloid systems because of their ability to compress the double layer and thereby reduce the electrostatic repulsive forces between the colloidal surfaces. In addition, these counter ions play an active role in the approach of the anionic polymer functional groups into the double layer of the colloid. However, these cations are unnecessary in a cationic polymer system, and to avoid their influence, no multivalent cations were used in my experiments.

My research with the E. coli-PEI system was intended to provide data applicable to existing water and wastewater treatment systems. For that reason, the experimental pH and ionic strength were intended to be representative of existing conditions. Babbit and Bauman (25), in a survey of 32 municipal wastewater systems, state

the pH range to be from 6.8 to 8.0, with a median of 7.3. Since earlier researchers had shown that neither the surface charge density of the bacteria (26) nor the optimum PEI concentration for flocculation (24) changed noticeably in the pH range 6 to 8, a pH of 7.0 was adopted for all experiments.

Based on data published by the United States Geological Survey (27), the ionic strength of public water supplies for forty of the largest cities in the United States varies between  $4 \times 10^{-4}$  and  $4 \times 10^{-2}$  moles per liter. Municipal sewage adds from 100 to 300 mg/l of total dissolved solids to the input water supply. The resulting ionic strength of municipal sewage therefore varies in the range  $2 \times 10^{-3}$  to  $5 \times 10^{-2}$  moles per liter. Unfortunately, ionic strengths within this range are too low to provide adequate current flow in the Coulter counter to detect the small bacteria. A slightly higher ionic strength of 0.06 M NaCl was adopted for all experimental work. This increase in ionic strength was not felt to have a significant impact on the applicability of the results to existing wastewater treatment systems.

## 6.2 Experimental Methods

In the experiments of this Chapter, 900 ml of stationary phase E. coli cells were removed from the chemostat and placed in the stirrer-reactor assembly (Figure 4.2). One hundred ml of specified PEI

concentration was then added to the E. coli suspension during a two minute rapid mix ( $G=190 \text{ sec}^{-1}$ ). The final suspension had a  $\text{pH}=7.0$  ( $\pm 0.1$ ),  $I=0.06 \text{ M NaCl}$ ,  $T = 25^{\circ}\text{C}$ , and a cell concentration of  $2.5(\pm 0.5) \times 10^7$  cells/ml before flocculation. The flocculation velocity gradient ( $G=0, 20, 40, \text{ or } 60 \text{ sec}^{-1}$ ) was set by regulating the angular velocity of the two-pronged stirrer to yield the desired torque (Equation 6-1). For turbidity measurements, a 50 ml sample was pipetted from the stirrer-reactor and placed in a Brice Phoenix scattering cell (Catalog Number T 101). For electrophoretic mobility measurements, a 20 ml sample was pipetted from the stirrer-reaction and placed in a Briggs microelectrophoresis cell. For refiltration rate measurements, a 50 ml sample was pipetted from the stirrer-reactor and placed in a Millipore filtration apparatus. In each case, care was taken to insure minimum disruption of floccules during the transfer step.

### 6.2.1 Applications of Coulter Counter/PHA/MCA

#### 6.2.1.1 Calibration Techniques

The current and amplification settings of the Model B Coulter Counter were determined for three different aperture diameters ( $11 \mu\text{m}$ ,  $30 \mu\text{m}$ , and  $70 \mu\text{m}$ ) by passing suspensions of monodisperse polystyrene latex in  $0.06 \text{ M NaCl}$  through the aperture. The settings, summarized in Table 6.2, provide strong signal to noise ratios and maintain the

<u>Aperture diameter</u>	<u>Particle diameter</u>	<u>Counter Settings</u>		<u>Peak channel</u>	<u>Logbase</u>
		<u>Amp.</u>	<u>Current</u>		
11 $\mu\text{m}$	1.3 $\mu\text{m}$	0.5	8	38	1.024
	2.0 $\mu\text{m}$	0.5	8	94	
30 $\mu\text{m}$	2.0 $\mu\text{m}$	2.0	4	24	1.045
	5.7 $\mu\text{m}$	2.0	4	95	
70 $\mu\text{m}$	5.7 $\mu\text{m}$	8.0	4	20	1.032
	9.5 $\mu\text{m}$	8.0	4	70	

Table 6.2 Summary of Calibration Data for Coulter Counter.

ratio of particle diameter  $d$  to aperture diameter  $D$  greater than 0.05 and less than 0.30.

A voltage pulse generator was used with the Nuclear Data Model 555 Pulse Height Analyzer (PHA) and Multichannel Analyzer (MCA) to determine the coarse and fine gain settings such that the logbase of input signals remained constant over the full range of channels, i. e., from channel 1 to 128. Varying the frequency of the voltage pulse, within the recovery time of the electronic circuitry, did not shift the channel of record.

A detailed particle size distribution could be obtained by using 80 channels of data from the 11  $\mu\text{m}$  aperture, 80 channels of data from the 30  $\mu\text{m}$  aperture, and 100 channels of data from the 70  $\mu\text{m}$  aperture. All 128 channels could not be utilized because of overlap between the 11 and 30  $\mu\text{m}$  apertures, and between the 30 and 70  $\mu\text{m}$  apertures. Bacteria of equivalent spherical diameter less than 1.13  $\mu\text{m}$  could not be detected by the 11  $\mu\text{m}$  aperture because of background electronic noise at this low signal level.

Prior to seeding the culture, the growth media was filtered through 0.45  $\mu\text{m}$  Millipore filters to remove any large particulate matter. After culture growth, plate counts and hemacytometer counts were made to verify the accuracy of the Coulter Counter measurements. As was noted by Mattern et al. (9), the results of the

Coulter Counter had better reproducibility than either of the other techniques.

#### 6.2.1.2 Aggregate Count and Size Distribution

Samples of the flocculating E. coli suspension were withdrawn from the reactor (Figure 4.2) with a 2 mm bore pipet to prevent aggregate breakup, and then diluted with 0.06 M filtered NaCl. The dilution ratio depended upon the number of aggregates per unit volume, i.e., the reactor suspension was diluted only to the degree necessary to insure significance of count and adequate relaxation time of the electronic circuitry. Since there is little difference in densities between the E. coli cells and the suspending electrolyte, sedimentation of the particle aggregates during the time required to make a count and size distribution was negligible. The aggregates did not appear to fragment as they passed through the aperture, in spite of the high shear forces encountered there (28).

The smaller apertures (11  $\mu\text{m}$  and 30  $\mu\text{m}$ ) were prone to blocking by the aggregated bacterial cells. Generally, blockages could be cleared with a small paint brush; the more difficult cases were cleared by briefly immersing (1 second) the entire aperture tube into the bath of an ultrasonic vibrator. Occasionally, single cells would adhere to the sides of the aperture, resulting in an effective reduction

in the aperture size, and therefore increased pulse heights. By using a stopwatch to record the sampling time, such minor blockages were immediately detected, and the aperture could be cleared with the ultrasonic vibrator.

Using the calibration techniques discussed earlier (Sections 5.2.3 and 6.2.1) aggregate size distributions were prepared from the Coulter counter data taken each hour after addition of the PEI. The aggregate count in each channel  $C_i$  was converted to aggregate count at diameter  $d_i$  via a computer program utilizing equations (5-22) and (5-23). This aggregate count, divided by the diameter change corresponding to the size range stored in each channel, yielded the differential particle size distribution.

#### 6.2.2 Light Scattering by E. coli Cells

Measurements of turbidity of cultures of bacteria have served in the past as a simple and relatively accurate method of determining the number of bacteria in suspension. In my experiments, a Brice Phoenix Model 2000 spectrophotometer was utilized to measure the intensity of light scattered at  $90^\circ$  and transmitted at  $0^\circ$  from a stationary phase culture of E. coli strain CR63. From the scattering intensity  $I_{90^\circ}/I_{0^\circ}$ , the turbidity may be calculated via equation (6-6) below, which utilizes the ratio of the galvanometer deflections recorded experimentally (29).

$$\tau = \frac{16 \text{ IC}}{3(1.049)h} (u^2 (R_w/R_c)) aF(G_s/G_w) \quad (6-6)$$

where IC = instrument correction factor

h = diaphragm width = 1.2 cm

u = refractive index of solution = 1.33

$R_w/R_c$  = refraction correction factor = 1.00

a = working standard constant

F = product of transmittances of neutral filters

$G_s$  = galvanometer deflection for light scattered from  
solution at  $90^\circ$

$G_w$  = galvanometer deflection for light transmitted through  
solution at  $0^\circ$

For an incident wavelength of 546 nm, the turbidity per cm of path-length is  $\tau = 0.048 F G_s / G_w$ .

Although determination of the turbidity from the ratio of deflections method is strictly valid only for Rayleigh scatterers, the turbidity so calculated was a constant fraction of the turbidity measured as the reduction in transmitted light intensity by a Gilford Model 300 spectrophotometer. This indicated that the scattering intensity technique could be used to measure the suspension turbidity. In addition, the turbidity of the E. coli suspension was found to vary linearly over the range  $3 \times 10^5$  to  $5 \times 10^7$  cells/ml; i. e.,

$$\tau = C \sum_i n_i R_i \quad (6-7)$$

where  $C$  = optical constant for the particular geometry of the instrument involved

$n_i$  = number of particles of diameter  $d_i$

$R_i$  = total scattering cross section of particle of diameter  $d_i$

The Brice-Phoenix instrument offers advantages in that the flocculated suspension can remain undisturbed in the scattering cell, and thus the progress of differential settling can be recorded. In addition, the scattering cells can be easily filled with the flocculating suspension, without subjecting the flocs to unnecessarily high shear forces and disruption.

### 6.2.3 Light Scattering by E. coli Aggregates

#### 6.2.3.1 Correlation of Turbidity with Aggregate Size Distribution

Although visual observation of bacterial agglutination and precipitation was recorded by Bordet (30) in 1899, the use of turbidity measurements to quantify light transmission in aggregating suspensions began in the 1950's. The turbidimetric technique generally consisted of a rapid mix of the suspended particles with the flocculating agent, followed by transmission measurements as the flocculated particles sedimented. The flocculation period, the sedimentation period, and the transmission measurement show wide variation with different

investigators. Table 6.3 summarizes the various techniques of recent use.

All of the above investigations utilized the turbidimetric technique as a qualitative rather than a quantitative measure of aggregate formation. In most cases, the suspension turbidity as measured was the eventual result of aggregation (e.g., the degree of settling of flocculated particles) rather than aggregation itself. Busch (37), however, measured the ratio of light scattered at  $90^\circ$  to that transmitted at  $0^\circ$  immediately after the flocculation period, thereby eliminating complications due to settling. He felt that the aggregation process itself would result in reduced scattering intensities, based on experiments with large polystyrene spheres. As shown in Figure 6.3, the scattering intensity decreased with increasing particle size at constant weight concentration of particles. Busch achieved similar reductions in the relative light scattered from flocculated bacteria, and concluded that they behaved similarly, in a light scattering sense, to the polystyrene spheres of increasing bead diameter, even though the bacteria floccules were uncoalesced.

The reduction in scattering intensity for the large polystyrene beads (Figure 6.3) is caused by the fact that their large diameter places them in the diffraction regime. Since  $\alpha = 64$  for  $7\mu\text{m}$  diameter particles when  $\lambda_0 = 456 \text{ nm}$ , and  $m = 1.20$ , then  $1 \ll \alpha(m-1) \ll \alpha$

<u>Particles</u>	<u>Flocculation</u>		<u>Sedimentation</u>		<u>Quantity Measured</u>	<u>Reference</u>
	<u>Period</u>	<u>Period</u>	<u>Period</u>	<u>Period</u>		
Clay	2 hrs stirring		0-4 hours		Residual turbidity	31
Bacteria	Rapid mix		$\frac{1}{2}$ -2 hours		" "	32
Bacteria	Rapid mix		2-18 hours		" "	33
Clay	$\frac{1}{2}$ hr @ 42 rpm		0- $\frac{1}{2}$ hour		" "	34
Algae	$\frac{1}{2}$ hr @ 42 rpm		1 hour		" "	34
Clay	20 min @ 100 rpm 20 min @ 15 rpm		15 min		" "	17
Clay	20 min @ 100 rpm 20 min @ 15 rpm		15 min		" "	35
Fluorite	5 min @ 800 rpm		3 min		" "	36
Bacteria	3 min rapid mix 20 min @ 40 rpm		0		Relative scattering intensity	37
Polystyrene	0-7 hours		12 hours		Residual Optical Density	18
Polystyrene	20 min @ 100 rpm 20 min @ 15 rpm		Variable		Residual relative turbidity	8

Table 6.3 Recent Applications of Turbidity Measurements to Flocculating Systems.

<u>Particles</u>	<u>Flocculation Period</u>	<u>Sedimentation Period</u>	<u>Quantity Measured</u>	<u>Reference</u>
Bacteria	10 min	1 hour	Residual relative turbidity	24
Clay	20 min @ 100 rpm 20 min @ 15 rpm	15 min	Residual turbidity	38
Algae	2 min @ 80 rpm 15 min @ 30 rpm	1 hour	" "	4
Virus	1 min @ 100 rpm 30 min @ 30 rpm	1½ hour	" "	39
Bacteria	5 min @ 150 rpm	45 minutes	" "	40
Clay	1 min rapid min 15 min stirring	45 minutes	Residual relative turbidity	41
Algae	10 min stirring	1 hour	Residual turbidity	42
Clay & polystyrene	10 min @ 100 rpm	20 minutes	Residual optical density Residual relative scattering	43
Bacteria	rapid mix 20 min @ 30 rpm	0	Relative scattering intensity	44

$$1. \text{ Relative scattering intensity} = \frac{(I_{90^\circ}/I_{0^\circ}) \text{ Particulate + polymer}}{(I_{90^\circ}/I_{0^\circ}) \text{ Particulate}}$$

$$2. \text{ Relative turbidity} = \frac{(\tau) \text{ Particulate + polymer}}{(\tau) \text{ Particulate}}$$

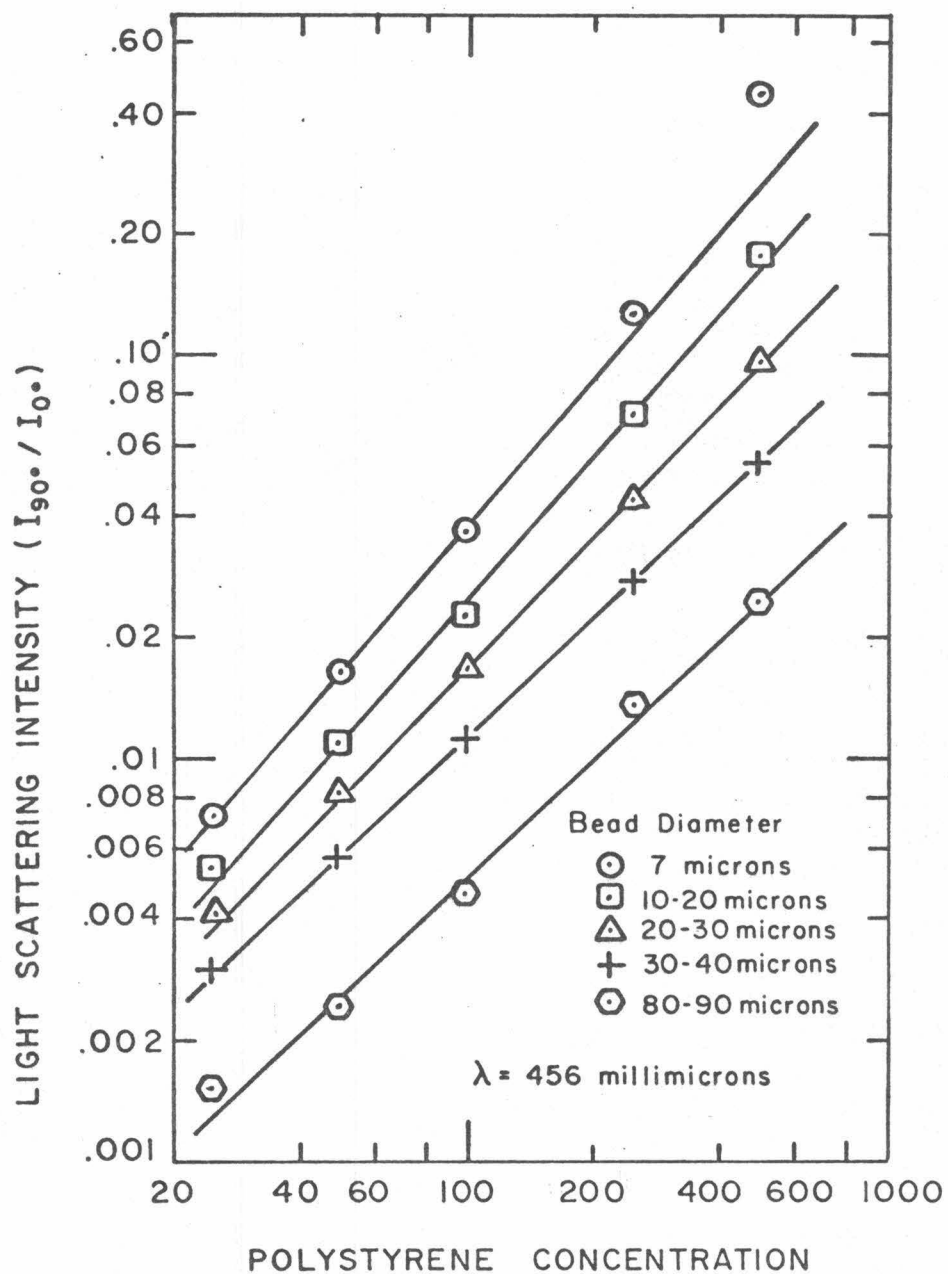


Figure 6.3 Light Scattering Intensity from Equal Weight Concentrations of Polystyrene Latex Spheres of Increasing Diameter. Adapted from Busch (37).

equals  $1 \ll 13 \ll 64$ , and equation (5-37) applies for approximate turbidity calculation. The number of particles decreases inversely as the third power of the radius, while the scattering of each particle is proportional to the square of the radius, so the turbidity will always decrease with increasing particle diameter.

In later experiments on coagulating PSL spheres, Birkner and Morgan (18) also recorded a decrease in the optical density as the size distribution of the aggregates broadened; i. e.; as the number of aggregates decreased and their size increased. This result is expected, since the single polystyrene latex particles ( $d=1.3 \mu\text{m}$ ,  $m = 1.20$ , and  $\lambda = 410 \text{ nm}$ ) are also in the diffraction regime ( $1 \ll \alpha$  ( $m-1) \ll \alpha$  equals  $1 \ll 2 \ll 10$ ) even before coagulation.

Thus far investigators in the wastewater field have been unable to correlate quantitatively the changes in particle size distribution of a coagulating suspension with corresponding changes in suspension turbidity (or scattering intensity at any angle). In the experiments of this chapter, particle size distributions and turbidity readings were recorded simultaneously from samples of the flocculating E. coli-PEI suspension. These data, together with the coalescence assumption and the Mie scattering-coefficient approximations, enabled quantitative comparisons to be made between the two measurement techniques.

In experiments with *E. coli* ( $d = 1.34 \mu\text{m}$ ,  $m = 1.06$ , and  $\lambda = 410 \text{ nm}$ ),  $\alpha(m-1) \ll 1 \ll \alpha$  equals  $0.6 \ll 1 \ll 10$  and therefore the singlet cells could be in the anomalous region, i. e., equation (5-35) would apply for approximate turbidity calculation. In this region, we anticipate that the turbidity of the small aggregates would increase linearly with the diameter. However, for the moderately successful flocculation caused by low molecular weight PEI (see Figures 6.10-6.16), the turbidity remained constant; for the very successful flocculation caused by the high molecular weight PEI (see Figures 6.18-6.21), the turbidity decreased. This result can be explained by considering the singlet cells and their aggregates to be in the anomalous diffraction regime. For aggregates up to  $5 \mu\text{m}$  in diameter ( $\alpha = 40$ ), turbidity remains insensitive to changes in the aggregate diameter since it is proportional to  $n_i r_i^3$ , a conservative parameter in a coagulating system. However, for aggregates greater than  $5 \mu\text{m}$  in diameter ( $\alpha > 40$ ), the scattering coefficient oscillates near the constant value 2, (Figure 5.10), and thus the turbidity is proportional to  $n_i r_i^2$ , which decreases in a coagulating system.

In each flocculation experiment, the turbidity and particle size distribution of the untreated *E. coli* suspension were measured. From this information, the optical constant could be determined, i. e.,

$$\tau = C \sum_i K_i n_i \pi r_i^2 \quad (6-8)$$

where C = optical constant

$$K_i = 2 - (4 \sin \rho) / \rho + 4(1 - \cos \rho) / (\rho)^2$$

$$\rho = 2\alpha(m-1)$$

$$n_i = \text{number of aggregates of radius } r_i$$

Schie and Rehberg (45) have measured the refractive index of E. coli as 1.41; this value was utilized here along with a solution refractive index of 1.33.

Once the optical constant was known, the turbidity of the flocculated suspension calculated from equation (6-8) could be compared with the experimentally measured turbidity. Correlations were made between particle size distributions and turbidity readings as the PEI molecular weight and dose were varied, but the velocity gradient was held constant at  $G = 20 \text{ sec}^{-1}$ . Other experiments indicated that the influence of varying the velocity gradient on either turbidity or particle size distribution measurements was minor.

#### 6.2.3.2 Relative Scattering Intensity of Flocculating E. coli

In an analysis of various techniques of qualitatively measuring flocculation effectiveness, Busch (37) determined that the relative scattering intensity is preferable to microscopic counting, bacterial

plating, and velocity settling; mainly because the light scattering technique does not require sample dilution or extensive measurement times.

Essentially this technique attempts to measure directly the decrease in scattered light at  $90^{\circ}$  and the increase in transmitted light at  $0^{\circ}$  for a suspension of aggregated particles over that recorded for a suspension of dispersed particles.

In my experiments, four consecutive hourly intensity readings were taken, the first occurring 60 minutes after the initial two minute rapid mix of E. coli and PEI. During the intervening flocculation period, the sample was stirred continuously at a predetermined value of G, either 20, 40, or 60 per second. These hourly scattering intensity readings were then compared directly to hourly scattering intensity readings of an untreated E. coli suspension. The relative scattering intensity of PEI flocculated E. coli cells was investigated as a function of PEI molecular weight, PEI dose, and intensity of agitation during four hours of mixing.

#### 6.2.3.3 Residual Relative Scattering Intensity of Flocculating E. coli

If light transmission measurements are made on a dispersion of large particles, the intensity of the transmitted light will gradually increase as the particles settle out under the influence of gravity.

Gumprecht and Sliepcevich (46) computed the size range of particles settling out during any interval of time via Stokes Law:

$$r = (9hu/2g(\rho_p - \rho_o)t)^{\frac{1}{2}} = k(t)^{-\frac{1}{2}} \quad (6-9)$$

where  $h$  = height from top of container to light beam

$u$  = viscosity of settling medium

$g$  = acceleration due to gravity

$(\rho_p - \rho_o)$  = difference in density of the dispersed particles and surrounding medium

Since a polydispersed system may be considered as being composed of a multitude of monodisperse systems, the transmission equation becomes

$$I/I_o = \exp(-\pi \int_{r_o}^{r_t} CKr^2 p(r) dr) \quad (6-10)$$

where  $C$  = correction to Mie theory reflecting size of particles and geometry of optical system

$p(r)$  = number of particles within interval  $dr$ ; the frequency distribution function

$r_t$  = maximum value of  $r$  at time  $t$

Differentiating equation (6-10) with respect to time yields

$$-d(\ln I)/dt = -d(\ln \tau)/dt = \pi CKr^2 p(r) dr/dt \quad (6-11)$$

where  $p(r)dr$  = number of particles in the size range between  $r$  and  $r+dr$  which irreplaceably drop out of the light beam during the time interval between  $t$  and  $t+dt$ .

By means of equation (6-9),  $r$  can be eliminated from equation (6-11), yielding

$$p(r) = (2t^{5/2} / \pi l k^3 CK) d(\ln I) / dt \quad (6-12)$$

Thus the frequency function can be determined from the time rate of decay of the intensity without making a priori assumptions regarding the form of the distribution or of the concentration of the particles. This method has been applied to polydispersed aerosols by Gumprecht and Sliepcevich (46) and by Kerker, Cox, and Shoenberg (47); however it has not been utilized in liquid suspensions. Major limitations appear to be control of convection currents, scattering complications caused by coagulation, and the height of the light beam, which must be negligibly small compared to the settling height of the chamber. Because of these limitations, no effort was made to correlate the turbidity of a settling, flocculated E. coli suspension with the particle size distribution. Instead the scattering intensity of settling, flocculated aggregates was compared to the scattering intensity of settling, untreated E. coli suspensions, as a function of PEI molecular weight, PEI dose, and time of settling. In spite of its qualitative nature, this technique has received widespread application in

determining the effectiveness of flocculants in producing the desired flocculation and sedimentation of colloidal particles (Table 6.3).

Following the two minute rapid mix of bacteria suspension and PEI solution, the flocculating suspension was gently stirred ( $G = 20 \text{ sec}^{-1}$ ) for 20 minutes, and then a 50 ml sample was removed for sedimentation within the Brice-Phoenix scattering cell. Residual relative scattering intensity readings were recorded at sedimentation times of 60, 120, 180, and 240 minutes following the rapid mix.

#### 6.2.4 Refiltration Rate of E. coli Aggregates

##### 6.2.4.1 Verification of Constant Porosity Assumption

In addition to the determination of the optimum polymer dose and the possible mechanism of flocculation (Sections 3.4 and 4.3.4), the refiltration technique can be utilized to determine the change in the mean aggregate diameter (Section 5.4.1). However, the filter bed porosity must remain constant irrespective of flocculation condition (Section 5.4.2).

The constant porosity assumption was verified for the E. coli-PEI system by filtering 50 ml of the flocculated suspension through a  $0.45 \mu\text{m}$  Millipore filter at seven different pressure differentials ranging from 100 mm Hg to 700 mm Hg in increments of 100 mm Hg. The filtrate was collected and refiltered through the filter cake and

septum at the same pressure differential. The product of the specific time of refiltration and the pressure differential was then plotted against the pressure differential as per Section 5.4.2.

Figure 6.4 shows the results of differential pressure variations on the specific resistance at three flocculant doses (underdosed, optimum, and overdosed) for two PEI molecular weights (PEI 6 and PEI 350). The connecting lines are drawn parallel to each other, thereby illustrating that changes in the refiltration rate are primarily attributable to changes in the specific surface area and not to variations in the porosity of the filter cake.

Not all the points fall on the parallel connecting lines, an indication that the porosity of the filter cake does vary irregularly with flocculation condition, a fact also observed by Busch (37). Carman (48) states that the specific resistance varies with the compressibility of the material, which may account for the recorded porosity changes during refiltration experiments of other investigators. Obviously, the extent of porosity changes with flocculation condition must be measured for each polymer-colloid system before the Carman-Kozeny equation can be used to determine specific surface areas.

Since the porosity of the filter cake in the PEI-E. coli system is essentially constant, the refiltration technique becomes a direct measure of the change in specific surface area, and thus of the change

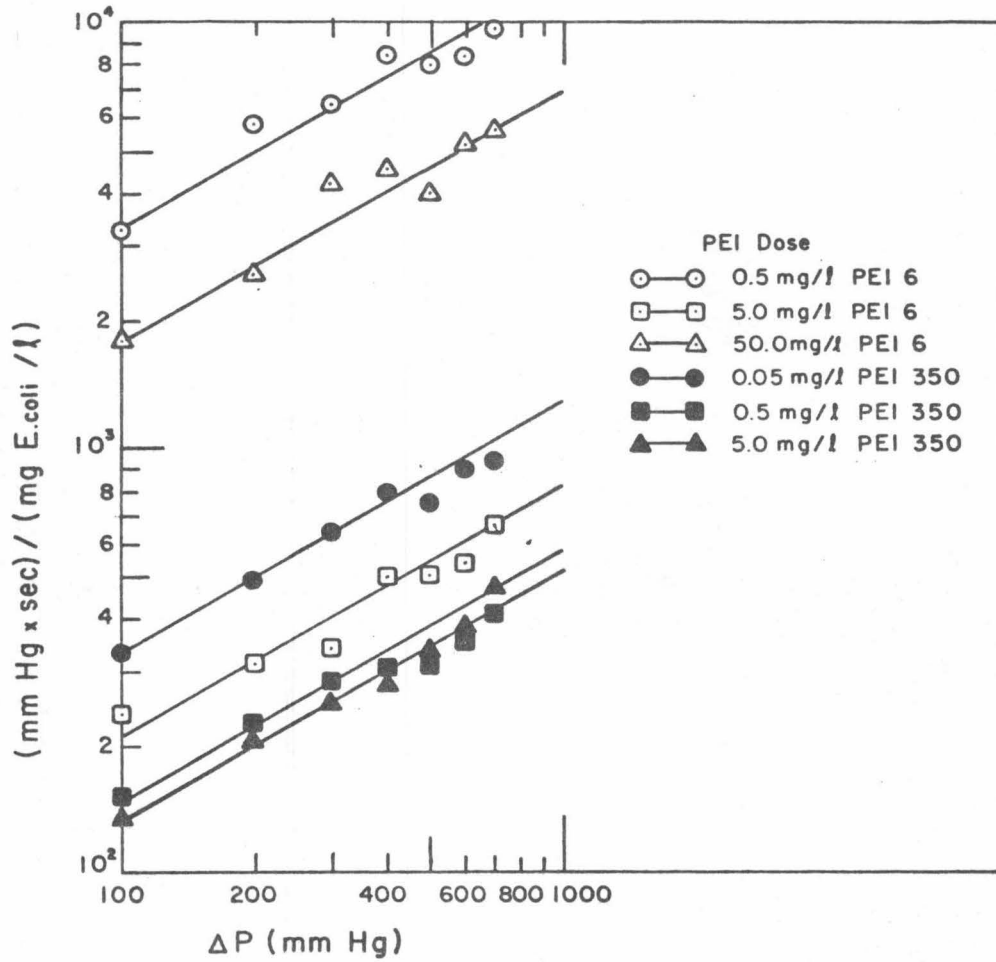


Figure 6.4 Plot of  $\Delta Pt/w$  Versus  $\Delta P$  (Equivalent to Plot of Specific Resistance Versus  $\Delta P$ ) for Varying Doses of PEI 6 and PEI 350.

in mean aggregate diameter. The refiltration technique therefore indicates the PEI flocculation effectiveness not only in the vacuum filtration process, but also in sedimentation, centrifugation, and filtration processes, since all are directly dependent on the square of the mean aggregate diameter.

#### 6.2.4.2 Influence of Velocity Gradient in Stirrer-Reactor on the Refiltration Rate

The refiltration technique, and the variation of refiltration times with PEI molecular weight and dose, have been presented in Sections 4.2.4 and 4.3.4, respectively. The same technique was utilized to determine the influence of varying the velocity gradient in the stirrer-reactor from  $G = 0$  to  $G = 60 \text{ sec}^{-1}$  on the refiltration rate. Since the refiltration time is inversely proportional to the square of the mean aggregate diameter, increases in refiltration time as the velocity gradient increases would indicate that the greater shear forces are causing floccule disruption.

Following the two minute rapid mix of E. coli with PEI the suspension was flocculated for 60 minutes at a predetermined velocity gradient ( $G = 0, 20, 40, \text{ or } 60 \text{ sec}^{-1}$ ). A 50 ml sample was removed from the stirrer-reactor and refiltered as per Section 4.2.4. For the purpose of correlating studies between Coulter counter measurements

and refiltration rate measurements, the E.coli aggregate surface area  $S$  and the specific surface area  $S_0$  were calculated from the particle size distribution determined from Coulter counter readings taken simultaneously with the refiltration experiments.

#### 6.2.5 Preparation of Electron Micrographs of E.coli Filter Cake

Electron micrographs of the E.coli filter cake were prepared to determine the structural differences between the cakes formed by high molecular weight PEI species which yielded excellent flow rates, and the cakes formed by low molecular weight PEI species which yielded poor flow rates. The refiltration experiments were conducted as per Section 4.2.4, except that 0.5  $\mu\text{m}$  Nucleopore filters were used in lieu of Millipore filters to provide better visual contrast.

The filter septum and cake were removed from the vacuum filtration apparatus, and were prepared for observation in the Scanning Electron Microscope using the procedure of Section 4.2.5. Only optimum flocculation doses: 5.0 mg/l for PEI 6 and 0.5 ml/l for PEI 350 were utilized in this Section.

### 6.3 Experimental Results

#### 6.3.1 Influence of PEI Molecular Weight, Dose, and Velocity Gradient on Reduction of Particle Count

Figure 6.5 presents the results of flocculation experiments

with the five molecular weight species at varying doses. Polymers of molecular weight less than  $10^3$  recorded less than a 70% reduction in the number of primary particles ( $(n_0 - n)/n_0 < 0.70$ ). Polymers of molecular weight greater than  $10^4$  achieved more than a 90% reduction in the number of primary particles for doses greater than 0.5 ml/l; however, a restabilization region was noted for doses greater than 5.0 mg/l. This restabilization corresponded to charge reversal on the bacteria cells, as determined by measurement of their electrophoretic mobility.

Figure 6.6 primarily illustrates the restabilization of the E. coli cells caused by PEI 350 doses in excess of 5.0 mg/l, as opposed to the virtually constant level of flocculation caused by PEI 12 doses far in excess of 5.0 mg/l. Also shown is the effect of long periods of stirring (up to 240 minutes) upon the degree of flocculation. For PEI 12, continuous stirring for four hours after dosing results in a 20% greater reduction in the number of particles than continuous stirring for only one hour. For PEI 350, the reaction is complete within one hour, and further stirring neither increases nor decreases the degree of flocculation. The results for PEI 6 and PEI 18 were analogous to those of PEI 12; and PEI 600 results were the same as those for PEI 350.

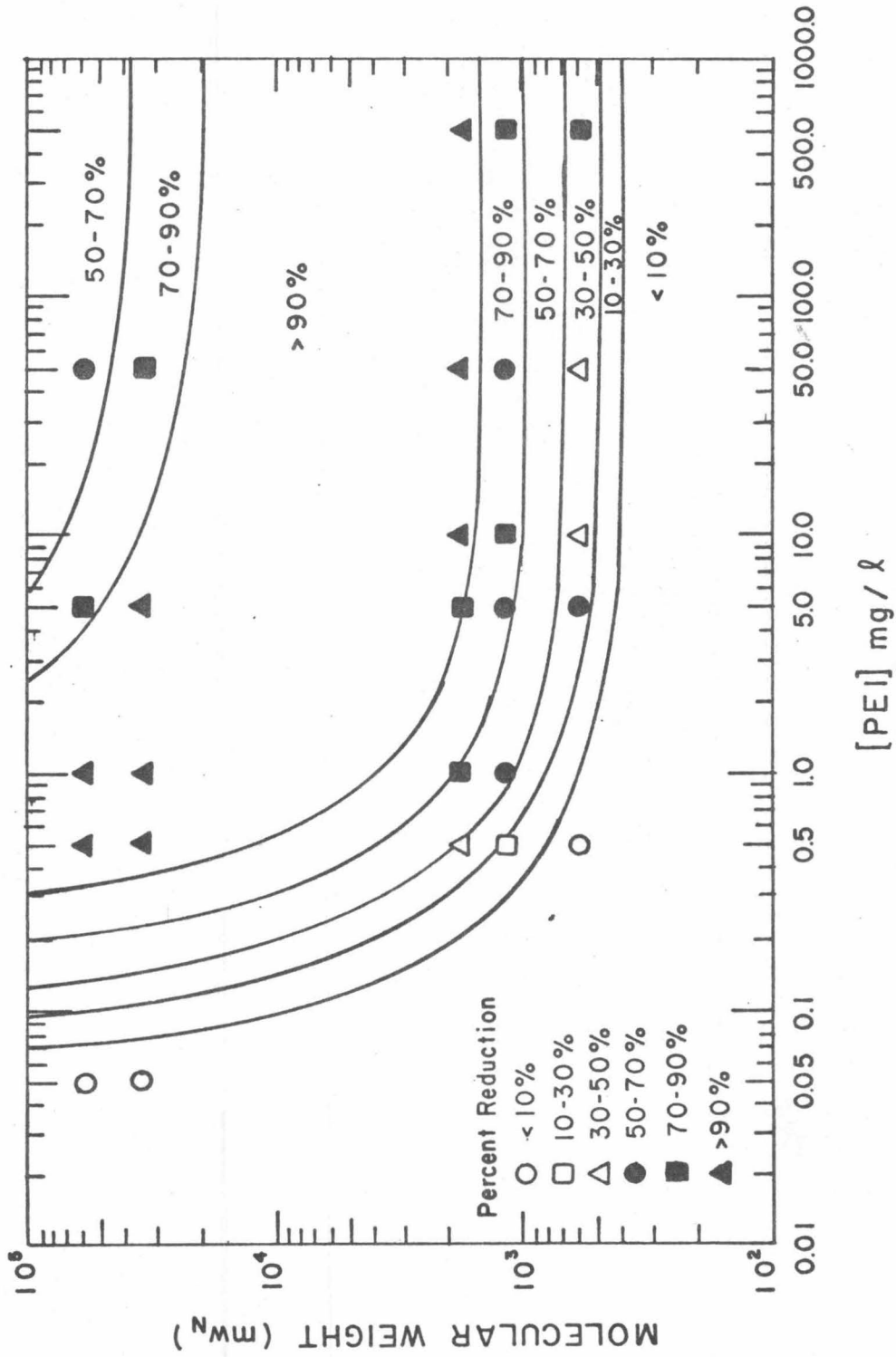


Figure 6.5 Log MW<sub>n</sub> - Log [PEI] Domains of Percent Reduction in Number of Particles after 60 Minutes of Flocculation at G=20 sec<sup>-1</sup>.

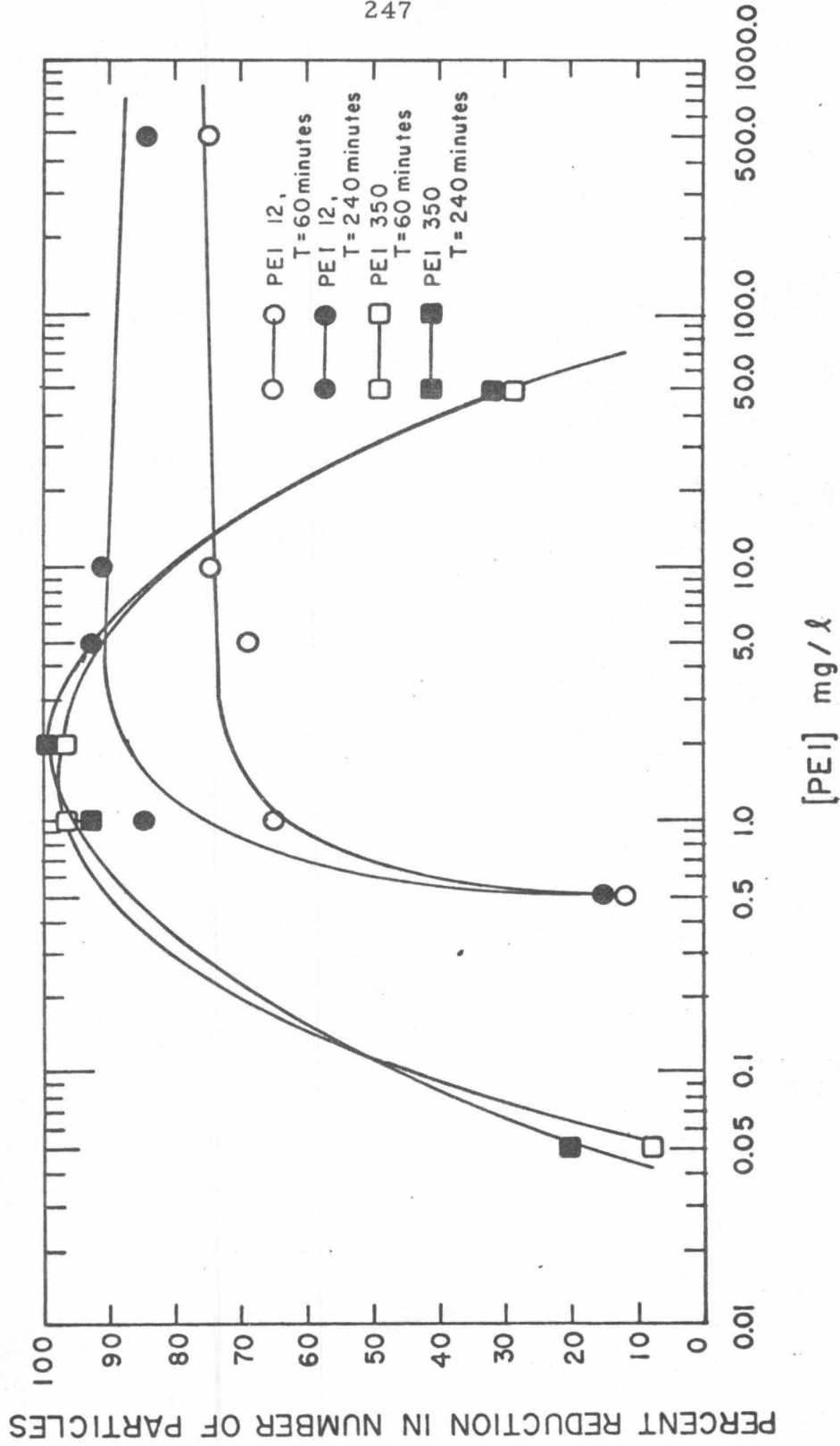


Figure 6.6 Percent Reduction in Number of Particles as a Function of PEI MW, [PEI], and Time of Flocculation at  $G=20 \text{ sec}^{-1}$ .

Experiments were conducted at shear gradients of 20, 40, and  $60 \text{ sec}^{-1}$  in order to determine the optimum shear gradient for reduction in particle count. As Figure 6.7 shows, only negligible differences exist between the percent reduction in particle count as the velocity gradient is increased from  $20 \text{ sec}^{-1}$  to  $60 \text{ sec}^{-1}$ . Obviously, the primary factors in flocculant effectiveness are molecular weight and dose; i. e., both the intensity of agitation, within the common treatment practice limits, and the time of agitation play very minor roles in the flocculation of E. coli with PEI. Additional studies have shown that the first order of magnitude reduction in primary particle population occurs within 5 minutes of addition of PEI 350 or PEI 600, and the second order of magnitude reduction in aggregate population occurs gradually over the remaining four hours of flocculation.

### 6.3.2 Influence of PEI Molecular Weight and Dose on Particle Size Distributions

Figure 6.8 reflects the change in the particle size distribution over a four hour period of stirring at  $G = 20 \text{ sec}^{-1}$  when no polymer has been added. The peak in the particle size distribution occurs roughly at the mean cell diameter  $1.3 \mu\text{m}$ . Cell aggregates are present, though in small concentrations. These aggregates are caused by bio-flocculation, which increases with time because of the continuous release of extracellular biopolymers, and to coagulation by the  $0.06\text{M}$

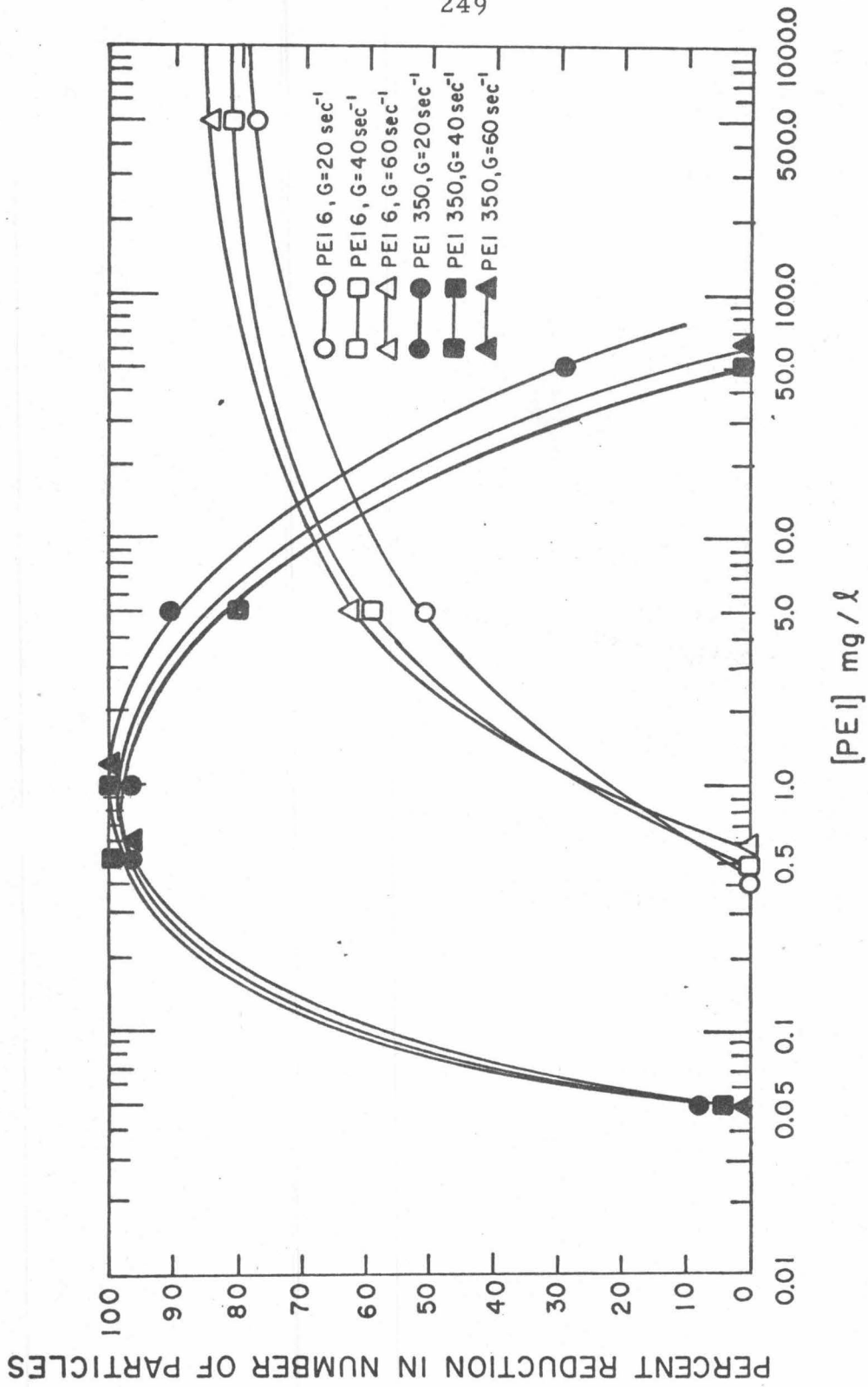


Figure 6.7 Percent Reduction in Number of Particles as a Function of PEI MW<sub>n</sub>, [PEI], and Magnitude of Velocity Gradient for 60 Minutes.

NaCl dilutant. Differential volume distribution spectrums, corresponding to each of the following number distributions, are contained in Appendix A.

Figures 6-9-6.11 are the particle size distributions for E.coli cells flocculated with underdosed (0.5 mg/l), optimum (5.0 mg/l), and overdosed (50.0 mg/l) concentrations of PEI 6. All three size distributions show that the degree of flocculation increases continually with agitation at  $G = 20 \text{ sec}^{-1}$ . At this molecular weight and agitation, most aggregates are concentrated in the range 1 to 4  $\mu\text{m}$ , with the number of the latter increasing with time as the number of the former decreases. Overdosing does not appear to cause restabilization of the E.coli cells, as evidenced by comparing Figure 6.10 with Figure 6.11.

Figures 6.12-6.14 are the particle size distributions for E.coli flocculated with underdosed (0.5 mg/l), optimum (5.0 mg/l), and overdosed (50.0 mg/l) concentrations of PEI 12. In contrast to Figures 6.9-6.10, there appears to be little change in degree of flocculation after one hour of stirring at  $G = 20 \text{ sec}^{-1}$ . In addition, there are more aggregates in the 4 to 8  $\mu\text{m}$  range, indicating increasing shear strength with increasing molecular weight. As with PEI 6, overdosing does not appear to cause restabilization of the E.coli cells.

FIGURE 6.8 DIFFERENTIAL SIZE DISTRIBUTION SPECTRUM

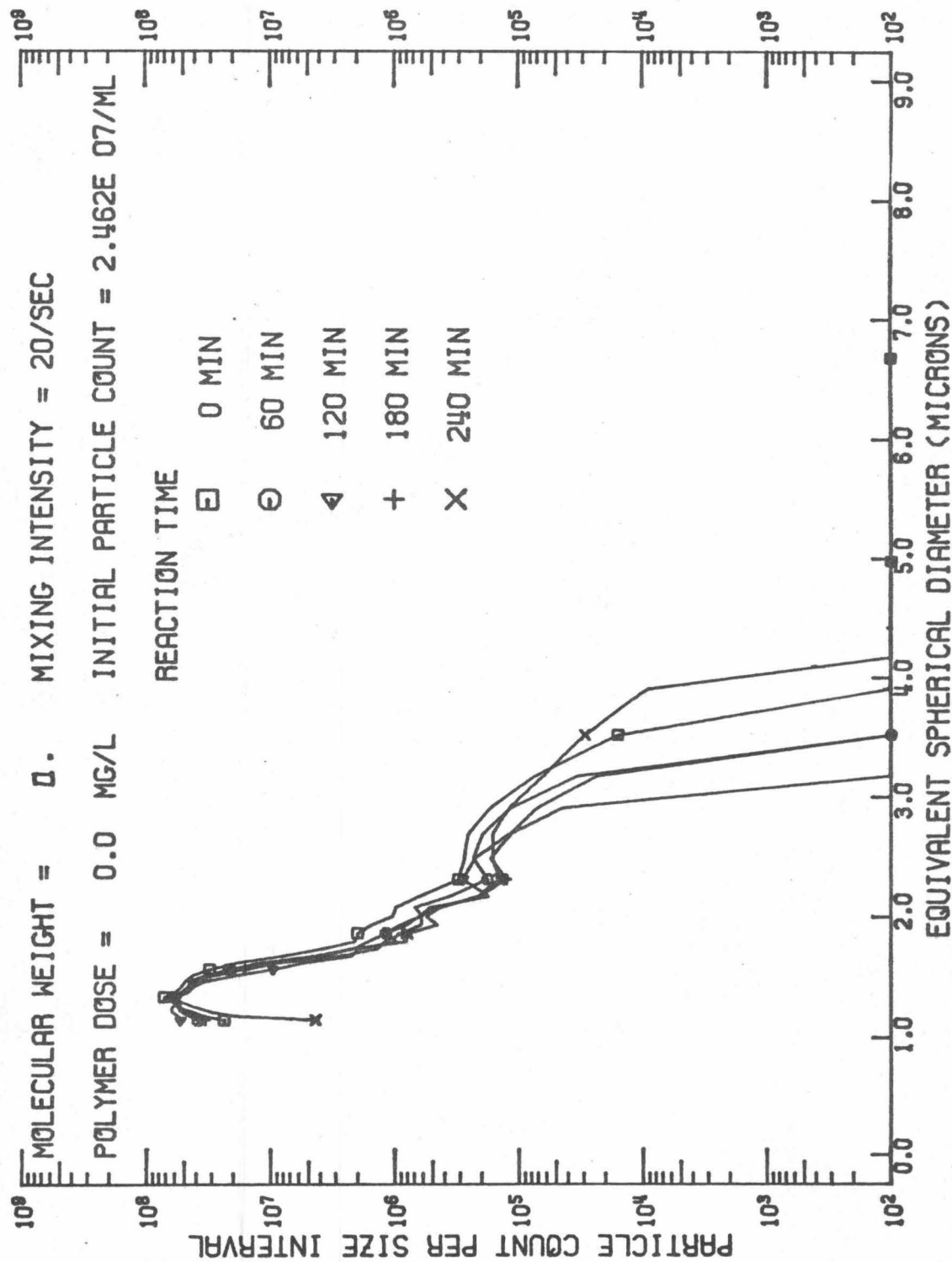


FIGURE 6.9 DIFFERENTIAL SIZE DISTRIBUTION SPECTRUM

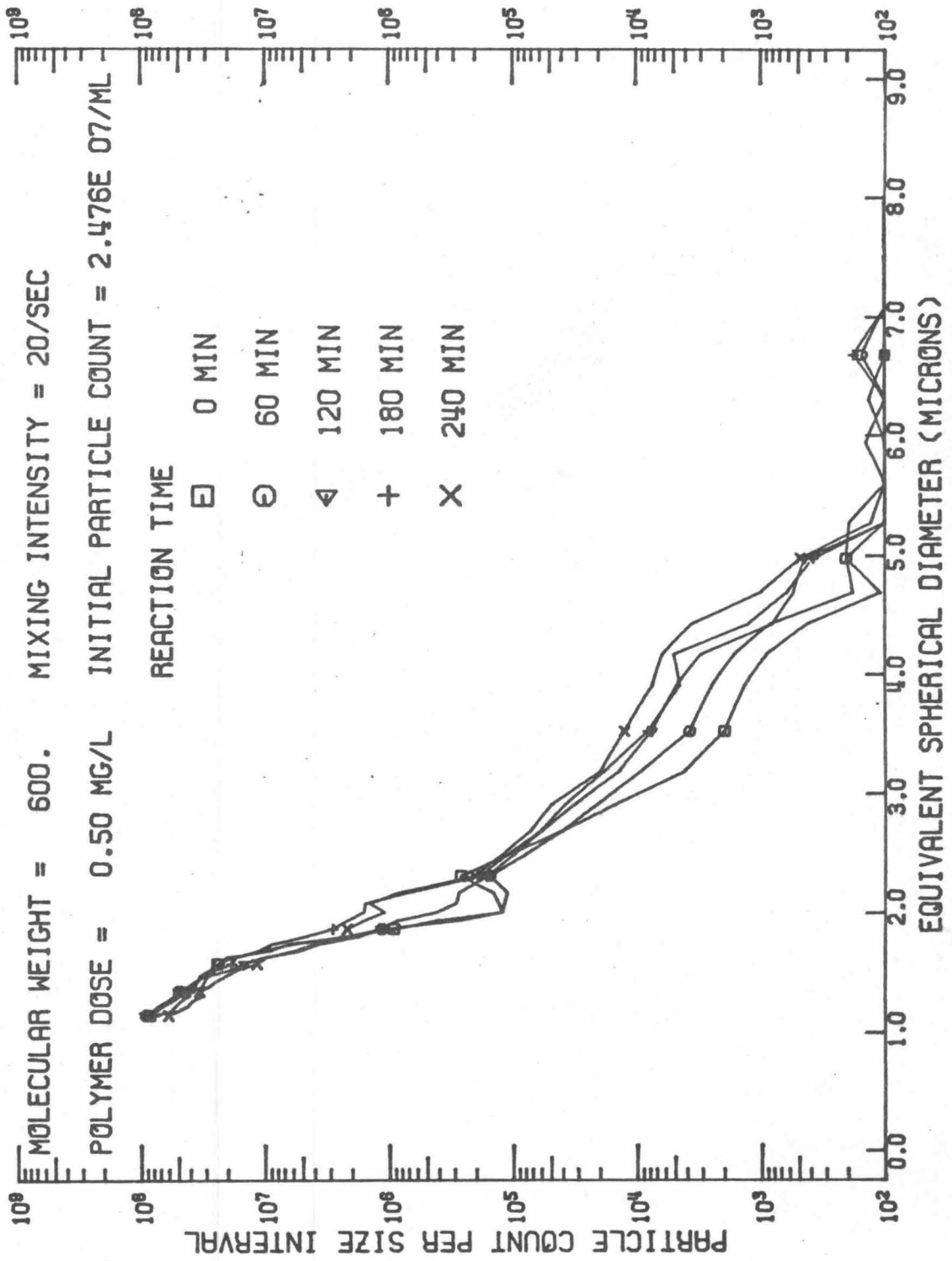


FIGURE 6.10 DIFFERENTIAL SIZE DISTRIBUTION SPECTRUM

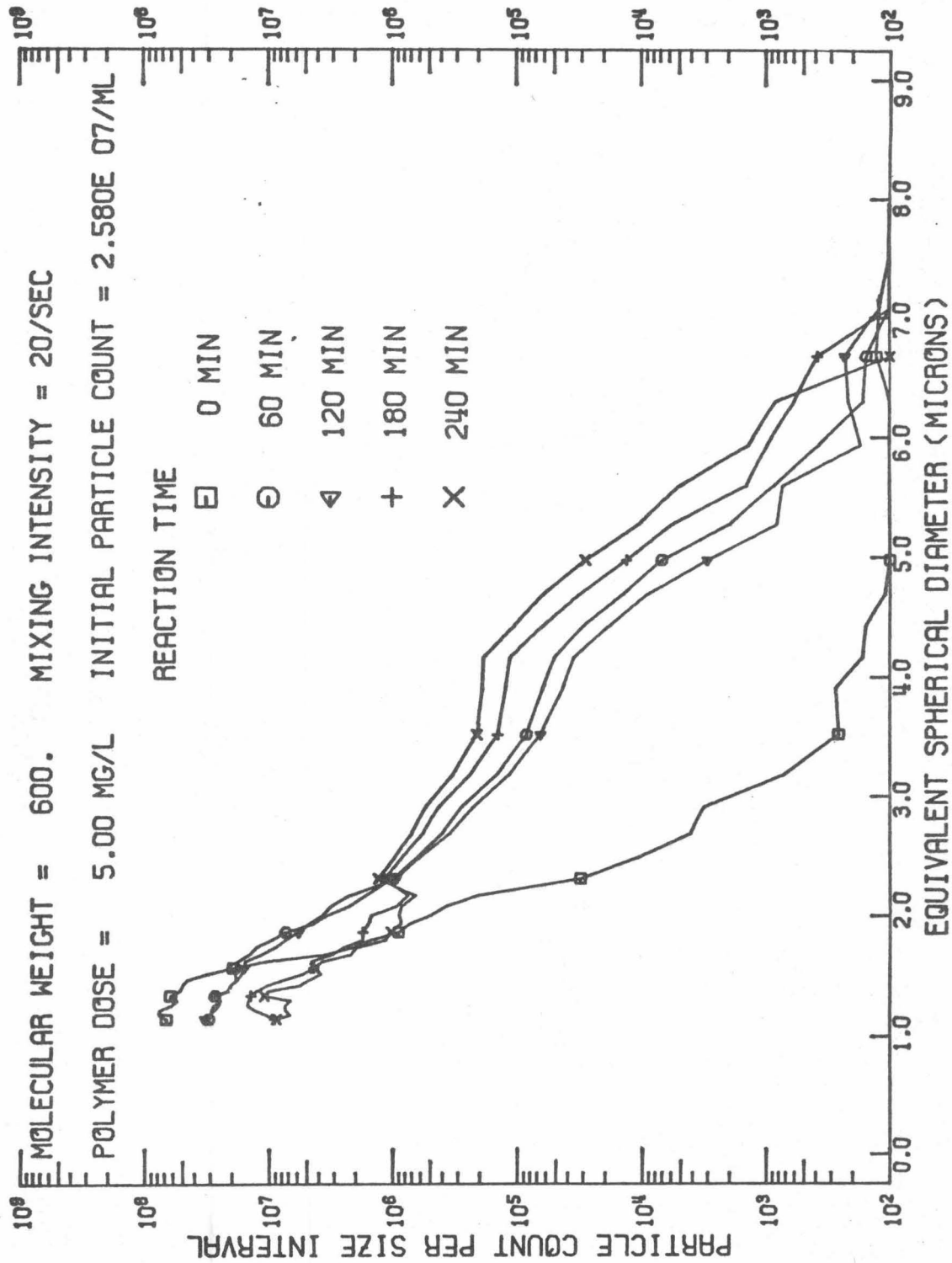


FIGURE 6.11 DIFFERENTIAL SIZE DISTRIBUTION SPECTRUM

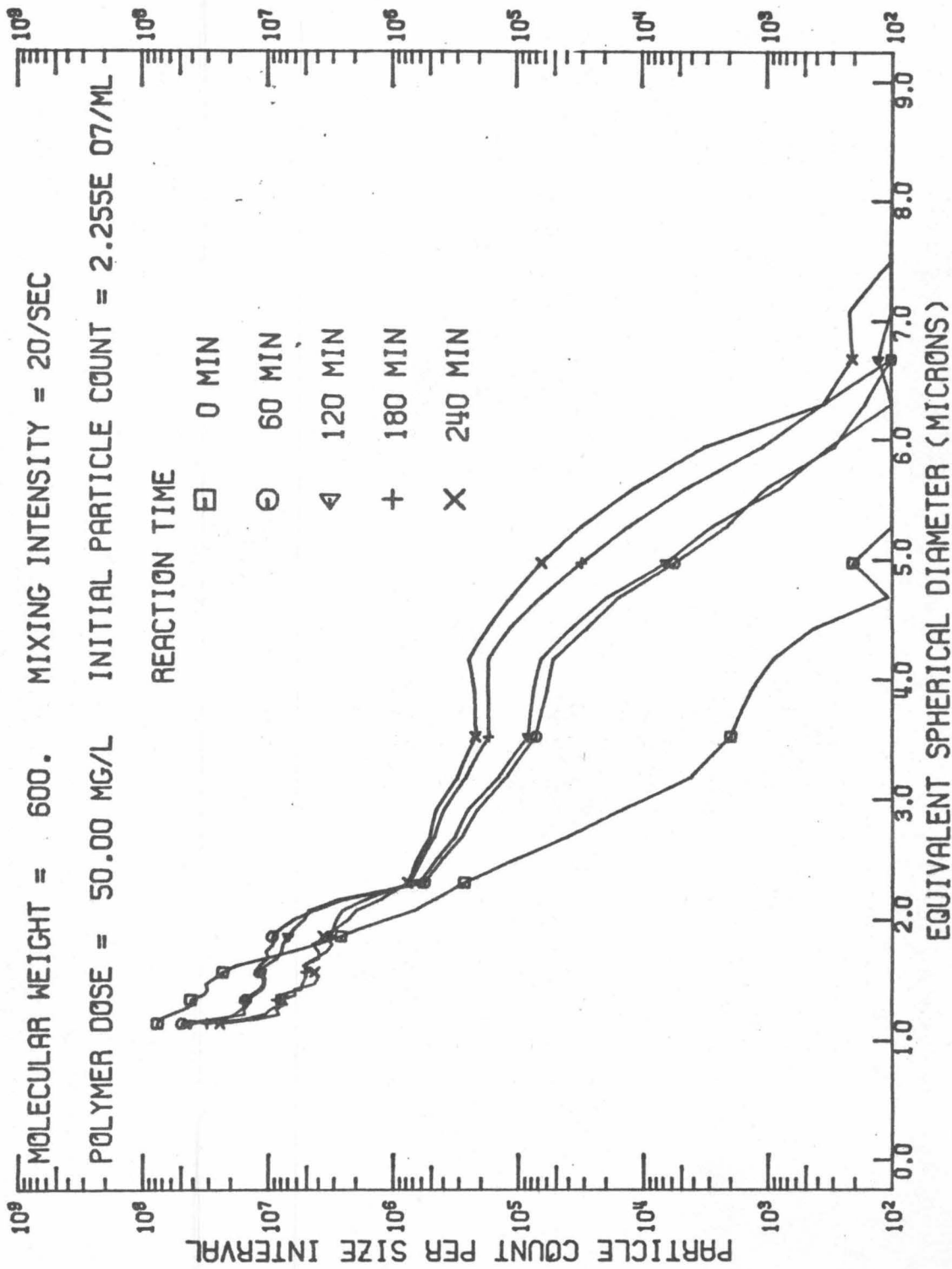


FIGURE 6.12 DIFFERENTIAL SIZE DISTRIBUTION SPECTRUM

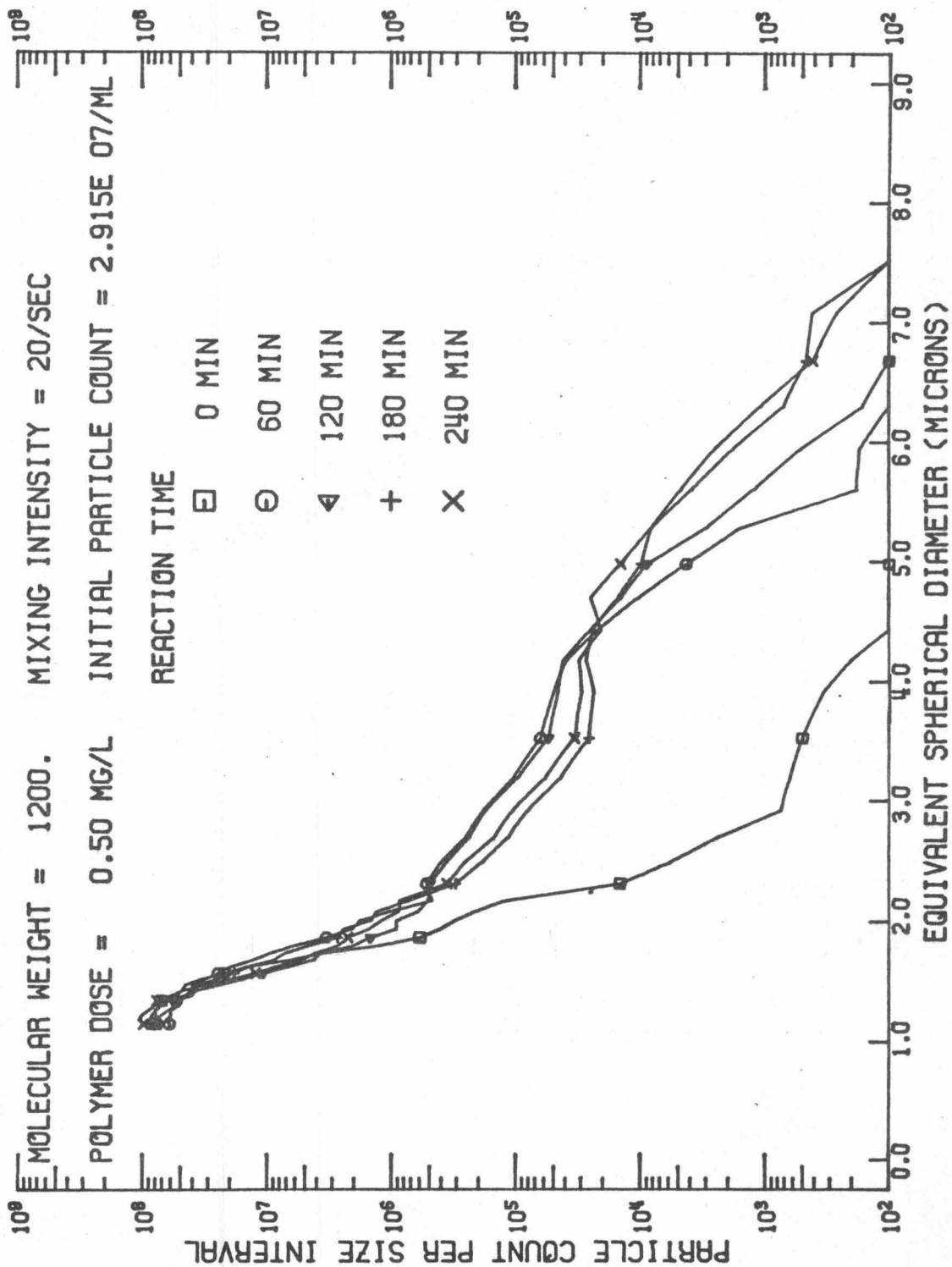


FIGURE 6.13 DIFFERENTIAL SIZE DISTRIBUTION SPECTRUM

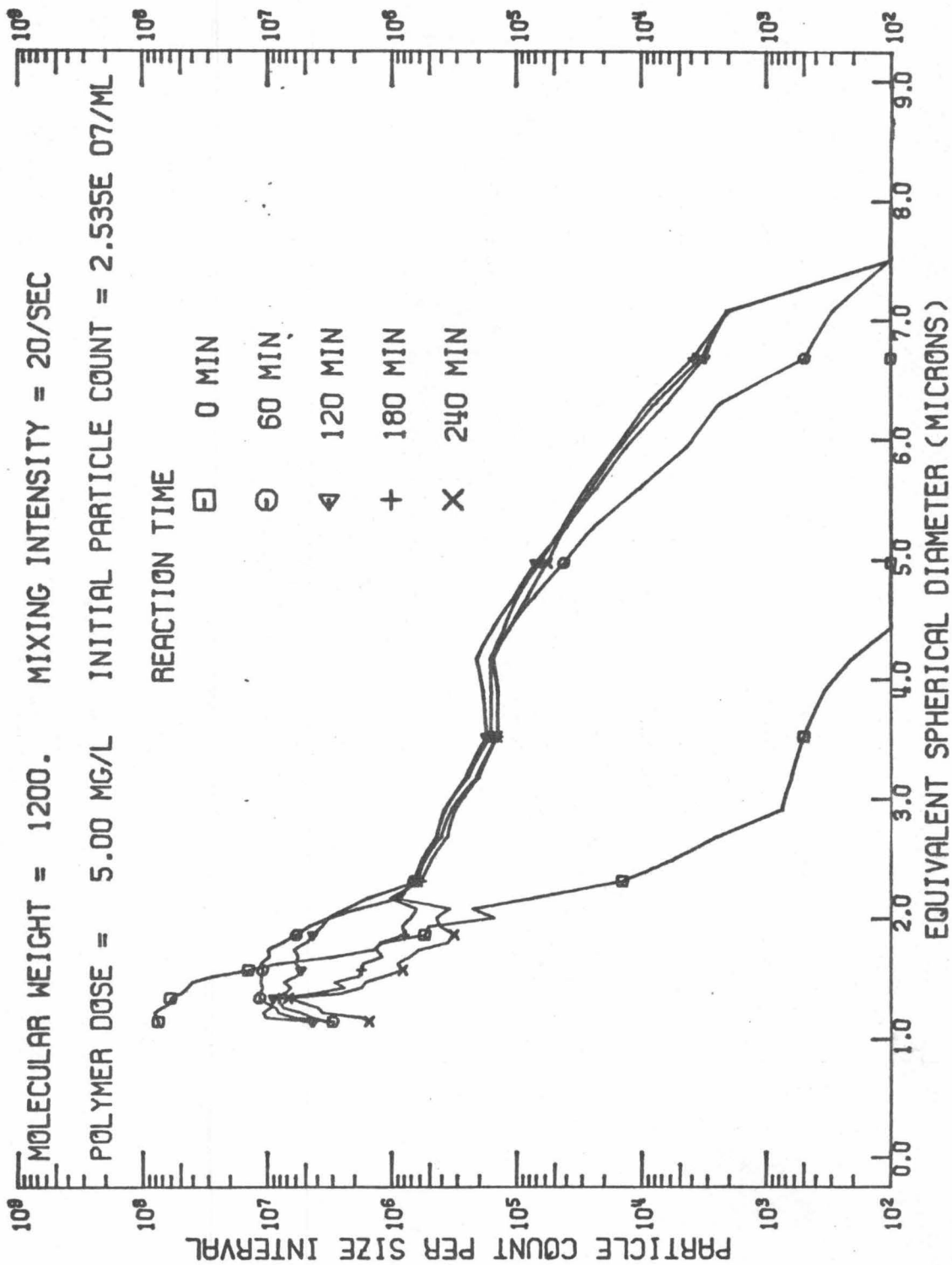
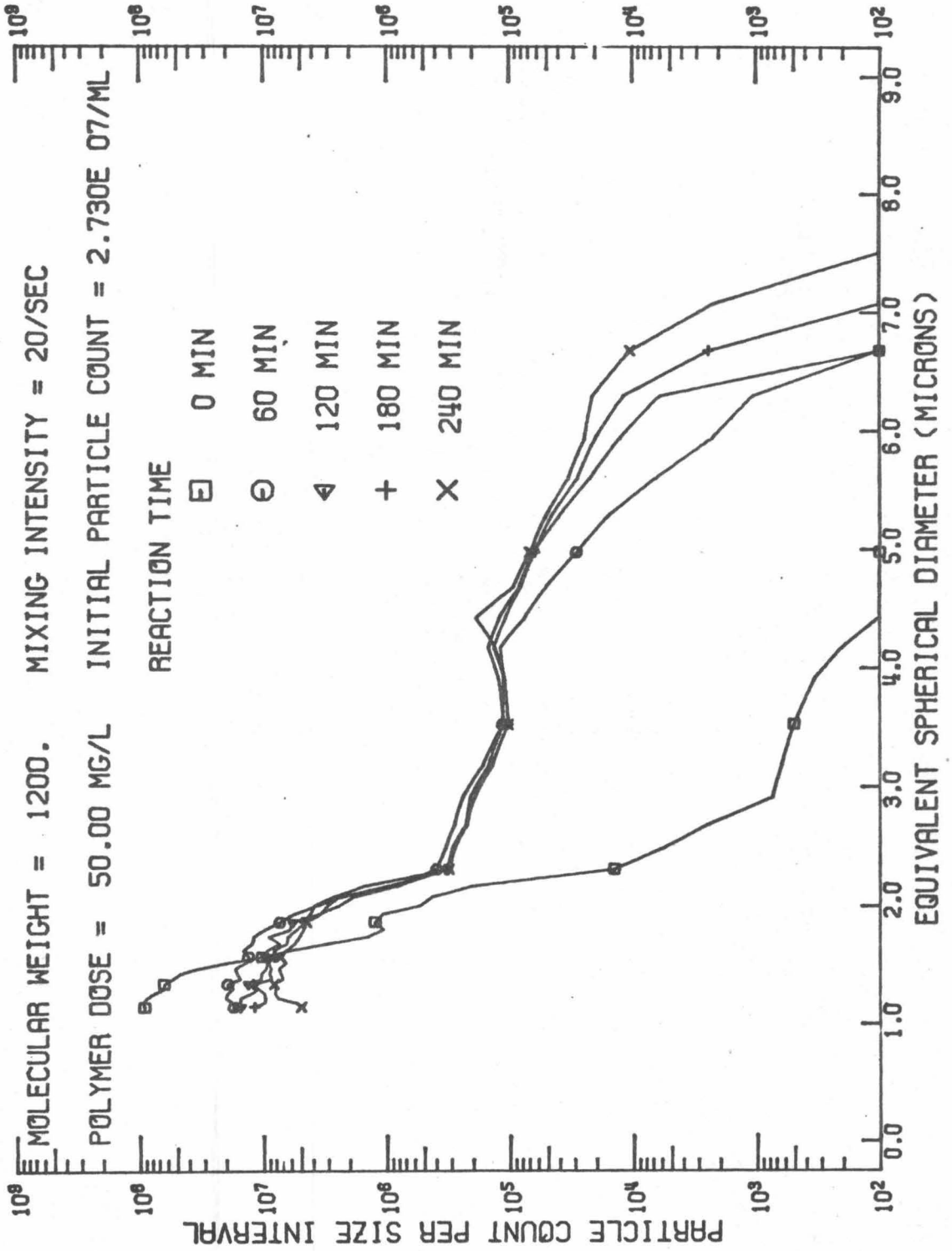


FIGURE 6.14 DIFFERENTIAL SIZE DISTRIBUTION SPECTRUM



Figures 6.15-6.16 are particle size distributions for E. coli cells flocculated with optimum (5.0 mg/l) and overdosed (50.0 mg/l) concentrations of PEI 18. There appears to be a continuous growth of larger aggregates in the 8 to 12  $\mu\text{m}$  range at the expense of the smaller 1 to 4  $\mu\text{m}$  aggregates. The increased shear strength with the higher molecular weight species is again reflected in the growth of aggregates in the 8 to 12  $\mu\text{m}$  region: PEI 6 and PEI 12 had virtually no aggregates in this particle size range.

Figures 6.17-6.19 are the particle size distributions for E. coli cells flocculated with underdosed (0.05 mg/l), optimum (0.5 mg/l), and overdosed (50.0 mg/l) concentrations of PEI 350. Figure 6.18 illustrates a dramatic decrease in the number of primary particles (from  $10^8$  cells  $\text{cm}^{-3}/\mu\text{m}$  to  $10^6$  cells  $\text{cm}^{-3}/\mu\text{m}$ ) and a dramatic increase in the size of the largest aggregates (greater than 12  $\mu\text{m}$ ). The growth of very large aggregates occurs at the expense of small (1 to 4  $\mu\text{m}$ ) and medium (4 to 8  $\mu\text{m}$ ) sized aggregates, both of which are an order of magnitude less in number than when flocculated with PEI 12 or PEI 18. Figure 6.19 illustrates the restabilization of small unit flocs (approximately 4  $\mu\text{m}$  in diameter) caused by overdoses of the high molecular weight PEI 350.

Figures 6.20-6.22 present essentially the same picture for PEI 600 as was given for PEI 350. In general, flocculation with the

high molecular weight species is characterized by a reduction in the numbers of primary particles by two orders of magnitude, the rapid growth of macroflocs (i. e. , larger than 12  $\mu\text{m}$  in diameter or 780 cells/aggregate), and the restabilization of smaller unit flocs by polymer overdoses.

### 6.3.3 Aggregate Light Scattering Results

The purpose of my light scattering experiments on the flocculating bacterial system was two-fold: First, to attempt correlation of light scattering measurements with Coulter counter size distributions, and second, to study the effect of system parameters, specifically polymer molecular weight, polymer dosage, mixing intensity, and sedimentation period, upon the relative scattering intensity and the residual relative scattering intensity.

#### 6.3.3.1 Correlation of Predicted Turbidity with Measured Turbidity

Although both the scattering intensity measurements and the Coulter counter size distributions are complicated by a variety of effects, good correlation was achieved between the two methods for a wide variety of flocculation conditions.

The turbidities calculated from the particle size distributions and equation (6-8) are within  $\pm 20\%$  of values measured experimentally in the Brice-Phoenix instrument. For flocculation with the low

FIGURE 6.15 DIFFERENTIAL SIZE DISTRIBUTION SPECTRUM

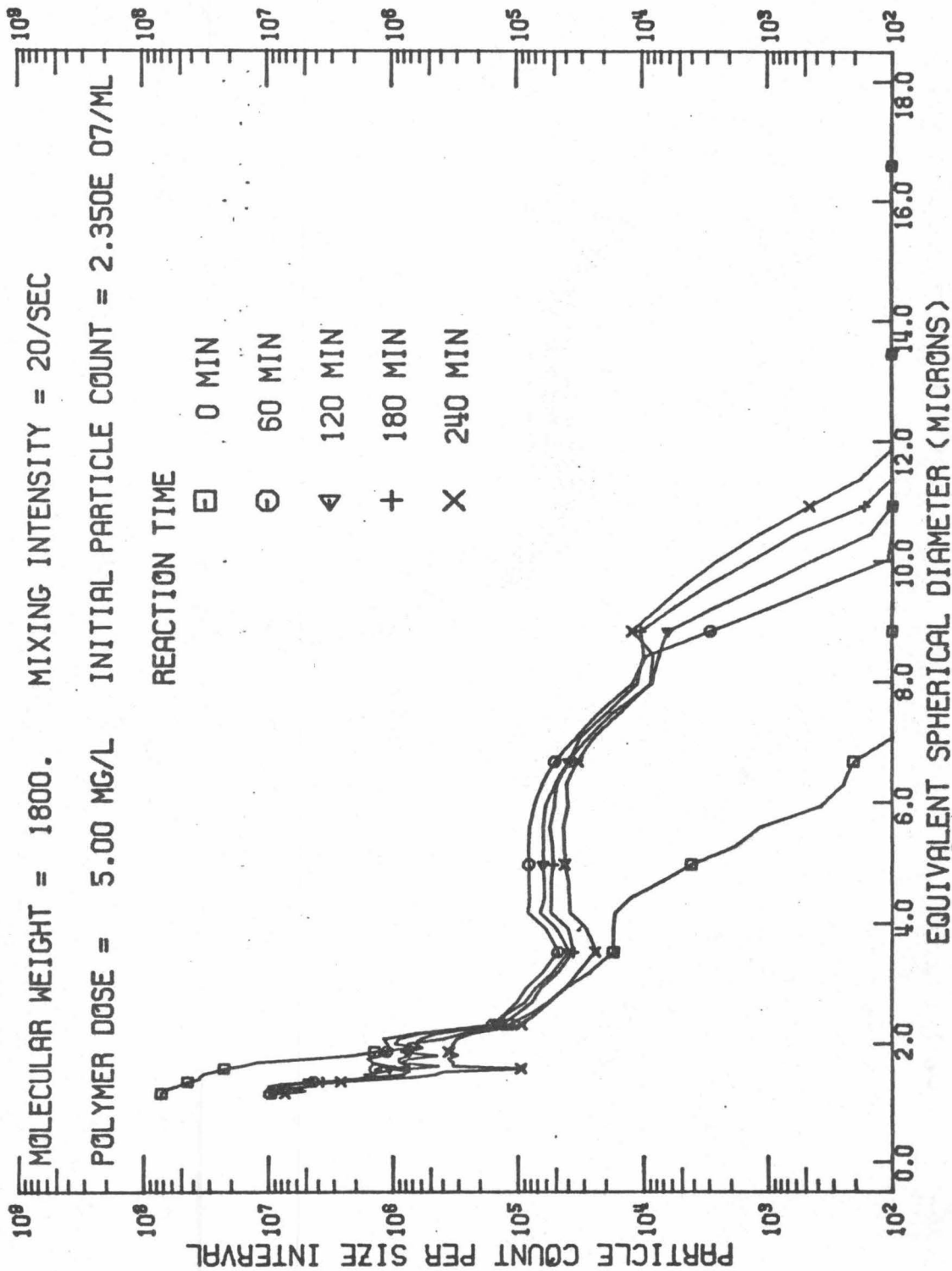


FIGURE 6.16 DIFFERENTIAL SIZE DISTRIBUTION SPECTRUM

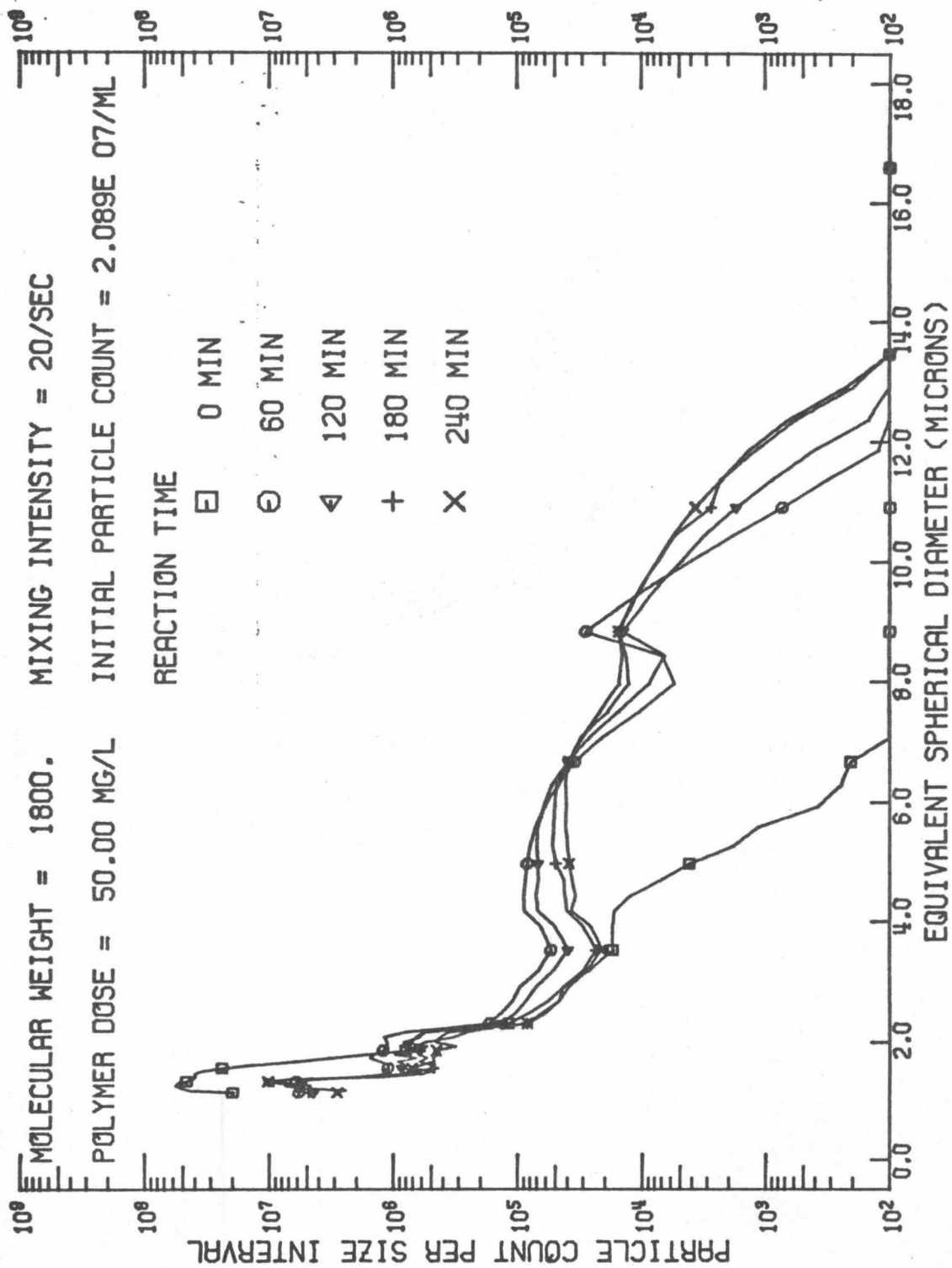


FIGURE 6.17 DIFFERENTIAL SIZE DISTRIBUTION SPECTRUM

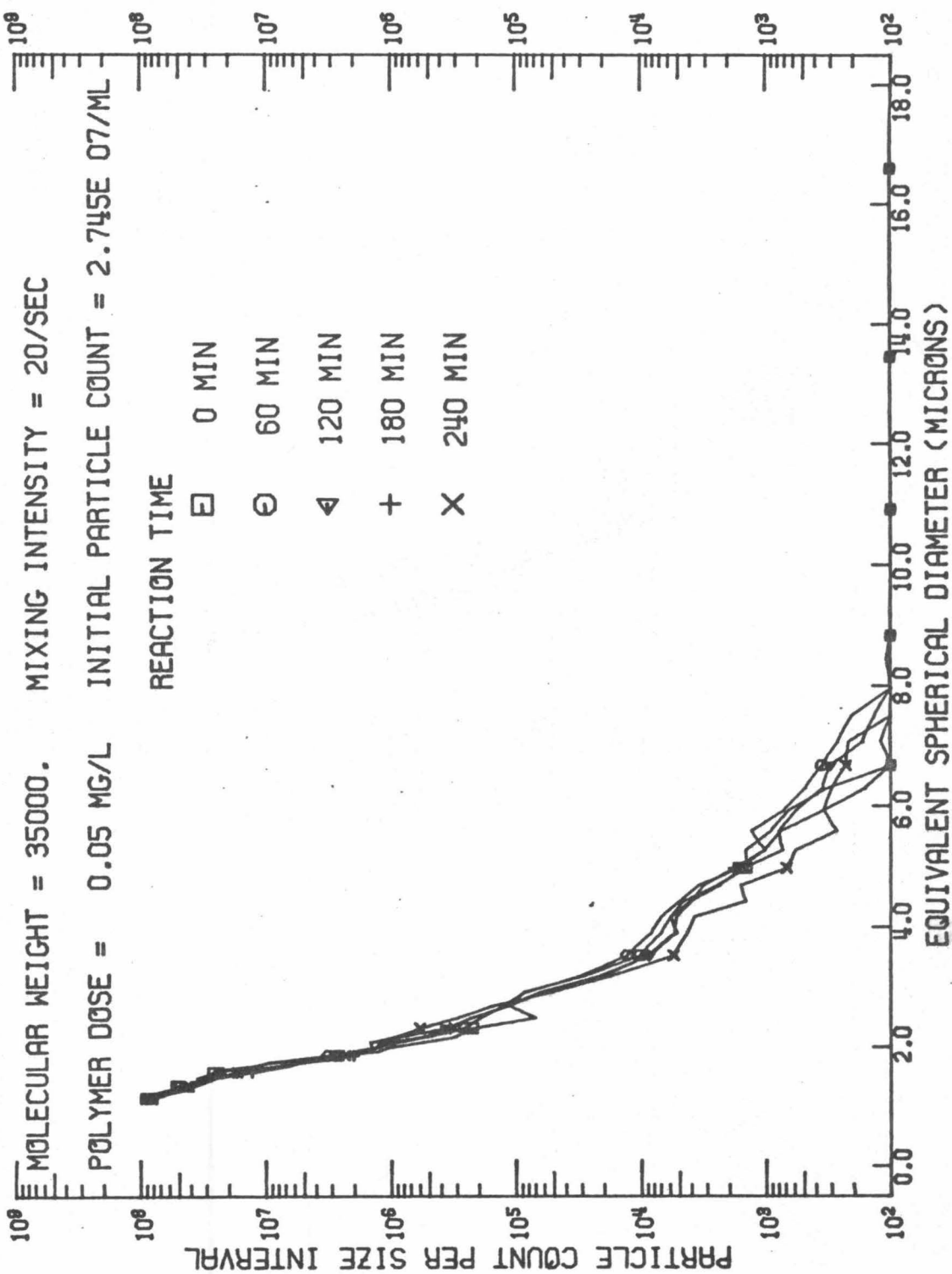


FIGURE 6.18 DIFFERENTIAL SIZE DISTRIBUTION SPECTRUM

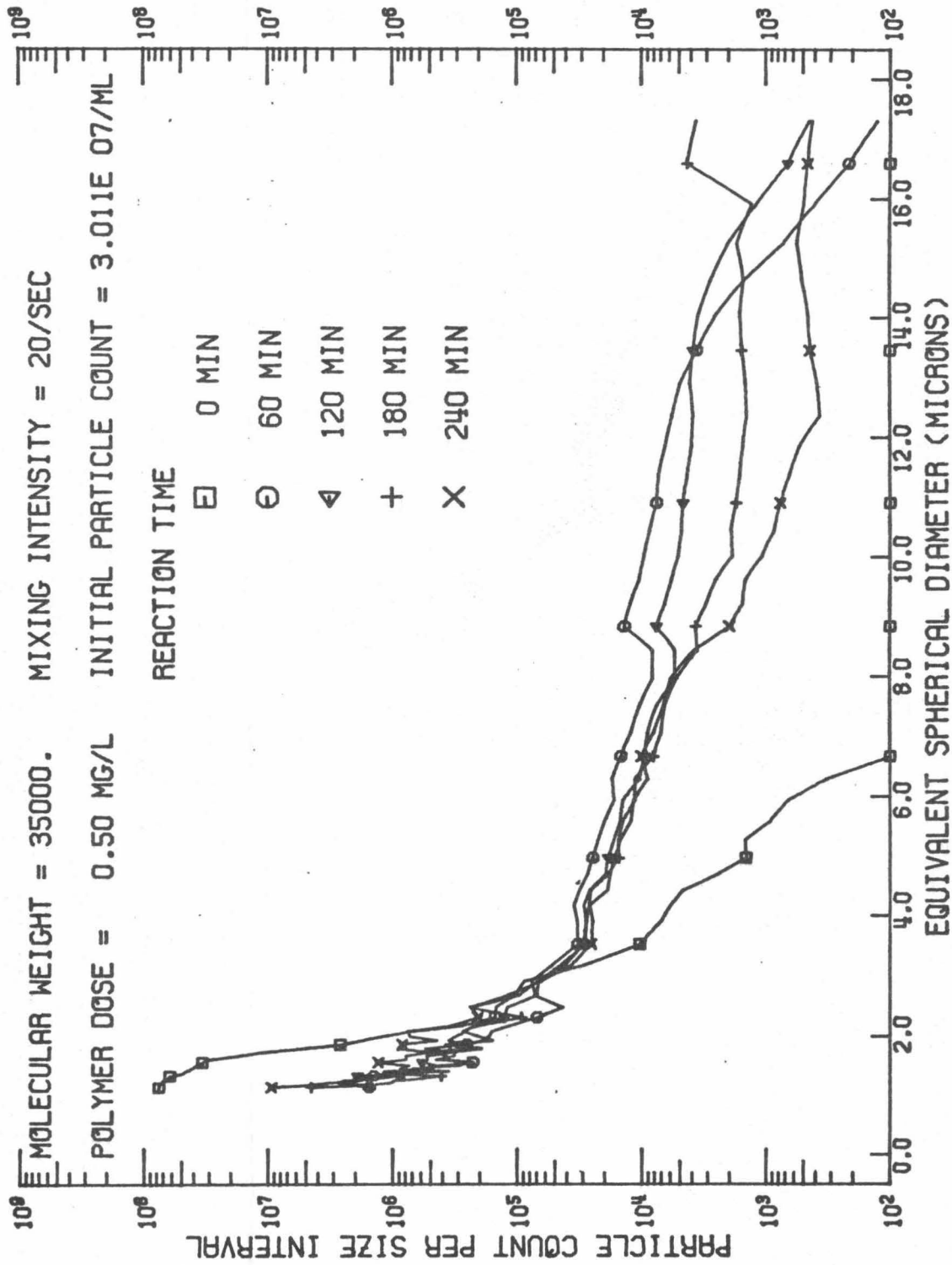


FIGURE 6.19 DIFFERENTIAL SIZE DISTRIBUTION SPECTRUM

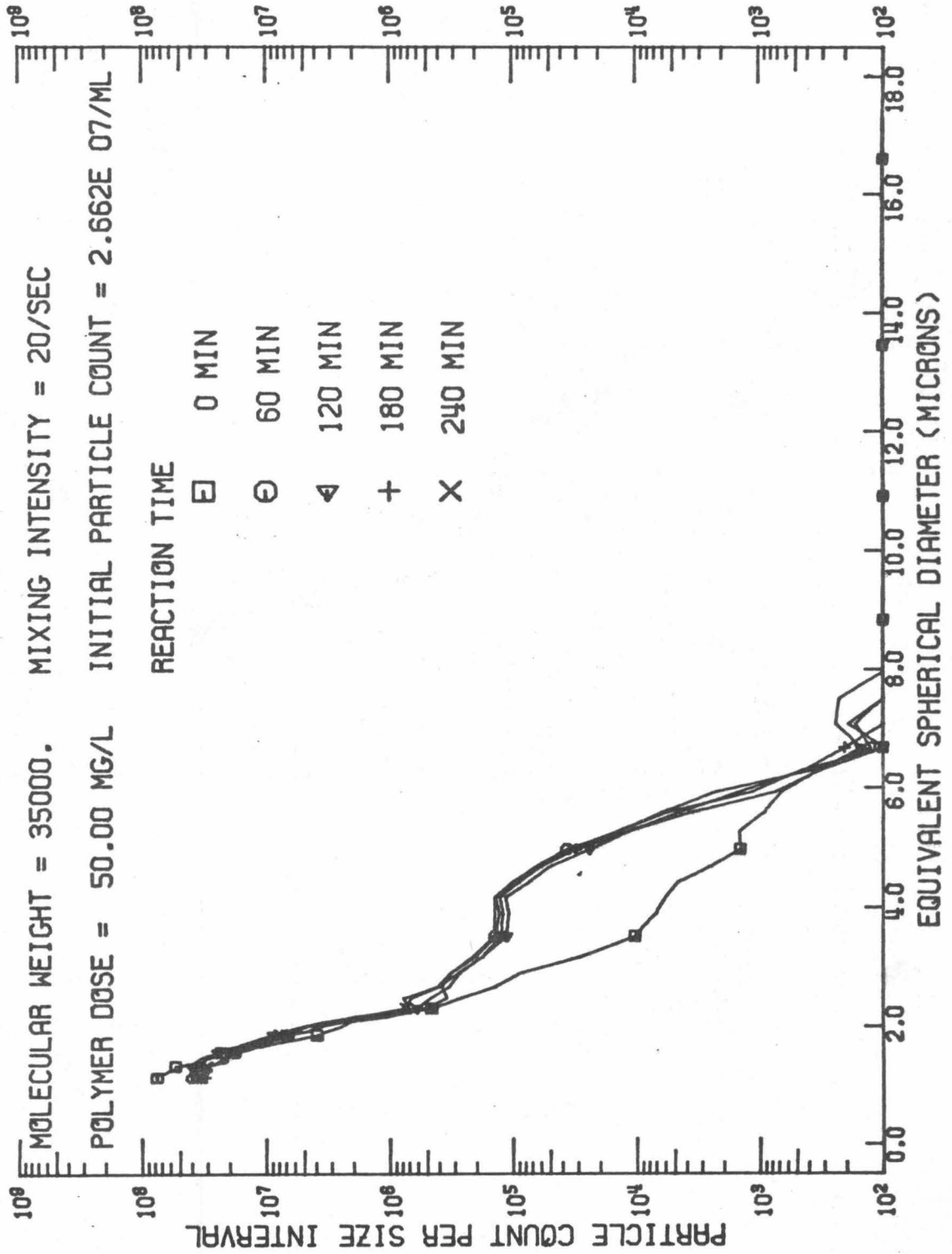


FIGURE 6.20 DIFFERENTIAL SIZE DISTRIBUTION SPECTRUM

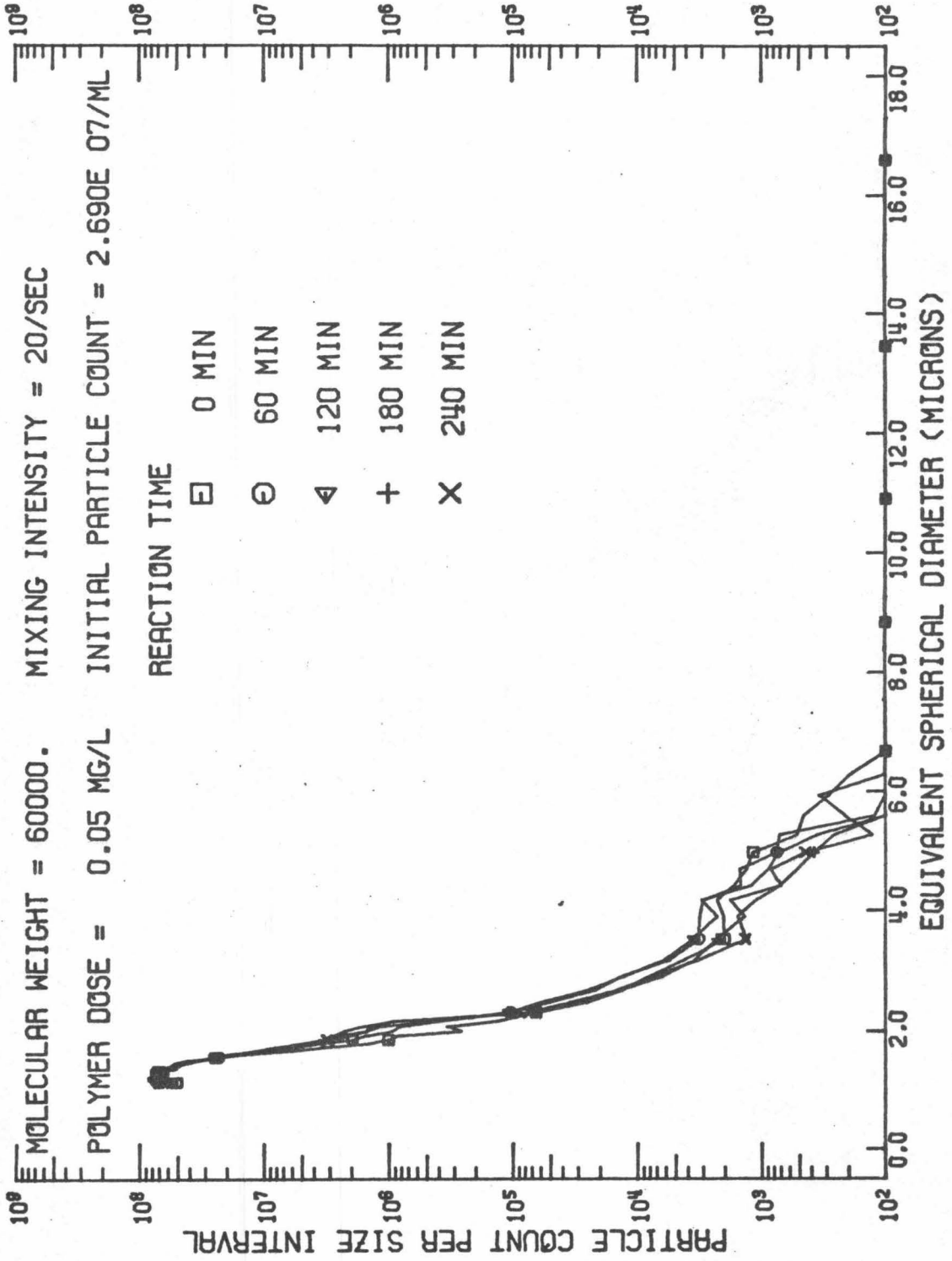


FIGURE 6.21 DIFFERENTIAL SIZE DISTRIBUTION SPECTRUM

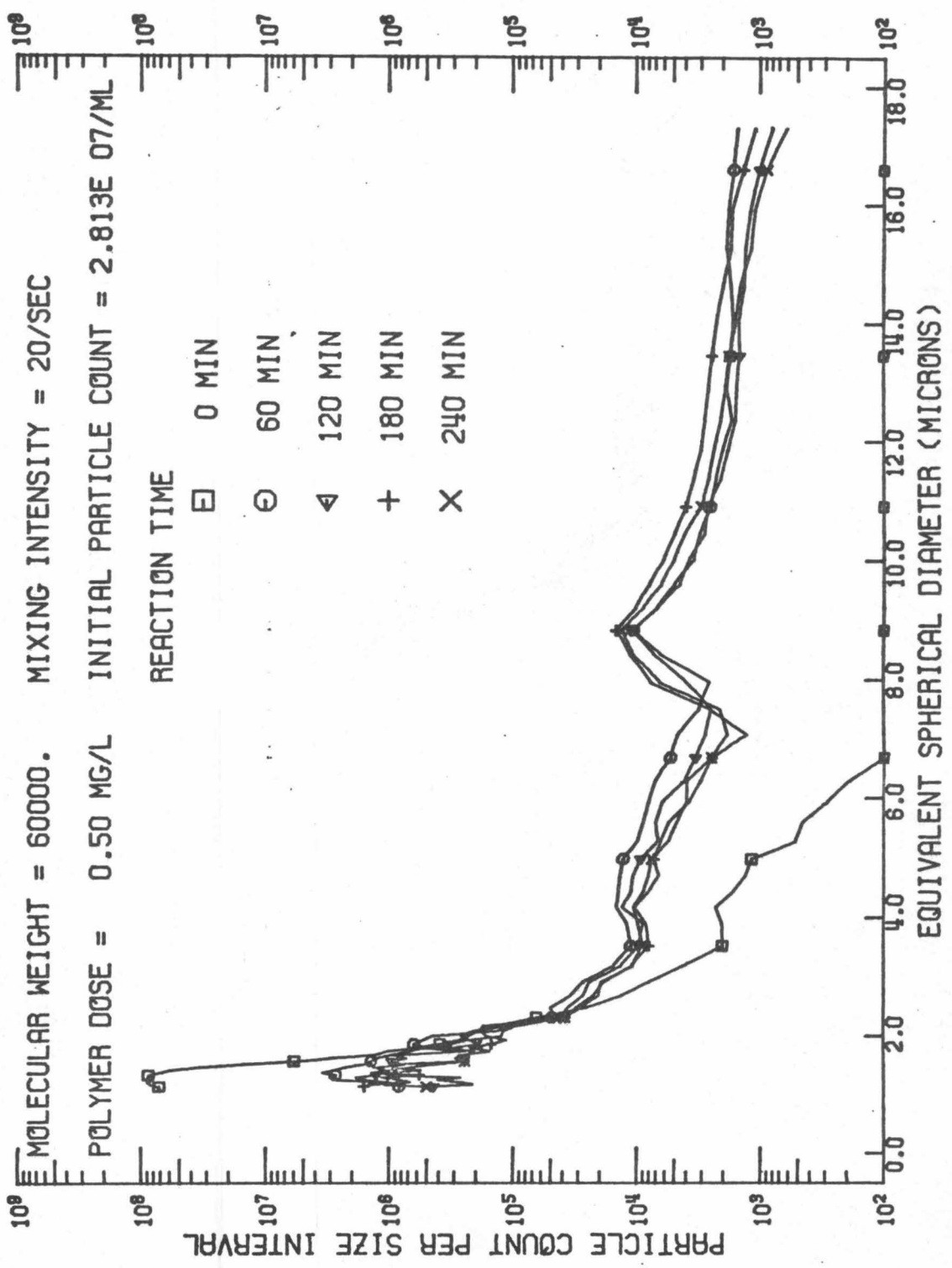
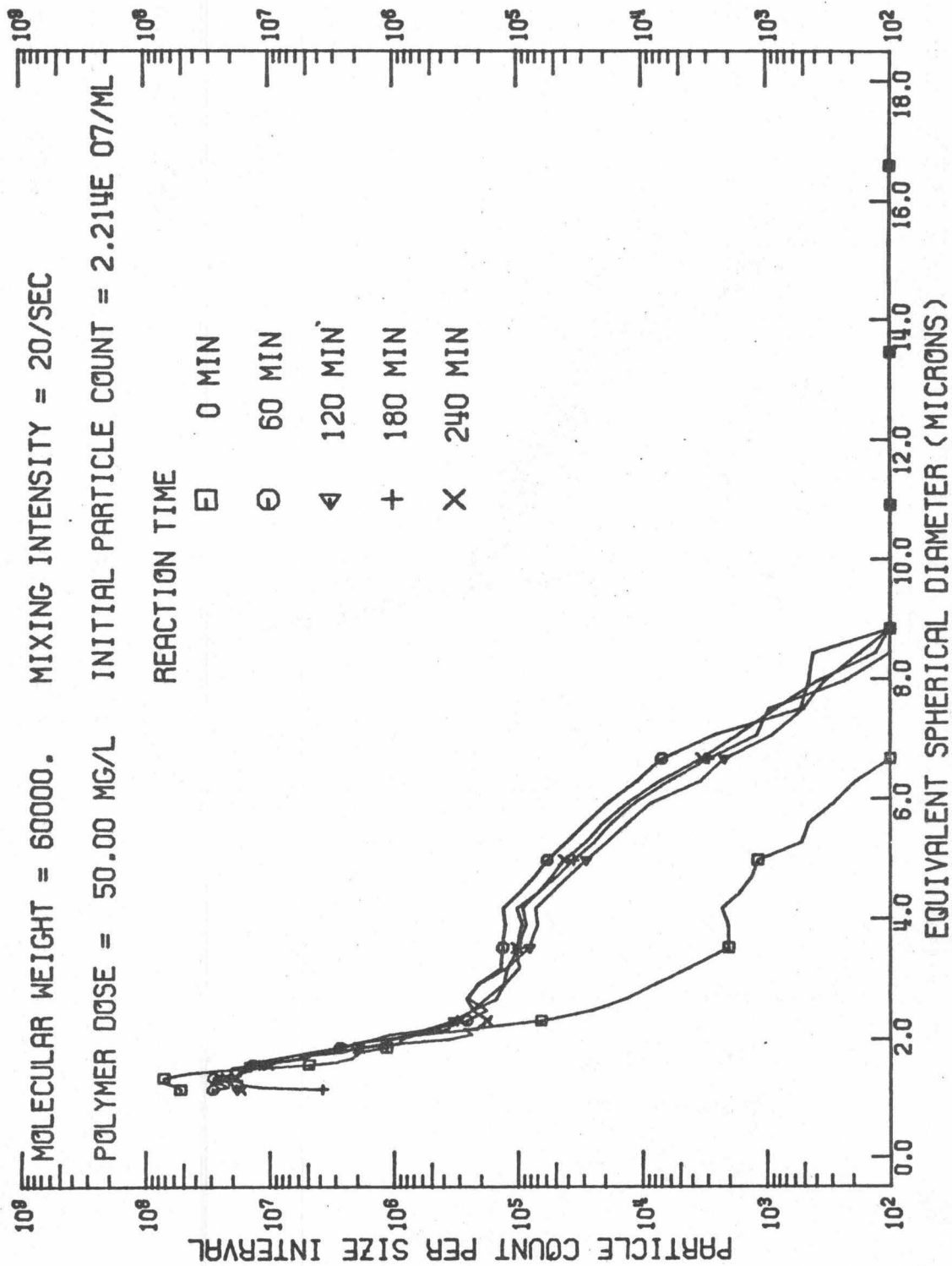


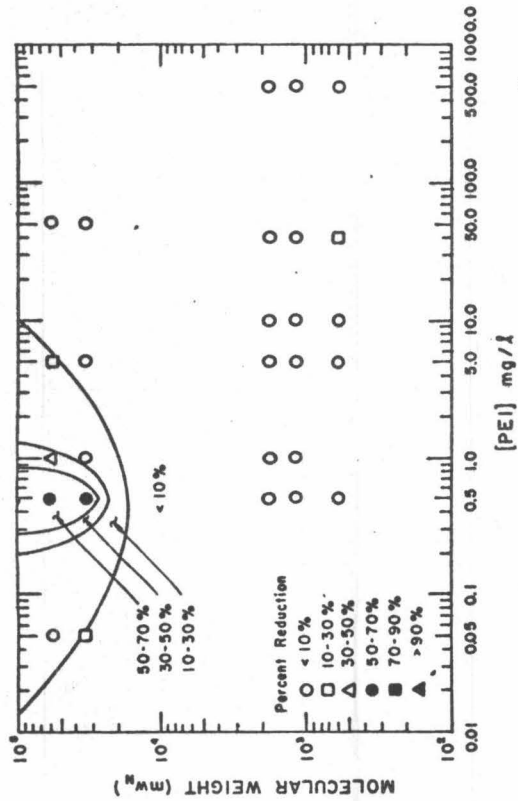
FIGURE 6.22 DIFFERENTIAL SIZE DISTRIBUTION SPECTRUM



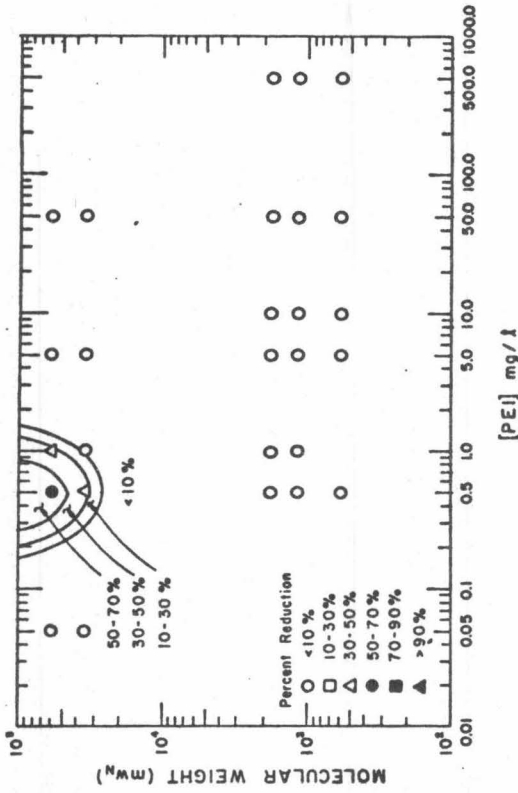
molecular weight species, the calculated turbidity was consistently larger than the experimental value: this was attributed to the over-estimation of the scattering cross section caused by the coalescence assumption and to interparticle interference of scattered light resulting in lower actual scattering intensities for aggregates. For flocculation with the high molecular weight species, the calculated turbidity was consistently smaller than the experimental value; attributable to the difficulty in accurately sizing very large aggregates with the Coulter counter technique. Considering an error of about 10% in estimating the scattering cross section for the assumed coalesced aggregate, and the error of up to 10% in operating the Coulter Counter, the correlation of experimental turbidities with those calculated from the anomalous diffraction - coalesced sphere model was felt to be good.

#### 6.3.3.2 Relative Scattering Intensity of Flocculating E. coli Suspensions

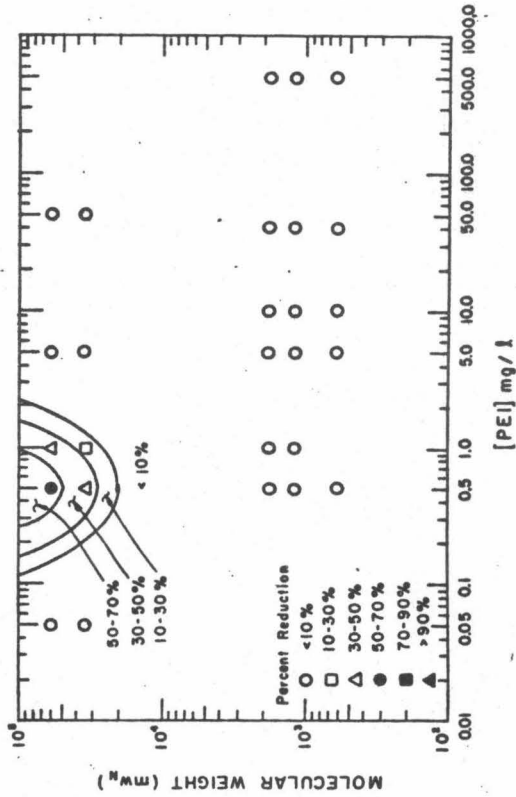
Figures 6.23 through 6.26 graphically display the percent reduction in relative scattering intensity of the flocculating suspension as a function of PEI molecular weight, dose, and duration of agitation at  $G = 20 \text{ sec}^{-1}$ . The figures show that, except at optimum concentrations of high molecular weight species, the relative scattering intensity decreases less than 10%.



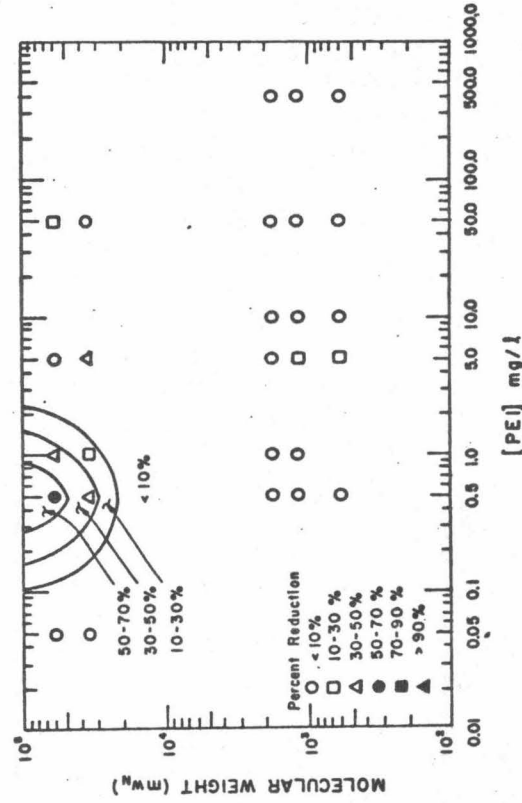
60 Minutes of Flocculation at  $G=20 \text{ sec}^{-1}$



120 Minutes of Flocculation at  $G=20 \text{ sec}^{-1}$



180 Minutes of Flocculation at  $G=20 \text{ sec}^{-1}$



240 Minutes of Flocculation at  $G=20 \text{ sec}^{-1}$

Figure 6.23-6.26 Log  $MW_n$  - Log  $[PEI]$  Domains of Percent Reduction in Relative Scattering Intensity.

This influence of different mixing intensities upon the relative light scattering intensity of bacterial suspensions flocculated with PEI 6 and PEI 350 is shown in Figure 6.27. If optimum flocculation is measured by the higher percent reduction in relative scattering intensity, then increasing the mixing intensity has a small adverse impact upon the flocculation efficiency.

Because the aggregates formed by the low molecular weight PEI are in the initial portion of the anomalous diffraction region, there is little difference between the relative scattering intensity of these aggregates and that of the primary particles. The intensity of agitation has little influence on the relative scattering intensity of these aggregates. The aggregates formed by the high molecular weight species are in the diffraction portion of the anomalous diffraction region, and thus there is a significant reduction (from 30 to 70%) in the relative scattering intensity of these aggregates. Once again however, the intensity of agitation has only a minor impact on the relative scattering intensity.

#### 6.3.3.3 Residual Relative Scattering Intensity of Flocculating E. coli Suspensions

As seen in a comparison of Figure 6.5 with Figures 6.23 - 6.26, the percent reduction in relative scattering intensity for

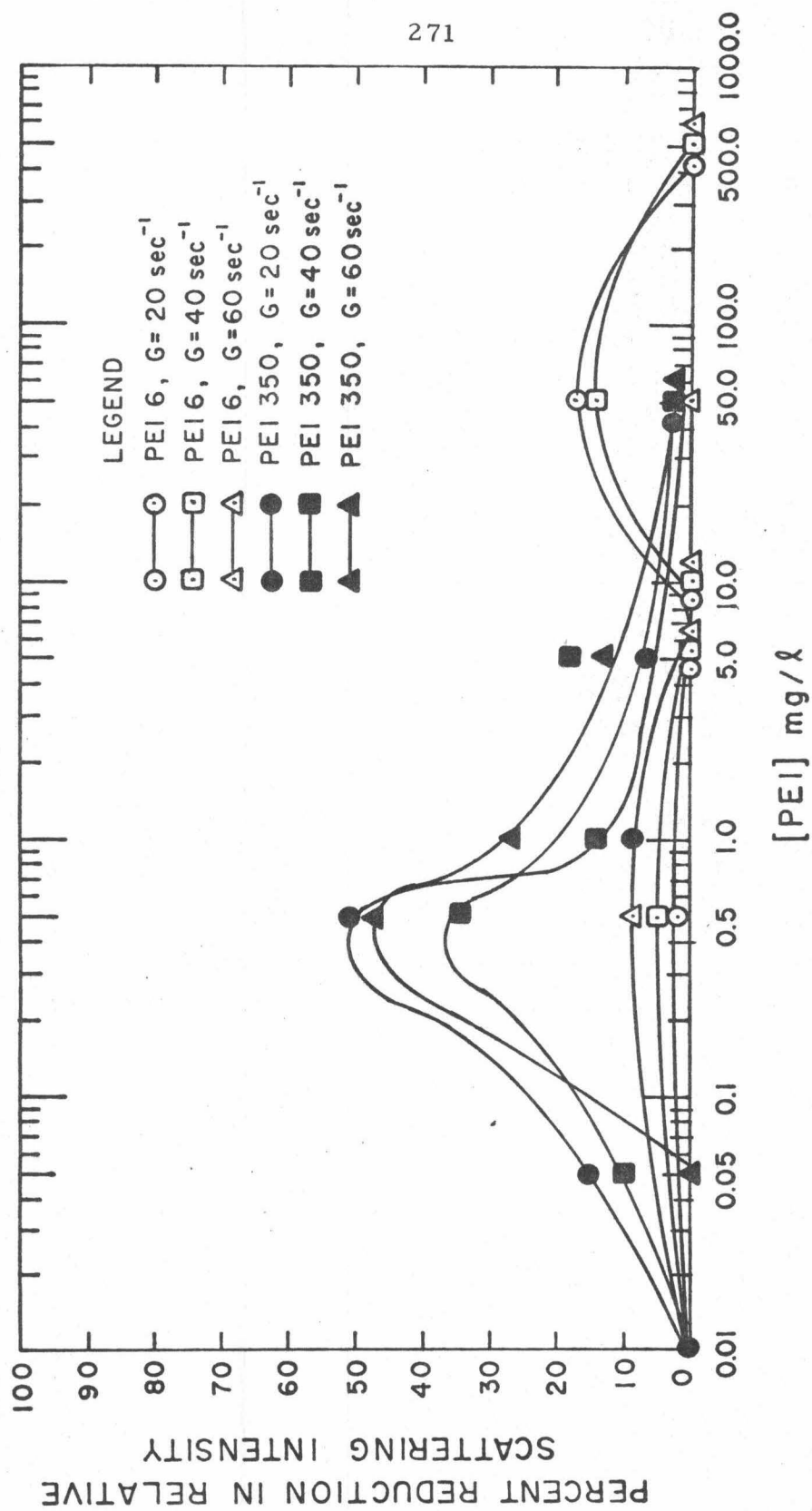
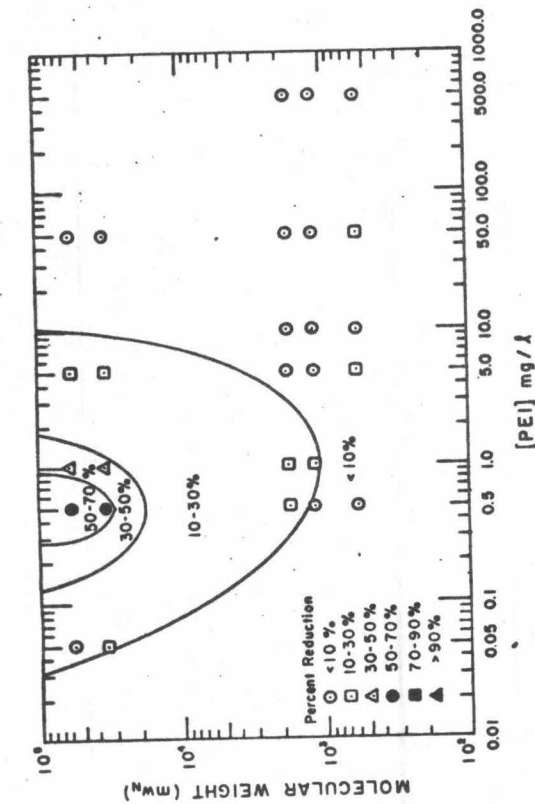


Figure 6.27 Percent Reduction in Relative Scattering Intensity as a Function of [PEI], PEI MW, and Intensity of Agitation for 60 Minutes.

flocculated suspensions can be a poor indicator of the degree of flocculation achieved. This is because aggregates in the anomalous diffraction regime scatter almost as much light as the dispersed individual cells; the small reduction in scattered light is caused by interparticle interference. The minor effect shown in Figures 6.23 to 6.26 is enhanced by measuring the relative scattering intensity after a specified sedimentation period. This allows the larger aggregates to settle out, thereby reducing the relative scattering intensity. The sedimentation period of prior investigators has generally been arbitrary in length, and the resulting scattering intensity is merely a qualitative measure of flocculation efficiency. Although the particle size distribution could theoretically be determined via the techniques of differential settling discussed in Section 6.2.3.3, the many problems with a flocculating system in aqueous media make the solution impractical.

Figures 6.28 through 6.31 graphically display the percent reduction in relative scattering intensity of the flocculated suspension after sedimentation versus the PEI molecular weight and concentration.

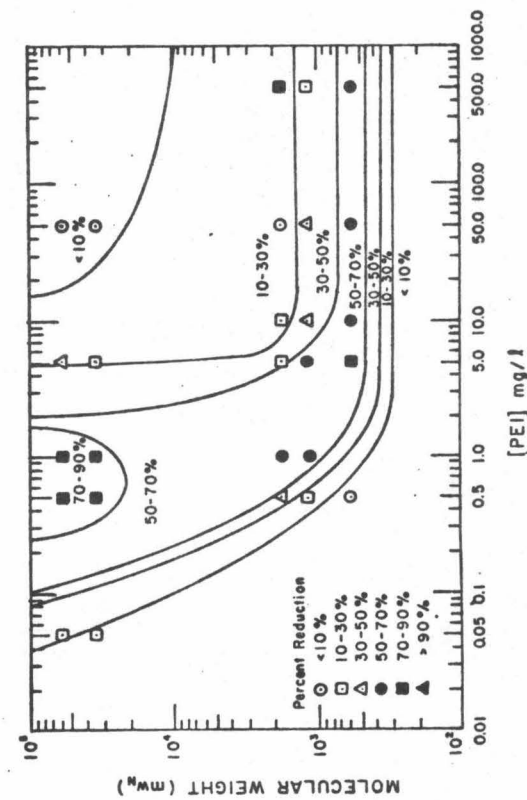
As expected, the relative scattering intensity after sedimentation shows a much larger percent reduction than that without sedimentation. The percent reductions in relative light scattering intensity after 240 minutes of sedimentation shown in Figure 6.31 are



60 Minutes of Sedimentation

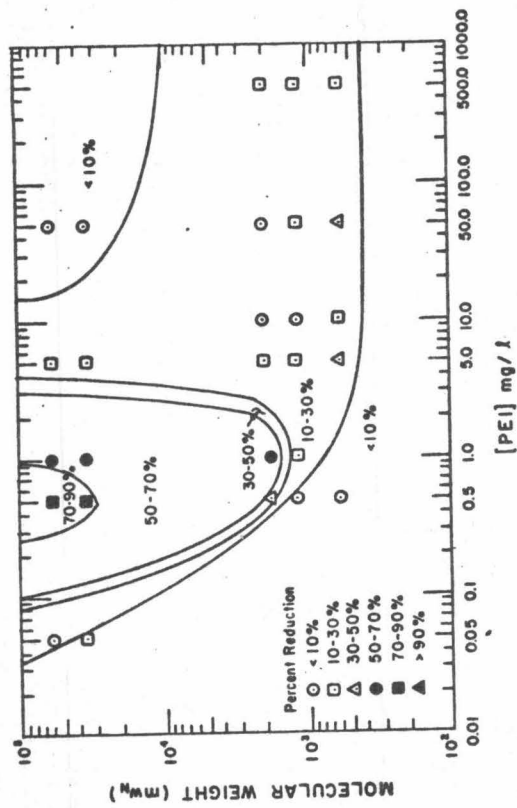
[PEI] mg/l

120 Minutes of Sedimentation



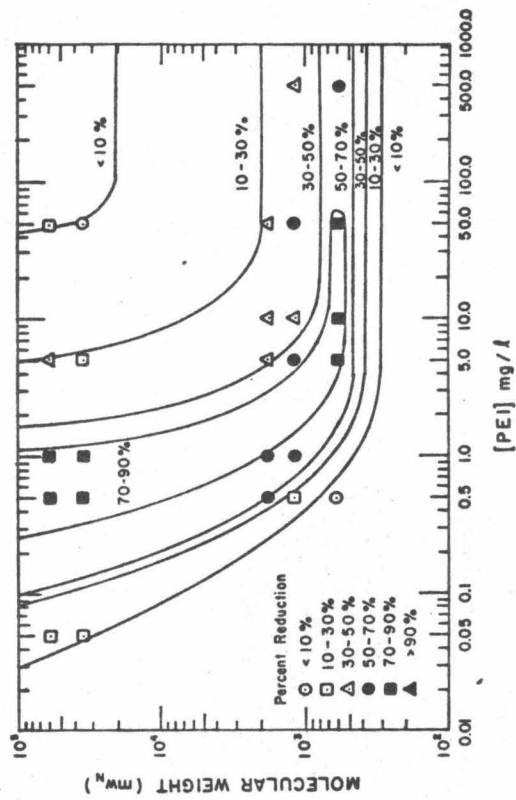
180 Minutes of Sedimentation

[PEI] mg/l



240 Minutes of Sedimentation

[PEI] mg/l



240 Minutes of Sedimentation

[PEI] mg/l

Figure 6.28-6.31 Log MW - Log [PEI] Domains of Percent Reduction in Residual Relative Scattering Intensity after 20 Minutes of Flocculation at  $G=20 \text{ sec}^{-1}$ .

essentially the same as the percent reductions in the number of particles shown in Figure 6.5. The arbitrary nature of the sedimentation period however, restricts the applicability of any such correlation solely to the E. coli-PEI system.

The influence of different mixing intensities (for 20 minutes following rapid mix) upon the residual relative light scattering intensity after 60 and 240 minutes of sedimentation for E. coli suspensions flocculated with PEI 6 and PEI 350 is shown in Figures 6.32 and 6.33. As in Figure 6.27, strong stirring ( $G = 40$  or  $60 \text{ sec}^{-1}$ ) of the E. coli-PEI suspension following the rapid mix produces a slightly smaller percent reduction in the relative scattering intensity, even after the long sedimentation period.

Figure 6.33 also illustrates a dramatic decrease in the percent reduction in relative scattering intensity caused by overdosing with high molecular weight polymer (35,000). Polymer doses in excess of 5.0 mg/l result in restabilization of the E. coli suspension at positive values of cell mobility. This restabilization effect is far less pronounced for low molecular weight polymer (PEI6), as shown in Figure 6.32.

Qualitative light scattering measurements recorded after a predetermined sedimentation period indicate that PEI molecular weight and dose are the two most important factors in achieving optimum

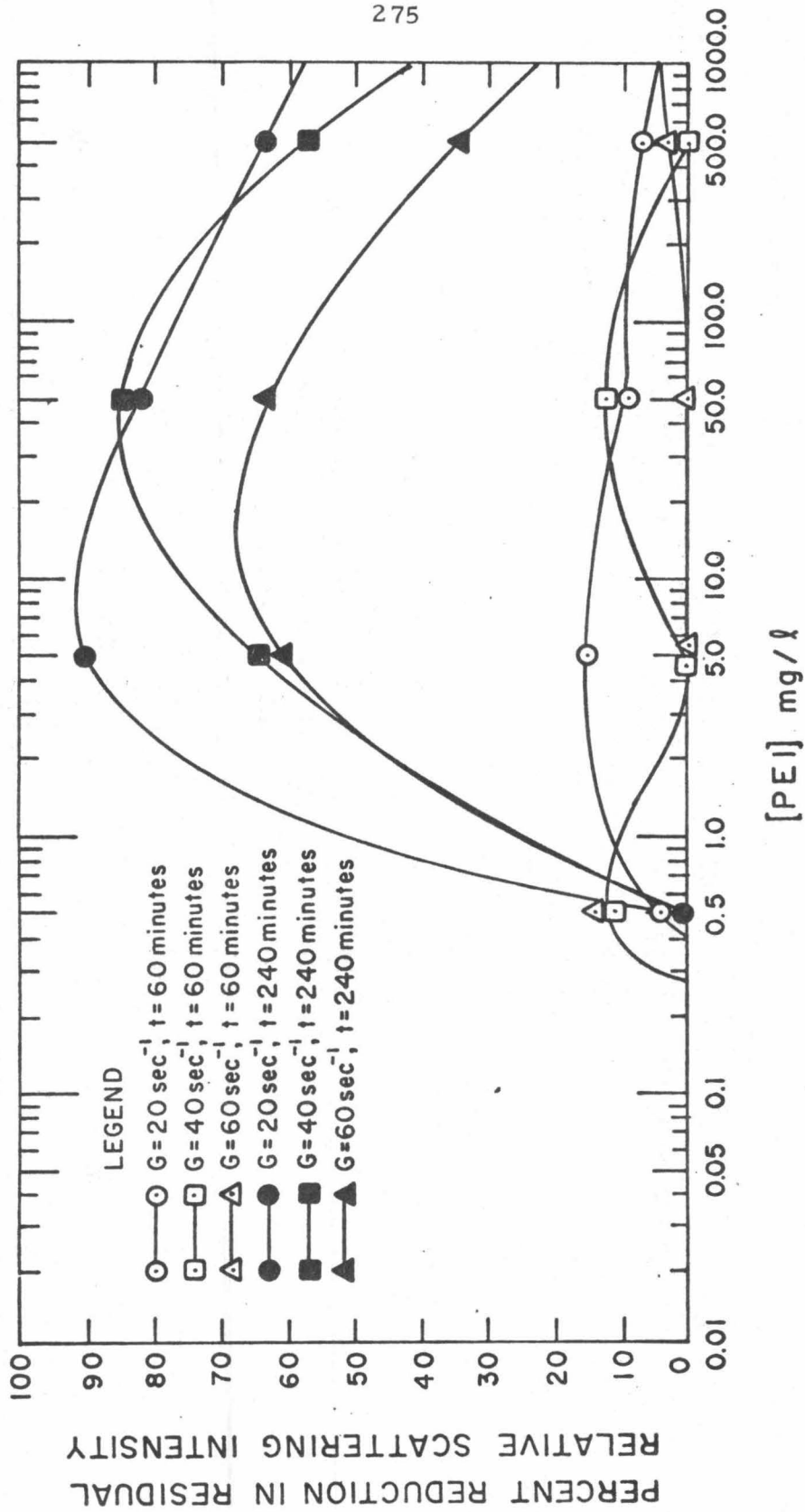


Figure 6.32 Percent Reduction in Residual Relative Scattering Intensity as a Function of [PEI], Intensity of Agitation, and Time of Settling. PEI  $MW_n = 600$ .

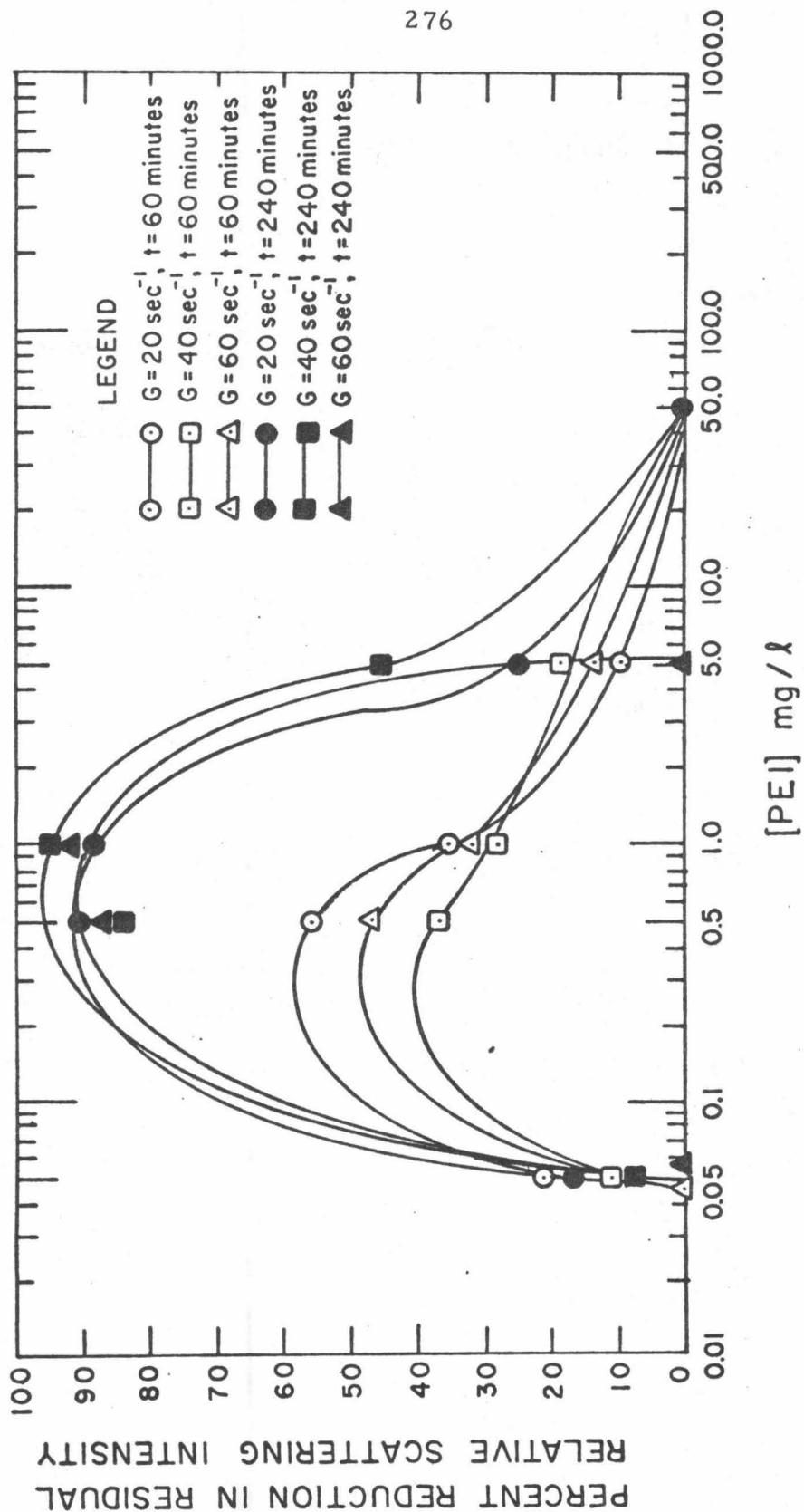


Figure 6.33 Percent Reduction in Residual Relative Scattering Intensity as a Function of [PEI], Intensity of Agitation, and Time of Settling.  $PEI MW_n = 35,000$ .

flocculation efficiency. Slightly higher turbidities were observed as the mixing intensity was increased, indicating that the increased shear forces were causing floc disruption. This disruption of flocs outweighed the advantage of increased interparticle collisions.

Prolonged sedimentation periods after flocculation dramatized the decrease in the residual relative scattering intensity. If properly employed, this sedimentation technique could be utilized for rapid assessment of optimum operating conditions.

#### 6.3.4 Refiltration Rate Results

##### 6.3.4.1 Influence of PEI Molecular Weight, Dose, and Velocity

###### Gradient on Reduction of Refiltration Time

Figure 6.34 presents the results of refiltration experiments with the five molecular weight species at varying doses. The refiltration time  $t$  was measured as the time required to refilter the filtrate of a 50 ml sample of the PEI-E. coli suspension through the filter cake and a 0.45  $\mu\text{m}$  Millipore filter at a pressure differential of 74 cm Hg. All measurements were taken after 60 minutes of stirring at  $G = 20 \text{ sec}^{-1}$  following PEI addition to the E. coli suspension. Figure 6.34 is similar to Figure 6.5 (Log MW - Log (PEI) Domains of Percent Reduction in Number of Particles) with the exception of low molecular weight polymer doses greater than 10 mg/l. Here the low

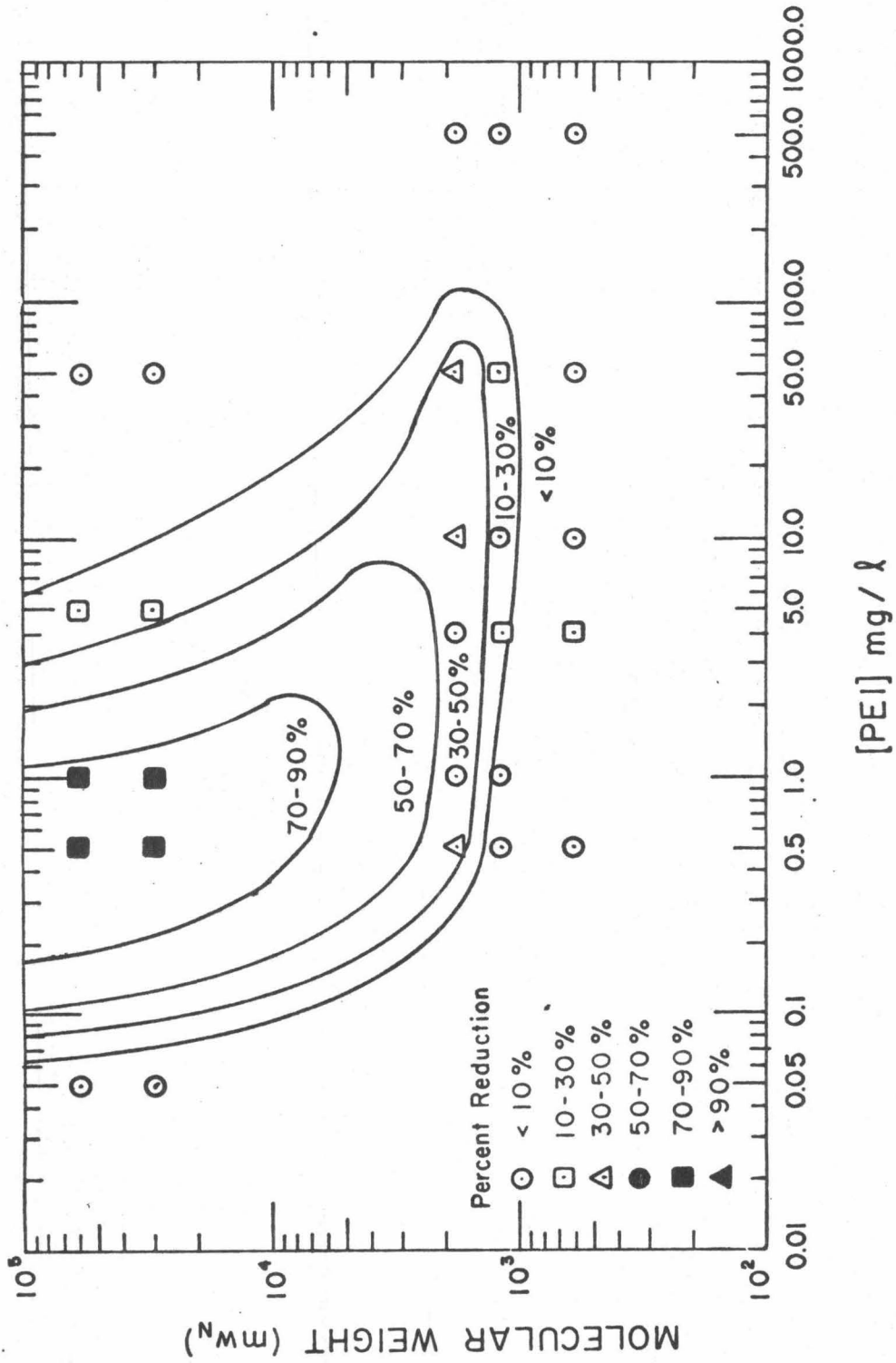


Figure 6.34 Log MW - Log [PEI] Domains of Percent Reduction in Refiltration Time after 60 Minutes of Flocculation at  $G=20 \text{ sec}^{-1}$ .

percent reduction in refiltration rate is caused by clogging of the interstices of the filter cake and filter septum with excess polymer (PEI 6, PEI 12, or PEI 18). The low percent reduction for high molecular weight species (PEI 350 and PEI 600) is caused by restabilization of the E. coli cells and microflocs, in addition to clogging of the interstices.

Refiltration experiments also show that the magnitude of the imposed velocity gradient, either 0, 20, 40, or 60  $\text{sec}^{-1}$  for 60 minutes, has little effect on the refiltration time. Figure 6.35 illustrates the minor differences in the percent reduction in refiltration time caused by varying the velocity gradient in flocculation studies with PEI 350. While Figures 6.6 and 6.7 showed that varying the velocity gradient had negligible effect on the number of aggregates in the flocculated suspension, Figure 6.35 shows that varying the velocity gradient also has negligible effect on the size of the aggregates.

#### 6.3.4.2 Correlation of Refiltration Times with Surface Area

##### Changes in a Flocculating Suspension

Squaring equation (5-42) and solving for the time of refiltration

t yields:

$$t = (V_f/A)^2 k'uw(1-\Phi)S_o^2 / (\Delta P g p \Phi^3) \quad (6-13)$$

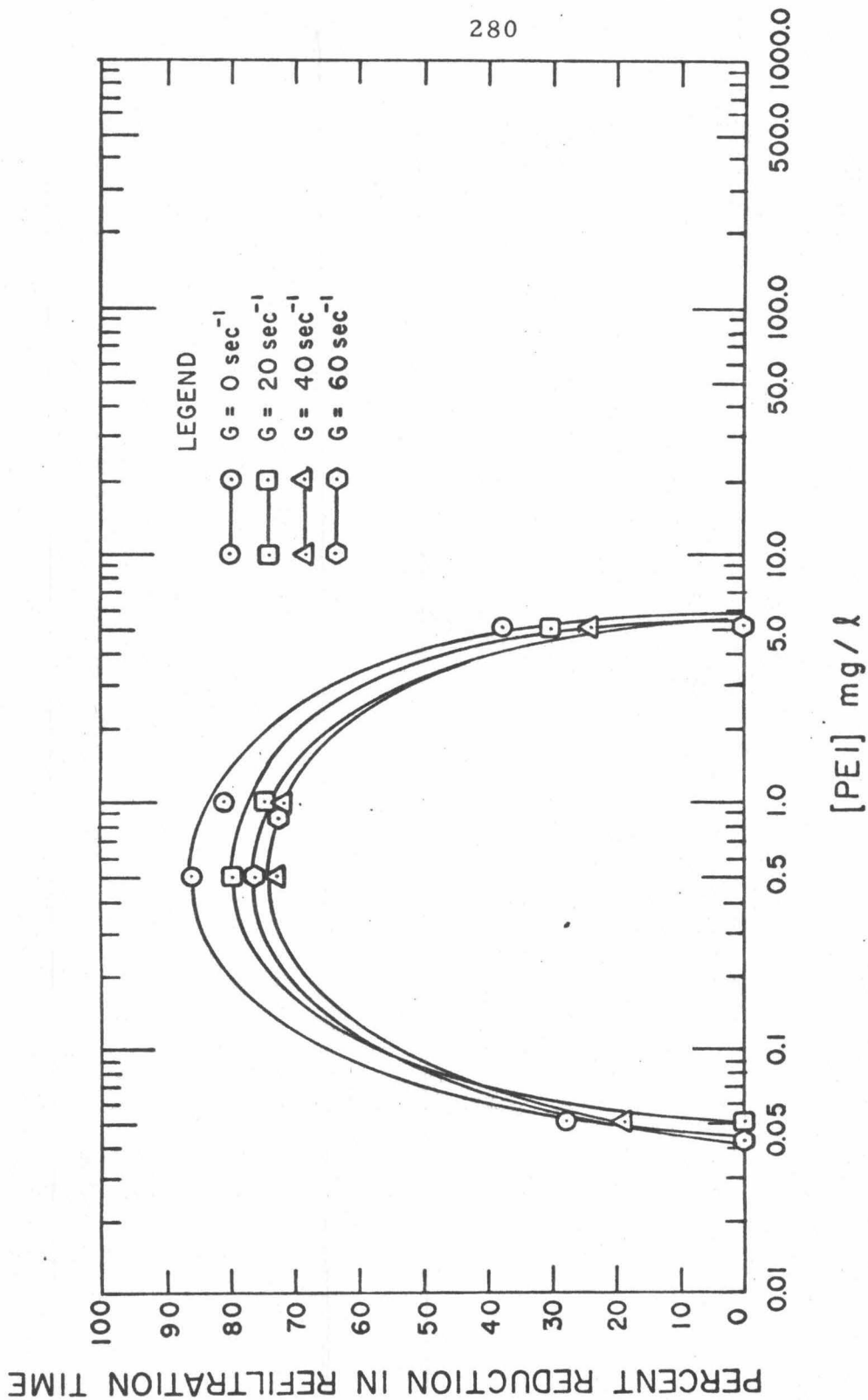


Figure 6.35 Percent Reduction in Refiltration Time as a Function of PEI 350 Concentration and Magnitude of Velocity Gradient.

where  $w = \rho_p V_p / V_f$

$V_p$  = volume of E. coli in suspension

$S_o = S/V_p$

$S$  = surface area of E. coli aggregates

Consequently,

$$t = [(V_f k' u w (1 - \Phi)) / (A^2 \Delta P g \Phi^3)] SS_o \quad (6-14)$$

$$t = K SS_o$$

where  $K$  is the product of the constant terms in brackets.

Thus the validity of the Carman-Kozeny equation, and the assumption of virtually constant porosity, can be checked by plotting the refiltration time versus PEI concentration, and the independently determined product  $SS_o$  versus PEI concentration, on the same graph. Figure 6.36 shows the correlation between Coulter counter data and refiltration times as a function of PEI dose for PEI 6 and PEI 12. At doses greater than 50 mg/l, the polymer clogs the filter cake and filter septum, resulting in high refiltration times. These refiltration times do not reflect restabilization of the particulate matter as shown by the value of the product  $SS_o$ . Figure 6.37 depicts the data correlation as a function of PEI dose for PEI 350 and PEI 600. The high refiltration times for doses greater than 5.0 mg/l are the result of both filter clogging and redispersion of flocs at large polymer doses. This redispersion effect is shown in the

Coulter counter data for  $SS_o$  at PEI concentrations greater than 5.0 mg/l.

The good agreement between refiltration and Coulter counter data substantiates earlier experiments that predicted the improvement in filtration rate as being caused by the reduction of specific surface area during the flocculation process. For high molecular weight PEI, the refiltration method appears especially valuable in quickly determining optimum polymer dosages.

#### 6.3.5 Electron Micrographs of E. coli Filter Cake

Even though the refiltration time appears to vary with the PEI concentration in the same manner as the product  $SS_o$ , examination of equation (1-11) reveals that minor increases in the porosity  $\phi$  will produce significant changes in the refiltration rate  $Q$ :

$$Q = \Delta P g A \phi^3 / (k_1 u L S_o^2 (1-\phi)^2) \quad (1-11)$$

In addition, the product  $SS_o$  is obtained from measurements of flocs in suspension, whereas the refiltration time is determined by the configuration of flocs layered onto a Millipore filter. In order to examine the effect of this layering, and the structure of the filter cake, electron micrographs were prepared of the filter cake produced by E. coli-PEI suspensions during refiltration experiments.

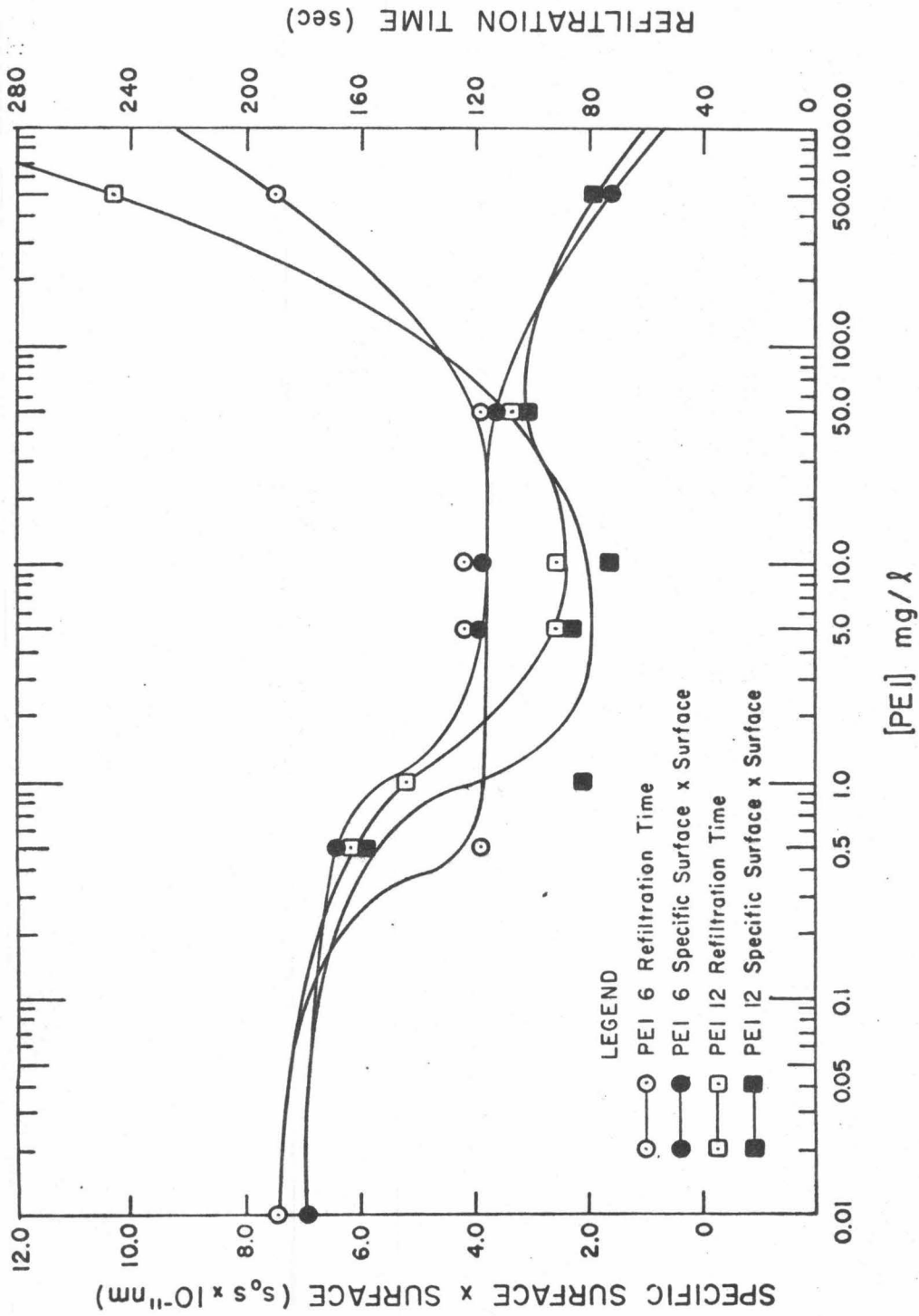


Figure 6.36 Comparison Between Plots of the Product Specific Surface Times Surface Versus PEI Dose and Refiltration Time Versus PEI Dose.

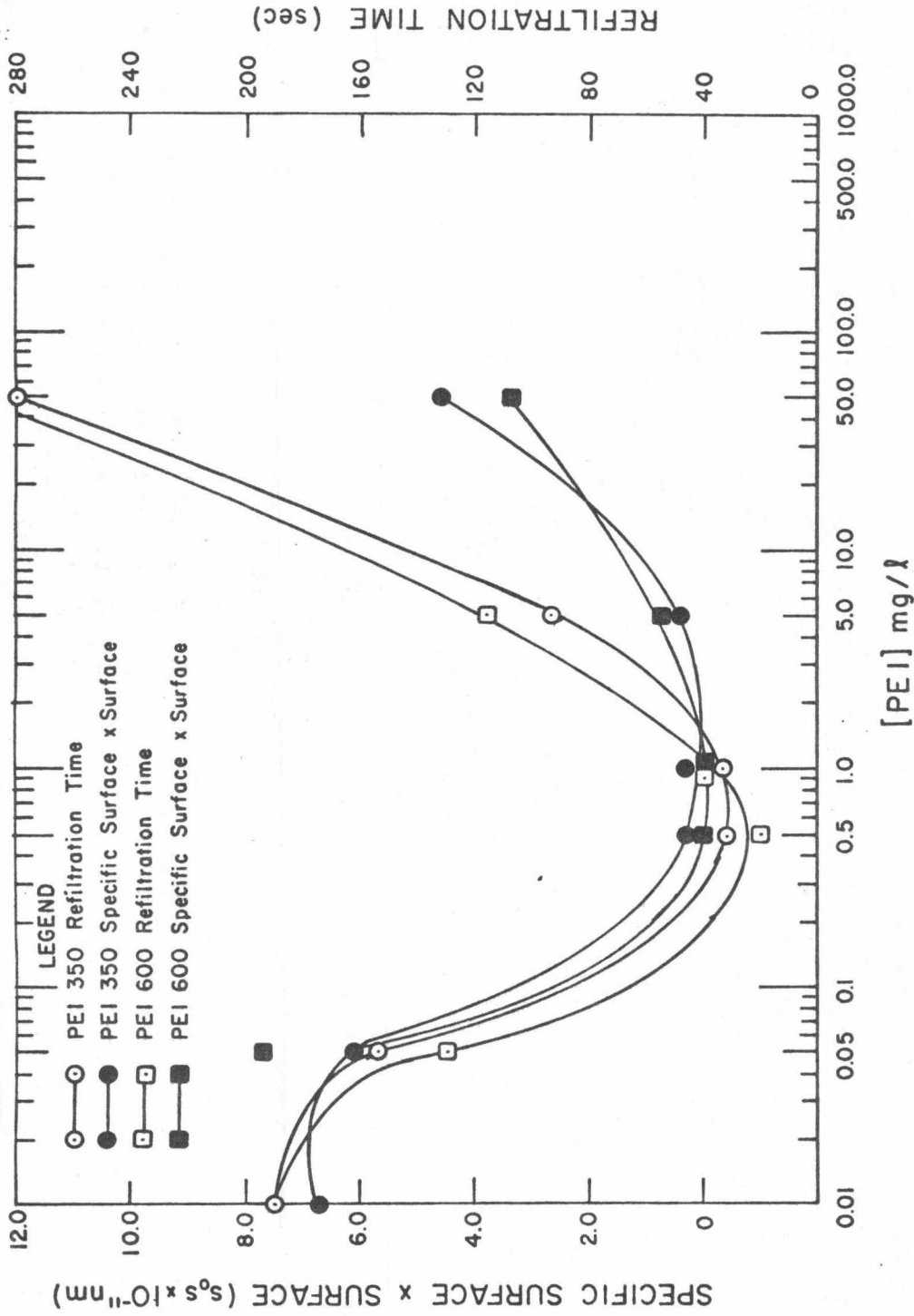


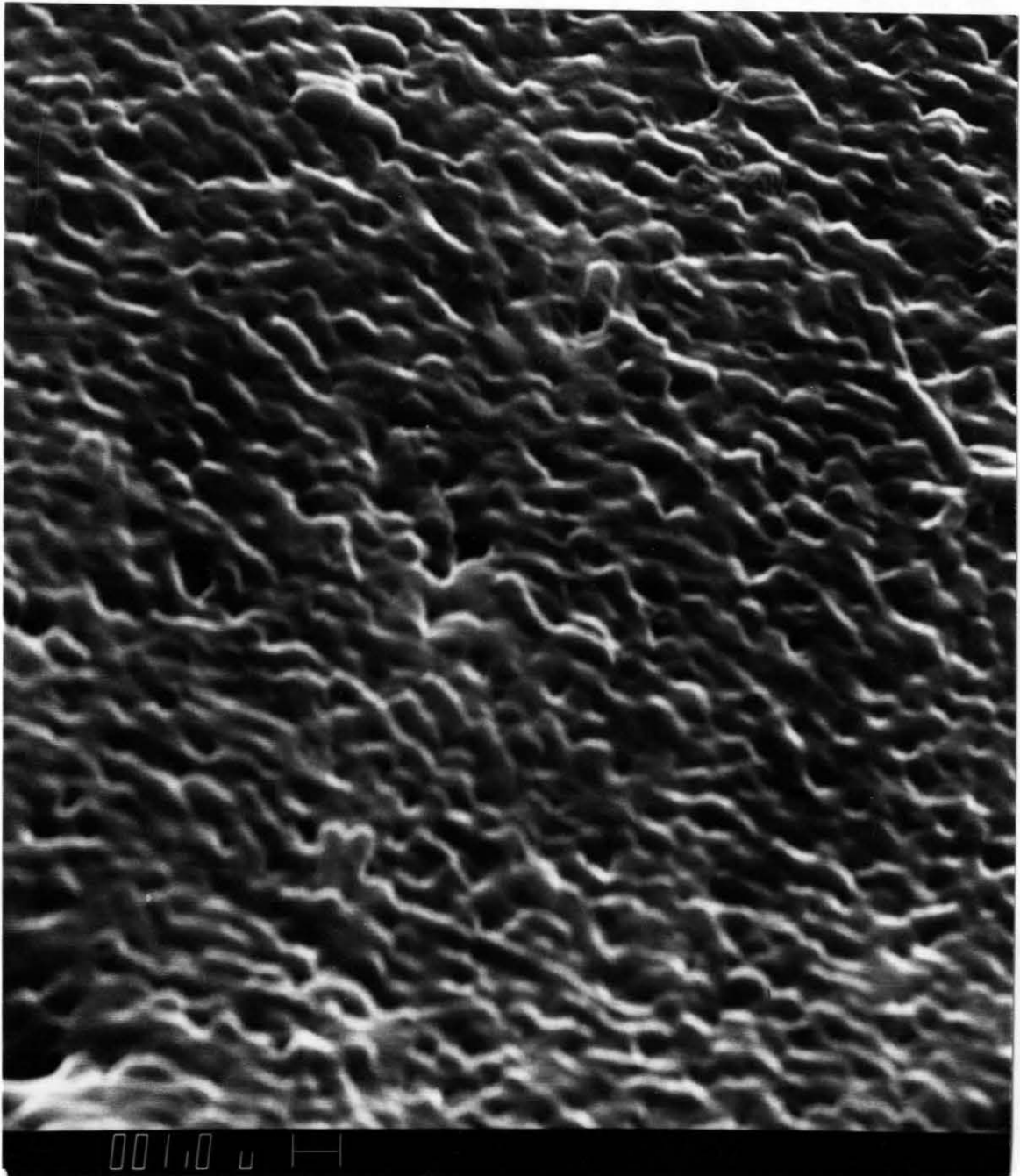
Figure 6.37 Comparison Between Plots of the Product Specific Surface Times Surface Versus PEI Dose and Refiltration Time Versus PEI Dose.

Photographs 6.1-6.4 depict the filter cake of E. coli flocculated with the optimum concentration (5.0 mg/l) of PEI 6. The cells appear closely packed, with many small channels for liquid passage. Photographs 6.5-6.8 depict the filter cake of E. coli flocculated with the optimum concentration (0.5 mg/l) of PEI 350. The cells appear to form a more open, three-dimensional structure with large channels for liquid passage. Whereas cells flocculated with PEI 6 have compacted under the friction pressure of liquid flow, those flocculated with PEI 350 appear to have maintained a rigid structure, indicating less realignment after initial contact between cells.

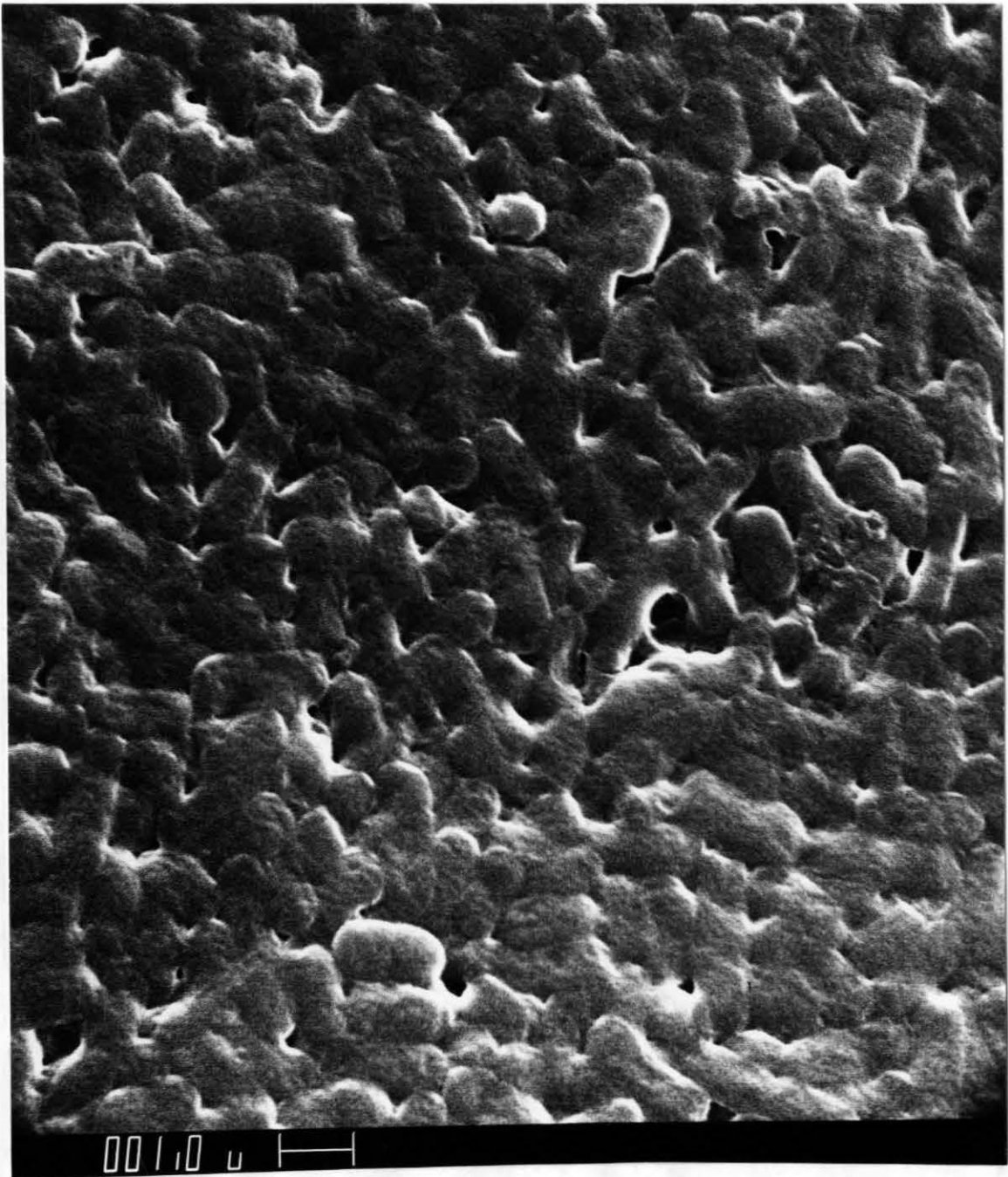
These micrographs indicate a higher filter cake porosity for the PEI 350 flocculated cells than for the PEI 6 flocculated cells. The greater refiltration rates observed with PEI 350 and PEI 600 are probably caused by a combination of smaller specific surface area and increased cake porosity over those recorded with PEI 6, PEI 12, and PEI 18.

#### 6.3.6 Electrophoretic Mobility of E. coli Aggregates

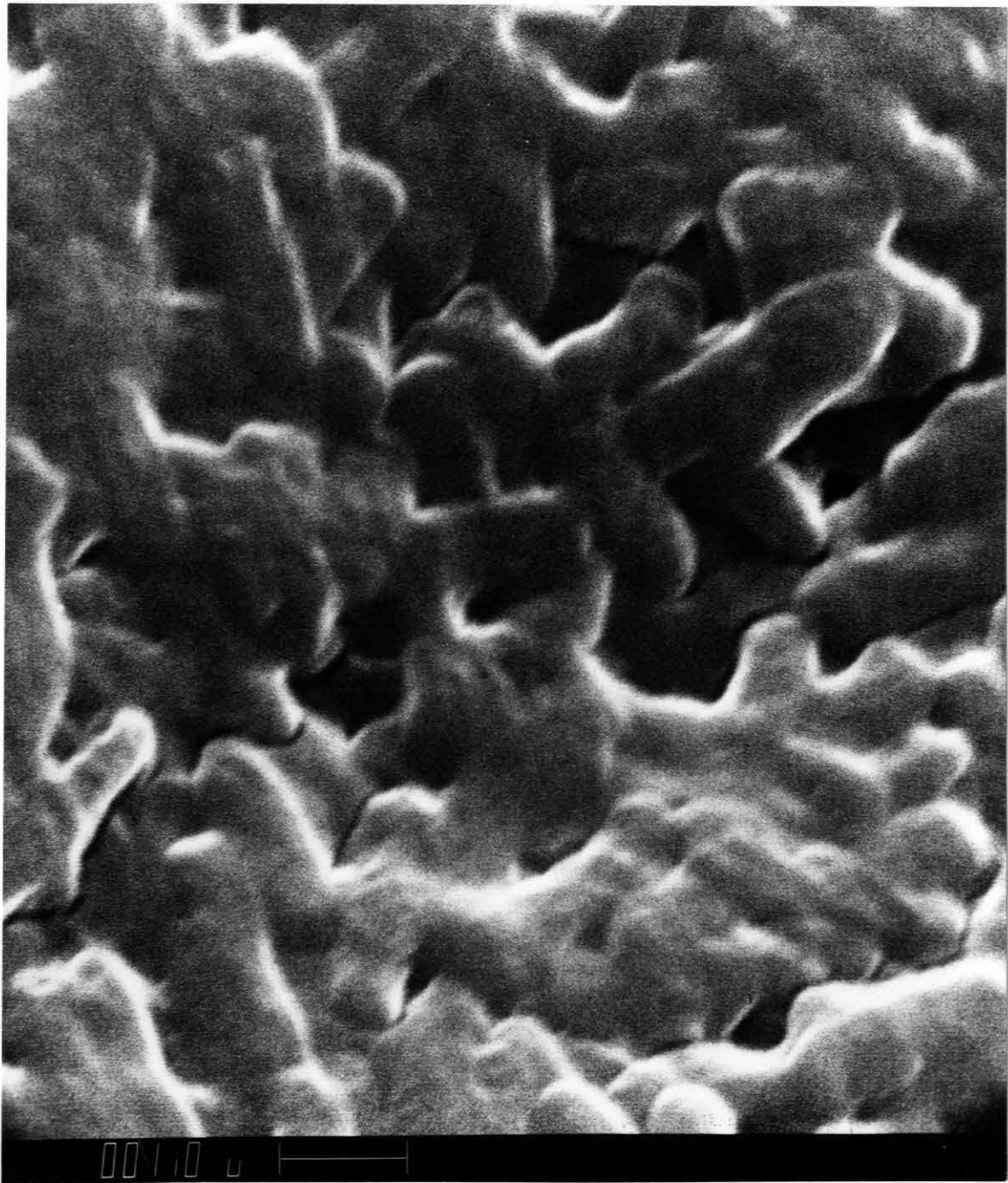
The effect of varying the PEI molecular weight and dose on the electrophoretic mobilities of E. coli aggregates was determined in Section 4.3.3. Variation of the stirrer-reactor velocity gradient did not have a measurable effect on the recorded electrophoretic mobilities,



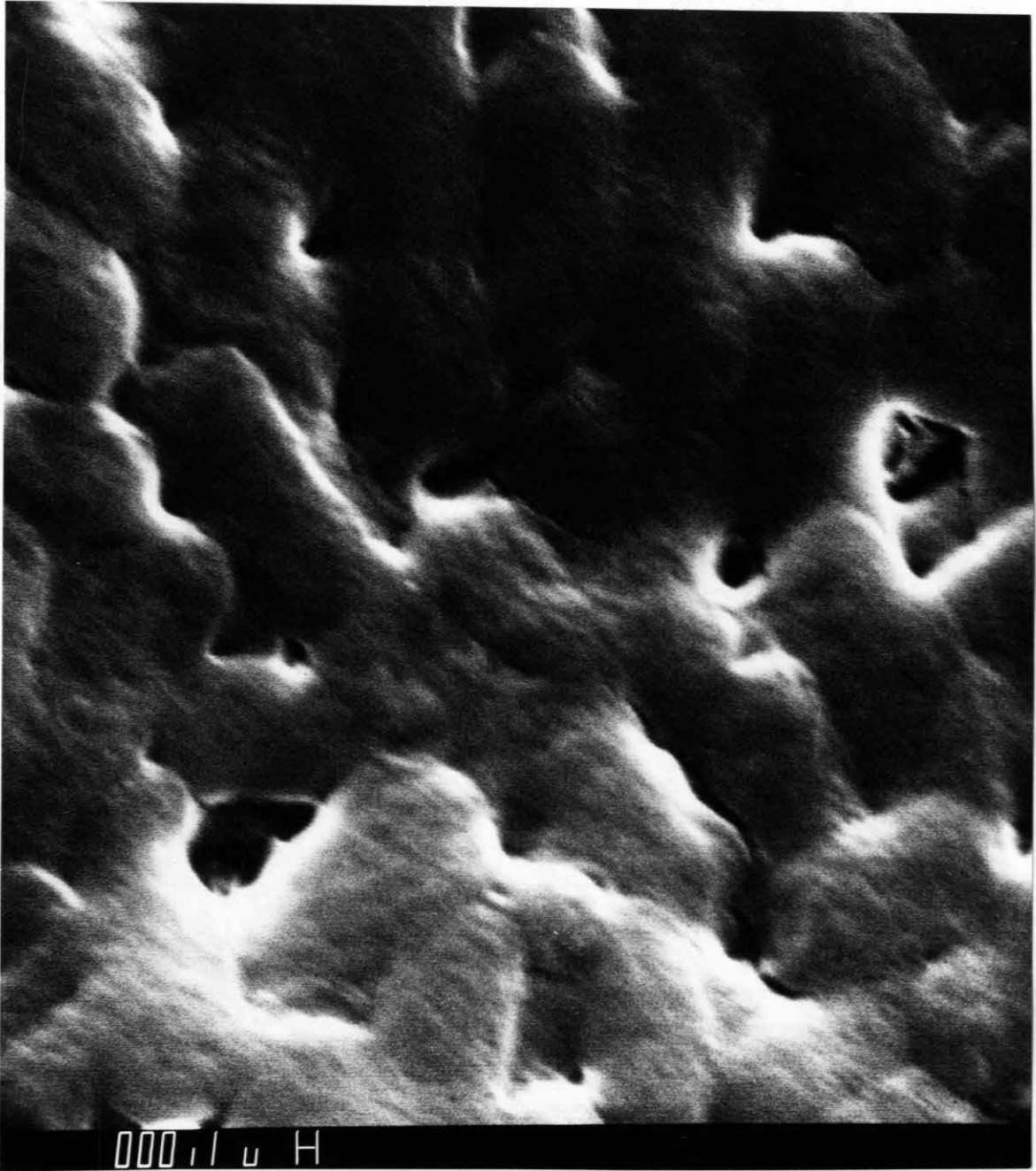
6.1 Electron Micrograph of Surface of Filter Cake Produced by Vacuum Filtration of E. coli Cells Flocculated with PEI 6. Total Magnification  $6.0 \times 10^3$ .



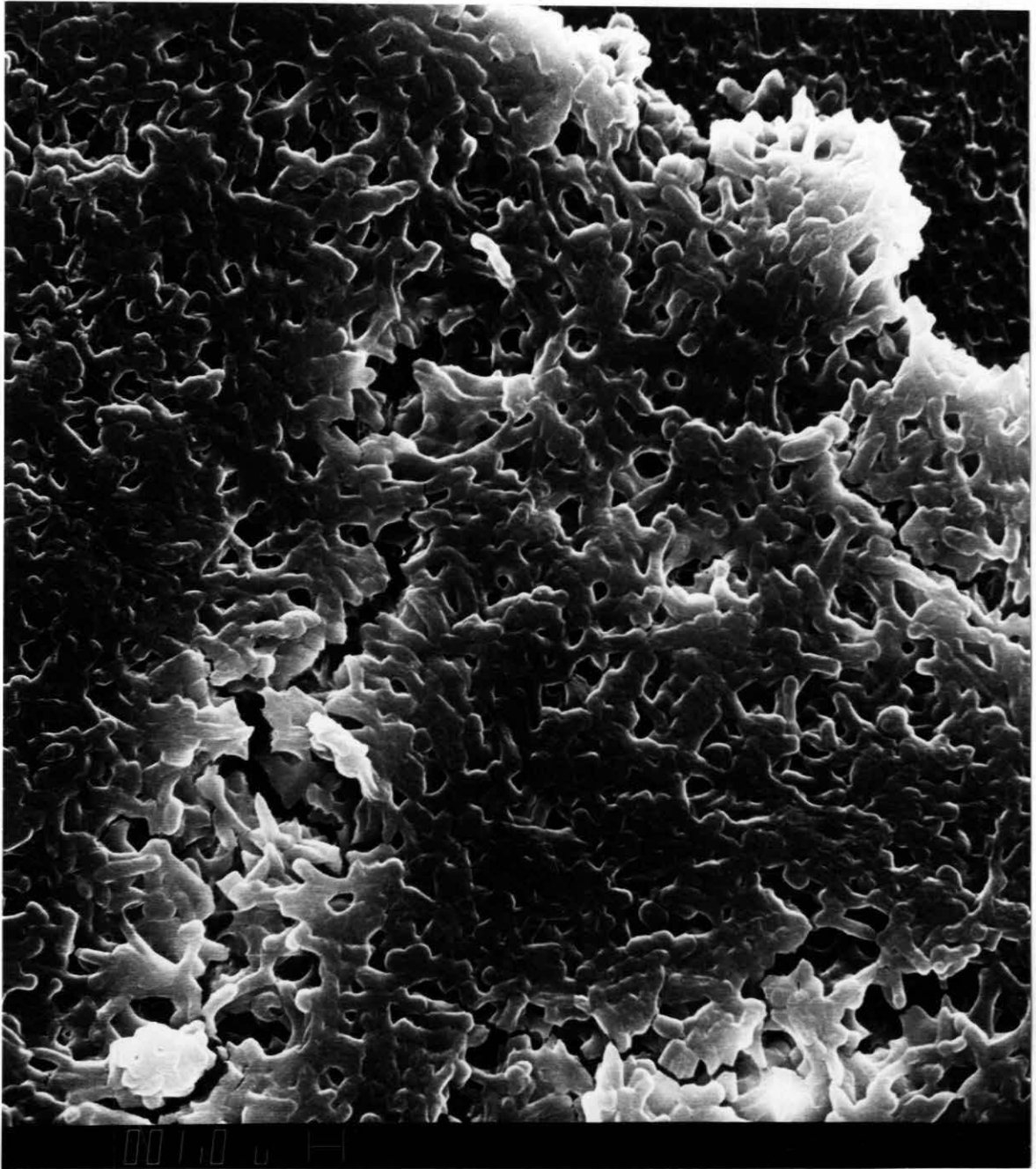
6.2 Electron Micrograph of Surface of Filter Cake Produced by Vacuum Filtration of *E. coli* Cells Flocculated with PEI 6. Total Magnification  $1.0 \times 10^4$ .



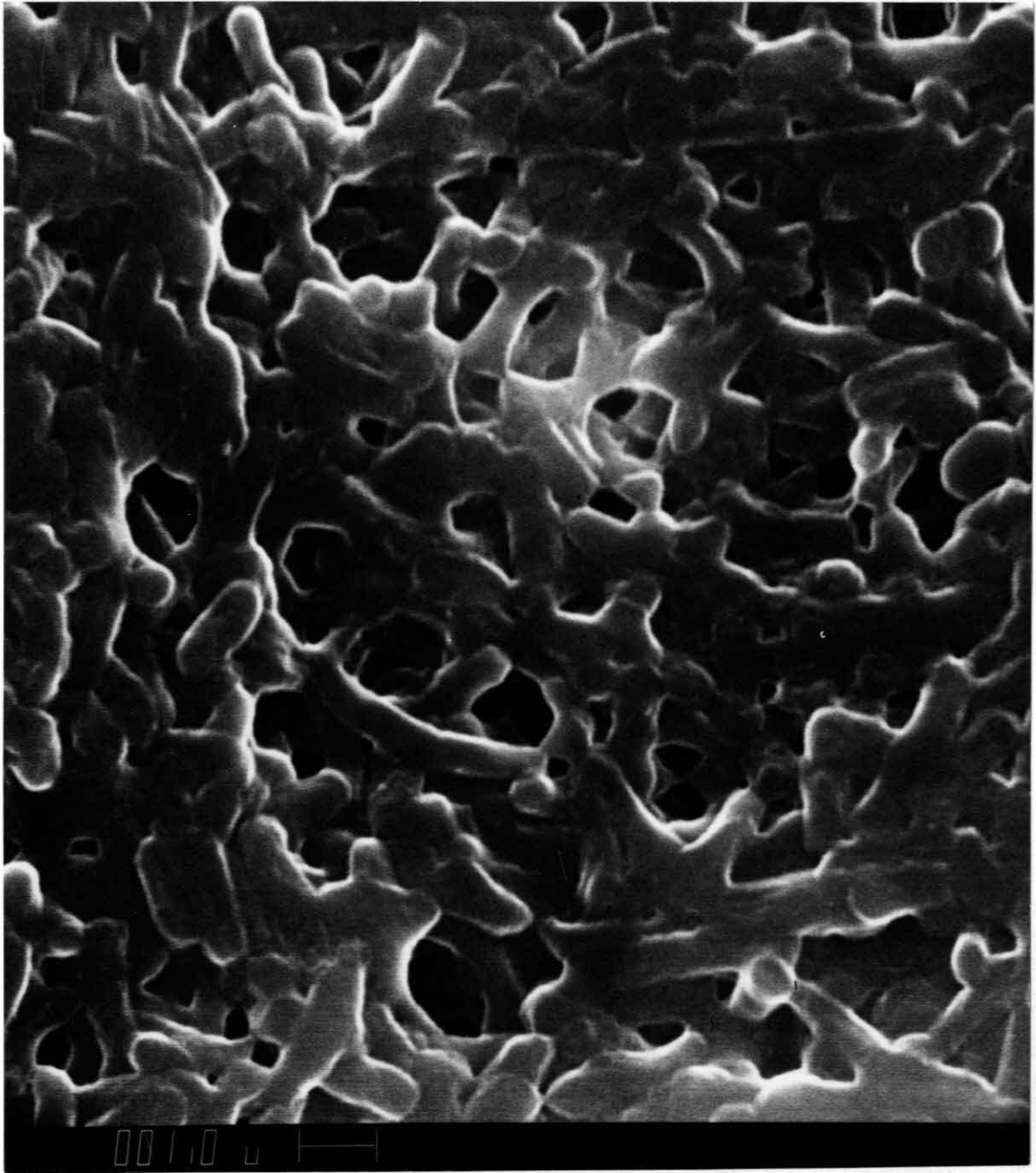
6.3 Electron Micrograph of Surface of Filter Cake Produced by Vacuum Filtration of *E. coli* Cells Flocculated with PEI 6. Total Magnification  $1.8 \times 10^4$ .



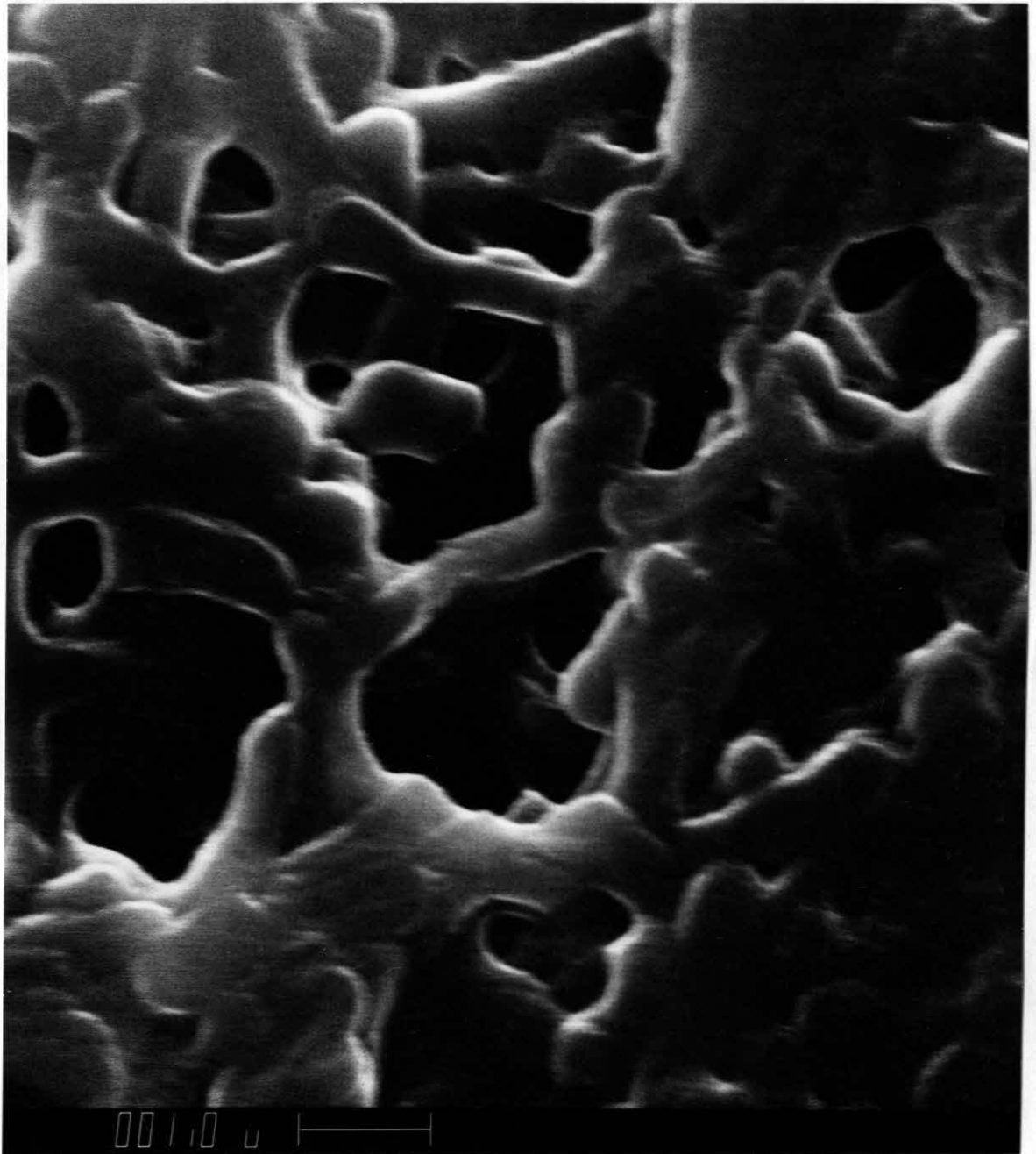
6.4 Electron Micrograph of Surface of Filter Cake Produced by Vacuum Filtration of E. coli Cells Flocculated with PEI 6. Total Magnification  $2.0 \times 10^4$ .



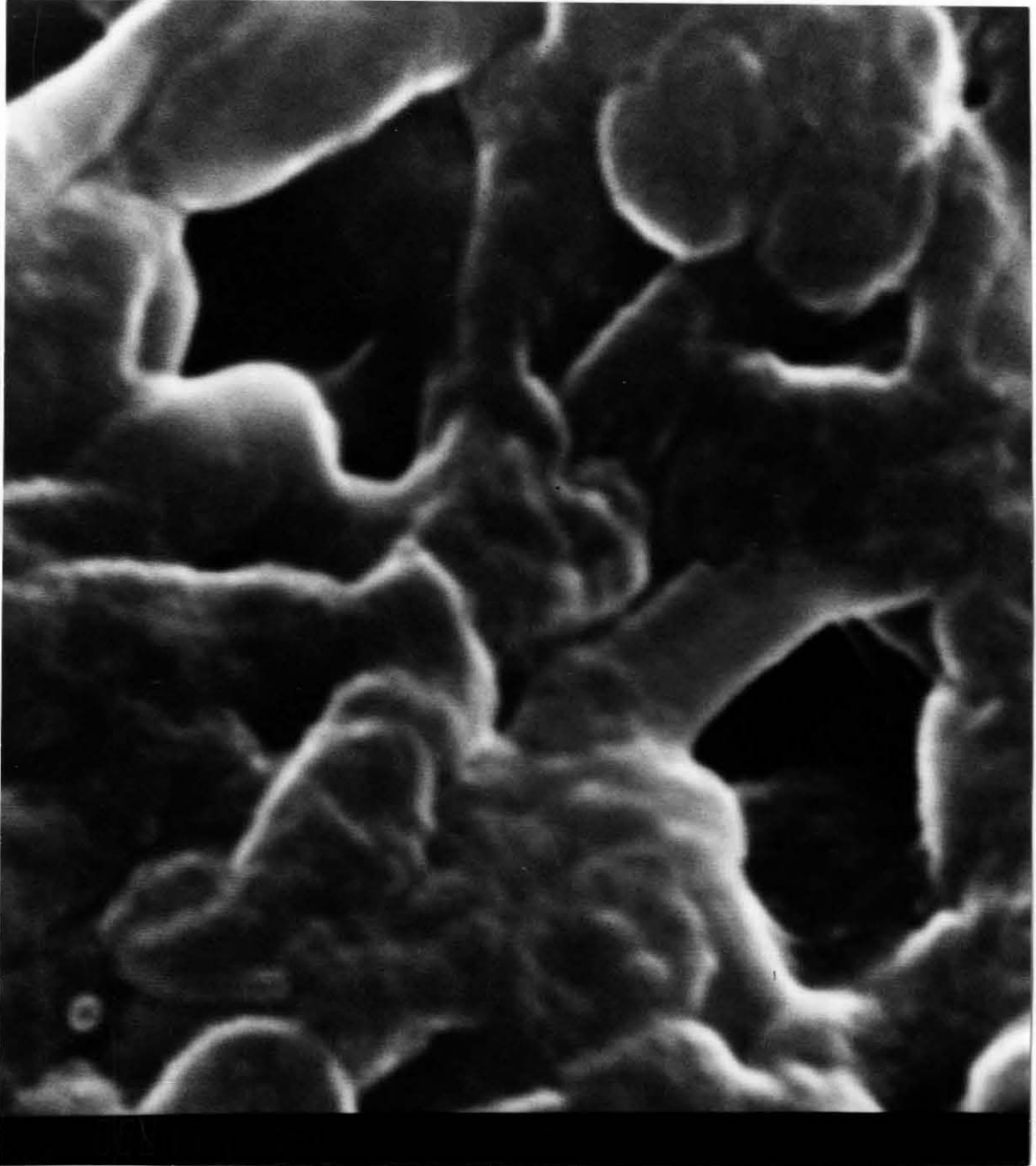
6.5 Electron Micrograph of Surface of Filter Cake Produced by Vacuum Filtration of *E. coli* Cells Flocculated with PEI 350. Total Magnification  $4.0 \times 10^3$ .



6.6 Electron Micrograph of Surface of Filter Cake Produced by Vacuum Filtration of E.coli Cells Flocculated with PEI 350. Total Magnification  $1.0 \times 10^4$ .



6.7 Electron Micrograph of Surface of Filter Cake Produced by Vacuum Filtration of E. coli Cells Flocculated with PEI 350. Total Magnification  $1.8 \times 10^4$ .



6.8 Electron Micrograph of Surface of Filter Cake Produced by Vacuum Filtration of E. coli Cells Flocculated with PEI 350. Total Magnification  $4.0 \times 10^4$ .

indicating that shear forces were not adequate to strip PEI molecules from the E. coli surface.

The electrophoretic mobility experiments conducted to provide information on the mechanism of E. coli flocculation (Section 4.3.3) are valuable as a means of measuring the change in mean aggregate diameter if the unbalanced charge density  $\sigma$  at the slipping plane is known (Equation 5-53). However,  $\sigma$  is an experimentally inaccessible quantity. Additional problems arise from the derivation of the fluid drag force on the aggregate, which requires an assumption as to the aggregate shape (usually assumed spherical).

In spite of these difficulties, the measured aggregate electrophoretic mobilities (Figure 4.8) qualitatively reinforce the results of other experimental techniques. The poor reduction in number of particles at large doses (greater than 3.0 mg/l) of high molecular weight species can be attributed to charge reversal and redispersion of the primary particles (Figure 4.8), as evidenced by the mobility data. Conversely, the continued effectiveness of low molecular weight species at large doses can be correlated with their inability to produce charge reversal. These same effects can be seen in the differential particle size distributions (Figures 6.19 and 6.22 for PEI 350 and PEI 600, Figures 6.11 and 6.14 for PEI 6 and PEI 12, respectively), relative scattering intensities (Figures 6.23-6.26), residual relative

scattering intensities (Figures 6.28-6.31), and refiltration rates (Figure 6.34). Electrophoretic mobility experiments provide an electrostatic justification for the observed phenomenon of restabilization at large doses of high molecular weight species.

Figure 4.8 illustrates that effective flocculation with cationic polymers occurs over a wide range of zeta potential values on either side of 0.0 potential. The common engineering practice of requiring the zeta potential to be within some limits,  $0.0 \pm x$  mv, for optimum flocculation could result in excessive use of expensive high molecular weight PEI, or in poor flocculation with low molecular weight PEI. The optimum dose and molecular weight must be determined specifically for the particular wastewater under consideration. Although the polymer dose for optimum flocculation cannot be determined directly from electrophoretic mobility measurements, once this dose is independently determined, the electrophoretic mobility technique provides a rapid and simple verification of proper operating conditions.

## REFERENCES CITED

## CHAPTER 6

1. Killenberger, E., and Sechaud, J., "Electron Microscope Studies of Phase Multiplication. II. Production of Phage-Related Structures During Multiplication of Phages T2 and T4", Virology, 3 (1957) 256-274.
2. Gomori, G., "Buffers in the Range of pH 6.5 to 9.6", Society Experimental Biology and Medicine, 62 (1946), 33-34.
3. Tenney, M. W., and Stumm, W., "Chemical Flocculation of Micro-organisms in Biological Waste Treatment", Journal Water Pollution Control Federation, 37 (1965), 1370-1388.
4. Tenney, M. W., Echelberger, W. F., Scheussler, R. G., and Pavoni, J. L., "Algal Flocculation with Synthetic Organic Polyelectrolytes", Applied Microbiology, 18 (1969), 965-971.
5. Busch, P. L., and Stumm, W., "Chemical Interactions in the Aggregation of Bacteria", Environmental Science and Technology, 2 (1968), 49-53.
6. Linke, W. F., and Booth, R. B., "Physical Chemical Aspects of Flocculation by Polymers", AIME Mining Transactions, 217 (1960), 364-371.
7. LaMer, V. K., Smellie, R. H., and Lee, P. K., "Flocculation, Subsidence, and Filtration of Phosphate Slimes. V. The Optimum Filtration Rate as a Function of Solid Content and Specific Area", Journal Colloid Science, 12 (1957), 566-574.
8. Black, A. P., and Vilaret, M. R., "Effect of Particle Size on Turbidity Removal", Journal American Water Works Association, 61 (1969), 209-214.
9. Mattern, C. F., Brackett, F. S., and Olson, B. J., "Determination of Number and Size of Particles by Electrical Grating: Blood Cells", Journal Applied Physiology, 10 (1957), 56-70.

10. Bateman, J. B., "Osmotic Responses and Light Scattering of Bacteria", Journal Colloid and Interface Science, 27 (1968), 458-474.
11. Verwey, E. J., and Overbeek, T. G., Theory of the Stability of Lyophobic Colloids, Elsevier, Amsterdam, 1948.
12. Tanford, C., Physical Chemistry of Macromolecules, John Wiley, New York, 1961.
13. Kasper, D. R., "Theoretical and Experimental Investigations of the Flocculation of Charged Particles in Aqueous Solutions by Polyelectrolytes of Opposite Charge", Ph.D. Thesis, California Institute of Technology, 1971.
14. Nevo, A., DeVries, A., and Katchalsky, E., "Interaction of Basic Polyamino Acids with Red Blood Cells", Biochimica Et Biophysica Acta, 17 (1955), 536-547.
15. LaMer, V. K., Smellie, R. H., and Lee, P. L., "Flocculation, Subsidence, and Filtration of Phosphate Slimes", Journal Colloid Science, 12 (1957), 230-239.
16. Healy, T. W., and LaMer, V. K., "The Adsorption-Flocculation Reactions of a Polymer with an Aqueous Colloidal Dispersion", Journal Physical Chemistry, 66 (1962), 1835-1838.
17. Black, A. P., Birkner, F. B., and Morgan, J. J., "Destabilization of Dilute Clay Suspensions with Labeled Polymers", Journal American Water Works Association, 57 (1965), 1547-1560.
18. Birkner, F. B., and Morgan, J. J., "Polymer Flocculation Kinetics of Dilute Colloidal Suspension", Journal American Water Works Association, 60 (1968), 179-191.
19. Camp, T. R., "Flocculation and Flocculation Basins", Transactions American Society of Civil Engineers, 120 (1955), 1-5.
20. Shinnar, R., and Church, J. M., "Predicting Particle Size in Agitated Dispersions", Industrial and Engineering Chemistry, 52 (1960), 253-256.

21. Cummins, C. S., "The Chemical Composition of the Bacterial Cell Wall", International Review of Cytology, 5 (1956), 25-50.
22. Thimann, K. V., The Life of Bacteria, Macmillan, New York, 1963.
23. Buchanan, R. E., "Agglutination", Journal Bacteriology, 4 (1919), 73-105.
24. Dixon, J. K., and Zielyk, M. W., "Control of the Bacterial Content of Water with Synthetic Polymeric Flocculants", Environmental Science and Technology, 3 (1969), 965-971.
25. Babbitt, H. E., and Bauman, E. R., Sewerage and Sewage Treatment, John Wiley, New York, 1958.
26. Moyer, L. S., "Changes in the Electrokinetic Potential of Bacteria at Various Phases of the Culture Cycle", Bacteriology, 32 (1936), 433-464.
27. United States Geological Survey, "The Industrial Utility of Public Water Supplies in the U.S.", Water Supply Paper 1299 (1952).
28. Hannah, S. A., Cohen, J. M., and Robeck, G. G., "Measurement of Floc Strength by Particle Counting", Journal American Water Works Association, 59 (1967), 843-858.
29. Instruction Manual, Phoenix Precision Instrument Company, Philadelphia, Pa., 1963.
30. Bordet, J., "Le Mechanisms de L'Agglutination", Annales de L'Institute Pasteur, 13 (1899), 225-250.
31. Ruehrwein, R. A., and Ward, D. W., "Mechanism of Clay Aggregation by Polyelectrolytes", Soil Science, 73 (1952), 485-492.
32. Avi-Dor, Y., and Yaniv, H., "Relation between Changes in the Stability of Pasteurella tularensis Suspensions and its Bacterial Population", Journal Bacteriology, 66 (1953), 1-5.
33. Hodge, H. M., and Metcalfe, S. N., "Flocculation of Bacteria by Hydrophilic Colloids", Journal Bacteriology, 75 (1958), 258-264.

34. Cohen, J. M., Rourke, G. A., and Woodward, R. L., "Natural and Synthetic Polyelectrolytes as Coagulant Aids", Journal American Water Works Association, 50 (1958), 463-478.
35. Black, A. P., Birkner, F. B., and Morgan, J. J., "The Effect of Polymer Adsorption on the Electrokinetic Stability of Dilute Clay Suspensions", Journal Colloid and Interface Science, 21 (1966), 626-648.
36. Slater, R. W., and Kitchener, J. A., "Characteristics of Flocculation of Mineral Suspension by Polymers", Discussions Faraday Society, 42 (1966), 267-284.
37. Busch, P. L., "Chemical Interactions in the Aggregation of Bacteria", Ph.D. Thesis, Division of Engineering and Applied Physics, Harvard University, 1966.
38. Birkner, F. B., and Edzwald, J. K., "Nonionic Polymer Flocculation of Dilute Clay Suspension", Journal American Water Works Association, 61 (1969), 645-651.
39. Thorup, R. T., Nixon, F. P., Wentworth, D. F., and Sproul, O. J., "Virus Removal by Coagulation with Polyelectrolytes", Journal American Water Works Association, 62 (1970), 97-101.
40. Peter, G., and Wuhrmann, K., "Contribution to the Problem of Bioflocculation in the Activated Sludge Process", 5th International Water Pollution Research Conference, 1970, II:1/1-1/9.
41. Pavoni, J. L., "Fractional Composition of Microbially Produced Exocellular Polymers and Their Relationship to Biological Flocculation", Ph.D. Thesis, Department of Civil Engineering, Notre Dame University, 1970.
42. Tilton, R. C., Murphy, J., and Dixon, J. K., "The Flocculation of Algae with Synthetic Polymeric Flocculants", Water Research, 6 (1972), 155-164.
43. Rembaum, A., Casson, D., and Morgan, J. J., "Flocculation of Colloidal Suspensions with Ionene Polymers", unpublished paper, 1972.

44. Harris, R. H., "The Effect of Extracellular Polymers and Inorganic Colloids on the Colloidal Stability of Bacteria", Ph.D. Thesis, Division of Engineering and Applied Physics, Harvard University, 1971.
45. Schie, P., and Rehberg, R., "Refractive Index of E.coli in Solutions of Sucrose", Biophysical Journal, 10 (1970), 211a.
46. Gumprecht, R. D., and Sliepcevich, C. M., "Measurement of Particle Sizes in Polydispersed Systems by Means of Light Transmission Measurements Combined with Differential Settling", Journal Physical Chemistry, 57 (1953), 95-97.
47. Kerker, M., Cox, A., and Shoenberg, M., "Maximum Particle Sizes in Polydispersed Aerosols", Journal Colloid Science, 10 (1955), 413-427.
48. Carman, P. C., "Fundamental Principles of Industrial Filtration", Transactions - Institution of Chemical Engineers, 16 (1938), 168-185.

## Chapter 7

## SUMMARY AND CONCLUSIONS

Many of the impurities present in water and wastewater systems occur as colloids which are removed by one of the conventional treatment practices: sedimentation, centrifugation, or filtration. Often the colloidal particles are too small to be efficiently removed by any of these techniques. Then the coagulation of this colloidal fraction into large aggregates becomes an essential step in the overall purification process.

The importance of destabilizing the colloidal particles and forming them into large compact aggregates is readily apparent in the equations describing the aggregate velocity in sedimentation and centrifugation, the removal efficiency in filtration, and filtrate flow rate in vacuum filtration. In each case, either the velocity or the efficiency of the phase separation step is directly dependent upon the square of the mean aggregate diameter times a porosity factor specific to each method.

Prior to the phase separation step, the colloidal particles must be destabilized to permit adhesion when interparticle contact occurs, and then transported in their suspending media to create contact opportunities. While the choice of coagulant and chemical

conditions advantageous to rapid destabilization is primarily determined by the surface chemistry of the colloids involved, the means of producing interparticle collisions is based in fluid and particle mechanics.

In general, the destabilization step can be thoroughly investigated in small laboratory batch experiments, and the results extrapolated to full-scale treatment facilities. In this research, the cationic polymer PEI was utilized to determine the mechanism by which polymer molecules destabilize an oppositely-charged colloidal suspension. An understanding of this mechanism is valuable to sanitary engineers in their selection of flocculants to solve specific treatment problems, and to polymer manufacturers in their synthesis of desired polymeric materials.

Unfortunately, laboratory experiments to determine the effectiveness of selected system variables ( $K$ ), the interparticle collision efficiency factor;  $G$ , the mean velocity gradient; and  $t$ , the detention time) in producing interparticle collisions are not readily extrapolated to full-sized plants. A range of values of  $G$  and  $Gt$  for water treatment facilities have been developed from years of experience, however, and this range was investigated in the laboratory with the E.coli-PEI system. At a minimum, these experimental results can be applied qualitatively in the design of pilot plant tests.

The third goal of this research was a quantitative comparison

of the techniques available to measure the extent of aggregation. A systematic analysis was made of four measurement techniques: electronic particle counting, light scattering, refiltration rate and electrophoretic mobility, to determine the functional dependence of each on known system parameters. Special emphasis was placed on determining the relationship between the experimentally measured quantity and the mean aggregate diameter. The theoretical relationships developed for light scattering, refiltration rate, and electrophoretic mobility techniques were then compared experimentally with the aggregate count and size distribution recorded by a Coulter electronic particle counter. Good correlation was found between the parameters measured experimentally by the different techniques, using samples from flocculated E. coli-PEI systems.

#### 7.1 Mechanism of E. coli Flocculation by PEI

A literature survey produced at least eight proposed mechanisms by which coagulants successfully aggregated hydrophilic biocolloids. Several of the mechanisms were restricted to a specific organism or growth condition, either of which could be encompassed in one of the more general explanations. Primarily the coagulants consisted of salts, multivalent hydrolysis species of metal ions, synthetic polymers (anionic, nonionic, or cationic), and extracellular

organic polymers; and the possible mechanisms involved compression of the double layer, adsorption-producing charge neutralization, adsorption-producing interparticle bridging, and entrapment in a precipitate (multivalent hydrolysis species only). While some coagulants produced biocolloid destabilization by one specific mechanism, others could achieve the same result by more than one mechanism, or by a combination of mechanisms. Cationic polymer molecules, for example, could be attracted into the diffuse double-layer surrounding an oppositely-charged colloidal particle, thereby reducing the interaction energy between approaching particles to the extent necessary to produce double-layer coagulation. Or the polymer molecules could adsorb completely onto the colloidal surface, neutralizing the repelling surface charges, and enabling van der Waals forces to draw the particles together. Or finally, the cationic polymer could adsorb partially to the colloidal surface through end sequences, leaving other end sequences free to attach to approaching colloidal particles, producing interparticle bridges of polymer molecules. Colloid destabilization by double-layer compression involves a constant concentration of coagulant irrespective of the concentration of colloidal material, while destabilization by either of the adsorption mechanisms involves a stoichiometric dependence of optimum coagulation dose on the concentration of colloidal material. The cationic polymer PEI was

selected for this research to determine which of the above mechanisms predominate in the coagulation of an oppositely-charged biocolloid.

The polyethylenimine polymers offered several advantages in the conduct of the research experiments. The wide molecular weight range of commercially available PEI species enabled comparisons to be made between observed characteristics solely on a molecular weight basis. For example, the number-average molecular weight varied from 600 to 60,000; the former being too small for destabilization by bridging, the later being in the range considered as the minimum for aggregation via the bridging mechanism with anionic polymers (1). The highly-branched PEI molecules provided the opportunity to study whether successful flocculation could occur without the long chain structure considered important to the bridging mechanism. And finally, the extent of polymer adsorption on the E. coli surface could be readily determined by measuring the initial and residual polymer concentrations via a light adsorption technique.

Table 4.1 summarizes the anticipated characteristics of E. coli-PEI flocs based on the characteristics attributed to each of the three major coagulation models. The investigation into the coagulation of E. coli by PEI was aimed at determining which mechanism predominates in the PEI molecular weight range 600 to 60,000 at pH 7.0 and ionic strength 0.06 M NaCl.

### 7.1.1 PEI Adsorption to E. coli Surface

Polyethylene species of all molecular weights were strongly adsorbed to the surface of E. coli cells. At pH 7.0, the protonated amino groups of the PEI molecule are attracted and bound to negative surface sites on the E. coli surface caused by the ionization of carboxyl or amino groups. The adsorption followed the shape of a Langmuirian isotherm, but the quantity adsorbed in the plateau region was far in excess of that which could be packed into a two-dimensional layer. The amount polymer adsorbed at the saturation plateau increased as a low power of the molecular weight:

$$A_s = 1.8 MW_n^{0.24} \quad (7-1)$$

In the Perkel and Ullman model (2), the value of the molecular weight exponent indicates the configuration of adsorbed polymer molecules after the first monolayer. The value 0.24 means that the PEI molecules in the overlayers have adsorbed in configuration intermediate between coiled spheres (0.33) and flat two-dimensional layers (0.00). If the polymer molecules were attached to the surface by a single segment, such as in a simple bridging model, then the exponent would be 1.00. The adsorbed configuration in the overlayers is the same as that envisioned for a highly branched PEI molecule in solution.

Using a linearized form of the Langmuir adsorption isotherm, the fraction of surface site coverage  $\theta$  was calculated over the range of PEI doses from  $10^{-1}$  to  $10^3$  mg/l. In addition, an optimum flocculation dose was measured for each molecular weight species, essentially based on the percent reduction in number of primary particles, but also considering the percent reductions in refiltration time and relative scattering intensity. From this information the fraction of surface site coverage at optimum flocculation doses for low molecular weight species (PEI 6, PEI 12, and PEI 18) was between 0.3 and 0.6, while for high molecular weight species (PEI 350 and PEI 600)  $\theta$  was between 0.01 and 0.03.

LaMer (3) has stated that flocculation via polymer bridging is optimized at values of  $\theta$  near 0.5, which coincides with the results for low molecular weight PEI species. In addition, between 5 and 10 monolayers of surface coverage are deposited at optimum flocculation doses of low molecular weight species, indicating that the molecules may adsorb through end segments after the first monolayer, as per the Jenckel and Rumbach model (4). The surface area of each monomer unit ( $C_2H_5N$ ) was calculated from known values of packing radii, yielding areas on the order of  $20 \text{ \AA}^2/\text{monomer}$ . This value was extrapolated to determine the surface coverage of a single PEI molecule, assuming a flat extended configuration.

For high-molecular-weight species (PEI 350 and PEI 600), the fraction of surface site coverage at optimum flocculation doses is so small that the initial adsorption models of Chapter 3 appear valid. In these models, the PEI molecules are essentially collapsed into two-dimensional layers by the strong attractive forces (5-8 kcal/mole) between extended segments and colloidal surface. In addition to the low degree of surface site coverage, optimum doses of high-molecular-weight species produce less than 1.5 monolayers of coverage.

A final item of importance derived from adsorption studies is the effect of saturation adsorption upon the extent of flocculation. For low-molecular-weight species, polymer adsorbed in excess of optimum conditions produced no noticeable destabilization of E. coli cells. Excess PEI doses did produce poorer refiltration rates, but this was attributed to blockage of the pores in the filter cake and filter septum rather than to increases in aggregate surface area caused by restabilization. For high-molecular-weight species, polymer adsorbed in excess of optimum conditions produced definite restabilization of the E. coli at positive values of electrophoretic mobility. Since this restabilization occurred at a  $\theta$  value of approximately 0.2, it cannot be attributed to oversaturation of surface sites. The restabilization is directly traceable to the charge reversal caused by excess adsorption of PEI species.

### 7.1.2 Electrophoretic Mobility of E. Coli Floccules

Irrespective of which mechanism predominated in the coagulation process, the addition of the cationic polymer PEI to a solution of oppositely-charged E. coli cells modified the electrophoretic mobility of these cells. If the primary mechanism was double-layer coagulation, an excess of cationic polymer molecular (counterions) accumulated in the electrolyte near the cell surface. As the bacterial cells reacted to the applied potential of the Briggs apparatus, a quantity of electrolyte, containing the counterions, moved with the primary particle. At optimum flocculation doses, the concentration of counterions in the immediate vicinity of the bacterial cell reduced the repulsive interaction energy to a level permitting the attractive van der Waals forces to produce aggregation. This counterion concentration is usually sufficient to reduce the electrophoretic mobility to values near zero, and this effect was observed with PEI 6 and PEI 12. However, an excess of cationic molecules will not reverse the electrophoretic mobility because of the increasing electrostatic repulsion between molecules of the same charge in the Gouy layer. Nevertheless, charge reversal was observed with PEI 18, PEI 350, and PEI 600.

If the primary mechanism was adsorption coagulation, the mobility at optimum flocculation may be a value other than zero. Kasper ( 5 ) has shown that the proper alignment of regions of

positive charge density where cationic polymer has adsorbed with uncovered regions of negative charge density can produce rapid destabilization at widely varying values of electrophoretic mobility. If segment-surface adsorption energies are strong enough, polymer molecules may adsorb through a few segments, leaving an unbalanced positive charge on other segments extending away from the surface. Consequently, excess polymer may produce positive mobility values, as was observed with PEI 18, PEI 350, and PEI 600.

If the primary mechanism was polymer bridging, then the electrophoretic mobility at optimum doses would usually not be zero. The extended polymer segments must be long enough to bridge the gap between particles created by the interaction of diffuse double layers, and electrostatic effects would play a subordinate role. Since the molecules adsorb through end sequences, more molecules are able to adsorb than a charge balance would permit, and thus excess doses can result in mobility reversal.

For the low molecular weight PEI species, optimum flocculation occurs at mobility values near zero. Excess doses of PEI 6 and PEI 12 are unable to reverse the negative mobility of the E. coli cells, whereas excess doses of PEI 18, PEI 350, and PEI 600 reverse and eventually stabilize the mobility at positive values. For the high molecular weight PEI species, optimum flocculation occurs at a wide range of mobility values on either side of 0.0.

### 7.1.3 Light Scattering from PEI Solutions

The light scattered by dilute solutions of PEI 18, PEI 350, and PEI 600 molecules was utilized to determine their respective weight-average molecular weights. The weight-average molecular weight is especially sensitive to large molecules, and consequently, would be an important indication of whether polymer bridging was physically possible. In addition to the molecular weight, the radius of gyration and an equivalent spherical radius was calculated from light scattering measurements. Low molecular weight species had equivalent spherical radii in the range 100 to 200 Å, while PEI 350 molecules had equivalent spherical radii near 1000 Å, and PEI 600 molecules had equivalent spherical radii near 2000 Å. Molecules of all species would be of sufficient length to form polymeric bridges, provided the surface potential between E. coli cells and suspending electrolyte does not exceed 100 millivolts (see Figure II-8 of Kasper (5)).

The radii of gyration of the PEI species were found to be related to the weight-average molecular weight via the equation

$$R_G = 0.05 MW_w^{0.7} \quad (7-2)$$

The experimental value of the exponent for the PEI molecules in solution indicates an open ellipsoid-shaped molecule, in agreement with earlier evidence of the molecular configuration. Calculations of

the mutual repulsion between ionized groups on the PEI molecule predict the molecules to be fully extended in a solution of ionic strength 0.06 M NaCl.

#### 7.1.4 Refiltration Rate of Filtrate Through E. Coli Filter Cake

The refiltration rate technique of LaMer and Healy (3) was utilized to determine the optimum flocculation dose for each of the five molecular weight species. As stated in Section 7.1.1, these optimum doses should coincide with a fraction of surface site coverage near 0.5. This condition was met only for PEI 6 and PEI 12, both of which produce poor refiltration rates when compared to the higher molecular weight species. The best refiltration rates for the E. coli PEI system were produced with the high molecular weight species at values of  $\theta$  ranging between 0.01 and 0.03; values which are in better accord with adsorption coagulation model of flocculation, than with the polymer bridging model.

#### 7.1.5 Electron Micrographs of Flocculated E. Coli Cells

E. coli aggregates were examined in a Scanning Electron Microscope to compare the separation distance between cells flocculated with PEI 6 with that recorded for cells flocculated with PEI 350. In both cases, the cells were observed as tightly bound together, with cell separation distances of approximately 100-200 Å. A single

bridging structure on the order of 500 Å in length was observed between cells flocculated with the optimum dose of PEI 350. Long fibular structures, such as those observed by Friedman, et al. (6) in their electron micrographs of Zoogloea ramigera, were not evident. Instead, the highly-branched PEI molecules appear to serve as a strongly-adsorbed polymeric glue which binds the colliding cells together.

#### 7.1.6 The Mechanism of E. Coli Flocculation by PEI

The results of the preceding experiment are summarized in Table 7.1, with the PEI species segregated into short ( $MW_n < 10^3$ ), medium ( $10^3 < MW_n < 10^4$ ), and long ( $MW_n > 10^4$ ) molecules. Although some experimental evidence exists that coagulation of E. coli cells by the double-layer compression mechanism is possible, and other evidence exists that coagulation by the polymer bridging mechanism is possible, the preponderance of data supports the adsorption coagulation mechanism as predominant in this system.

The strong adsorption of PEI to the E. coli cells and the stoichiometric dependence of optimum coagulation dose on the concentration of colloidal material (7) eliminates the physical double-layer mechanism.

The polymer bridging mechanisms were discarded primarily because of the low degree of surface site coverage observed at optimum

Phenomenon	Species
	PEI 6 PEI 12, PEI 18 PEI 350, PEI 600

Adsorption

Configuration of polymer molecules at saturation adsorption All species adsorb in ellipsoid configuration

Surface site coverage at optimum flocculation  $\theta > 0.4$   $0.3 < \theta < 0.6$   $\theta < 0.1$

Monolayers of surface coverage All species adsorb in many monolayers

Effect of excess adsorption on flocculation no effect no effect Restabilization from charge reversal

Electrophoretic Mobility

Mobility at optimum flocculation Usually not zero for all species  
 Mobility at excess adsorption near zero near zero Positive mobility

Light Scattering

PEI molecule size  $r < 100 \text{ \AA}$   $r < 200 \text{ \AA}$   $r < 2000 \text{ \AA}$   
 PEI molecule configuration extended extended extended

Refiltration Rate

poor poor excellent

Intercellular Structure

Electron microscope closely packed generally closely packed

Table 7.1 Summary of Characteristics of E. coli-PEI Floccs as a Function of PEI Species

flocculant doses of PEI 350 and PEI 600. This low surface site coverage indicates the presence of many negative charge sites which strongly attract extended positive segments to the surface, as expected from the theoretical discussion of Chapter 3. For this reason even the large molecules measured by light scattering, although of sufficient size to form polymeric bridges, are tightly bound to the E.coli surface.

Although the degree of surface site coverage at optimum flocculant doses of PEI 6 and PEI 12 is much higher, the majority of these molecules is too small to provide adequate chain length for bridging structures. Intercellular separation distances greater than 100 - 200 Å in length are attributed to imperfect dehydration of the flocs during preparation of the EM grids, and are an indication of the strength of the interparticle bonds produced by the adsorbed PEI.

All of the evidence of Table 7.1 can be interpreted in terms of the adsorption coagulation mechanism of flocculation. Recent theoretical and experimental studies by Kasper ( 5 ) and Gregory ( 8 ) have elucidated the adsorption coagulation mechanism in terms of a charge mosaic model.

According to this charge mosaic model, the relatively low degree of surface site coverage at optimum flocculation results in regions of positive charge density where cationic polymer has adsorbed, and uncovered regions of negative surface charge density. The proper

alignment of these regions on colliding particles results in mutual attraction and flocculation. On a larger scale, these interactions produce an open three-dimensional floc of excellent filterability.

Kasper has shown theoretically that as the polymer molecular weight increases, less polymer and consequently less surface site coverage are required to produce successful flocculation via the charge mosaic model. Both of these theoretical predictions have been substantiated by the results in the E. coli-PEI system.

## 7.2 Comparison of Methods of Measuring Extent of Aggregation

A survey of methods for measuring the extent of aggregation revealed that most methods may be categorized as either direct measurement, optical measurement, sedimentation/filtration measurement, or electrostatic charge measurement. In Chapter 5, a theoretical analysis was made of four experimental techniques: electronic particle counting, light scattering intensity, refiltration rate, and electrophoretic mobility, which were felt to be representative of the four measurement categories. This analysis found that each of the experimental techniques possessed serious limitation to their direct application in recording the extent of aggregation produced within a coagulating system. Nevertheless, once these limitations were recognized, procedures were developed to correct the shortcomings and to utilize these techniques to study the aggregation

of E. coli by PEI. These procedures can be applied to other coagulating systems with minor changes to reflect the particular attributes of the colloid and coagulant.

#### 7.2.1 Electronic Particle Counting and Size Distribution

The basic theory of electronic particle counting and sizing for singlets has been thoroughly developed over the past 20 years. Only recently however have difficulties been observed in extending this theory to the sizing of aggregates ( 9 ). These difficulties are traced to the porosity of the aggregates, and especially to the separation distance between primary particles as reflected by the aggregate porosity. If the primary particles within an aggregate are tightly bound together, then the pulse produced by the passage of this aggregate through the aperture of the Coulter counter is directly proportional to the number of singlets in the aggregate. However, as the porosity of the aggregate increases, and thus the separation distance between singlets also increases, two problems arise in properly sizing the aggregates. If a small aperture is used, the aggregate elongates within the critical measuring volume, resulting in insufficient pulse height to accurately reflect the aggregate size. If a larger aperture is used, the aggregate shape is not affected, but the aperture sizing system (aperture, current, and amplification) is required to size and sum the many smaller pulses

created by the primary particles which comprise the total aggregate. Generally, only the small aperture is able to precisely detect and size singlet particles: the larger apertures only detect tightly bound singlet cells, and then the system response is only a partial response to the total particulate volume within the aggregate.

A solution to this problem was found by relating the aggregate porosity, as determined from calculations and current literature, to the number of singlet cells within the aggregate. In addition, the conservation of volume condition existing between the unflocculated and flocculated state was utilized to establish an asymptotic value of the aggregate porosity. The resulting equations, which compensated for the effects of aggregate porosity on the recorded pulse height, were successfully applied to a wide variety of flocculating conditions produced during the coagulation of E. coli by PEI.

#### 7.2.2 Light Scattering Intensity of Aggregated Particles

Because of the size-refractive index regime of E. coli cells, there existed two possible interpretations of the light scattered by aggregates of these cells. The first treatment considered the aggregates as composed of rod-like Rayleigh-Gans scatterers which were coagulated into a mixture of three different configurations: linear, planar, and close-packed three-dimensional. Using an assumption as to the relative concentrations of these configurations, the scattered light could be

corrected by the application of aggregate form factors to yield a theoretical scattering intensity. This treatment was discarded as unworkable for a system of aggregates with many possible sizes and shapes.

Alternatively, the aggregates were considered as coalesced into large Mie scatterers, such that the turbidity of flocculating particles was represented by

$$\tau = \sum_i n_i \pi r_i^2 K_i \quad (7-3)$$

where  $n_i$  = number of aggregates of equivalent spherical radius  $r_i$

$r_i$  = equivalent spherical radius

$K_i$  = Mie scattering coefficient for aggregates of equivalent spherical radius  $r_i$

In this treatment, the turbidity of a suspension of aggregates coalesced from primary particles was highly dependent upon the particle size regime involved. Depending upon the particle size and refractive index, approximations to the exact Mie scattering coefficient can be utilized in lieu of the complicated exact formulation. If the number of aggregates and their equivalent spherical radii are known from Coulter counter measurements, then a suspension turbidity can be predicted using the coalesced sphere approach with approximate Mie scattering coefficients.

### 7.2.3 Refiltration Rate Through Filter Bed of Aggregated Particles

The ability of the refiltration technique to record changes in the mean aggregate diameter is directly related to whether the porosity of the filter cake is dependent or independent of the flocculation condition. A theoretical analysis of the equation for the specific resistance of the filter cake revealed that changes in this quantity are directly proportional to changes in the specific surface area, provided that the porosity of the filter cake is independent of flocculation condition. Therefore, this constant porosity condition must be satisfied by independent means before the refiltration rate technique can be used to measure the extent of aggregation. As with electronic particle counting and scattering intensity measurement, each aggregate must be considered as a coalesced sphere which is packed into the filter cake by the pressure differential.

### 7.2.4 Electrophoretic Mobility of Aggregated Particles

The electrophoretic mobility of aggregated particles was shown to be directly proportional to the product of the unbalanced charge density at the slipping plane and the square of equivalent spherical diameter

$$v_a = K\sigma d_a^2 \quad (7-4)$$

where  $\sigma$  = unbalanced charge density

$d_a$  = equivalent spherical diameter at slipping plane

Since the unbalanced charge density cannot be measured experimentally, electrophoretic mobility measurements are of limited usefulness in determining the extent of aggregation produced by adding a cationic flocculant to an oppositely-charged colloid.

In the experiments with the E. coli-PEI system, the aggregates produced at each PEI dose appeared to move at approximately the same velocity, almost independently of relative size. This condition would indicate that the coalescence assumption is a poor one when applied to electrophoretic mobility measurements. If the aggregate is considered merely as a collection of primary particles, with each particle maintaining separate identity with respect to surface charge neutralization and drag coefficient, then the equation for electrophoretic mobility is

$$v_a = \frac{E\sigma d_o}{3u} \quad (7-5)$$

where E = electric field strength

$d_o$  = diameter of primary particle

u = absolute viscosity

While (7-5) reflects the dependence of the aggregate velocity on the unbalanced charge density, the influence of the adhesion between cells on the drag coefficient has been neglected.

#### 7.2.5 Quantitative Correlation of Experimental Data

An important part of my research was directed at using the E. coli-PEI system to make quantitative comparisons between the results recorded by light scattering, refiltration rate, and Coulter counter techniques.

Values of suspension turbidity, predicted from particle size distributions using the approximate Mie scattering coefficients for coalesced aggregates in the anomalous diffraction regime, were within  $\pm 20\%$  of experimentally measured values. This correlation was felt to be good since it covered a wide range of flocculation conditions and several major assumptions, notably with respect to aggregate porosity in sizing, and aggregate coalescence in scattering.

The large aggregates formed by PEI 350 and PEI 600 occupied a portion of the anomalous diffraction regime in which the Mie scattering coefficient was essentially independent of aggregate diameter. The turbidity of a suspension of these aggregates decreased as the mean aggregate diameter increased. The smaller aggregates formed by PEI 6, PEI 12, and PEI 18 occupied a portion of the

anomalous diffraction regime in which the scattering coefficient was approximately linearly dependent on the aggregate diameter. The turbidity of a suspension of these aggregates was a conservative parameter even as flocculation increased between primary particles.

The use of the Carmen-Kozeny filtration equation, and the assumption of constant filter cake porosity irrespective of flocculation conditions, were verified by simultaneously plotting the product of the specific surface times the surface (determined from Coulter counter data) and the refiltration time against the PEI dose. Very good correlation was found in the shape of these curves, especially for PEI 350 and PEI 600 (Figures 3.36 and 3.37). Electron micrographs of PEI 350 flocculated cells in the filter cake revealed a few large channels between tightly-clustered cells. Other micrographs of PEI 6 flocculated cells revealed more small channels between the flocculated cells, and considerable clogging of the interstices.

7.3 Influence of Selected Variables on the Extent of E. Coli  
Aggregation by PEI

Four experimental techniques (electronic particle counting, light scattering, refiltration rate, and electrophoretic mobility) were used to measure the extent of E. coli aggregation as the PEI molecular weight, PEI dose, the intensity of agitation G, and the time of agitation t were varied.

The effectiveness of cationic polymers in producing flocculation via the adsorption coagulation mechanism is highly molecular weight dependent. For example, Rubini et al. (10) found that lysine polypeptides of molecular weight 14,000 and 26,000 were much more effective in the aggregation of red blood cells than were molecules of molecular weight 1,000 and 3,000. Studies by Tilton et al. (11-13) placed the differentiation point between unsuccessful and successful flocculation at molecular weight 1,000. A similar molecular-weight dependence was readily apparent in my investigations with the E. coli-PEI system.

The relative effectiveness of PEI species in producing the flocculation of E. coli was separated into three approximate molecular-weight regimes:  $MW_n < 10^3$ ,  $10^3 < MW_n < 10^4$ , and  $MW_n > 10^4$ , corresponding to poor, average, and excellent flocculation respectively. The results of my experiments with five PEI species within these molecular-weight regimes are tabulated in Table 7.2.

Measurement Technique	$<10^3$	Molecular Weight $10^3 - 10^4$	$>10^4$
<u>Direct</u>			
% reduction in cell count	<70	70 to 99	>99
diameter of largest aggregates	d=4 to 8 $\mu\text{m}$	d=8 to 12 $\mu\text{m}$	d=16 to 20 $\mu\text{m}$
<u>Optical</u>			
% reduction in relative scattering intensity (60 min stirring at G=20 $\text{sec}^{-1}$ )	<10	<10	10 to 70
% reduction in residual relative scattering intensity (60 min sedimentation)	<10	10 to 30	30 to 70
<u>Sedimentation/Filtration</u>			
% increase in refiltration rate	<10	10 to 70	70 to 90
<u>Electrostatic Charge</u>			
electrophoretic mobility ( $\mu\text{m}/\text{sec}/\text{volt}/\text{cm}$ )	-0.55 to -0.40	-0.55 to +0.25	-0.75 to +1.05

325

Table 7.2 Summary of PEI Effectiveness in Producing Flocculation as a Function of PEI Molecular Weight.

The increased flocculant effectiveness with higher molecular-weight species is attributed to the formation of stronger contacts between colliding cells. The resulting aggregates are able to increase in size because the interparticle bonds are more resistant to the imposed shear forces than those formed by low-molecular-weight species.

The ability of these interparticle bonds to withstand shear is evidenced in electron micrographs of the filter cake formed in refiltration experiments. The open three-dimensional structure remains intact as the filtrate passes through the large channels between tightly bound cells. The small amount of high-molecular-weight polymer required to produce this structure is less prone to block the filter cake interstices than is the required larger dose of low-molecular-weight polymer.

PEI 350 and PEI 600 doses at optimum flocculation (0.3 to 1.0 mg/l) were an order of magnitude smaller than PEI 6, PEI 12, and PEI 18 doses (3.0 to 10.0 mg/l) at optimum flocculation. The charge mosaic model of Kasper ( 5 ) explains the successful flocculation produced by small doses, and low surface site coverages, of high-molecular-weight cationic polymers. These polymers produced flocculation by neutralizing, and then reversing, the surface charge density at specific adsorption sites. In addition to the reduction of the double-layer repulsion, this charge mosaic effect created electrostatic

attraction between oppositely-charged sites. In contrast, the low-molecular-weight species adsorbed to the surface, but did not produce regions of positive charge density, as evidenced by their failure to produce mobility reversal even at very high PEI concentrations. Low-molecular-weight species produced flocculation by neutralization of the negative surface charge density, and the subsequent reduction of the interparticle interaction energy.

Doses of the high-molecular-weight species greater than 3.0 mg/l were adsorbed to the E. coli surface, with increasing numbers of segments extending from the surface as the fraction of surface site coverage increased. These doses produced mobility reversal and initiated redispersion of the macroflocs into microflocs. Since the fraction of surface site coverage for low-molecular-weight species producing optimum flocculation ranged between 0.4 and 0.8, few available sites existed for additional adsorption at higher doses. Consequently, additional adsorption had no measurable redispersion effect.

The collision rate equations proposed by Smoluchowski for perikinetic and orthokinetic flocculation were used to estimate the particle concentration following the two minute rapid mix ( $G=190 \text{ sec}^{-1}$ ) and 60 minutes of either quiescence ( $G=0$ ) or agitation at a predetermined mixing intensity ( $G=20, 40, \text{ or } 60 \text{ sec}^{-1}$ ). These calculations (Table 6.1) predicted greater reduction in the number of particles as the mixing

intensity increased. Experimentally, this did not occur, since the percent reductions in number of particles were virtually identical irrespective of mixing intensity in the range  $G=20 \text{ sec}^{-1}$  to  $G=60 \text{ sec}^{-1}$ . (Figure 6.7). Birkner and Morgan (14) found the experimental rate constants proposed by Smoluchowski were valid only during the first 10 minutes of flocculation: my experiments indicated that before 60 minutes of mixing, deflocculation processes, caused by higher shear stresses at  $G=40 \text{ sec}^{-1}$  and  $G=60 \text{ sec}^{-1}$ , resulted in particle concentrations the same as those produced at  $G=20 \text{ sec}^{-1}$ .

For perikinetic flocculation, the initial rapid mix period produced some large aggregates which settled rapidly, sweeping along other particles moving at a slower rate. Thus reductions in number of aggregates for perikinetic flocculation were within a few percent of those recorded for stirrer suspensions, in spite of theoretical predictions to the contrary.

As the flocculation period increased from 60 minutes to 240 minutes at  $G=20 \text{ sec}^{-1}$ , the particle count and particle size distribution remained essentially constant for E. coli aggregates formed by PEI 350 or PEI 600. (Figures 6.6, 6.17-6.22). Thus the duration of agitation had no measurable impact on aggregate formation after the first hour. Experiments showed that the first order of magnitude reduction in primary particle concentrations occurred within six minutes of PEI 350

or PEI 600 addition, and the second order of magnitude reduction occurred very gradually over the remaining four hours of flocculation.

The duration of agitation (from  $t=60$  minutes to  $t=240$  minutes) did produce a 10 to 20 percent increase in the reduction of particle count for E. coli aggregates formed by PEI 6, PEI 12, and PEI 18. (Figure 6.6). These reductions in particle count coincided with a gradually broadening of the particle size distribution spectrums (Figures 6.9-6.16).

Relative light-scattering experiments and refiltration rate experiments supported the conclusions arrived at by electronic particle counting and sizing techniques:

1. The primary factors in PEI effectiveness are molecular weight and dose (Figures 6.23-6.26, 6.27, 6.34).
2. The intensity of agitation, within common treatment practice limits, and the duration of agitation play very minor roles in the flocculant effectiveness (Figure 6.27, 6.33, 6.35).

#### 7.4 Engineering Applications

All four of the measurement techniques employed in this research were found to possess serious limitations to their practical application in the sanitary engineering field. These limitations, while not insurmountable, point to the need for continued research in the

measurement of flocculant effectiveness. The following list summarizes the major limitations of the four measurement techniques utilized in this research.

1. Coulter Counter/PHA/MCA
  - a. Multiple apertures are required to detect complete size distributions from primary particles to the largest aggregates.
  - b. An aggregate porosity assumption is required to account for the stretching of the signal pulse in small apertures and the incomplete signal in large apertures.
  - c. Expensive and sophisticated peripheral equipment is required to analyze primary data.
2. Turbidity and residual relative scattering intensity
  - a. Turbidity increases, remains constant, or decreases with flocculation, depending upon the size regime of the aggregates involved. A particle size distribution is required to properly evaluate the scattering coefficients and to interpret turbidity readings.
  - b. Interpretation of data is complicated by relative refractive index, heterogeneity of aggregate size and shape, and multiple scattering effects.

3. Refiltration rate
  - a. A constant filter cake porosity irrespective of flocculation condition is required to evaluate changes in the specific surface area.
  - b. Blockage of interstices of filter cake and filter septum with excess polymer can result in incorrect evaluation of the degree of flocculation.
4. Electrophoretic mobility
  - a. Changes in the mean aggregate diameter can only be evaluated if the unbalanced charge density at the slipping plane and the aggregate drag coefficient are known.
  - b. Optimum aggregation often occurs at zeta potential values considerably removed from 0.0 potential.

From an engineering viewpoint, the refiltration technique of LaMer and Healy was found to be the best overall measure of PEI effectiveness in flocculating E. coli. The technique requires very little equipment, is easy to perform, is reproducible, and provides results that correlate well with those obtained via more sophisticated techniques.

As stated in the introduction to this thesis, the timely application of cationic polymers to wastewater treatment flows could result in a more rapid flocculation of dispersed microorganisms and non-assimilated macromolecular material than is currently possible through bioflocculation. Figure 6.8, for example, shows that bioflocculation does produce some aggregation of E. coli over the four-hour test period; however, this effect is minor when compared to the very rapid changes in particle size distribution produced by 0.5 mg/l of PEI 350 (Figure 6.18) or PEI 600 (Figure 6.21).

My research has shown that there is no need for flocculation tanks when strongly-adsorbing cationic polymer is employed as the flocculating agent. The addition of cationic polymer in a rapid mixing chamber, plus flow through pipes, pumps, and the secondary sedimentation tank will provide adequate contact opportunity between dispersed particles. Additional contact will occur as the larger aggregates fall through the suspension in the sedimentation tank, impacting on slower moving particles.

The high molecular weight PEI species were most effective as flocculant at concentrations of 1 part PEI:100 parts microorganisms. Currently PEI 600 costs \$3.70 per pound of 100% PEI, based on the purchase of 55 gallon drums. The effective flocculation of 100 pounds of microorganisms (dry weight) could be achieved with \$3.70 of PEI 600.

Under comparable conditions, Tenney and Stumm (15) found alum ( $\text{Al}_2(\text{SO}_4)_3 \cdot 18\text{H}_2\text{O}$ ) effective as a flocculant at concentrations of 70 parts alum:100 parts microorganisms. However, in spite of the 70 times greater dose required than with PEI, alum costs only \$0.03 per pound, and thus the flocculant cost per 100 pounds of microorganisms is \$2.10.

The flocculant cost differential will be partially offset by other factors, such as significantly smaller sludge dewatering and handling costs, and the elimination of extensive flocculation basins when PEI is used. Other possible advantages to the use of cationic PEI are the preferential reaction with soluble phosphates (7) and the toxicity to E. coli at optimum flocculant doses.

#### 7.5 Modeling of Flocculation/Sedimentation Process

The flocculation of dispersed colloidal particles into aggregates as they move through a basin can be expressed by the following differential equation for a small volume element within the basin:

$$\begin{aligned} \frac{dn(a_k, \bar{r}, t)}{dt} + \nabla \cdot [(\bar{v}(\bar{r}, t) + \bar{v}_s(a_k))n(a_k, \bar{r}, t) = \\ D(a_k)\nabla^2 n(a_k, \bar{r}, t) + \frac{1}{2} \sum_{i+j=k} B(a_i, a_j, G, \kappa)n(a_i, \bar{r}, t)n(a_j, \bar{r}, t) \\ - \sum_{i=1}^{\infty} B(a_i, a_k, G, \kappa)n(a_i, \bar{r}, t)n(a_k, \bar{r}, t) + \sum_{i=1}^{\infty} S(a_{i+k}, G, \gamma)n(a_{i+k}, \bar{r}, t) \\ - S(a_k, G, \gamma)n(a_k, \bar{r}, t) \end{aligned} \quad (7-5)$$

where  $n$  = concentration of aggregates of radius  $a$

$a_k$  = radius of aggregate of  $k$  singlets

$\bar{r}$  = position vector of aggregate

$t$  = time

$\bar{v}$  = displacement velocity vector

$\bar{v}_s$  = sedimentation velocity vector

$D$  = diffusion coefficient

$B$  = collision frequency factor

$S$  = shear frequency factor

$G$  = velocity gradient

$\kappa$  = collision efficiency factor

$\gamma$  = shear efficiency factor

The diffusion coefficient for large particles in aqueous media will be negligibly small, thereby making  $D(a_k) \nabla^2 n(a_k, \bar{r}, t)$  insignificant in comparison with the remaining terms.

If the process under consideration occurs in a well-mixed flocculation basin,  $v_s(a_k)$  will be independent of position, and consequently  $\nabla \cdot v_s(a_k) = 0$ . In this case, the change in particle concentration of each size will be caused by the sum of gains and losses from coagulation plus gains and losses from shear plus losses as the particles leave the basin. The process may be further simplified by operating

in the batch mode, so that  $\bar{v}(\bar{r}, t) = 0$  and no losses will result from aggregates leaving the basin.

During the initial period of operation of the batch flocculation basin, the change in particle concentration will be primarily caused by the coagulation of singlet particles, neglecting contributions from the shear terms. Then the generation of particles  $n_k$  will be the difference between effective collisions of  $n_i$  with  $n_j$  minus effective collisions of  $n_i$  with  $n_k$ . The expression for shear coagulation of discrete particles is

$$\frac{dn_k}{dt} = \frac{1}{2} \sum_{i+j=k} \frac{4}{3} (a_i + a_j)^3 n_i n_j G \kappa - \sum \frac{4}{3} (a_i + a_k)^3 n_i n_k G \kappa \quad (7-6)$$

Assuming a relatively monodisperse system of particles, i.e.,  $a_i = a_j$ , and summing over all  $k$  results in

$$\ln \frac{N}{N_0} = - \frac{4\kappa V_m G}{\pi} t \quad (7-7)$$

where  $N_0$  = initial concentration of particles

$N$  = concentration of particles at time  $t$

$V_m$  = volume fraction of particles to media

From equation (7-7), the collision efficiency factor  $\kappa$  at each value of  $G$  can be determined by measuring the change in total particle concentration.

Continued operation of the batch flocculation basin will result in the shearing of large aggregates  $n_{k+i}$  into smaller aggregates  $n_k$  and  $n_i$ , and in the loss of some  $n_k$  aggregate to shear. The number of effective shear gains and losses is hypothesized to be a function of the aggregate size, aggregate number, velocity gradient, and a shear efficiency factor depending on the strength of the interparticle bonds. If an equilibrium aggregate size  $a_e$  results from a balancing of gains and losses from coagulation and shear, then this equilibrium situation can be utilized to determine the shear frequency factor and shear efficiency factor at each  $G$ .

After four hours of continuous agitation, all the PEI-E. coli systems had achieved an equilibrium size of aggregates (Table A.1). The high-molecular weight species had achieved virtual equilibrium in number and volume distribution within 60 minutes of flocculation (Figures A.10-A.15), while the low-molecular weight species exhibited continued growth of aggregates in the larger size ranges over the full four hour flocculation period (Figures A.2-A.9). Further research in this area should be conducted with highly monodisperse particles which do not present the problems of bacterial cells: i. e., bioflocculation and loss of volume in endogeneous respiration. My experiments do indicate that the shear efficiency factor is dependent upon the strength of the interparticle bond; the low molecular weight species

forming weaker bonds which result in smaller aggregates as compared with the high molecular weight species (Figures A.3, A.6, A.8, A.11, and A.14). Once the combined generation and loss of aggregates from coagulation and shear are evaluated, then the batch flocculation basin can be studied in the continuous flow mode as represented by equation (7-5).

If the process under consideration occurs in a sedimentation basin with negligible velocity gradient induced coagulation and shear, equation (7-5) must be modified to include collisions from differential settling, and removal as aggregates reach the bottom of the basin.

In the first case, the number of collisions  $J_{ij}$  per unit volume and time can be estimated from the size and number of particles in a unit volume of fluid,

$$J_{ij} = \pi(a_i + a_j)^2 (v_{si} - v_{sj}) n_i n_j \quad (7-8)$$

where  $v_{si}$  = settling velocity of aggregates of size  $a_i$

The associated vertical distance is one within the small volume element that enables the upper, larger particle to catch up with the lower, smaller particle in unit time. As with shear induced coagulation, both gains and losses to the particle concentration  $n_k$  will occur as a result of differential settling.

The path taken by discrete particle settling in a horizontal-flow sedimentation basin is the vector sum of the displacement velocity  $\bar{v}$  and the sedimentation  $\bar{v}_s$ . All particles with a settling velocity  $v_s > v_o$  are removed,  $v_o$  being the velocity of the particle falling through the full depth  $h_o$  of the sedimentation basin in the detention time  $t_o$ .

$$v_o = \frac{h_o}{t_o} = \frac{V/A}{V/Q} = \frac{Q}{A} \quad (7-9)$$

where  $V$  = volume of sedimentation basin

$A$  = surface area of sedimentation basin

$Q$  = volume rate of flow

In addition, if  $n_o$  particles possessing a settling velocity  $v_s \leq v_o$  are distributed throughout the suspension, then the proportion  $n/n_o$  of particles removed in a horizontal-flow basin is

$$\frac{n}{n_o} = \frac{h}{h_o} = \frac{v_s t_o}{v_o t_o} = \frac{v_s}{v_o} = \frac{v_s}{Q/A} \quad (7-10)$$

The aggregate diameter required to insure removal by a sedimentation basin is obtained by equating  $v_o$  of equation 7-9 with  $v_a$  of equation 1-4.

$$d_a = \left( \frac{18ut_o}{g((\rho_p - \rho_o)(1-f))h_o} \right)^{\frac{1}{2}} \quad (7-11)$$

Substituting typical values ( $t_o = 2$  hours,  $h_o = 12$  ft.,  $\rho_p = 1.12$ ,  $f = 0.65$ ) in equation 7-11 yields an aggregate diameter of  $150 \mu\text{m}$ .

Since the largest diameters recorded in my experiments were only of the order 25  $\mu\text{m}$ , growth of particle size by differential settling becomes an important factor in the operation of conventional treatment facilities.

#### 7.6 Summary

This research verified the charge mosaic model of colloid flocculation for the E. coli-PEI system. High-molecular-weight PEI molecules not only neutralized the negative surface charge on the E. coli cells, but also reversed the charge at polymer adsorption sites, resulting in alternating patches of positive polymer and negative surface. The resulting flocs significantly reduced suspension turbidity and re-filtration time. Low-molecular-weight PEI molecules produced flocculation solely by reduction of the interparticle repulsive forces by adsorption onto the oppositely-charged surface.

A modification to the current procedure of measuring aggregate size in the Coulter counter was proposed and tested in flocculating E. coli-PEI suspensions. This modification, which accounts for the effect of aggregate porosity on the counter response, was found to be applicable over a broad range of flocculation conditions. Utilizing a coalesced sphere model, the changes in aggregate size distribution were correlated directly with turbidity and re-filtration rate measurements.

The effectiveness of PEI in producing the desired aggregation of E. coli cells was highly molecular weight dependent. Only the high-molecular-weight species produced significant increases in aggregate size. Both the intensity of agitation in the stirrer-reactor assembly, and the duration of agitation were found to be relatively unimportant, within the limits of current treatment practice.

## REFERENCES CITED

## CHAPTER 7

1. Jones, G. P., Friedrich, R. E., MacWilliams, D. C., "Factors in Flocculation Mechanism", Presented at American Institute of Chemical Engineers' Meeting, New Orleans, 1962.
2. Perkel, R., and Ullman, R., "The Adsorption of Polydimethylsiloxanes from Solution", Journal Polymer Science, 54 (1961), 127-148.
3. LaMer, V. K., and Healy, T. W., "Adsorption-Flocculation Reactions of Macromolecules at the Solid-Liquid Interface", Review of Pure and Applied Chemistry, 13 (1963), 112-133.
4. Jenckel, E., and Rumbach, B., "The Adsorption of High Molecular Weight Material from Solution", Zeitschifte Electrochemie, 55 (1961), 612-618.
5. Kasper, D. R., "Theoretical and Experimental Investigations of the Flocculation of Charged Particles in Aqueous Solutions by Polyelectrolytes of Opposite Charge", Ph.D. Thesis, California Institute of Technology, 1971.
6. Friedman, B. A., Dugan, P. R., Pfister, R. M., and Remsen, C. C., "Structure of Exocellular Polymers and Their Relationship to Bacterial Flocculation", Journal Bacteriology, 98 (1969), 1328-1334.
7. Dixon, J. K., and Zielyk, M. W., "Control of the Bacterial Content of Water with Synthetic Polymeric Flocculants", Environmental Science and Technology, 3 (1969), 551-558.
8. Gregory, J., "Rates of Flocculation of Latex Particles by Cationic Polymers", Journal Colloid and Interface Science, 42 (1973), 448-456.
9. Neis, U., Eppler, B., and Hahn, H., "Quantitative Analysis of Coagulation Processes in Aqueous Systems: An Application of the Coulter Counter Technique", unpublished paper, 1974.

10. Rubini, J., Stahman, M., and Rasmussen, A., "Agglutination of Red Cells by Synthetic Lysine Polypeptides", Proceedings Society Experimental Biology and Medicine, 76 (1951), 659-662.
11. Tilton, R., Murphy, J., and Dixon, J., "The Flocculation of Algae with Synthetic Polymeric Flocculants", Water Research, 6 (1972), 155-164.
12. Dixon, J. K., LaMer, V. K., and Linford, H. B., "Factors Affecting Filtration Rates of Flocculated Silica", Journal Water Pollution Control Federation, 39 (1967), 647-658.
13. Dixon, J. K., LaMer, V. K., Li, C., Messinger, S., and Linford, H. B., "Effect of the Structure of Cationic Polymers on the Flocculation and the Electrophoretic Mobility of Crystalline Silica", Journal Colloid and Interface Science, 23 (1967), 465-473.
14. Birkner, F. B., and Morgan, J. J., "Polymer Flocculation Kinetics of Dilute Colloidal Suspensions", Journal American Water Works Association, 60 (1968), 175-191.
15. Tenney, M. W., and Stumm, W., "Chemical Flocculation of Microorganisms in Biological Waste Treatment", Journal Water Pollution Control Federation, 37 (1965), 1370-1388.

## Appendix A

## DIFFERENTIAL VOLUME DISTRIBUTION SPECTRA

Differential volume distribution spectra were prepared from the particle size data measured by the Coulter counter for the various E. coli-PEI systems. The raw data for the volume distribution spectra, Figures A.1-A.15, correspond to that utilized in the preparation of the number distribution spectra, Figures 6.8-6.23.

Volume distribution spectra enable the researcher to record the shift in total aggregate volume from the initial large concentration at the singlet diameter to the final volume distribution of the aggregated particles, over the time period of the experiment. In addition, the volume distribution provides a means of identifying the equilibrium aggregate diameter, i. e., the aggregate diameter at which the largest volume concentration occurs. While the equilibrium aggregate diameter may be obscured in the number distribution spectrum by the large number of small particles, the volume distribution will identify the aggregate size, or range of sizes, which are in equilibrium with the imposed coagulation and shear conditions.

Table A.1 summarizes the information derived from Figures A.1-A.15. The diameter at the largest volume concentration increases with increasing PEI molecular weight. In most cases, two distinct peaks are recorded, the first corresponding to the large number of

uncoagulated singlet-doublet particles, and the second to the equilibrium value produced. Over the four hour coagulation period, the low molecular weight PEI-E. coli system exhibits a continuous shift in aggregate volume from the singlet-doublet peak to the equilibrium value (Figures A 3-A.4, A.6-A.9). This effect is not exhibited by the high molecular weight species, which have achieved equilibrium values within the first 60 minutes of agitation. Overdoses of PEI 350 and PEI 600 produce some aggregates, probably before the surface sites became saturated, and a large concentration of stabilized singlets.

Figure	PEI MW <sub>n</sub>	[PEI] mg/ℓ	Diameter at Largest Volume Concentration μm	Range of Aggregate Diameters in Equilibrium with Coagulation and Shear Conditions μm
A.1	0	0.0	1.5	1.3 - 1.7
A.2	600	0.5	1.5	1.3 - 1.7
A.3	600	5.0	1.7, 4.5	1.3-2.0, 2.3-4.7
A.4	600	50.0	2.0, 4.5	1.7-2.2, 4.0-5.0
A.5	1200	0.5	1.5	1.3 - 1.7
A.6	1200	5.0	1.8, 4.5	1.6-2.1, 4.0-5.0
A.7	1200	50.0	1.8, 4.5	1.6-2.1, 4.2-6.5
A.8	1800	5.0	2.0, 7.0	1.8-2.2, 5.0-9.0
A.9	1800	50.0	1.5, 2.0 9.0	1.4-1.6, 1.8-2.2, 6.0-11.0
A.10	35000	0.05	1.5	1.2 - 1.7
A.11	35000	0.5	13.0	11.0 - 15.0
A.12	35000	50.0	1.5, 4.5	1.3-1.7, 3.5-5.0
A.13	60000	0.05	1.5	1.2 - 1.7
A.14	60000	0.5	16.0	9.0 - 19.0
A.15	60000	50.0	1.5, 4.5	1.3-1.7, 4.0-5.0

Table A.1 Diameters of Largest Volume Concentrations, and Range of Aggregate Diameters in Equilibrium with Coagulation and Shear Conditions as Functions of PEI MW<sub>n</sub> and PEI Dose.

FIGURE A.1 DIFFERENTIAL VOLUME DISTRIBUTION SPECTRUM

MOLECULAR WEIGHT = 0. MIXING INTENSITY = 20/SEC

POLYMER DOSE = 0.0 MG/L INITIAL PARTICLE COUNT = 2.462E 07/ML

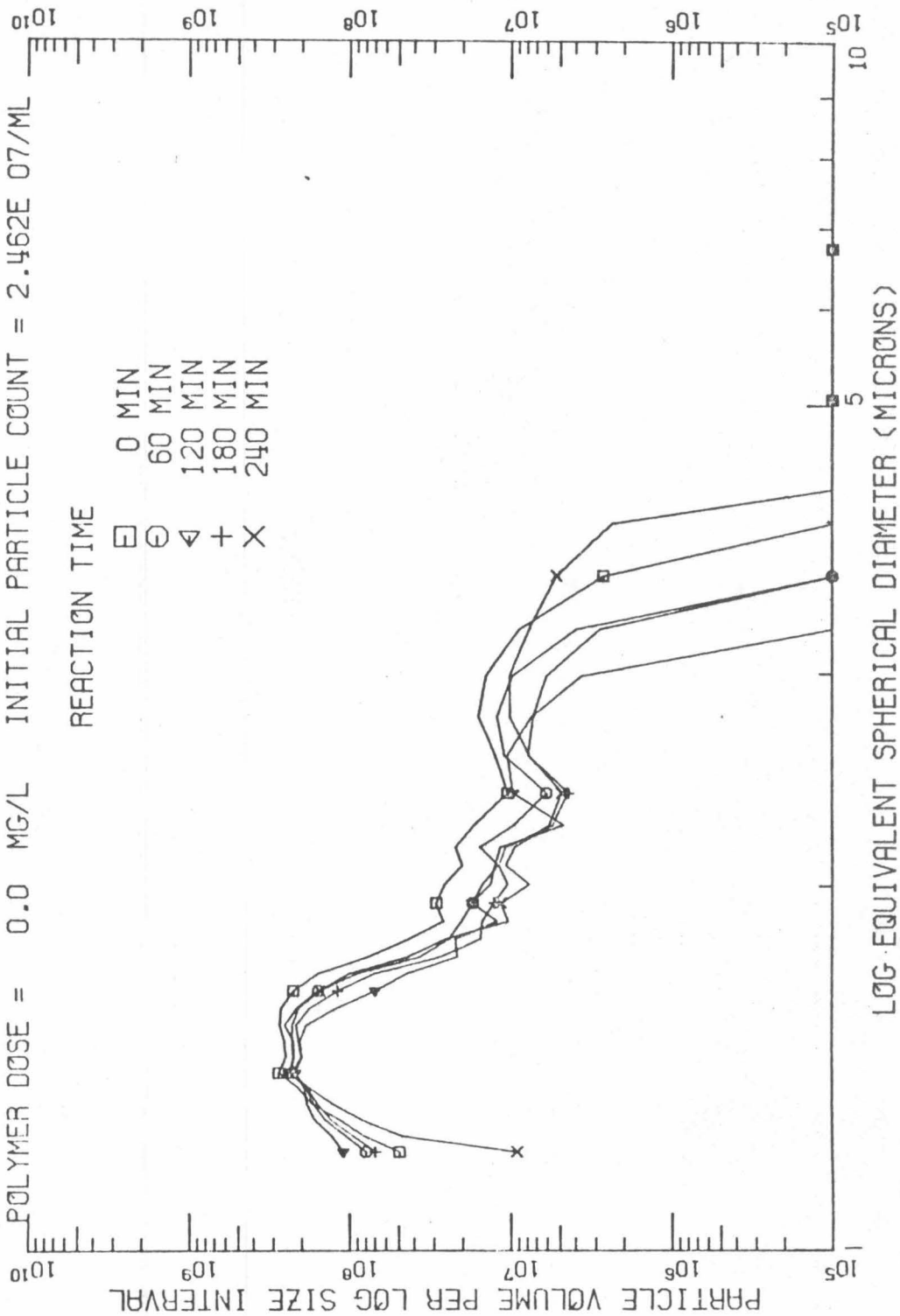


FIGURE A.2 DIFFERENTIAL VOLUME DISTRIBUTION SPECTRUM

MOLECULAR WEIGHT = 600. MIXING INTENSITY = 20/SEC

POLYMER DOSE = 0.50 MG/L INITIAL PARTICLE COUNT = 2.476E 07/ML

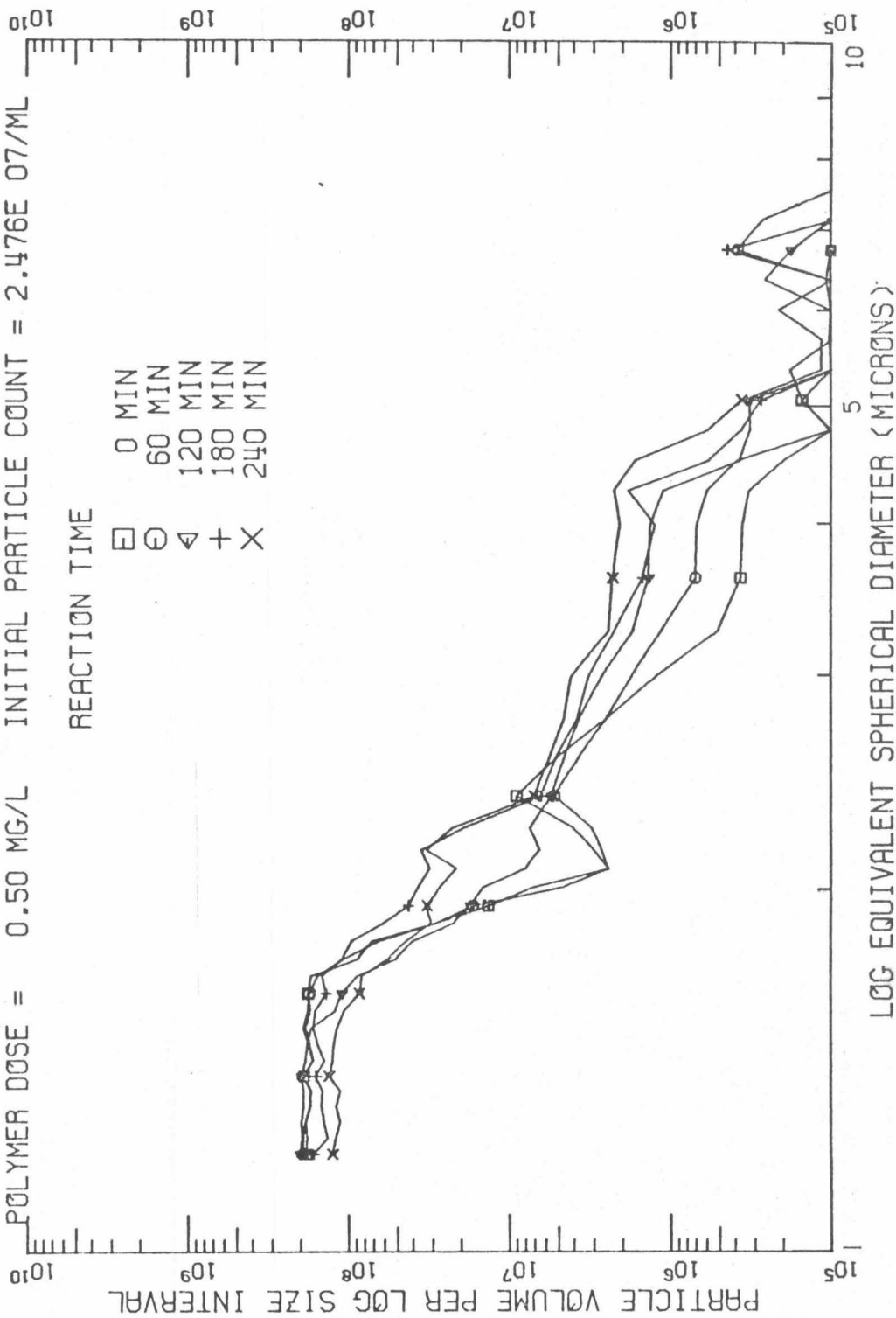


FIGURE A.3 DIFFERENTIAL VOLUME DISTRIBUTION SPECTRUM

MOLECULAR WEIGHT = 600. MIXING INTENSITY = 20/SEC

POLYMER DOSE = 5.00 MG/L INITIAL PARTICLE COUNT = 2.580E 07/ML

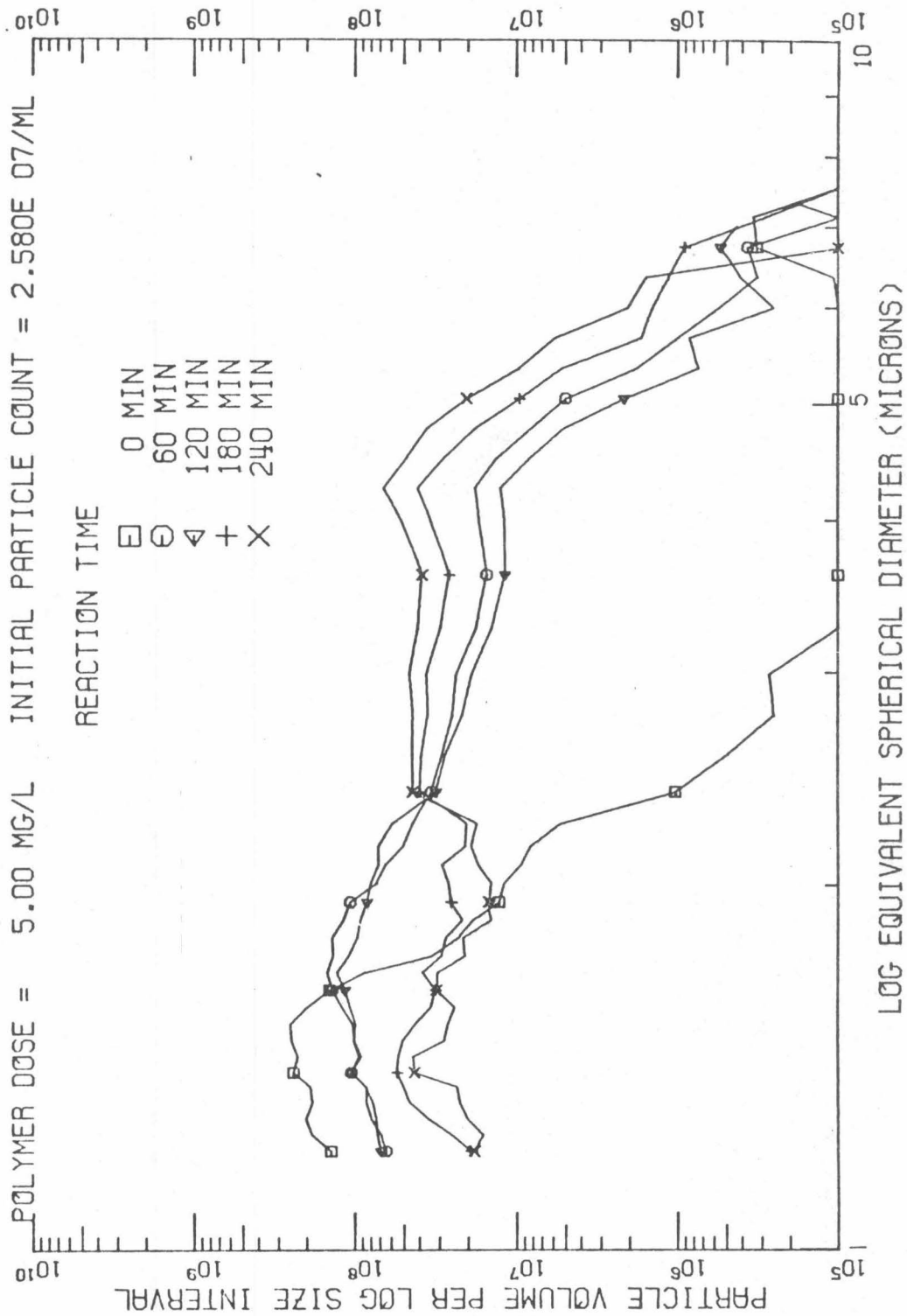


FIGURE A.4 DIFFERENTIAL VOLUME DISTRIBUTION SPECTRUM

MOLECULAR WEIGHT = 600. MIXING INTENSITY = 20/SEC

POLYMER DOSE = 50.00 MG/L INITIAL PARTICLE COUNT = 2.255E 07/ML

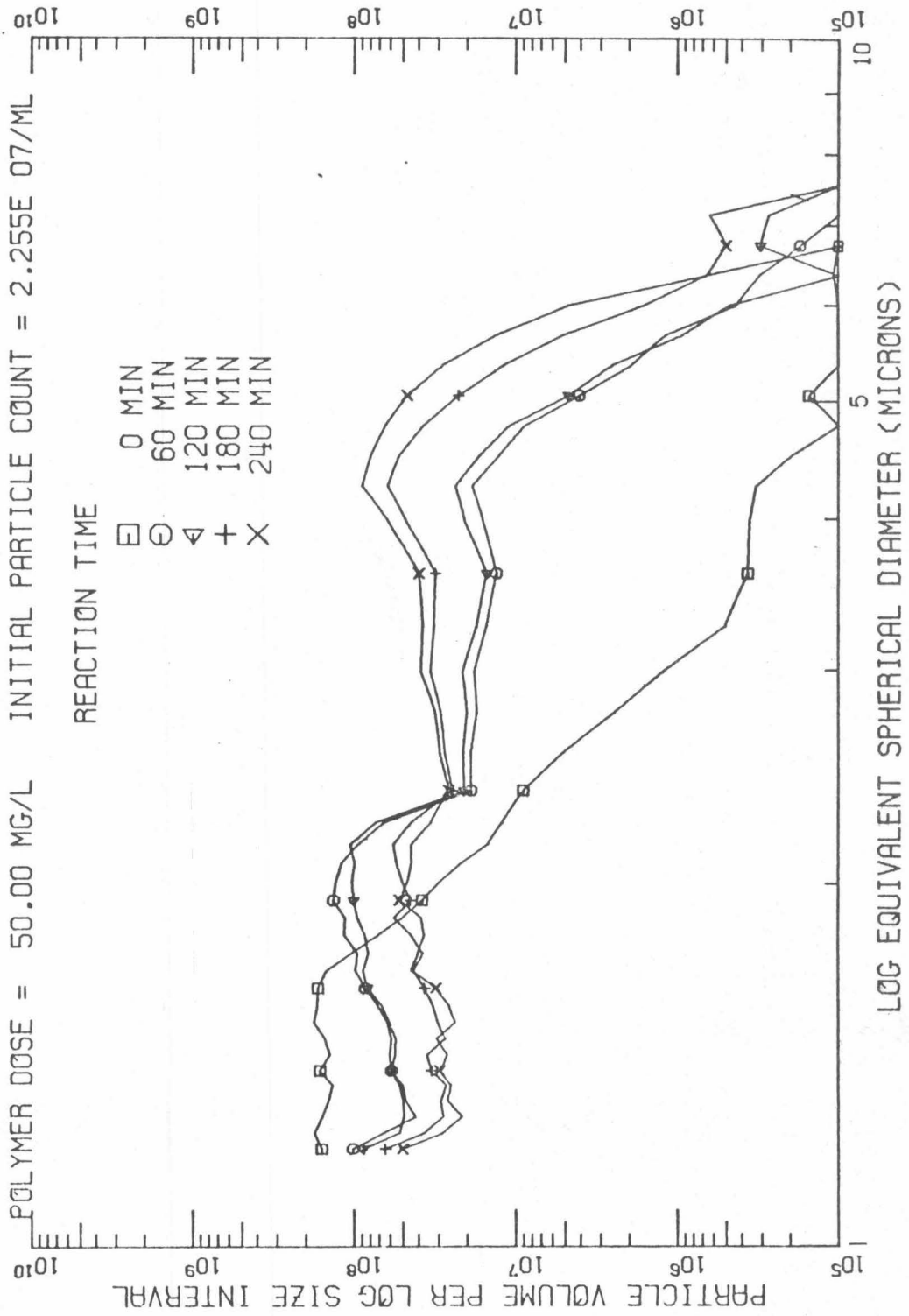


FIGURE A.5 DIFFERENTIAL VOLUME DISTRIBUTION SPECTRUM

MOLECULAR WEIGHT = 1200. MIXING INTENSITY = 20/SEC

POLYMER DOSE = 0.50 MG/L INITIAL PARTICLE COUNT = 2.915E 07/ML

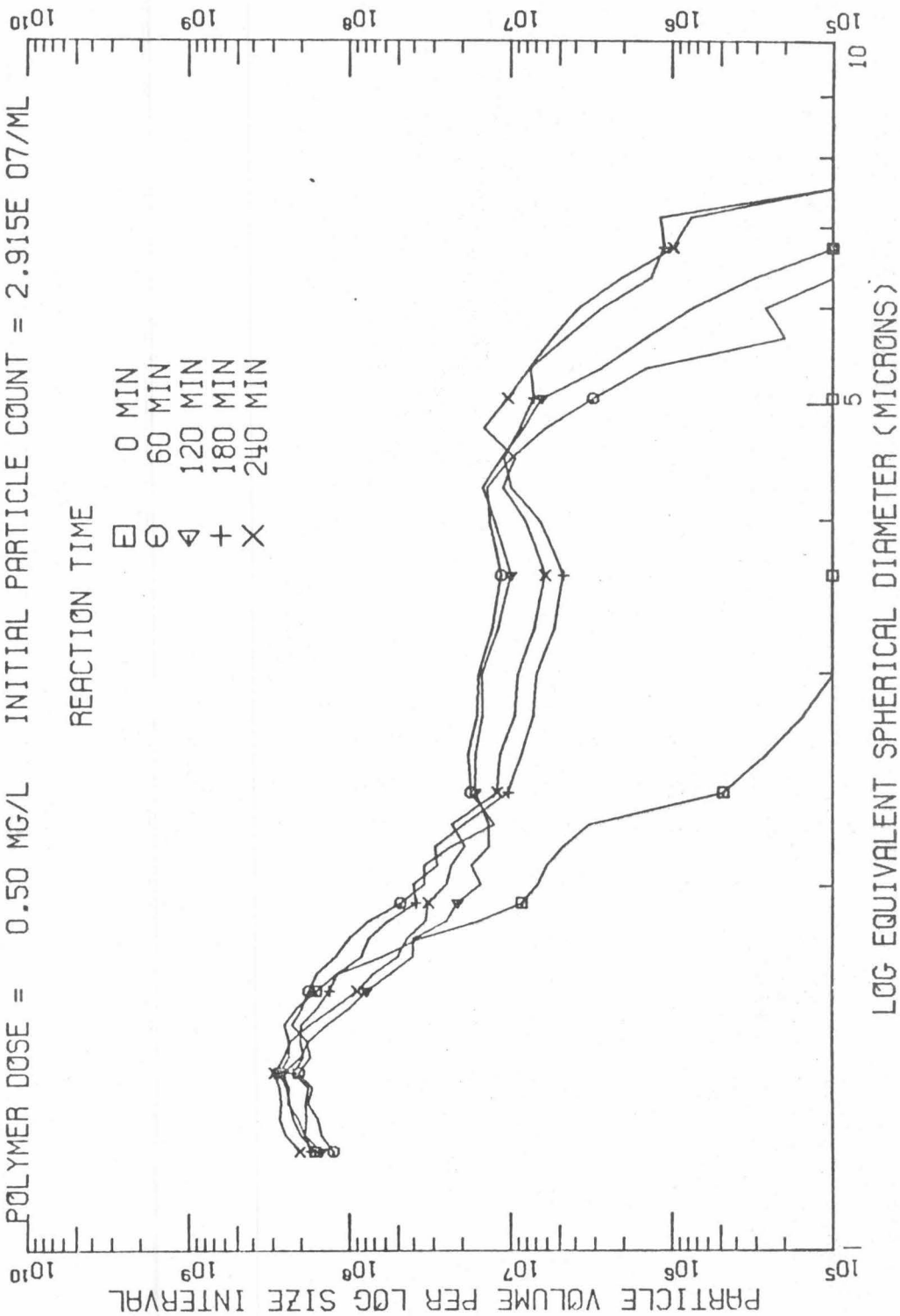


FIGURE A.6 DIFFERENTIAL VOLUME DISTRIBUTION SPECTRUM

MOLECULAR WEIGHT = 1200. MIXING INTENSITY = 20/SEC

POLYMER DOSE = 5.00 MG/L INITIAL PARTICLE COUNT = 2.535E 07/ML

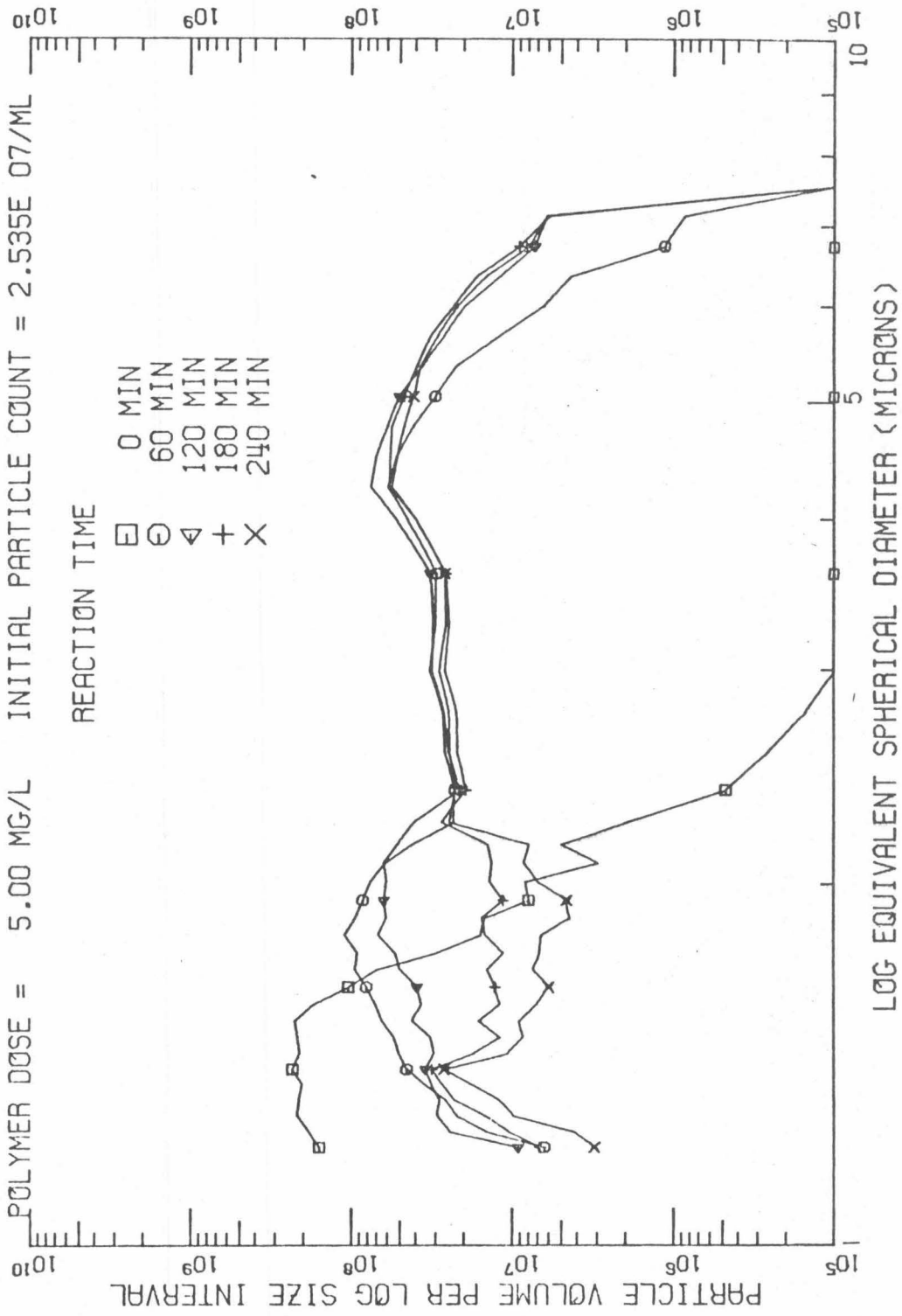


FIGURE A.7 DIFFERENTIAL VOLUME DISTRIBUTION SPECTRUM

MOLECULAR WEIGHT = 1200. MIXING INTENSITY = 20/SEC

POLYMER DOSE = 50.00 MG/L INITIAL PARTICLE COUNT = 2.730E 07/ML

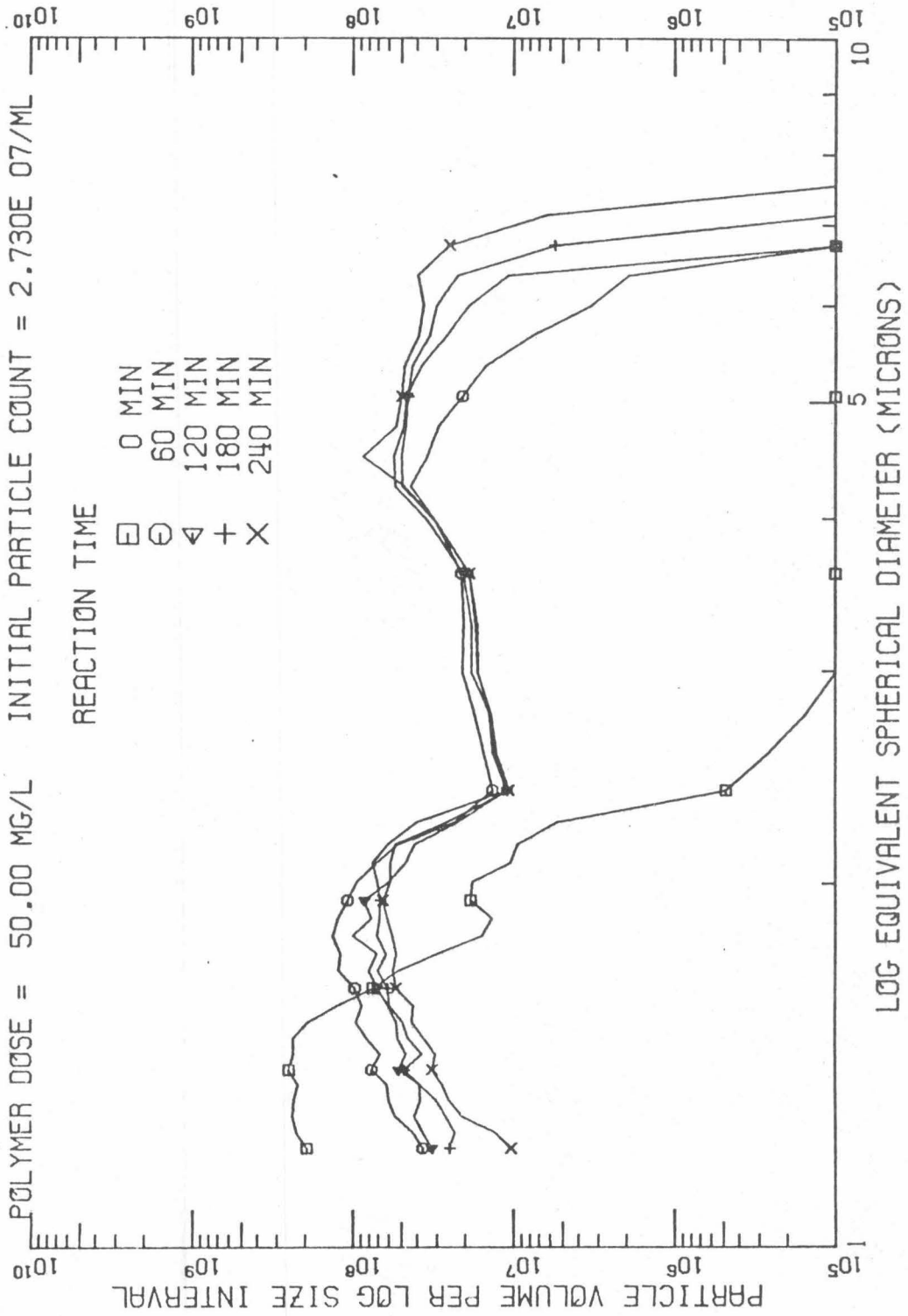


FIGURE A.8 DIFFERENTIAL VOLUME DISTRIBUTION SPECTRUM

MOLECULAR WEIGHT = 1800. MIXING INTENSITY = 20/SEC

POLYMER DOSE = 5.00 MG/L INITIAL PARTICLE COUNT = 2.350E 07/ML

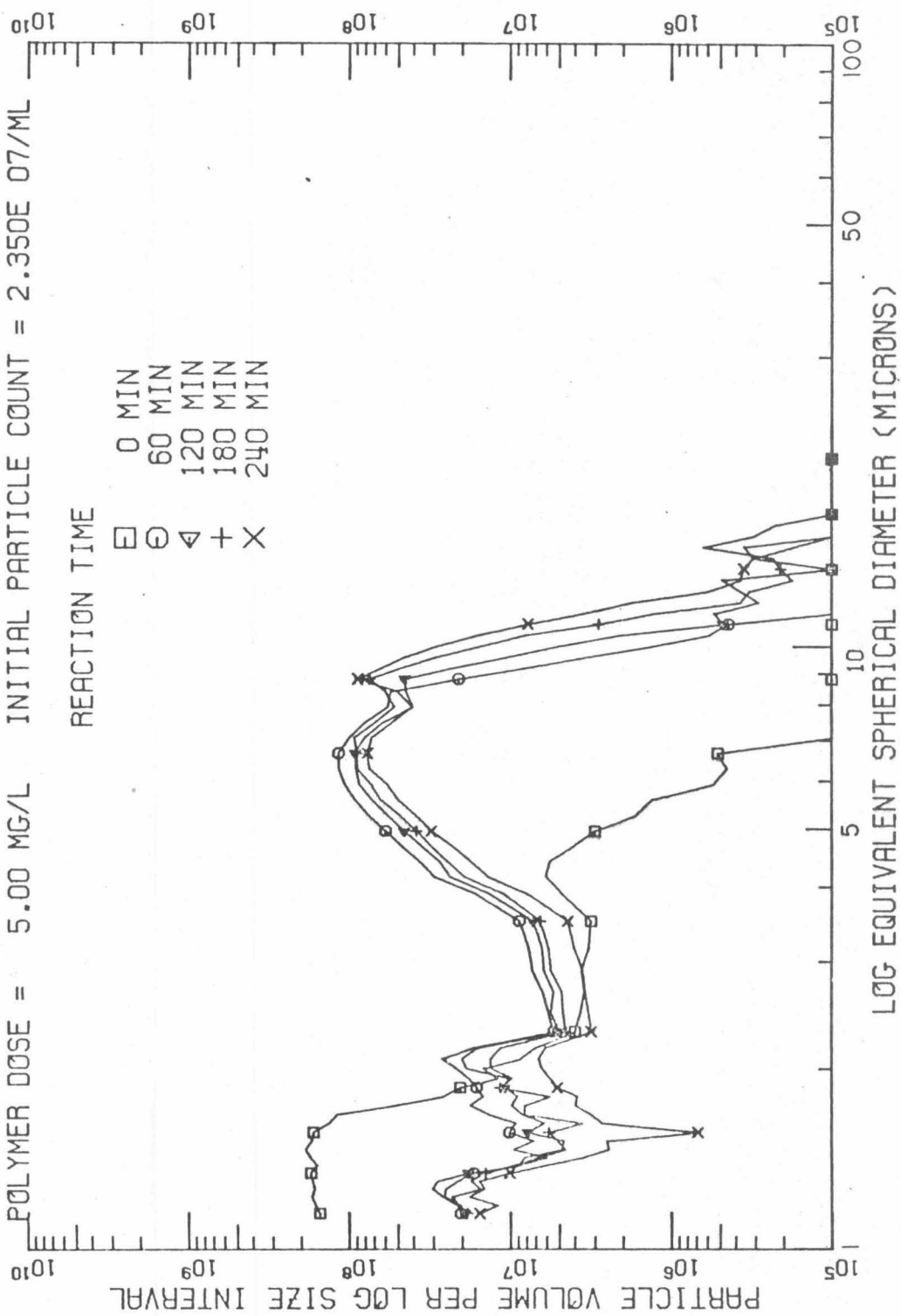


FIGURE A.9 DIFFERENTIAL VOLUME DISTRIBUTION SPECTRUM

MOLECULAR WEIGHT = 1800. MIXING INTENSITY = 20/SEC

POLYMER DOSE = 50.00 MG/L INITIAL PARTICLE COUNT = 2.089E 07/ML

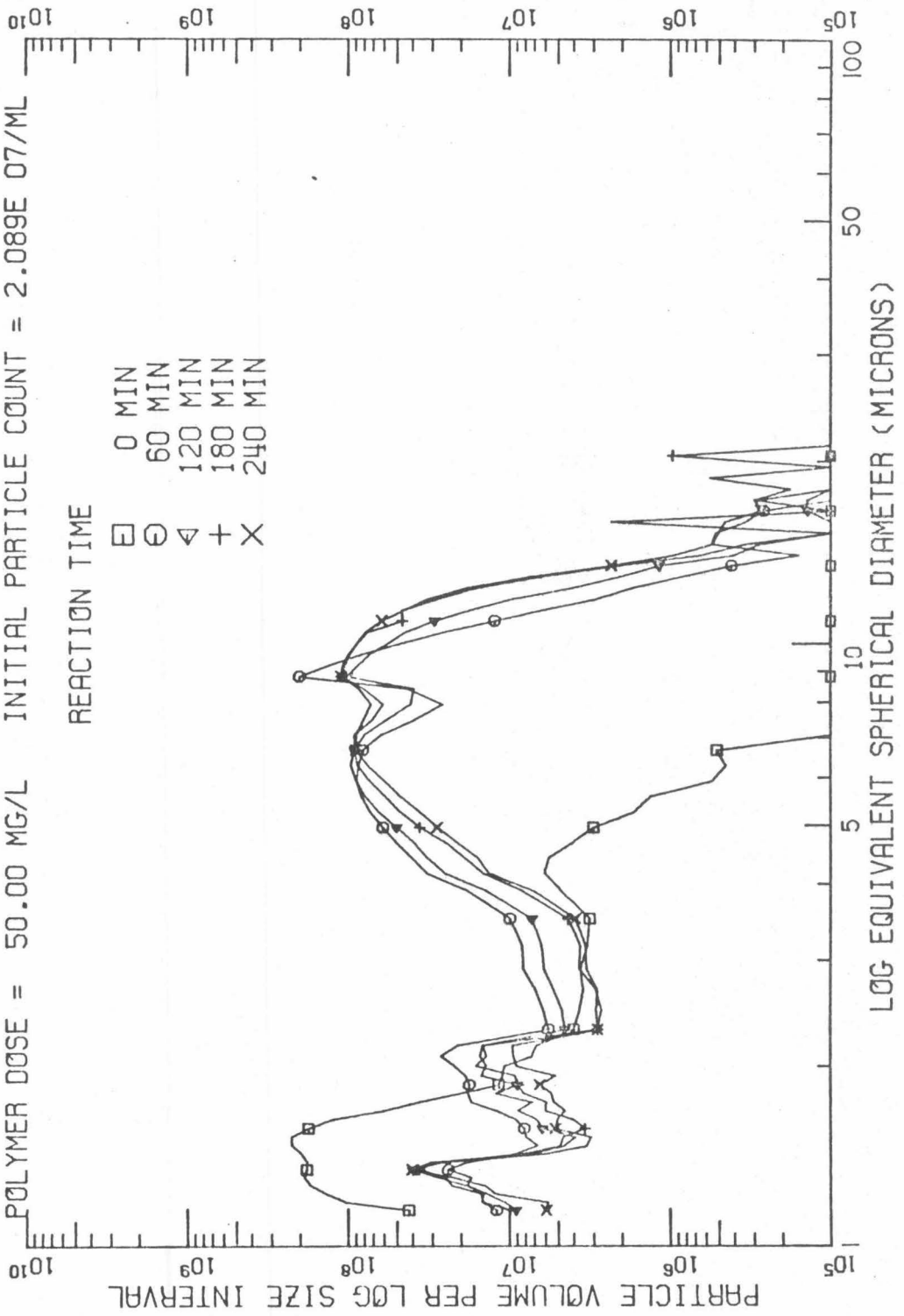


FIGURE A.10 DIFFERENTIAL VOLUME DISTRIBUTION SPECTRUM

MOLECULAR WEIGHT = 35000. MIXING INTENSITY = 20/SEC

POLYMER DOSE = 0.05 MG/L INITIAL PARTICLE COUNT = 2.745E 07/ML

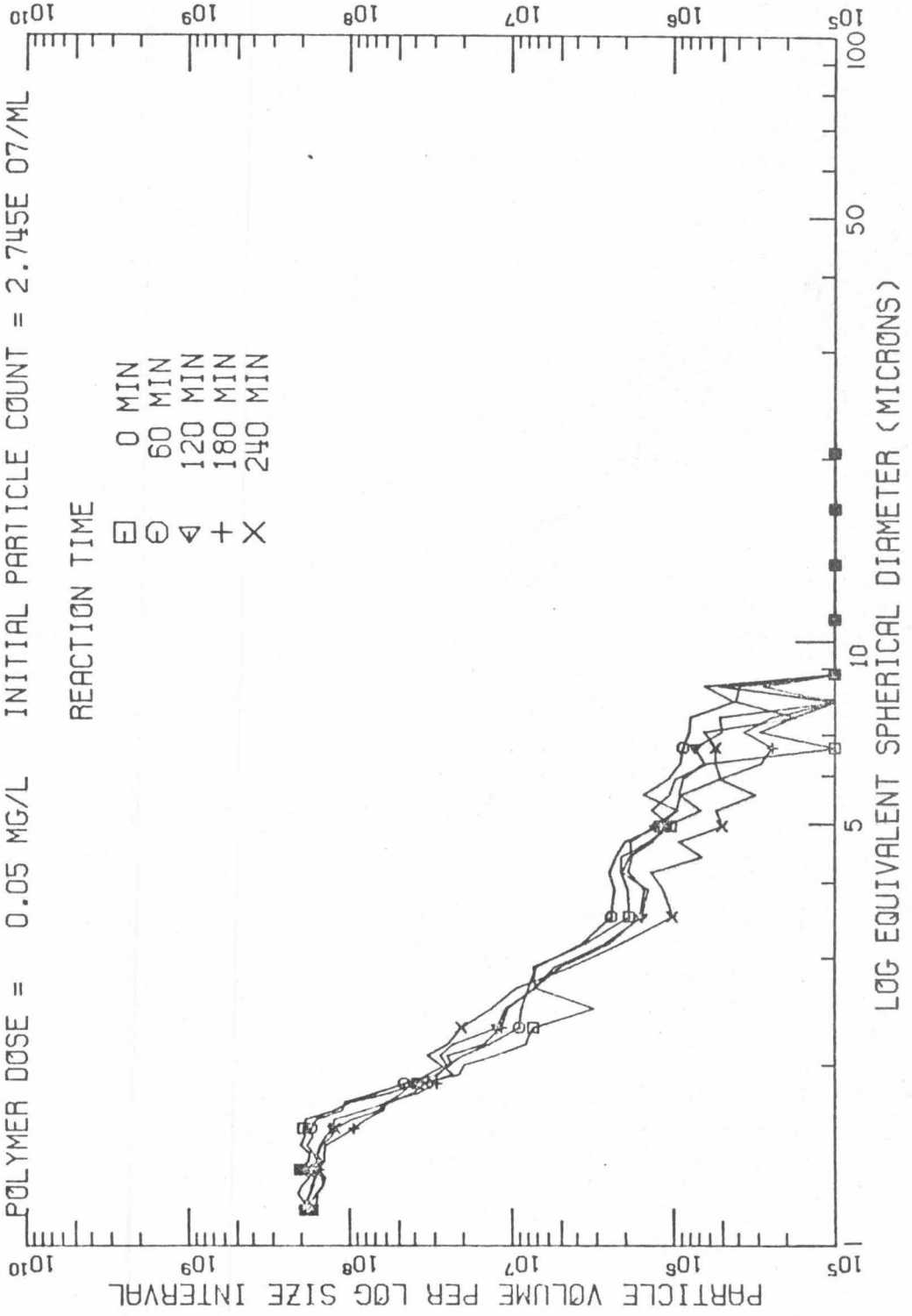


FIGURE A.11 DIFFERENTIAL VOLUME DISTRIBUTION SPECTRUM

MOLECULAR WEIGHT = 35000. MIXING INTENSITY = 20/SEC

POLYMER DOSE = 0.50 MG/L INITIAL PARTICLE COUNT = 3.011E 07/ML

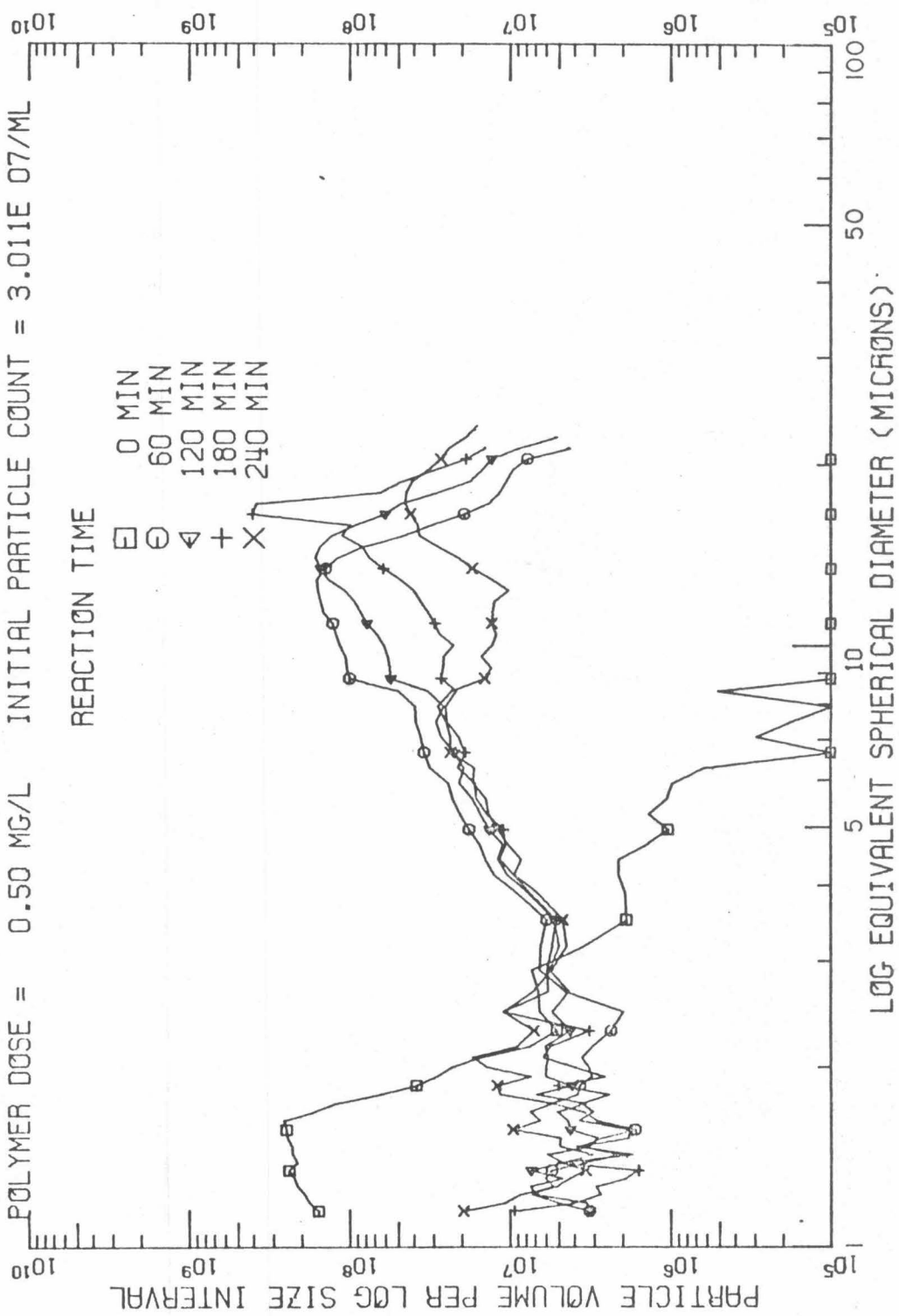


FIGURE A.12 DIFFERENTIAL VOLUME DISTRIBUTION SPECTRUM

MOLECULAR WEIGHT = 35000.

MIXING INTENSITY = 20/SEC

POLYMER DOSE = 50.00 MG/L

INITIAL PARTICLE COUNT = 2.662E 07/ML

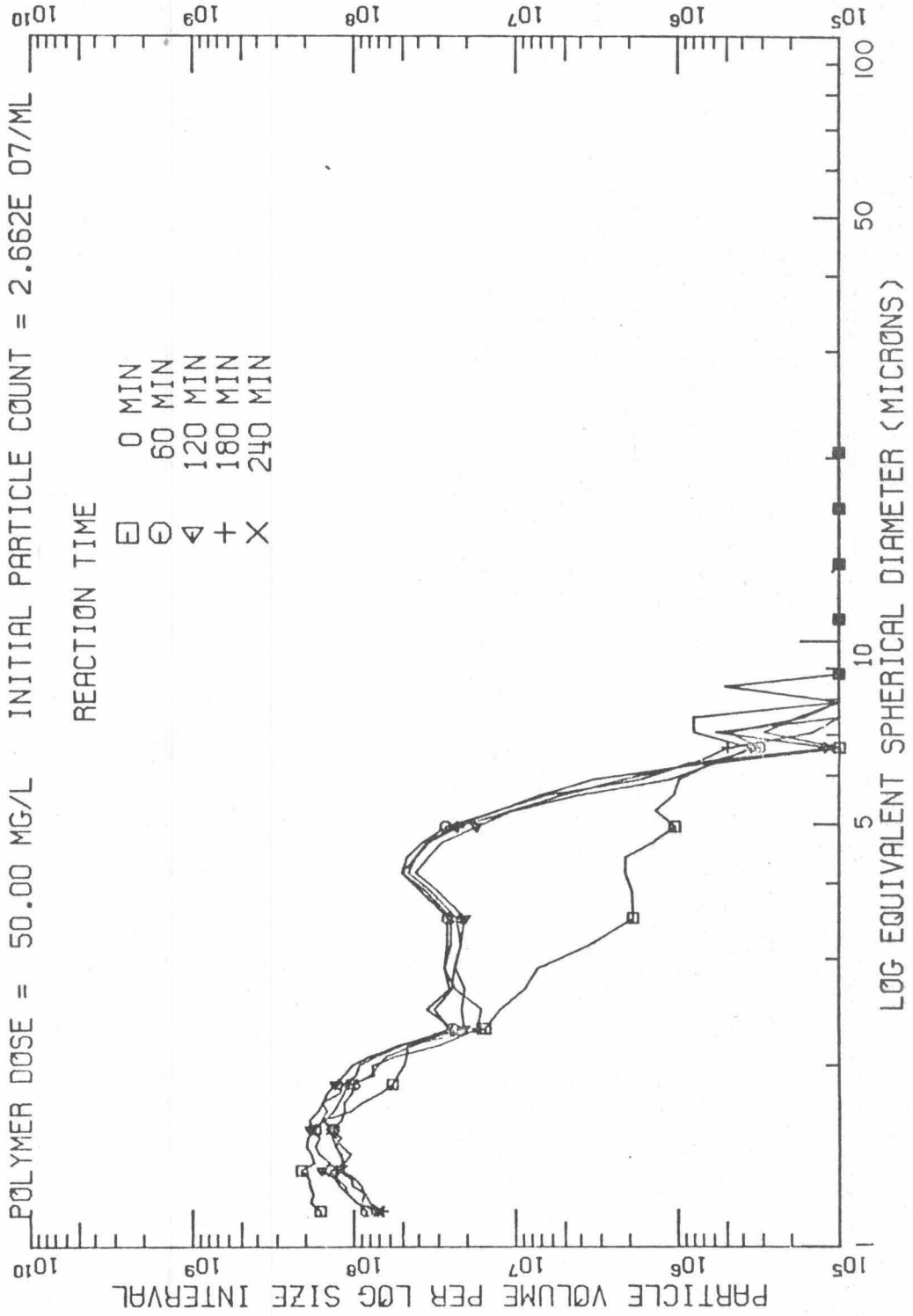


FIGURE A.13 DIFFERENTIAL VOLUME DISTRIBUTION SPECTRUM

MOLECULAR WEIGHT = 60000. MIXING INTENSITY = 20/SEC  
 POLYMER DOSE = 0.05 MG/L INITIAL PARTICLE COUNT = 2.690E 07/ML

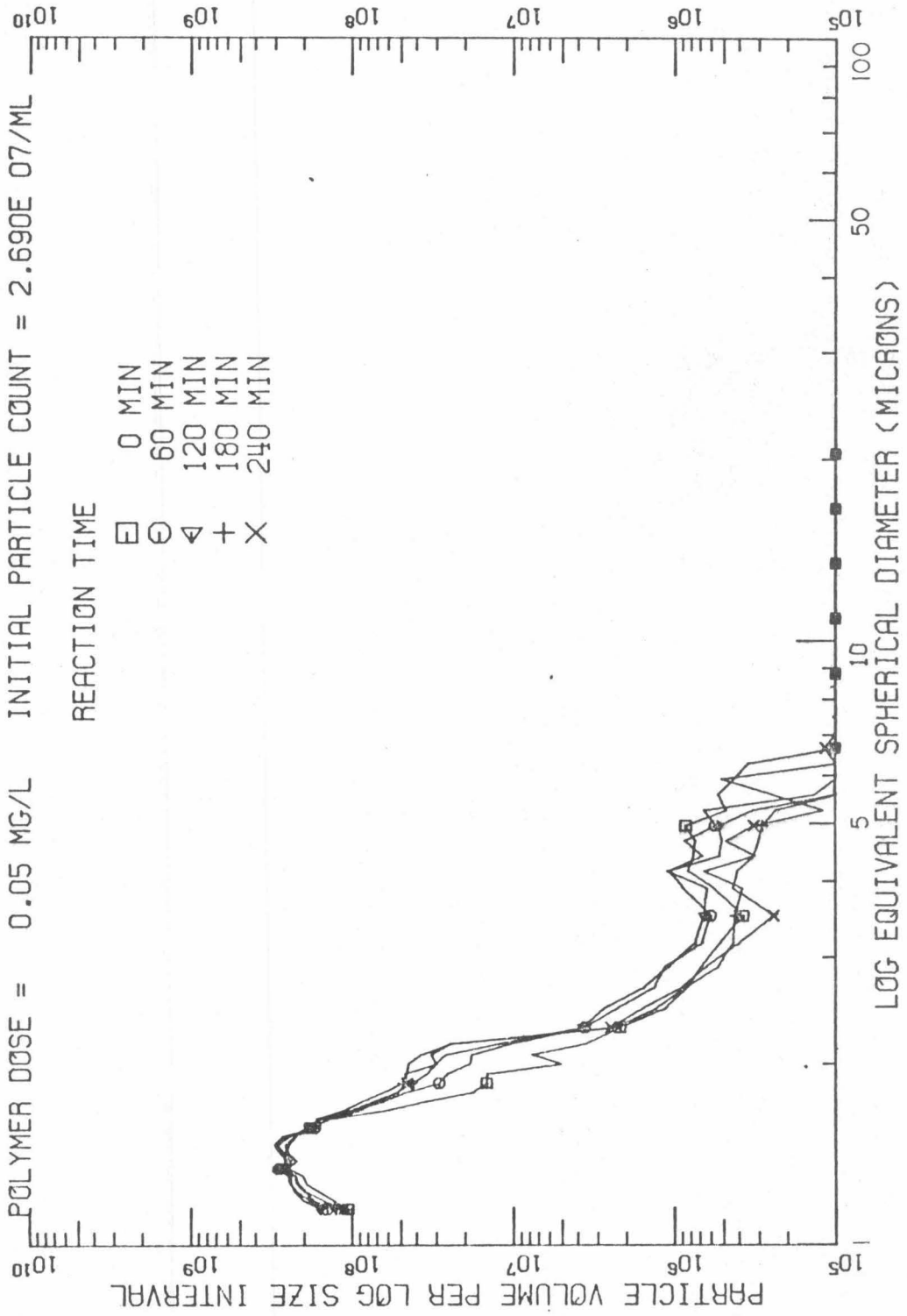


FIGURE A.14 DIFFERENTIAL VOLUME DISTRIBUTION SPECTRUM

MOLECULAR WEIGHT = 60000. MIXING INTENSITY = 20/SEC

POLYMER DOSE = 0.50 MG/L INITIAL PARTICLE COUNT = 2.813E 07/ML

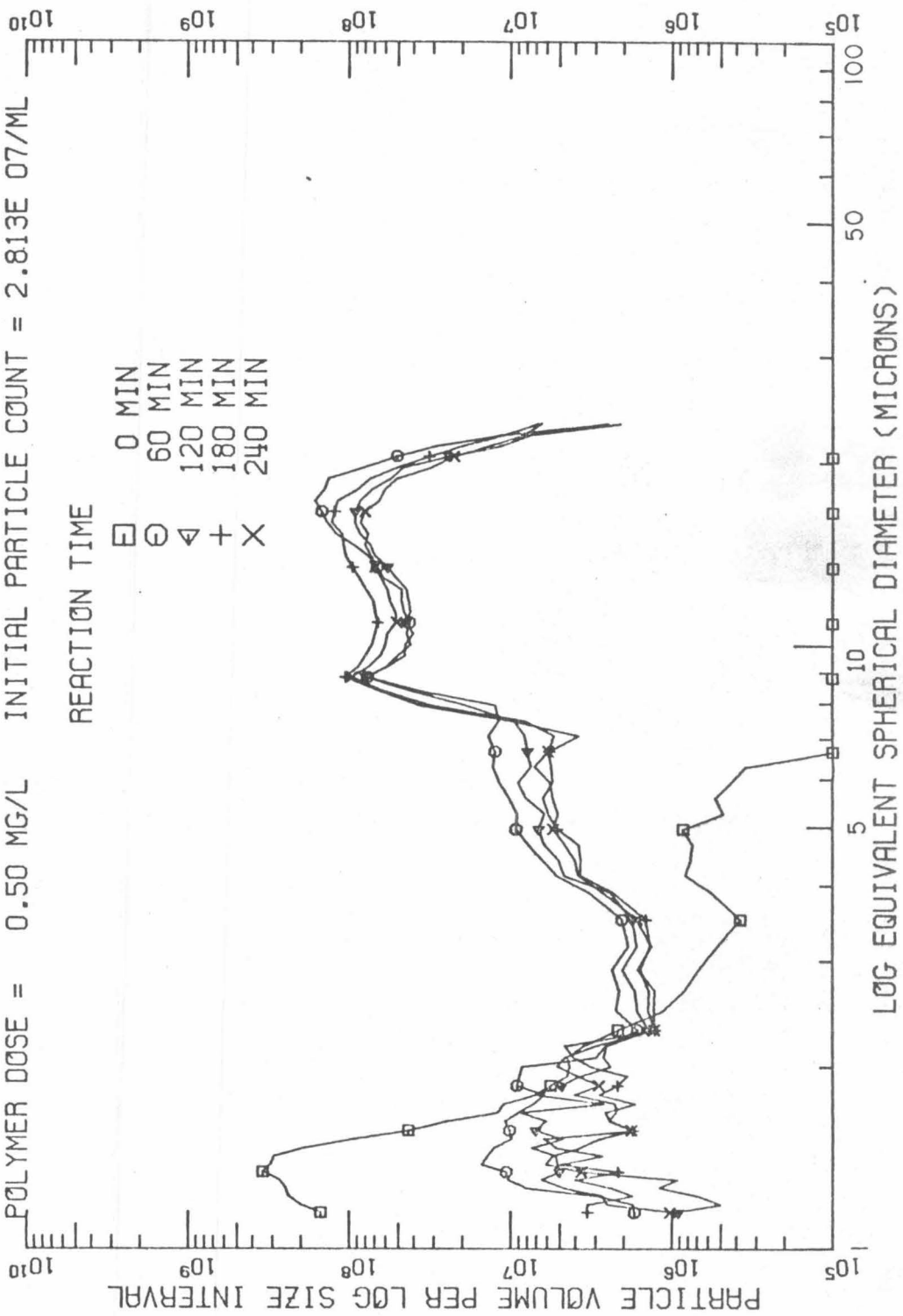


FIGURE A.15 DIFFERENTIAL VOLUME DISTRIBUTION SPECTRUM

MOLECULAR WEIGHT = 60000. MIXING INTENSITY = 20/SEC

POLYMER DOSE = 50.00 MG/L. INITIAL PARTICLE COUNT = 2.214E 07/ML

